University of Alberta

Hazard Analysis of Reactivated Earth Slides in the Thompson River Valley, Ashcroft, British Columbia

by

Arash Eshraghian

©

A thesis submitted to the Faculty of Graduate Studies and Research
in partial fulfillment of the requirements for the degree of

Doctor of Philosophy
in
Geotechnical Engineering

Department of Civil and Environmental Engineering

Edmonton, Alberta
Fall 2007

Library and
Archives Canada

Published Heritage
Branch

395 Wellington Street
Ottawa ON K1A 0N4
Canada

Bibliothèque et
Archives Canada

Direction du
Patrimoine de l'édition

395, rue Wellington
Ottawa ON K1A 0N4
Canada

Your file Votre référence
ISBN: 978-0-494-32953-5
Our file Notre référence
ISBN: 978-0-494-32953-5

NOTICE:
The author has granted a non-exclusive license allowing Library and Archives Canada to reproduce, publish, archive, preserve, conserve, communicate to the public by telecommunication or on the Internet, loan, distribute and sell theses worldwide, for commercial or non-commercial purposes, in microform, paper, electronic and/or any other formats.

The author retains copyright ownership and moral rights in this thesis. Neither the thesis nor substantial extracts from it may be printed or otherwise reproduced without the author's permission.

AVIS:
L'auteur a accordé une licence non exclusive permettant à la Bibliothèque et Archives Canada de reproduire, publier, archiver, sauvegarder, conserver, transmettre au public par télécommunication ou par l'Internet, prêter, distribuer et vendre des thèses partout dans le monde, à des fins commerciales ou autres, sur support microforme, papier, électronique et/ou autres formats.

L'auteur conserve la propriété du droit d'auteur et des droits moraux qui protège cette thèse. Ni la thèse ni des extraits substantiels de celle-ci ne doivent être imprimés ou autrement reproduits sans son autorisation.

In compliance with the Canadian Privacy Act some supporting forms may have been removed from this thesis.

While these forms may be included in the document page count, their removal does not represent any loss of content from the thesis.

Conformément à la loi canadienne sur la protection de la vie privée, quelques formulaires secondaires ont été enlevés de cette thèse.

Bien que ces formulaires aient inclus dans la pagination, il n'y aura aucun contenu manquant.

Canada

Dedication

I dedicate this thesis to my parents and lovely sisters. Without their patients, understanding, support, and most of all love, the completion of this work would not have been possible.

Abstract

A risk analysis approach may provide a more appropriate methodology for dealing with uncertainties in slope engineering compared to traditional deterministic analysis. Hazard analysis is a main part of a risk analysis process. The movement rates of an active earth slide may vary significantly; therefore, the hazard analyses of such landslides anticipated need to count for the consequences from the range of movement rates.

Since the Canadian Pacific Railway and Canadian National Railway constructed their main rail lines in western Canada in 1885 and 1905, respectively, both companies have had to contend with eleven large, translational, retrogressive earth slides in the Thompson River Valley south of Ashcroft, British Columbia. Geotechnical investigations of these slides provided a unique opportunity to develop and test a new methodology for the hazard analysis of active translational earth slides enouncing different movement rates. The results of all the site investigations since the 1980s were gathered in a geographical information system data base and combined with new geological studies within this area to provide a broader perspective of the deposition units within the study area. Then, groundwater modeling and deterministic stability analyses revealed the mechanical processes that triggered the slides' movements. Later, a review of reactivated translational landslides cases around the world gave a better understanding of the range of the possible movement rates of slides during their reactivations and its correlation with pore pressure on the slides rupture surfaces. Finally, a hazard analysis of a sample slide was conducted to show the methodology for calculating the probability of the reactivation movement rate of such slides.

This study shows that the slides' reactivations in the Ashcroft area are triggered by the Thompson River in a drawdown and toe erosion mechanism. The rate of movement changes non-linearly with the pore pressure on the slides' rupture surfaces. The amount of acceleration after the reactivation initiation depends on the material type and stress level on the rupture surfaces. The analysis also highlighted the importance of the toe erosion protection system in preventing the beginning of movement and preventing the change of rate from slow reactivations to rapid reactivations.

Acknowledgments

I would like to express my sincere gratitude to Dr. C.D. Martin whose continual technical and financial support, guidance, and constant vision were instrumental in achieving the goals of this work and is extremely appreciated. I also thank Dr. N.R. Morgenstern for his valuable help and advice. His guidance, comments and valuable ideas will never be forgotten.

Gratitude is extended to each of the professors within the geotechnical group, particularly Dr. R. Chalaturnyk, Dr. D.H. Chan, Dr. P.K. Robertson, Dr. J.D. Scott and Dr. D.C. Sego, who contributed to both personal and professional development during these studies. Special thank is extended to Dr. D.M. Cruden who helped in geological engineering and provided guidance toward better understanding of the geology of the study area.

My most sincere appreciation is extended to the Canadian National railway, Canadian Pacific Railway, and Transport Canada for their financial support of this project. I like thank Mr. Tim Keegan, Brian Nachtigal, and Chris Bunce for their help in this project.

Mrs. Emily Herd help with GIS program is appreciated. The laboratory assistance provided by Steve Gamble was extremely valuable. Special thanks are extended to Gerry Cyre for his help with site investigation. I am also grateful for tireless secretarial efforts provided during various stage of thesis research by Mrs. S. Petaske.

I am thankful to all my friends and colleagues at the university, who endured the difficult and happy moments of this adventure. Very special thanks must go to

Mehran Panahi, Mehrdad Panahi, Dung Nguyen, Ali Azad, Ardeshir Sharif-Abadi, Mazda Irani, Andrew Corkum, Changho Lim, and Silawat Jeepavipoolvarn. Their friendship and help made the difficulties bearable.

Last but not least, the support encouragement and love my family has been constantly showing are truly appreciated. Special thanks to my mother who never fail to show her love and support! The support provided by my father through last three decades is deeply appreciated.

Table of Contents

Chapter 1

Introduction

1.1. BACKGROUND 1

1.2. RESEARCH PURPOSE 3

1.3. SCOPE AND LIMITATIONS 3

1.4. RESEARCH OBJECTIVES 4

1.5. ORGANIZATION OF THESIS 5

1.6. REFERENCES 7

Chapter 2

Overview of Landslides in the Thompson River Valley, Ashcroft, British Columbia

2.1. GEOLOGY OF THE ASHCROFT AREA 11

- 2.1.1. Surficial Geology of the Study Area 12
- 2.1.2. Quaternary History of the Ashcroft Area 12
- 2.1.3. Geological Units 13

2.2. GEOTECHNICAL CHARACTERISTICS OF THE SLIDES 15

- 2.2.1. Movement Characteristics 15
- 2.2.2. Controlling Laws and Parameters 16
- 2.2.3. Predisposal Factors 17

2.2.4. Triggering Factors 18
2.2.5. Mechanism of Failure 19
2.3. CONCLUSIONS 21
2.4. REFERENCES 22

Chapter 3

Characteristics of Earth Slides in Ashcroft Area

3.1. GEOLOGY 37
3.1.1. Quaternary history of the Ashcroft area 38
3.2. SLIDES IN THE ASHCROFT AREA 40
3.2.1. Slide CN50.9 (Slide 1, Figure 3.1) 41
3.2.2. Goddard Slide (Slide 2, Figure 3.1) 43
3.2.3. North Slide (Slide 3, Figure 3.1) 46
3.2.4. South Slide (Slide 4, Figure 3.1) 47
3.2.5. Basque Slide (Slide 5, Figure 3.1) 48
3.3. RUPTURE SURFACES AND SOIL PARAMETERS 48
3.4. LANDSLIDE CAUSES 51
3.4.1. Triggering causes 51
3.4.2. Preparatory Causes 52
3.5. MOVEMENT BEHAVIOUR 54
3.5.1. Retrogression Movement 54
3.5.2. Reactivation Movement 55
3.6. CONCLUSIONS 58
3.7. REFERENCES 59

Chapter 4

Movement Triggers and Mechanisms of the Earth Slides in the Thompson River Valley

4.1. INTRODUCTION 89

4.2. GEOLOGY AND MOVEMENT HISTORY 92

4.3. SLIDE WITH EFFECTIVE RIVER EROSION PROTECTION (SLIDE CN50.9) 94

4.3.1. Instrumentation 94

4.3.2. Groundwater System Modeling 95

4.3.2.1. Procedure 96

4.3.2.2. Results 98

4.3.3. Stability Analyses 99

4.3.3.1. Procedure 100

4.3.3.2. Results 101

4.4. SLIDE WITHOUT EFFECTIVE RIVER EROSION PROTECTION (THE GODDARD SLIDE) 102

4.4.1. Instrumentation 102

4.4.2. Groundwater System Modelling 103

4.4.2.1. Procedure 103

4.4.2.2. Results 104

4.4.3. Stability Analyses 106

4.4.3.1. Procedure 106

4.4.3.2. Results 107

4.5. SUMMARY OF SLIDE KINEMATICS AND DEFORMATION PATTERNS ... 108

4.5.1. Slide CN50.9 108

4.5.2. The Goddard Slide 110

4.6. CONCLUSIONS 113

4.7. REFERENCES 114

Chapter 5

A Review of Movements of Reactivated Translational Earth Slides

5.1. CAUSAL FACTORS 144

5.2. PORE-PRESSURE-INDUCED ACCELERATION 145

- 5.2.1. Geometry 146
- 5.2.2. Soil Properties 146
- 5.2.3. Rate of Movement 146

5.3. MOVEMENT BEHAVIOUR 147

- 5.3.1. Correlation for the start of reactivation 148
- 5.3.2. Correlation for rate of reactivation movement 149

5.4. DISCUSSION 151

5.5. CONCLUSIONS 153

5.6. REFERENCES 154

Chapter 6

Hazard Analysis of an Active Earth Slide in the Thompson River Valley, Ashcroft, British Columbia

6.1. INTRODUCTION 181

6.2. BACKGROUND 183

- 6.2.1. Landslide Characterization 183
  - 6.2.1.1. Reactivation Movement Rate 185
  - 6.2.1.2. Retrogression Movement Rate 187

6.2.2. Trigger Characterization (Thompson River) 187
6.2.2.1. The Thompson River Discharge 188
6.2.2.2. The Thompson River Level 189
6.2.2.3. Probability of River Flood in the Railway Lifetime 190

6.3. PROBABILISTIC STABILITY ANALYSES 191

6.3.1. Seepage Analyses 191

6.3.2. Deterministic Stability Analyses 191

6.3.3. Material Uncertainties 192

6.3.4. Sensitivity Analyses 193

6.3.5. Results of Probabilistic Stability Analyses 194

6.3.6. Uncertainties in Results of the Probabilistic Stability Analyses 195
6.3.6.1. Groundwater Modeling Uncertainty 195
6.3.6.2. Toe Erosion Uncertainty 196
6.3.6.3. Total Uncertainty 196

6.4. PROBABILITY OF DIFFERENT MOVEMENT RATES 197

6.5. CONCLUSIONS 204

6.6. REFERENCES 205

Chapter 7

Summary and Conclusions

7.1. SUMMARY 234

7.3. CONCLUSIONS 238

7.4. SUGGESTED FUTURE RESEARCH 240

Appendix 1

Effect of the Thompson River on the Stability of Earth Slides in Ashcroft Area (South Slide)

A1.1. INTRODUCTION 242

A1.2. GEOLOGY AND MOVEMENT HISTORY 243

A1.3. GROUNDWATER SYSTEM 244

- A1.3.1. Piezometric Data 244
- A1.3.2. Groundwater Modeling 244
  - A1.3.2.1. Procedure 245
  - A1.3.2.2. Result 246

A1.4. STABILITY ANALYSES 247

- A1.4.1. Procedure 247
- A1.4.2. Results 249

A1.5. DISCUSSION 249

A1.6. CONCLUSIONS 251

A1.7. REFERENCES 252

Appendix 2

Cross Sections of the Earth Slides in Ashcroft Area

A2.1. INTRODUCTION 262

A2.2. PROCESS 262

A2.3. ASHCROFT AREA SLIDES' CROSS SECTIONS 267

- A2.3.1. Slide CN50.9 267

A2.3.2. Goddard Slide 271

A2.3.3. North Slide 276

A2.3.4. South Slide........ 286

A2.3.5. Basque Slide 290

A2.3.6. Conclusions 294

Appendix 3

Soil Tests

A3.1. INTRODUCTION........ 295

A3.2. CONSOLIDATION TEST 297

A3.3. DIRECT SHEAR TESTS........ 301

A3.4. MOISTURE CONTENT AND INDEX TESTS........ 306

A3.5. PARTICLE-SIZE DISTRIBUTION........ 315

A3.6. MINERALOGY TESTS 333

A3.7. CONCLUSIONS........ 336

List of Tables

Table 2.1. Volumes and areas of four of the landslides in the Ashcroft area. 25

Table 2.2. Estimated overburden pressure and previous deposit height in the Ashcroft area (based on Skempton 1969). 25

Table 2.3. Surfaces of rupture elevation of the studied slides in the Ashcroft area. 25

Table 3.1. Volumes and areas of the five active landslides (Figure 3.1) 64

Table 3.2. Soil parameters of glaciolacustrine unit (unit 2) at the Thompson River valley 65

Table 3.3. Surface of rupture elevations in different slides 66

Table 3.4. Summary of slide movements in the Ashcroft area 67

Table 3. 5. Average pore pressure ratio (r_u) and rate of movement at each movement period for the deeper rupture surface of Slide CN50.9 68

Table 4.1. Summary of the slide movements. 120

Table 4.2. Material properties used in groundwater modeling of the slides in Ashcroft area. 121

Table 4.3. Comparing the result of steady state seepage analysis and the minimum piezometric head of piezometers installed in Slide CN50.9. 121

Table 4.4. Residual and peak strengths used in the stability analyses. 122

Table 4.5. Change in the Factor of Safety for the reactivation blocks in Slide CN50.9 during year 2002. 122

Table 5.1. Studied cases of reactivated translational earth slides. 162

Table 5. 2. Causal factors of studied, reactivated, translational, earth slides. 166

Table 5.3. List of studied slides show rate sensitivity to pore pressure changes on their rupture surfaces with enough information for detailed movement behaviour study. 168

Table 5.4. Information on geometry of the slides 169

Table 5.5. Information on material properties of rupture surfaces. 170

Table 5.6. Rate versus pore pressure on rupture surface changes for 17 studied slides. 171

Table 5.7. Slope of movement line in root rate axes and r_{u0}. 172

Table 5.8. Different Acceleration Factor (A.F.) for the slides with similar material on their rupture surfaces. 173

Table 6.1. Dimension of translational blocks in Slide CN50.9. 210

Table 6.2. Return periods of the Thompson River yearly discharge. 210

Table 6.3. Probability of different Thompson River flood return periods in the designed lifetime of the railway (100 years). 211

Table 6.4. Soil properties used in seepage analyses 211

Table 6.5. The material properties used in Slide CN50.9's deterministic stability analyses 212

Table 6.6. Definitions of the variability in soil parameters used in probabilistic slope stability analysis 212

Table 6.7. Sensitivity of blocks' factor of safety to change in soil parameters 213

Table 6.8. Range of changes in the probability of Factor of Safety being less than 1.1 (P(FS<1.1)) by uncertainty in the groundwater system modeling for each of the four blocks in Slide CN50.9. 214

Table 6.9. Range of changes in the probability of Factor of Safety being less than 1.1 (P(FS<1.1)) by uncertainty in the amount of toe erosion in each of the five blocks in Slide CN50.9 214

Table 6.10. Definition of the total uncertainty of the probabilistic stability analysis results' trend line based on uncertainties in groundwater modeling and toe erosion 215

Table 6.11. Probability of the blocks' different movement rate classes in the design lifetime of the project (100 years) 215

Table A1.1 Summary of piezometric elevation data from piezometers installed in South Slide. 254

Table A1.2 Material properties were used in groundwater modeling of South Slide. 254

Table A1.3 Residual and peak properties of material on the South Slide rupture surfaces. 255

Table A3.1 South Slide borehole and sample information 296

Table A3.2 Consolidation specimen's information. 297

Table A3.3 Consolidation loading stages. 298

Table A3.4 Consolidation test result's summary. 298

Table A3.5 Coefficient of volume compressibility calculation data. 300

Table A3.6 Coefficient of consolidation and hydraulic conductivity data. 301

Table A3.7 Specimens general information. 302

Table A3.8 Atterberg limit calculation sheet (specimen 1). 307

Table A3.9 Atterberg limit calculation sheet (specimen 2). 308

Table A3.10 Atterberg limit calculation sheet (specimen 3). 309

Table A3.11 Atterberg limit calculation sheet (specimen 4). 310

Table A3.12 Atterberg limit calculation sheet (specimen 5). 311

Table A3.13 Atterberg Limit calculation sheet (specimen 6). 312

Table A3.14 Atterberg limit calculation sheet (specimen 7). 313

Table A3.15 Atterberg limit calculation sheet (specimen 8). 314

Table A3.16 Results of water content and Atterberg Limit tests. 315

Table A3.17 Hydrometry test data sheet (test 1, specimen 1). 316

Table A3. 18 Hydrometry test data sheet (test 2, specimen 1). 317

Table A3.19 Hydrometry test data sheet (test 1, specimen 2). 318

Table A3.20 Hydrometry test data sheet (test 2, specimen 2). 319

Table A3.21 Hydrometry test data sheet (test 1, specimen 3). 320

Table A3.22 Hydrometry test data sheet (test 2, specimen 3). 321

Table A3.23 Hydrometry test data sheet (test 1, specimen 4). 322

Table A3.24 Hydrometry test data sheet (test 2, specimen 4). 323

Table A3.25 Hydrometry test data sheet (test 1 specimen 5). 324

Table A3.26 Hydrometry test data sheet (test 2 specimen 5). 325

Table A3.27 Hydrometry test data sheet (test 1 specimen 6). 326

Table A3.28 Hydrometry data sheet (test 2 specimen 6). 327

Table A3.29 Hydrometry data sheet (test 1 specimen 7). 328

Table A3.30 Hydrometry data sheet (test 2 specimen 7). 329

Table A3.31 Hydrometry data sheet (test 1 specimen 8). 330

Table A3.32 Hydrometry data sheet (test 2 specimen 8). 331

Table A3.33 Summary of particle size distribution analysis result. 332

Table A3.34 SEM specimens' general information. 333

Table A3.35 X-ray fluorescence (energy dispersive x-ray micro fluorescence) test results on specimens. 335

Table A3.36 Summary of test results on soil specimens from clay-silt sediment, unit 2, South Slide. 337

Table A3.37 Summary of test results on clay-silt sediments in South Slide. 338

List of Figures

Figure 2.1. Landslides in the area south of Ashcroft, BC, between 50° 10′ to 50° 20′ N and 121° 15′ to 121° 20′ W. (Slide CN51, Goddard Slide, North Slide, South Slide, and Nepa Slide are discussed in this paper). 26

Figure 2.2. Stratigraphy of Quaternary sediment fill in Thompson River Valley at Ashcroft and their approximate elevations. 27

Figure 2.3. Silt clay layers (unit 2, Figure 2.4), at the toe of the Goddard Slide, south of Ashcroft. 28

Figure 2.4. Unit 3, at the scarp of the Goddard Slide, south of Ashcroft (see Figure 2.1 for location). 28

Figure 2.5. Wisconsin till (unit 6 in Figure 2.2) at the main scarp of the South Slide, south of Ashcroft (see Figure 2.1 for location). 29

Figure 2.6. Sample of rhythmically bedded glaciolacustrine silt and clay sediments (unit 2), sample from South Slide (see Figure 2.1 for location). 29

Figure 2.7. Typical slip surface shape for the slides in the Ashcroft area (Goddard Slide lower slip surface in this case). 30

Figure 2.8. Comparing the Thompson River level in an active year (1982) and non-active year (1981) (data from Kamloops station). 31

Figure 2.9. Daily difference between daily Thompson River level and average Thompson River level (Kamloops station). 31

Figure 2.10. Cumulative Thompson River level difference form its average river level (Kamloops station) 32

Figure 2. 11. Slide activity versus maximum cumulative Thompson River level difference from average Thompson River level (river data from Kamloops station). 32

Figure 2. 12. Slide CN51 plan, the location of the piezometers, and section A-B shown in Figure 2.13. 33

Figure 2.13. Piezometers locations at cross-section A-B at the toe of Slide CN51 (see Figure 2. 12 for location). 34

Figure 2.14. Sample responses of piezometers installed at the toe of the slides (Bh1, toe of Slide CN51, see Figs 2.12, 2.13). 34

Figure 2.15. Groundwater surfaces for slip surface 2 (shallower slip surface) at the toe of Slide CN51 (see Figure 2.1 for slide location and Figure 2.13 for slip surface location). 35

Figure 3.1. Landslides south of Ashcroft, BC, between 50° 10′ to 50° 20′ N and 121° 15′ to 121° 20′ W. 69

Figure 3.2. Contact between the overlying sediments and the Ashcroft Formation (marine argillite, siltstone, sandstone, conglomerate, and minor carbonate of Jurassic age) at CN mileage 54 (see Figure 3.1 for location). 70

Figure 3.3. Geological units in the earth slides and highland terraces in Ashcroft area (the horizontal distance is not to scale). 71

Figure 3.4. Silt and clay layers in unit 2, at the Goddard Slide toe (Figure 3.1). 72

Figure 3.5. Sample of silt-clay layer, unit 2, from a borehole at South Slide (Figure 3.1). 72

Figure 3.6. Sand, silt, and diamicton of unit 3 at Goddard Slide scarp (Figure 3.1). 73

Figure 3.7. Silt, clay, and diamicton (till) unit 6 at South Slide scarp (Figure 3.1). 73

Figure 3.8. A view from the east of Slide CN50.9 with its three scarps, CN track, Thompson River, and toe berm (Figure 3.1)(the slide wide is 600 m at the river level). 74

Figure 3.9. A plan view of Slide CN50.9 showing the cross-section line, scarps, and borehole positions. 75

Figure 3.10. Cross section through Slide CN50.9 showing rupture surfaces, stratification, and borehole locations (see Figure 3.10 for cross-section position). 76

Figure 3.11. Simplified sliding process since deglaciation at Slide CN50.9 (Figure 3.1). 77

Figure 3.12. Piezometer locations at Slide CN50.9. 78

Figure 3.13. Responses of piezometers installed in Borehole Bh1 at the toe of Slide CN50.9 (see Fig. 3.12 for location of Borehole Bh1) 78

Figure 3.14. A digital elevation model of the Goddard Slide looking from the southwest showing four scarps, borehole locations, CPR rail line, a scour hole in the Thompson River bed, wet area after 1982 reactivation of the slide area, and limits of 1886 retrogression and 1982 reactivation. At river level the slide is 400m wide. 79

Figure 3.15. Bedded sequence showing the northeast (into the slope) dipping beds at the toe of the Goddard Slide bulging up (See Figure 3.14 for location). 80

Figure 3.16. Cross section after the Goddard 1982 Slide and surface profile before the Goddard 1982 Slide. 81

Figure 3.17. New cracks developing at the toe of the Goddard slide observed in May 2005 (probably developed in fall 2004). 82

Figure 3.18. Cracks at the Goddard Slide toe resulted from Thompson River erosion. 82

Figure 3.19. View of the South Slide from the west with its three scarps, CN and CPR rail lines, borehole locations, a scour hole in the Thompson River bed, and the Black Canyon tunnel. At river level the slide is 700 m wide. 83

Figure 3.20. Cross section through the South Slide. 84

Figure 3.21. A 3-dimensional view of the Basque Slide from the northwest. At river level the slide is 350 m wide. 85

Figure 3.22. Cross section through the Basque Slide. 86

Figure 3. 23. SEM photographs of Sample A, the plastic brown clay layer forming the shear zone of the South Slide, and Sample B, the silty clay layer at South Slide. 87

Figure 3.24. Comparison of the Thompson River level in an active year (1982) and non-active year (1981) with the average flow for 1911 to 2000. 87

Figure 3.25. Thompson River level, groundwater level and movement rate on the deeper rupture surface in Slide CN50.9 between April 2001 and January 2004. 88

Figure 3.26. Relationship between movement rate of Slide CN50.9 and pore-pressure ratio for the deeper rupture surface during reactivation. 88

Figure 4.1. Study area south of Ashcroft, BC, between 50° 10′ to 50° 20′ N and 121° 15′ to 121° 20′ W in a view from south showing the location of the Goddard Slide and Slide CN50.9. 123

Figure 4.2. Correlation between the annual Thompson River's maximum Cumulative River Level Difference from its normal river level and slides in Ashcroft area with a noticeable increase in their rate of movement. 124

Figure 4.3. Geological units in Slide CN50.9 and the Goddard Slide (the horizontal distance is not to scale). 124

Figure 4.4. A view from north to Slide CN50.9 shows its crown terrace, four scarps, CN rail, and old and new extension toe berms at toe. (Photograph by T. Keegan). 125

Figure 4.5.A. Slide CN50.9 cross section showing the rupture surfaces, stratification, and borehole (see Figure 1 for cross-section line) 126

Figure 4.5.B. Piezometers installed at the Slide CN50.9 toe. 127

Figure 4.6. Responses of the piezometers installed in the boreholes at Slide CN50.9 to the Thompson River level changes. Elevation head of piezometer P1 in borehole Bh1 is equal to the river level (data from Tim Keegan, personal communication 2005). 128

Figure 4.7. Slide CN50.9 movement versus rupture surface pore pressure changes with the Thompson River level fluctuation measured in borehole Bh1 (A) on the deeper rupture surface, (B) on the shallower rupture surface (the flat portion of the shallow piezometer in (B) reflects elevation of the tip). 129

Figure 4.8. Hydraulic conductivity function and storage function for glacial till in Slide CN50.9. 130

Figure 4.9. Groundwater system in Slide CN50.9 calculated for the minimum Thompson River level. 131

Figure 4.10. Change of groundwater system and seepage velocity vectors at Slide CN50.9 toe modeled by a transient seepage analysis for 2002. 132

Figure 4.11. Change of elevation head at the location of piezometers installed in borehole Bh1 (see Figure 4.5-B) from the transient seepage analysis. 133

Figure 4.12. Comparison between modeled and real response of piezometer P1 in borehole Bh1 (Figure 4.5-B). The flat portion in the measured piezometer response reflects the piezometer tip elevation at 282.8 m. 133

Figure 4.13. Stability of Slide CN50.9 and change of Factor of Safety with the Thompson River levels measured in 2002 (a normal year with a maximum CRLD close to zero). 134

Figure 4.14. Effect of the toe berm construction on the stability of toe blocks, block R-3 and block R-4, with the 2002 Thompson River level fluctuation cycle. 135

Figure 4.15. A digital elevation model of the Goddard Slide, looking from the south-west and showing five scarps, borehole locations, the CPR rail line, a scour hole in the Thompson River bed, the seepage locations after the 1982 reactivation at the slide area, and the limits of the 1886 retrogression and 1982 reactivation. At the river level, the slide is 400m wide. 136

Figure 4.16. Cross section after the Goddard 1982 reactivation showing borehole and piezometer locations, ground profile before the Goddard 1982 reactivation, the CPR rail line, five translational blocks, and the stratigraphy of the slide (see Figure 1 and Figure 15 for location of the section). 137

Figure 4.17. Data from piezometers installed in the Goddard Slide post-reactivation: (A) main body and foot and (B) crown. The frequent readings were stopped in 1985. 138

Figure 4.18.A. Groundwater system modeled for the Goddard Slide during the maximum Thompson River level in 1982 (before the 1982 reactivation). 139

Figure 4.18.B. Groundwater system modeled for the Goddard Slide during the maximum Thompson River level in 1997 (after the 1982 reactivation). 140

Figure 4.19. Change in the Goddard Slide factor of safety with the Thompson River fluctuation: (A) Pre-1982 reactivation geometry in 1982 and (B) Post-1982 reactivation geometry in 1997. 141

Figure 4.20. Change of factor of safety of the Goddard Slide within last 150 years. 142

Figure 4.21. Cracks at the Goddard Slide toe (A) resulted from toe erosion by the Thompson River at the active erosion site (see Figure 4.15 for location), and (B) resulted from the toe block (block R-4) translational movement (see Figure 4.15 for tension crack location). 142

Figure 5.1. Relative frequency of reactivation triggers of studied translational earth slides. 174

Figure 5.2. Movement acceleration with pore pressure ratio (ru) increasing on the slides' rupture surfaces. 174

Figure 5.3. Anali-Paty movement acceleration curve in rate axes and Anali-paty movement acceleration line in square root rate axes. 175

Figure 5.4. Pore pressure ratio (r_u) versus square root rate movement line of some of the slides. 176

Figure 5.5. Change of r_{u0} with slide's geometry and material property characteristics. 177

Figure 5.6. Factor of Safety for starting the slides' reactivation. 178

Figure 5.7. Acceleration Factor versus Factor of Safety at the time of starting the slides' reactivation. 179

Figure 5.8. Acceleration Factor (A.F.) versus plasticity index (PI) of material on rupture surface. 179

Figure 5.9. Acceleration Factor (A.F.) versus Ductility Factor. 180

Figure 6. 1. Slide CN50.9 in study area south of Ashcroft, British Columbia, between 50° 10′ to 50° 20′ N and 121° 15′ to 121° 20′ W. 216

Figure 6. 2. Slide CN50.9 cross section showing the rupture surfaces, stratification, boreholes, four reactivation blocks, and a retrogression block. 217

Figure 6. 3. Correlation between pore pressure ratio during drawdown period and movement rate for reactivation blocks. 218

Figure 6.4. Increase in the trend line of the yearly discharge of Thompson River since 1970s. 219

Figure 6.5. (A) Comparison of the yearly discharge data from 1970 to 2003 and the best fit probabilistic distribution and (B) the lognormal probability function resulting from the best fit on yearly discharge data. 220

Figure 6.6. The Thompson River average discharge in a normal year, calculated by using peak date correction and without using peak date correction. 221

Figure 6.7. Correlation between the Thompson River level at Slide CN50.9 and the Thompson River discharge 221

Figure 6.8. The Thompson River level for different yearly discharge return periods 222

Figure 6.9. Probability of different Thompson River flood return periods within the designed railway lifetime period 222

Figure 6.10. Correlation between the Thompson River flood return period and the Thompson River discharge 223

Figure 6.11. Comparison of piezometric modeled response and measured response (from Eshraghian et al. submitted) 223

Figure 6.12. Deterministic stability analysis results with the Thompson River level fluctuation from the Thompson River 2-year return period discharge for (A) reactivation toe blocks, and (B) retrogression and main blocks 224

Figure 6.13. A sample material property probability distribution (in this case, the residual friction angle of the disturbed clay-silt layer) 225

Figure 6.14. The Factor of Safety distribution calculated for block R-3 by using a Thompson River discharge return period of 2 years 225

Figure 6.15. Change in the reactivation blocks' probability of Factor of Safety being less than 1.1 with the Thompson River yearly discharge 226

Figure 6.16. Change in the reactivation block pore pressure ratio (ru) with the Thompson River yearly discharge 227

Figure 6.17. Change in the probability of Factor of Safety being less than 1.1 for the retrogressive block (block B-5) with river discharge 228

Figure 6.18. Range of possible toe erosion at Slide CN50.9 228

Figure 6.19. Definition of the uncertainty around the trend line fitted on the probabilistic stability analysis (in this case, for the probability of Factor of Safety being less than 1.1 for block R-5) 229

Figure 6.20. Flowchart for calculating probability of different movement rates within the life time of the railway (100 years) 230

Figure 6.21. Histogram frequency distribution of movement rate for two translational blocks on shallower and deeper rupture surfaces 231

Figure 6.22. Frequency of different movement rate classes for reactivation blocks defined within Slide CN50.9. The duration of calculation is the design life time of the railway (100 years). 232

Figure 6.23. Frequency of different movement rate classes for retrogression block (B-5, Figure 6.2) 233

Figure A1.1 Study area south of Ashcroft, BC, between 50° 10′ to 50° 20′ N and 121° 15′ to 121° 20′ W. 256

Figure A1.2 3-dimensional view of the South Slide with its three scraps, scour hole at the Thompson River bed, borehole locations, and cross-section line. The slide is 600 metres wide at the river level. 257

Figure A1.3 South Slide's cross section with its three translational blocks, possible future retrogression, and piezometer locations. 258

Figure A1.4 Modeled groundwater system for the maximum and minimum Thompson River level in 1997. 259

Figure A1.5 Modeled piezometer responses to the Thompson River level fluctuation in 1997. 260

Figure A1.6 Stability of the South Slide in (A) 1997 after erosion took place and before repairing the toe berm protection and the eroded part (B) 2002 after repairing the toe berm protection and the eroded part. 261

Figure A1.7 Change of Factor of Safety for toe block R-3 during the 1997 flood event. 261

Figure A2.1 Sample ground surface DTM made in Surpac program (north of Basque Slide). 263

Figure A2.2 Stratigraphy of sediment fill units in Thompson River Valley at Ashcroft and their approximate elevations. 265

Figure A2.3 Geological units in the earth slides and highland terraces in Ashcroft area (the horizontal distance is not to scale). 265

Figure A2.4 A plan view of Slide CN50.9 with cross-section and boreholes locations. 268

Figure A2.5 Pre-slide stage in Slide CN50.9, Ashcroft area. 269

Figure A2.6 Slide CN50.9 after first retrogression on shallower rupture surface. 269

Figure A2.7 Slide CN50.9 after first sliding on deeper rupture surface. 270

Figure A2.8 Slide CN50.9 after second retrogression on the deeper rupture surface. 270

Figure A2.9 Slide CN50.9 end result of sliding process modeling after toe river erosion. 271

Figure A2.10 Slide CN50.9 current stratigraphy based on borehole information and sliding modeling. 271

Figure A2.11 Goddard slide boreholes and cross-section location. 273

Figure A2.12 Goddard Slide pre-slide situation. 274

Figure A2.13 Goddard Slide after the first retrogression on the shallower rupture surface. 274

Figure A2.14 Goddard Slide after the second retrogression on the shallower rupture surface. 274

Figure A2.15 Goddard Slide after the third retrogression on the deeper rupture surface. 275

Figure A2.16 Goddard Slide after the fourth retrogression on the deeper rupture surface and before the 1982 reactivation. 275

Figure A2.17 Goddard Slide after the 1982 reactivation. 275

Figure A2.18 Current Goddard cross section. 276

Figure A2.19 North Slide's boreholes and cross-section location. 277

Figure A2.20 North Slide pre-slide stage. 279

Figure A2.21 North Slide after the first retrogression. 280

Figure A2.22 North Slide after the second retrogression. 281

Figure A2.23 North Slide after the third retrogression. 282

Figure A2.24 North Slide after the fourth retrogression. 283

Figure A2.25 North Slide after the most recent retrogression (fifth retrogression). 284

Figure A2.26 North Slide current cross section. 285

Figure A2.27 A plan view of South Slide with the cross-section line close to the centre of slide and boreholes. 286

Figure A2.28 South Slide pre-retrogression stage. 288

Figure A2.29 South Slide after the first retrogression on the shallower rupture surface. 288

Figure A2.30 South Slide after the second retrogression on the deeper rupture surface. 289

Figure A2.31 South Slide after the most recent retrogression on the deeper rupture surface. 289

Figure A2.32 Current South Slide cross section. 290

Figure A2. 33 A plan view of Basque Slide showing the section line, boreholes, and slide extend. 291

Figure A2.34 Basque Slide pre-slide stage. 292

Figure A2.35 Basque Slide after the first retrogression on the shallower rupture surface. 292

Figure A2.36 Basque Slide after the second retrogression by movement on the deeper rupture surface. 293

Figure A2.37 Basque Slide after the most recent retrogression on the deeper rupture surface. 293

Figure A2.38 Basque cross section. 294

Figure A3.1 South Slide 296

Figure A3.2 Cumulative log-time gauge reading for consolidation test on the selected specimen. 299

Figure A3.3 Void ratio versus log P and coefficient of consolidation (C_v^t) versus log P. 300

Figure A3.4 Specimen one direct shear test graph. 303

Figure A3.5 Specimen two direct shear test graphs. 303

Figure A3.6 Specimen three direct shear test graphs. 304

Figure A3.7 Specimen four direct shear test graphs. 304

Figure A3.8 Specimen five direct shear test graphs. 305

Figure A3.9 Specimen six direct shear test graphs. 305

Figure A3.10 Specimen seven direct shear test graphs. 306

Figure A3.11 Liquid limit curve for specimen one. 307

Figure A3.12 Liquid limit curve for specimen 2. 308

Figure A3.13 Liquid limit curve for specimen 3. 309

Figure A3.14 Liquid limit curve for specimen 4. 310

Figure A3.15 Liquid limit curve for specimen 5. 311

Figure A3.16 Liquid limit curve for specimen 6. 312

Figure A3.17 Liquid limit curve for specimen 7. 313

Figure A3.18 Liquid limit curve for specimen 8. 314

Figure A3.19 Average particle size distribution curve for specimen 1. 317

Figure A3.20 Average particle size distribution curve for specimen 2. 319

Figure A3.21 Average particle size distribution curve for specimen 3. 321

Figure A3.22 Average particle size distribution curve for specimen 4. 323

Figure A3.23 Average particle size distribution curve for specimen 5. 325

Figure A3.24 Average particle size distribution curve for specimen 6. 327

Figure A3.25 Average particle size distribution curve for specimen 7. 329

Figure A3.26 Average particle size distribution curve for specimen 8. 331

Figure A3.27 Summary of particle size distribution curves of all tested specimens from clay-silt unit. 332

Figure A3.28 Four specimens from clay-silt unit (unit 2) for mineralogy tests. 334

Figure A3.29 Gold coated specimens ready for Scanning Electronic Microscope. 334

Figure A3.30 SEM pictures of four tested specimens from South Slide borehole DH04-13. 335

Figure A3.31 Peak strength envelope from direct shear tests for three classes of material in clay-silt unit, unit 2. 339

Chapter 1

Introduction

1.1. BACKGROUND

Risk analysis includes hazard analysis and consequence analyses (Fell et al. 2005). Hazard is the probability that a particular danger (threat) occurs within a given period of time. Landslide hazard analysis is the process of identification and characterization of the potential landslides (danger characterization) together with evaluation of their corresponding frequency of occurrence (analysis of frequency) (Fell et al. 2005).

The first step toward a landslide hazard analysis is landslide characterization. In this stage, information regarding the topography, geological settings, hydrogeology, history of movement, geotechnical characterization of slide, mechanisms and dimensions of the slide, mechanics of shearing and strength of rupture surface, assessment of stability, and assessment of deformations and travel distance need to be collected (Fell and Hartford 1997). Cruden and Varnes (1996) suggested a landslide classification based on information about state, distribution, style, rate of movement, water content, type of material, and type of movement. Their classification commonly is used in landslide characterization and is used in this thesis.

Frequency analysis can be done in different ways. They include historical data of slope failures in similar conditions, direct subjective assessment, empirical correlations with trigging event, and formal probabilistic methods (El-Ramly 2001). El-Ramly (2001) suggested that probabilistic slope analysis methods are more appropriate for site-specific studies. After hazard analysis, the next step in landslide risk analysis is consequence analysis. Consequence analysis comprises two main steps, estimating the elements at risk and assessing their vulnerability (El-Ramly 2001). Assessing the vulnerability needs evaluation of probability of landslide impacting the element at risk at a certain location. This probability depends on the type and usage of the impact facility, the mobility of the element at risk, the presence of and efficiency of warning system, and the velocity of the landslide. Among these parameters, only the velocity of landslide is a pure geotechnical problem, the other parameters need coworkers from other disciplines working closely with a geotechnical engineer for a complete vulnerability calculation. Leroueil et al. (1996) considered four stages of slope movements for a landslide as pre-failure stage, onset of failure, post-failure stage, and reactivation stage. The velocity of a landslide may be very different in each of these stages of movement.

Frequency analysis of a landslide may be done by using probabilistic methods and taking into account the uncertainty in slope geometry, shear strength, failure mechanism, and piezometric pressures. Morgenstern (1995) mentioned that these uncertainties are mainly from three sources: (1) parameter uncertainty, (2) model uncertainty, and (3) human uncertainty. Such problems with so many uncertain parameters can be better analyzed using a probabilistic slope stability analysis in a quantitative risk analysis framework. El-Ramly (2001) presented samples of probabilistic slope stability analyses and quantitative risk analyses for slides. In his analyses, and all previous cases of quantitative risk analyses, there was an assumption for the rate of movement after failure. Normally this assumption is based on engineering judgment and previous experiences with similar slopes in the study area. This part of landslide risk analysis still needs to be quantified properly because it affects the consequence of the slide movement (failure). In the case of active earth slides the rate of movement may be anything from extremely slow to very rapid (Hungr et al. 2005). A slower movement rate may damage the facilities but loss of life due to this type of movement is unlikely. On the other hand rapid and very rapid movements may impose risk of life. Therefore, doing a probabilistic analysis of different rate of movement is useful for such cases.

1.2. RESEARCH PURPOSE

Large translational landslides associated with glacial lake sediments in preglacial valleys are common hazards within river valleys in western Canada. Western Canada is covered by glacial sediments deposited during different glaciation periods (Fulton 1969). Trunk Rivers have cut through these glacial sediments since the last glaciation in the area (approximately 10,000 years ago). This river down-cutting left benches of glacial sediments and relatively deep and steep river valleys. This relatively rapid river down-cutting may have caused recurring translational sliding, in many cases in a retrogressive way, within these valleys (Evans et al. 2005). Most of these slides are active and their rates of movement change with the changes in conditions. Current landslide hazard analysis practice does not address the different possible rates of movement. Instead it analyses the slide with the assumption of a specific movement rate in case of failure. Hazard analysis of an active landslide needs probabilistic calculation of different possible movement rates.

1.3. SCOPE AND LIMITATIONS

The Canadian railway industry has been exposed to ground hazards, including earth slides, since their first transcontinental line was constructed in the late 1800s (Bunce et al. 2005). As a result, railways in Canada are developing a formal risk management process for ground hazards (Bunce et al. 2005). Both the CN and CPR companies have had to contend with eleven large, translational, retrogressive earth slides in the Thompson River Valley south of Ashcroft, British Columbia. Study of these landslides' causes started since 1800s (Stanton 1898). The six most active of these have been subjects of modern geotechnical studies since the early 1980s (Eshraghian et al. in-press). The slides move on two sub-horizontal rupture surfaces in a glaciolacustrine clay-silt unit within this Quaternary sediment sequence (Eshraghian et al. in-press). Canadian National Railway (CN) and Canadian Pacific Railway (CPR) companies initiated a detailed geotechnical investigation of slides in this area since 1980s (Eshraghian et al. in-press).

Rail lines can tolerate relatively slow, small movements as routine track maintenance can adjust for these deflections (Chris Bounce personal communication, 2006). However, while the landslides in Ashcroft area today are normally slow moving, rapid to very rapid movements that have blocked the Thompson River in some cases have occurred in the past (Clague and Evans, 2003). Therefore, calculating the probability of different rates of movement was essential for a risk assessment of these active translational earth slides. Using previous geotechnical investigation data and conducting new investigations on these slides gave an opportunity for developing the state-of-art for a probabilistic movement frequency analysis of active landslides.

1.4. RESEARCH OBJECTIVES

This Ph.D. project originated to conduct research on the earth slides in Ashcroft area with the global objective of developing techniques for calculating movement rate probabilities of reactivated earth slides. The general objectives of this Ph.D. project are summarized as follows:

- Determining the main trigger for the studied earth slides' movements in the Ashcroft area (study area).

- Understanding the different effects that a down-cutting river (like the Thompson River) through glacial sediments may have on the movement of slides in their valleys.

- Developing a correlation for movement of reactivated translational earth slides.

- Developing the methodology for hazard analysis of reactivated earth slides with wide range of rates during their pre-failure stage, first time failure, and reactivation stage.

1.5. ORGANIZATION OF THESIS

This thesis is organized into five main chapters (Chapter 2 through 6), a conclusion chapter, and three appendices. Each of the main chapters has been either published or is awaiting publication in conferences proceedings and/or journals. The chapters have been organized in a relative chronological fashion with each being unique in focus. Some similarities are observed within the chapters and the reader will observe the successively enhanced analysis sponsored through extended research.

Chapter 2 introduces the study area in the Thompson River Valley in Ashcroft, British Columbia. This chapter presents the result of general geological information, weather data, and river data analyses which reveals the main trigger of slides movement within this valley.

To complete the geological study of the slides in the study area, **Chapter 3** presents slides' characteristics including their movement behaviour, material information and geometry besides some geological detail.

To complete the investigation about the landslides' movement mechanism, **Chapter 4** presents the more detailed stability analyses and investigates the mechanisms of slide movement. Two sample earth slides (Slide CN50.9 and the Goddard Slide) in this valley with and without toe erosion protection are selected to investigate different mechanisms of movement and the ways in which Thompson River act as trigger for the slide movements.

A key problem inherent in characterization of slide movements is the unpredictable movement behaviour of the slide. The start of movement and how it would accelerate after starting were needed to achieve the objectives of the research. Because the best way of assessing a landslide's potential for rapid movement is to compare it with similar case histories whose failure stage has already taken place (Hungr et al. 2005) **Chapter 5** presents the result of study of 60 cases of translational earth slides at their post-failure stage. The results of this study are useful for defining the movement behaviour of the slide which can be used in the hazard analysis.

In **Chapter 6,** results of previous investigations, slide characterization, and study of movement behaviour of case histories is used to make a frequency analysis of different blocks in a sample landslide (Slide CN50.9) in the study area. This chapter presents the methodology for conducting a quantitative frequency of movement analysis which can be used for other similar cases in this area or similar cases everywhere else.

Chapter 7 includes a brief discussion of the methodology, investigation, and process of hazard analysis based on frequency of movement rate analysis which may help guide the use of similar methods for other cases of reactivated slides with wide ranges of possible post-failure movement rates. The discussion is followed by conclusions gathered and recommendations for future research pursuits.

In **Appendix 1** effects of the Thompson River on stability of another sample earth slide (South Slide) in the study area is studied through groundwater and stability modeling. **Appendix 2** shows the process of making cross-sections for the slides. The cross-sections were made based on geology of the area, the borehole information, and also simulation of process of sliding for each slide. Another appendix, **Appendix 3** presents the result of laboratory tests on samples from boreholes in the slides.

1.6. REFERENCES

Bunce, C.M., Martin, C.D., and Abbott, B. 2005. An overview of the Canadian railway ground hazard research program. *In* Proceedings of The International Conference on Landslide Risk Management. *Edited by* O. Hungr, R. Fell, R. Couture, and E. Eberhardt. Vancouver, Canada. 31 May - 3 June. A.A. Balkema, Supplementary Volume, On CR-ROM, p. 8.

Clague, J.J., and Evans, S.G. 2003. Geological framework of large historic landslides in Thompson River Valley, British Columbia. Environmental and Engineering Geoscience, **9**(3): 201-212.

Cruden, D. M., and Varnes, D. J. 1996. Landslide types and processes. In Landslides: Investigation and Mitigation. Edited by Turner, A.K., Schuster, R.L.,. Transportation Research Board, Special report 247. pp. 36-75.

Cruden, D.M., and Varnes, D.J. 1996. Landslide types and processes. *In* Landslides Investigation and Mitigation: Special report 247. National Research Council (U.S.). Transportation Research Board, pp. 36-75.

El-Ramly, H. 2001. Probabilistic analyses of landslide hazards and risk: bridging theory and practice. Ph.D thesis, University of Alberta, Edmonton.

Eshraghian, A., Martin, C.D., and Cruden, D.M. 2007. Complex earth slides in the Thompson River Valley, Ashcroft, British Columbia. Environmental and Engineering Geoscience. 13:161-181

Evans, S. G., Cruden, D. M., Bobrowsky, P. T., Guthrie, R. H., Keegan, T. R., Liverman, D. G. E., and Perret, D. 2005. Landslide risk assessment in Canada; a review of recent developments. In Proceedings of the International Conference on Landslide Risk Management, Vancouver, Canada, 31 May- 3 June 2005. A.A. Balkema. pp. 351-434.

Fulton, R.J. 1969. Glacial Lake History, Southern Interior Plateau, British Columbia. Geological Survey of Canada Paper 69-37: p.14.

Fell, R., and Hartford, D. 1997. Landslide risk management. *In* Landslide Risk Assessment. Edited by D.M. Cruden and R. Fell. Balkema, Roterdam.

Fell, R., Ho, K.K.S., Lacasse, S., and Leroi, E. 2005. A framework for landslide risk assessment and management. *In* Proceedings of the International Conference on Landslide Risk Management. *Edited by* O. Hungr, R. Fell, R. Couture, and E. Eberhardt. Vancouver, Canada. 31 May- 3 June 2005. pp. 3-25.

Hungr, O., Corominas, J., and Ebehardt, E. 2005. Estimating landslide motion mechanism, travel distance and velocity. In Proceedings of the International

Conference on Landslide Risk Management. Edited by O. Hunger, R. Fell, R. Couture, and E. Eberhardt. Vancouver, Canada. 31 May - 3 June. A.A. Balkema, Vol.1, 99-128.

Leroueil, S., Locat, J., Vaunat, J., Picarelli, L., Lee, H., and Faure, R. 1996. Geotechnical characterization of the slope movements. *In* Proceedings of the 7th International Symposium on Landslides. *Edited by* K. Senneset. Trondheim, Norway. 17-21 June 1996. A. A. Balkema, Rotterdam, Vol.1, pp. 53-74.

Morgenstern, N.R. 1995. Managing risk in geotechnical engineering. *In* Proceedings of the 10th Pan American Conference on Soil Mechanics and Foundation Engineering. Guadalajara, Mexico.

Stanton, R. B. 1898. The great land-slides on the Canadian Pacific Railway in British Columbia. Proceedings of the Institution of Civil Engineers, **132**: 1-48.

Chapter 2

Overview of Landslides in the Thompson River Valley, Ashcroft, British Columbia[1]

Thompson River Valley is a vital section of the strategic national transportation corridor that runs through southern British Columbia. Main rail lines of the Canadian Pacific Railway (CPR), completed in 1885, and the Canadian National Railway (CN), completed about 30 years later, are located in this corridor (Clague and Evans 2003). The study area is located between Ashcroft town and Spence's Bridge (50° 10′ to 50° 20′ N and 121° 15′ to 121° 20′ W) just south of Ashcroft town. This area has a history of landsliding which has created problems for both CPR and CN. When the landslides were rapid, they blocked the river, disrupted rail traffic and caused fatalities. When they move slowly, the rails need repairing every few years. Some of the slides created short-lived upstream reservoirs. Figure 2.1 shows the locations and names of the landslides in Thompson River Valley. Table 2.1 gives the areas and volumes of few of the landslides in this area.

The slides in this area are retrogressive, translational earth slides which have been moving very slowly since the first time sliding happened. According to Christiansen and Sauer (1984) retrogressive landslides in the Canadian Great Plains occur mainly in overconsolidated marine, Upper Cretaceous clay shales or in normally consolidated Quaternary glacial lake sediments. In this later case they are moving on a rhythmically bedded silt and high plastic clay layer.

---

[1] Published paper:

A version of this chapter has been published in the refereed Proceedings of the International Conference on Landslide Risk Management. Eshraghian, A., Martin, C. D., and Cruden, D. M. 2005. Landslides in the Thompson River Valley between Ashcroft and Spence's Bridge, British Columbia. In Proceedings of the International Conference on Landslide Risk Management, Vancouver, Canada, May 31 to June 4, 2005. pp. 437-446.

2.1. GEOLOGY OF THE ASHCROFT AREA

The Ashcroft area is part of the Thompson Plateau, a subdivision of the Interior Plateau. It is characterized by rolling uplands separated from each other by deep valleys. The Thompson River flows south and has down cut through thick glacial sediments and is relatively immature (Porter et al. 2002).

Most of the Quaternary landforms and surficial materials can be related to the last glaciation and are thus late-Pleistocene. A variety of Quaternary sediments occurs in the area, especially within the major valleys where a deep valley fill has been dissected and terraced by postglacial down-cutting of the trunk rivers (Duffell and McTaggart 1952).

The landslides occurred in a 10-km reach of Thompson Valley, within a thick Quaternary valley fill dominated by glaciolacustrine sediments. Failure occurred on the steep walls of an inner valley that formed during the Holocene when Quaternary sediments filling the broader Thompson River Valley were incised. The valley fill sequence consists dominantly of permeable sediments, the exception being a unit of rhythmically bedded silt and clay near the base of the Pleistocene sequence (Clague and Evans, 2003).

Hodge and Freeze (1977) and also Clague and Evans (2003) mentioned that groundwater flow systems in southern British Columbia show the possibility of generation of high pore pressures in less permeable sediments in discharge zones at the base of terraces underlain by a succession of Pleistocene deposits similar to that in Thompson Valley at Ashcroft.

2.1.1. Surficial Geology of the Study Area

The surficial materials in the area are tills, fluvial, fluvioglacial, lacustrine and colluvial deposits. The surficial geology map is produced by Geological Survey of Canada (Ryder 1976).

Surficial till dates from the last glaciation (Armstrong et al. 1965). Most of the areas mapped as drift (between Ashcroft and the Ashcroft Slide and also beside the Goddard Slide) are probably till, but may include small areas of fluvioglacial gravels, glaciolacustrine sediments, and recent alluvium (Ryder 1976).

2.1.2. Quaternary History of the Ashcroft Area

Most of the Quaternary landforms and surficial materials of the Ashcroft map-area can be related to the last Fraser Glaciation (Armstrong et al. 1965). Ice covered all but the highest peaks of the Coast Mountains in the area and generally flowed from the east and west into the Thompson Valley. In the Thompson River Valley ice flow was from north to south. Deglaciation occurred by the thinning and stagnation of ice over most of the Ashcroft area. Several phases of deglaciation may be identified, each represented by characteristic landforms and surficial deposits (Fulton 1969).

Johnsen and Brennand (2004) distinguished development of two late-glacial, ice-dammed lakes within the Thompson Basin: Glacial Lake Thompson and Glacial Lake Deadman. The lakes were narrow (width to length ratio of ~3:100). Glacial Lake Thompson was 140 m deep and Glacial Lake Deadman about 50 m. They had higher elevations at Ashcroft and lower elevation near Spence's Bridge with tilting about 1.7 m/km. According to Johnsen and Brennand (2004), these lakes were more extensive than previously thought and they lengthened and lowered as ice decayed.

There was an ice dam south of Spence's Bridge. Also they estimated the lake bottom at approximate elevation 420 m asl. (Johnsen and Brennand 2004).

Figure 2.1 shows the extent of the highest terrace of the Thompson (at 420 m asl.) which is perhaps formed by the bottom of glacial lake Deadman (glacial lake deposit in Figure 2.1). Fulton (1969), Ryder (1976), Clague and Evans (2003) and Johnsen and Brennand (2004) described the glacial history of the area in more detail.

2.1.3. Geological Units

The Quaternary sediment fill in Thompson Valley near Ashcroft consists of deposits of three glaciations. Figure 2.2 shows the Quaternary sediments of the valley similar to one produced by Clague and Evans (2003). The elevations of the boundaries between the units are the elevations found in the boreholes in Slide CN51 near Ashcroft (see Figure 2.1 for location). The sediment boundaries should have tilts similar to the Glacial Lakes (1.7 m/km) so the boundary elevations in the other slides can be lower than shown in Figure 2.2.

The three glacial sequences are separated by unconformities produced by erosion and mass wasting during intervening interglaciations. The oldest exposed sediments are cemented, oxidized, folded and faulted sand and gravel with minor lenses of diamicton (unit 1, Figure 2.2). These sediments are interpreted by Clague and Evans (2003) to be ice-contact materials, deposited against decaying masses of glacier ice at the end of a Pleistocene glaciation but their age is uncertain (Clague and Evans 2003).

At sites south of Ashcroft, the till and the oxidized sand and gravel are overlain by rhythmically bedded silt and clay of lacustrine or glaciolacustrine origin (unit 2 in Figure 2.2). Figure 2.3 shows the silt-clay layer at the toe of the Goddard Slide. The darker layers in the picture have more clay content. It is up to 45 m thick and consists of silt and clay couplets, ranging from less than 1 cm to several tens of centimetres thick. Previous study of the samples from this layer suggested that these sediments are at least several hundred thousand years old and thus of Middle or Early Pleistocene age (Clague and Evans 2003).

A second glacial sequence (unit 3, Figure 2.2) overlies the Middle or Early Pleistocene. It consists of poorly sorted, intertonguing silt, sand, gravel, and diamicton. They are interpreted by Clague and Evans (2003) as glaciolacustrine. This unit, unlike units 1 and 2, is not significantly weathered. Figure 2.4 shows this unit at the scarp of the Goddard Slide.

Sediments deposited during the last (Late Wisconsin or Fraser) glaciation (units 4-7, Figure 2.2) overlie unit 3. Clague and Evans (2003) defined the Fraser glacial sequence in the Ashcroft area as being comprised of, from bottom to top, units 4 to 7, defined below.

Unit 4 is a thick unit of horizontally bedded, pebble-cobble gravel. This unit is braided-river channel gravels deposited by melt-water streams during the initial advance of glaciers into the area early during the Fraser Glaciation.

Unit 5 is horizontally bedded silt and sand containing some isolated stones. This unit is probably glaciolacustrine sediments that were deposited when glaciers blocked the regional drainage and impounded a lake in this part of Thompson Valley.

Unit 6 is matrix-supported diamicton. This unit is till dating to the time of Late Wisconsin glacier occupation of the area. Figure 2.5 shows this unit at the main scarp of the South Slide.

Unit 7 is poorly sorted, weakly stratified gravel, grading up into sand and silt. This unit is glaciolacustrine sediments laid down during deglaciation when the regional drainage was again blocked by glacier ice.

At most sections in the study area, the Fraser Glaciation sequence is incomplete, consisting of only one or two of the four units described above. The Fraser Glaciation sediment sequence described above is locally overlain by horizontally bedded, pebble-cobble gravel (unit 8, Figure 2.2) deposited by Thompson River and its tributaries. These sediments date to the Pleistocene-Holocene transition, immediately after the lakes in Thompson Valley drained about 10,000 years ago (Clague and Evans 2003).

2.2. GEOTECHNICAL CHARACTERISTICS OF THE SLIDES

2.2.1. Movement Characteristics

According to Leroueil (2001) in order to have a complete geotechnical characterization of slope movements the information about type of movement, type of material and stage of movement are required.

Types of movements are those proposed in the geomorphological classifications of slides suggested by Cruden and Varnes (1996). They linked geology and landslide activity. The slides in the Ashcroft area are moving on a surface of rupture which is planar so they are translational slides. They are very slow moving slides with movement rates in the order of 2 to 10 cm per year. There is evidence that the surfaces of rupture of the slides are extending upslope while the movement is downslope, therefore the slides are retrogressive. The movement repeated following the enlargement of the slip surface therefore those slides are multiple landslides.

These slides have moved rapidly in the past, which in some cases caused transportation problems and also damming of the Thompson River, but now they are moving very slowly. As they are moving along the pre-existing slip surface they are reactivated slides. Therefore, for this kind of slides the soil is not likely to display strain softening and movement rate will be generally small (Leroueil 2001). Movement rate in these landslides varies with the seasonal changes in pore water pressure as discussed below. Therefore they are active slides in post failure stage of movement.

In summary, the slides in the Ashcroft area are reactivated retrogressive multiple translational earth slides that are very slow to extremely slow moving.

2.2.2. Controlling Laws and Parameters

As the slides are in post-failure stage and moving along pre-existing surfaces of rupture, the controlling Mohr-Coulomb parameters are the residual parameters. Due to possible rate effects on shear resistance, parameters should be obtained with laboratory tests at the same shear rates as in the field.

Clay beds in unit 2 (see Figure 2.2), which are the main part of the surfaces of rupture in those slides, are highly plastic; plasticity indices of most samples range from about 15% to 55%, and liquid limits range from 45% to almost 90% (Porter et al. 2002). Residual friction angles, estimated using the empirical correlation of Stark and Eid (1994), are 10-12°. Keegan et al. (2003) used similar residual friction angle for this material in their analyses.

The samples around the surfaces of rupture show activities in the range of 0.6 to 0.9. Perhaps the real activity of the clay material responsible for the slides is even higher. If it was possible to take the sample only from the clay layer in the rhythmically bedded clay-silt layer, a higher activity might be detected. Figure 2.6 shows a sample from this unit. The darker layer has more clay content.

Skempton (1969) found a correlation between the liquidity index and effective overburden pressure (or overburden material height) for normally consolidated clay sediments. This correlation can be used for estimating the overburden material height of overconsolidated clays. Table 2.2 shows the result using Skempton's approach on the samples from different slides in the Ashcroft area. The samples were taken from the undisturbed part of the rhythmically bedded silt and clay layer (unit 2) (CPR and CN reports). The results show this unit is overconsolidated.

2.2.3. Predisposal Factors

The stratigraphy of the valley fill predisposes it to failure. The role of clayey glaciolacustrine sediments older than the Fraser Glaciation is significant for the stability of slopes in many valleys in central British Columbia. Clague (1988) found that similar units control landsliding in a complex Pleistocene sediment sequence in the Fraser River Valley. The disturbance by overriding ice or early slope movements may create pre-sheared discontinuities that predispose these units to failure (Clague and Evans 2003).

By importing all the information from slide inclinometers, borehole logs, geological study of the area and site visit information to a geographical information system, it became clear that all the studied slides are sliding on two surfaces of rupture. Both of these surfaces of rupture are in the rhythmically bedded glaciolacustrine silt and clay unit (unit 2 in Figure 2.2).

The surfaces of rupture are at different elevations in different landslides but their elevation differences are about 6.5 metres in average. Table 2.3 shows the elevations of the slip surfaces for the studied slides. As shown in Table 2.3 the elevations for rupture surface decrease toward the South. This is in agreement with the tilting of the Glacial Lakes found by Johnsen and Brennand (2004). Figure 2.7 shows the shape of Goddard Slide lower rupture surface.

The slides in the Thompson River Valley have side slopes between 9° to 16°. The places with higher slope angles are controlled by bedrock.

2.2.4. Triggering Factors

A trigger is an external stimulus that causes a near-immediate response in the form of a landslide by rapidly increasing the stresses or by reducing the strength of the slope materials. It can be intense rainfall, earthquake shaking, volcanic eruption, storm waves, or rapid stream erosion (Wieczorek 1996).

The rainfall in the area has been increasing since the 1920s (Porter et al. 2002). Despite this rainfall increase the area is quite dry and efforts to find some correlation with slide movements were not successful.

But the situation is different for the level of Thompson River. For example the Thompson River level for two different years (1981 and 1982) and the average Thompson River level from Kamloops station are shown in Figure 2.8. During 1982, some slide activities occurred in the Thompson corridor, among them was the Goddard Slide which disrupted the CPR operations at the end of September (CPR reports). As can be seen in Figure 2.8, the Thompson River level during 1982 (active year) was significantly above normal. Similar situations can be seen in other years when slide movements occur.

Figure 2.9 shows the differences between the average Thompson River level and the daily Thompson River level from 1980 to 1986. As can be seen in this figure during 1982, the difference was positive and stayed positive for a while. The other interesting point is that although during 1985 the river level was even higher than river level during 1982, no slides occurred so it is not only the river level that affects slide activities but the area under this differential graph is also important (the period of time they stayed high).

In order to have a quantitative number for comparing the years in this way the cumulative river level difference from average river level (CRLD) was calculated (Figure 2.10) for 1980 to 1986. As shown in this figure the only year in this period with a positive (CRLD) is 1982 which was the only year with slide activity in the area during this period.

Similar behaviour is seen for other years. If the pick point of the cumulative river level difference from average river level (CRLD) for each year is selected as a quantitative number for that year and compared with the number of slides activities in the study area a close correlation can be found (Figure 2. 11). Figure 2. 11 shows that the years with positive maximum cumulative river level difference from average river level difference are active years. Similar results can be found by using data from Spence's Bridge station (south of study area). Data prior to 1970 is sparse and no conclusions related to slide movements can be drawn.

2.2.5. Mechanism of Failure

Clague and Evans (2003) mentioned some possibilities of increasing pore water pressures in the landslides in this area which would cause failures of the slides. There is a silty gravel layer (unit 1 in Figure 2.2) just above bedrock and under the rhythmically bedded silt and clay layer (unit 2 in Figure 2.2). As this unit has higher permeability than unit 2 it can act as an aquifer. Piezometers at the toe of Slide CN51 and South Slide show an artesian pressure in this unit. It is believed that this artesian pressure may affect the slide activity in the area.

Figure 2. 12 shows the locations of the piezometers at the toe of Slide CN51 and Figure 2.13 shows the cross-section A-B of the toe part of the slide. Figure 2.14 shows the measurement results of piezometers installed at the toe of Slide CN51 (borehole P1) and shows the deeper piezometers have higher heads. All piezometers respond to changes in the river level but the shallower the piezometer, the more the response. It takes some time for the piezometers to equalize after the river level peaks. Similar behaviour can be seen in other piezometers.

Comparing the piezometers installed in different boreholes showed the piezometers near to the toe of the slide respond more quickly to the river level changes than piezometers near the back scarp. The readings from piezometers installed near to the back scarp show no artesian pressures at that part of the slide.

From these results it can be said that the scarp is generally a recharge area and the toe is a discharge area most of the time. Because of the higher permeability of unit 1, water from the scarp moves through this unit and then comes up near to the toe. It results in an artesian pressure at the toe. On the other hand, when the Thompson River level starts rising the water from the river seeps toward the slide mass and may offset the artesian conditions but the river does not stay at this high level for sufficient time to let the system reach equilibrium. Therefore, the top part of the rhythmically bedded silt and clay layer (unit 2) may be more affected by the river level changes than the lower part. In the years that the Thompson River level stays at the higher level for a longer time the piezometers show the greatest increase in pore water pressures.

Figure 2.15 shows the ground water surface for slip surface 2 for Slide CN51. Due to the complexity of the ground water system in this area the ground water surface for slip surface 1 (deeper slip surface) is different from the ground water surface for slip surface 2 (shallower slip surface). For the study period (year 2002 and 2003) the maximum river level and ground water surface happened in June 2002 but the minimum river level happened in March 2002 while the minimum ground water surface belongs to the April 2002. Figure 2.15 shows that the change in ground water level is greatest for the portion of the slide near to the river. The pore water pressure on slip surface 2 at the toe is very low during the low river level periods while during high river level periods it is quite high. The pore water change on this slip surface is more than 180% compared to the minimum pore water pressure on this surface. The change for slip surface 1 (deep slip surface) is about 80%.

The other interesting point is the location of the slip surfaces. While slip surface 2 is almost at the minimum river level, slip surface 1 is located in the river bed (similar situation can be seen in other slides in the area). The river level changes can have some stabilization effects during its high level period while during its low level period, this stabilization force is removed. In this study period the calculated minimum factor of safety for the shallow slide was about 1.06 while for the deep slide it was about 1.2. Therefore the mechanism of increased movement may be a rapid drawdown mechanism due to change of the Thompson River level in the late summer and early fall. Similar instability caused by a drop in river level has been documented along riverbanks in Winnipeg, Manitoba, by Tutkaluk et al. (1998).

2.3. CONCLUSIONS

The slides in the Ashcroft area are reactivated retrogressive multiple very slow to extremely slow moist translational earth slides which are moving on pre-sheared surfaces. Understanding the geological stratigraphy of the valley fill is essential before undertaking a geotechnical analysis of those slides. The stratigraphy of the area is complex which can cause complex underground water seepage through the slide bodies. The sliding occurs through the rhythmically bedded silt and clay layer (unit 2) and contact of this unit with unit 3 on two rupture surfaces. Those two rupture surfaces can be the locations of weak layers in Unit 2 and 3. Preliminary findings suggest that all the slides may be moving on the same geological layer but proving this idea still needs more study.

The main trigger event for recent slide movements appears to be related to the river water level changes. If the river has a higher than average level for a significant duration the pore water pressure on the rupture surfaces increases. When the river level falls back to its traditional seasonal lower levels the pore water pressure is not equalized and the supporting load at the toe applied by river water is removed. Therefore it is believed that a rapid drawdown mechanism may significantly contribute to the slide movements.

2.4. REFERENCES

Armstrong, J.E., Crandell, D.R., Easterbrook, D.J. and Noble, J.B. 1965. Late Pleistocene stratigraphy and chronology in southwestern British Columbia and western Washington. Geological Society America Bulletin. **76**: 321-330.

Christiansen, E.A. and Sauer, E.K. 1984. Landslide styles in the Saskatchewan River Plain: a geological appraisal. Proceedings of the 37th Canadian Geotechnical Conference, Toronto. C. G. Society. **1**: 35-48.

Clague, J.J. 1988. Quaternary stratigraphy and history, Quesnel. British Columbia. Geographie Physique Quaternaire. **42**: 279-288.

Clague, J.J. and Evans, S.G. 2003. Geological framework of large historic landslides in Thompson River Valley, British Columbia. Environmental and Engineering Geoscience. **9**: 201-212.

Cruden, D.M., and Varnes, D.J. 1996. Landslide types and processes. *In* Landslides Investigation and Mitigation: Special report 247. National Research Council (U.S.). Transportation Research Board, pp. 36-75.

Duffell, S. and McTaggart, K.C. 1952. Ashcroft map-area, British Columbia. Geological Survey of Canada. Memo 262, P.122.

Flint, R.F. and Irwin, W.H. 1939. Glacial geology of Grand Coulee Dam, Washington. Geological Society America Bulletin. **50**:661-680.

Fulton, R.J. 1969. Glacial Lake History, Southern Interior Plateau, British Columbia. Geological Survey of Canada Paper 69-37: p.14.

Hodge, R.A.L. and Freeze, R.A. 1977. Groundwater flow systems and slope stability. Canadian Geotechnical Journal. **14**: 466-476.

Johnsen, T.F. and Brennand, T.A. 2004. Late-glacial lakes in the Thompson Basin, British Columbia: paleogeography and evolution. Canadian Journal of Earth Science. **41**: 1367-1383.

Keegan, T., Abbott, B., Cruden, D., Bruce, L. and Pritchard, M. 2003. Railway ground hazard risk scenario: River erosion: Earth-slide. In Proceedings of the 3rd Canadian Conference on Geotechnique and Natural Hazards, Edmonton, Alberta. The Canadian Geotechnical Society: 269-277.

Leroueil, S. 2001. Natural slopes and cuts: movement and failure mechanisms. Geotechnique. **51**: 197-243.

Porter, M. J., Savigny, K. W., Keegan, T.R., Bunce, C.M. and MacKay, C. 2002. Controls on stability of the Thompson River landslides. In Proceeding of the 55th

Canadian Geotechnical Conference, Niagara. Southern Ontario Section of the Canadian Geotechnical Society. pp. 1393-1499.

Ryder, J. M. 1976. Terrain inventory and quaternary geology Ashcroft, British Columbia. Geological Survey of Canada Paper 74-49.

Skempton, A. W. 1969. The consolidation of clays by gravitational compaction. Journal of the Geological Society. **125**: 373-411.

Stark, T. D. and Eid, H. T. 1994. Drained residual strength of cohesive soils. Journal of Geotechnical Engineering. **120**: 856-871.

Tutkaluk, J., Graham, J. and Kenyon, R. 1998. Effects of riverbank hydrology on riverbank stability. In Proceeding of the 51st Canadian Geotechnical Conference, Edmonton, Alberta.Canadian Geotechnical Society. pp. 283-288.

Wieczorec, G. F. 1996. Landslide triggering mechanisms. In Landslide Investigation and Mitigation: Special Report 247. National Research Council (U.S.) Transportation Research Board, 76-90.

Table 2.1. Volumes and areas of four of the landslides in the Ashcroft area.

Slide Name	Area×10^4 (m^2)	Volume×10^6 (m^3)
Slide CN51	15.06	3.27
Goddard	9.71	1.95
North Slide	58.67	21.36
South Slide	27.46	9.03

Table 2.2. Estimated overburden pressure and previous deposit height in the Ashcroft area (based on Skempton 1969).

Slide Name	Equivalent deposit height (m)	Equivalent Deposit Elev. (m) asl.	Current Ground Elev. (m) asl.
Goddard	337.5	607.2	296.7
North Slide	400	660.3	300.3
Nepa Slide	412.5	668.7	272.2

Table 2.3. Surfaces of rupture elevation of the studied slides in the Ashcroft area.

Slide Name	River Elevation (m)	Surface elevation (m)	
		Slip surface 1	Slip surface 2
Slide CN51	282.6	275.7	280.9
Goddard Slide	275.8	270.6	278.1
North Slide	273.2	264.2	269.4
South Slide	269.0	263.7	272.7

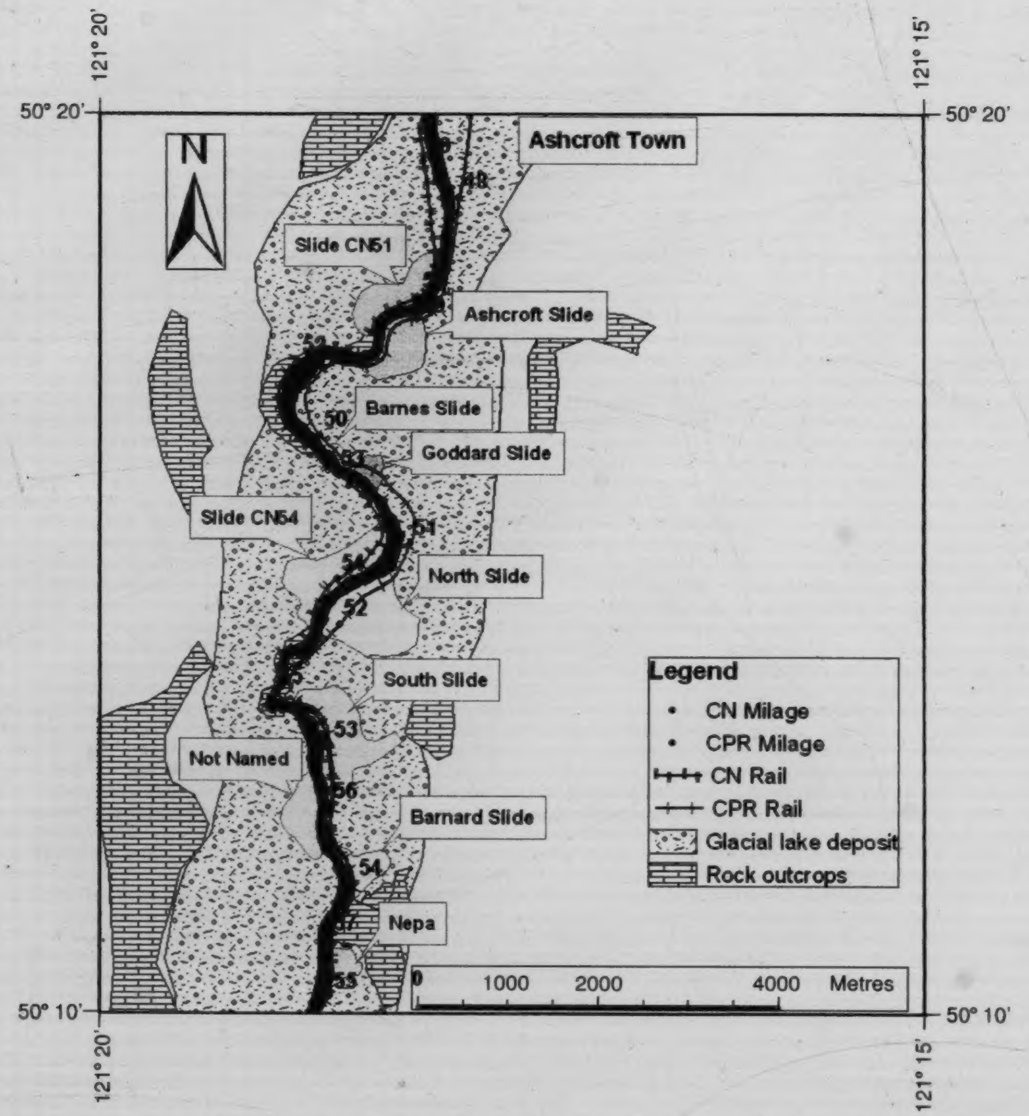
121° 20'
121° 15'
50° 20'
50° 10'
N
Ashcroft Town
48
Slide CN51
Ashcroft Slide
50
Barnes Slide
Goddard Slide
Slide CN54
51
North Slide
52
South Slide
53
Not Named
56
Barnard Slide
54
Nepa
57
55
Legend
• CN Milage
• CPR Milage
CN Rail
CPR Rail
Glacial lake deposit
Rock outcrops
0
1000
2000
4000
Metres

Figure 2.1. Landslides in the area south of Ashcroft, BC, between 50° 10′ to 50° 20′ N and 121° 15′ to 121° 20′ W. (Slide CN51, Goddard Slide, North Slide, South Slide, and Nepa Slide are discussed in this paper).

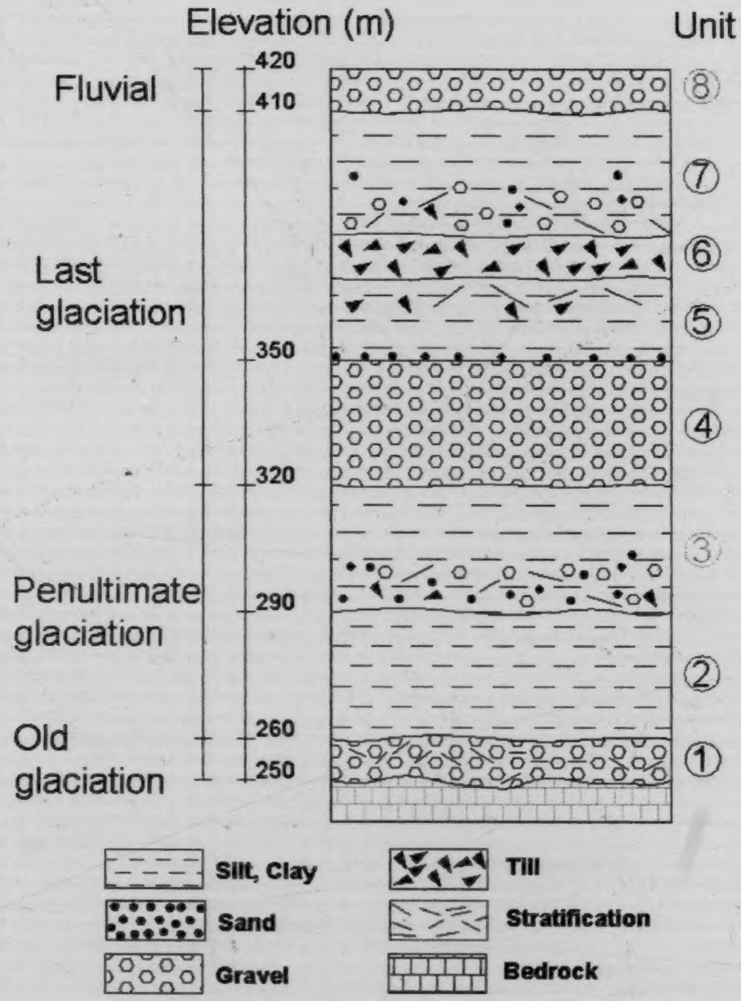
Elevation (m)
Unit
Fluvial
Last glaciation
Penultimate glaciation
Old glaciation
420
410
350
320
290
260
250
⑧
⑦
⑥
⑤
④
③
②
①
Silt, Clay
Sand
Gravel
Till
Stratification
Bedrock

Figure 2.2. Stratigraphy of Quaternary sediment fill in Thompson River Valley at Ashcroft and their approximate elevations.

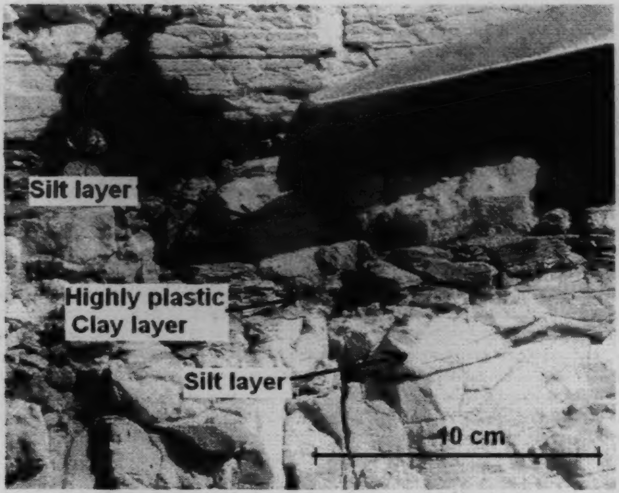
Silt layer
Highly plastic Clay layer
Silt layer
10 cm

Figure 2.3. Silt clay layers (unit 2, Figure 2.4), at the toe of the Goddard Slide, south of Ashcroft.

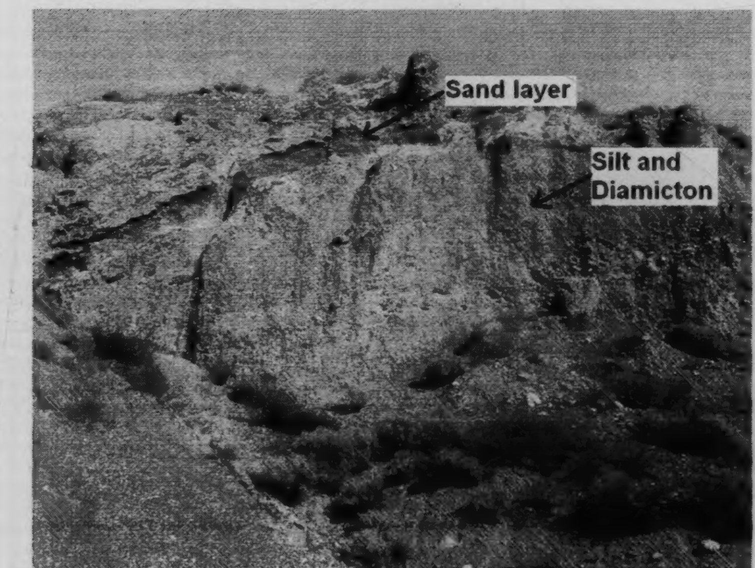
Sand layer
Silt and Diamicton

Figure 2.4. Unit 3, at the scarp of the Goddard Slide, south of Ashcroft (see Figure 2.1 for location).

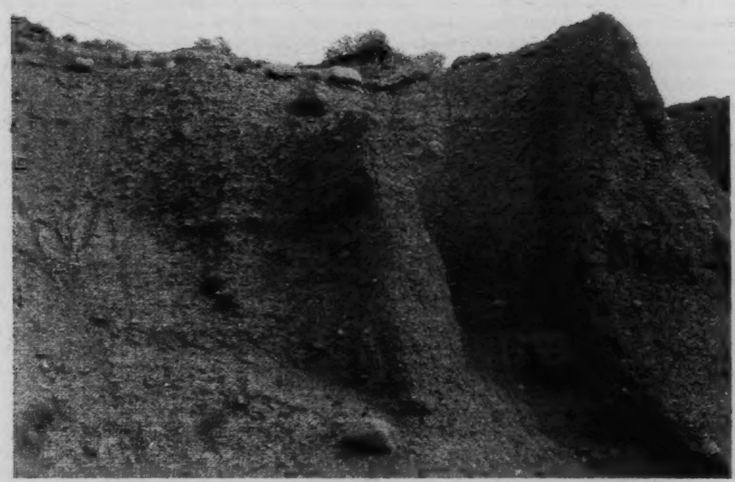

Figure 2.5. Wisconsin till (unit 6 in Figure 2.2) at the main scarp of the South Slide, south of Ashcroft (see Figure 2.1 for location).

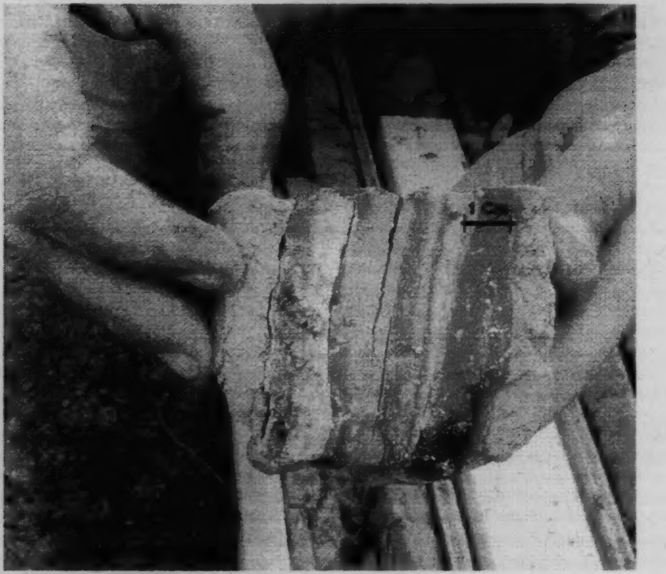

Figure 2.6. Sample of rhythmically bedded glaciolacustrine silt and clay sediments (unit 2), sample from South Slide (see Figure 2.1 for location).

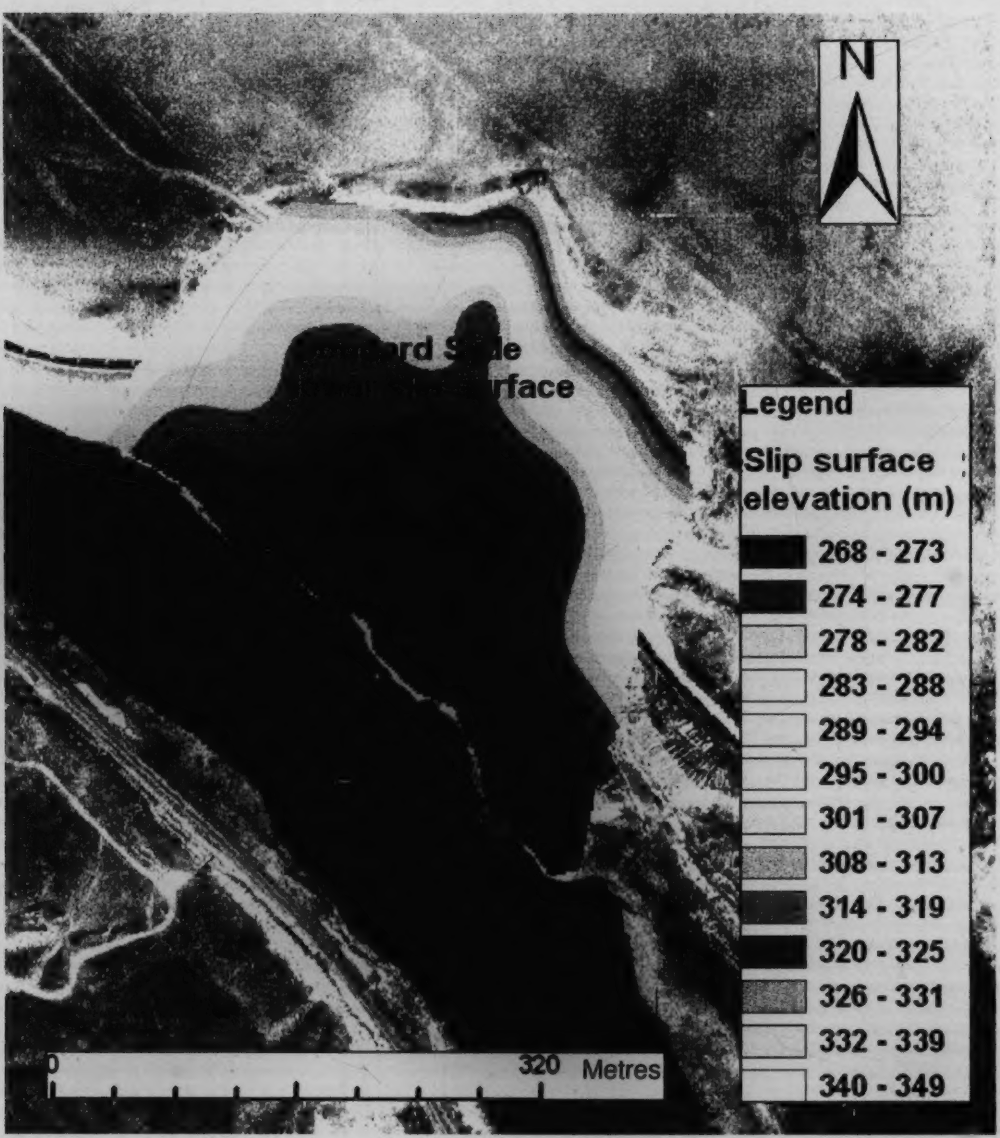
N
Goddard Slide
lower slip surface
Legend
Slip surface elevation (m)
268 - 273
274 - 277
278 - 282
283 - 288
289 - 294
295 - 300
301 - 307
308 - 313
314 - 319
320 - 325
326 - 331
332 - 339
340 - 349
0
320 Metres

Figure 2.7. Typical slip surface shape for the slides in the Ashcroft area (Goddard Slide lower slip surface in this case).

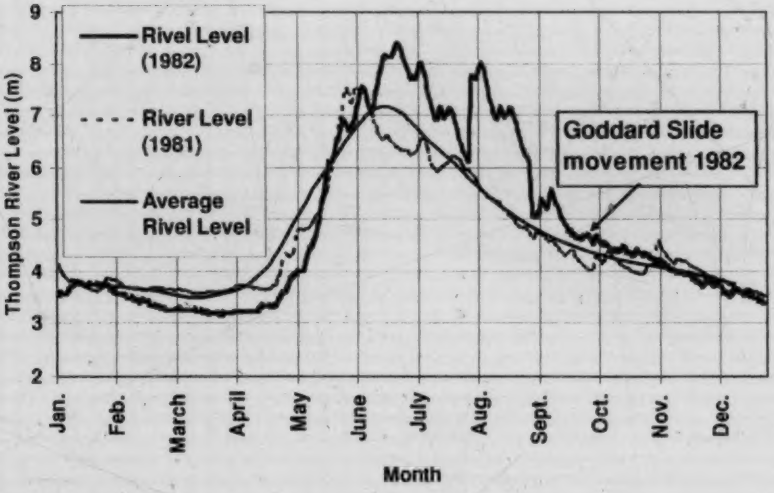

Figure 2.8. Comparing the Thompson River level in an active year (1982) and non-active year (1981) (data from Kamloops station).

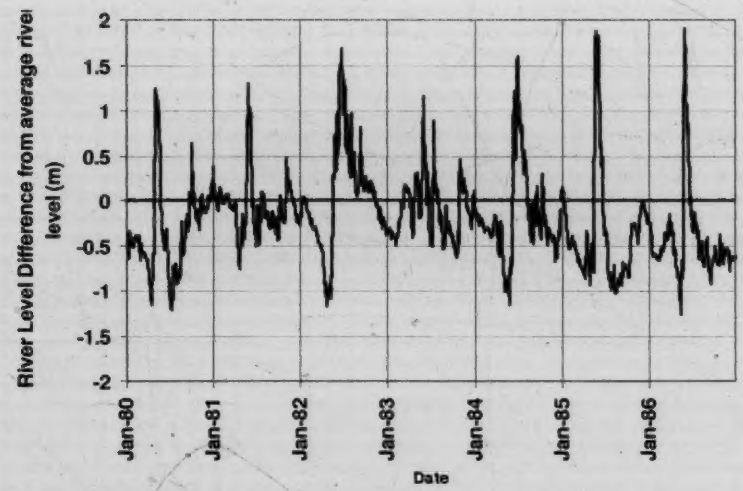

Figure 2.9. Daily difference between daily Thompson River level and average Thompson River level (Kamloops station).

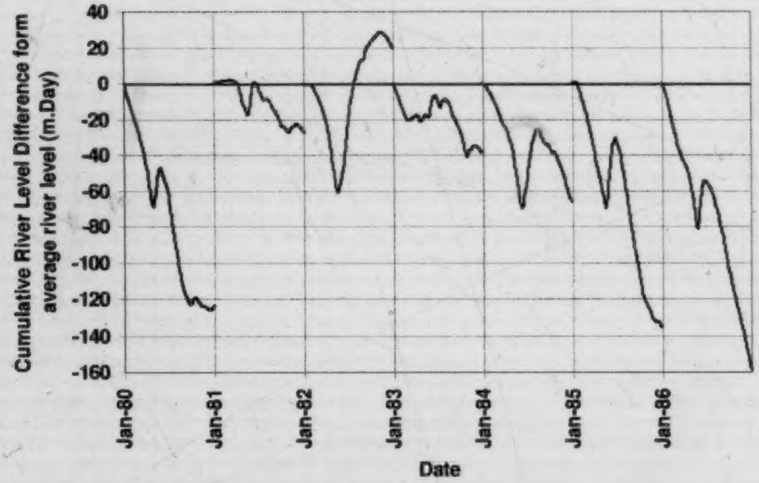

Figure 2.10. Cumulative Thompson River level difference form its average river level (Kamloops station)

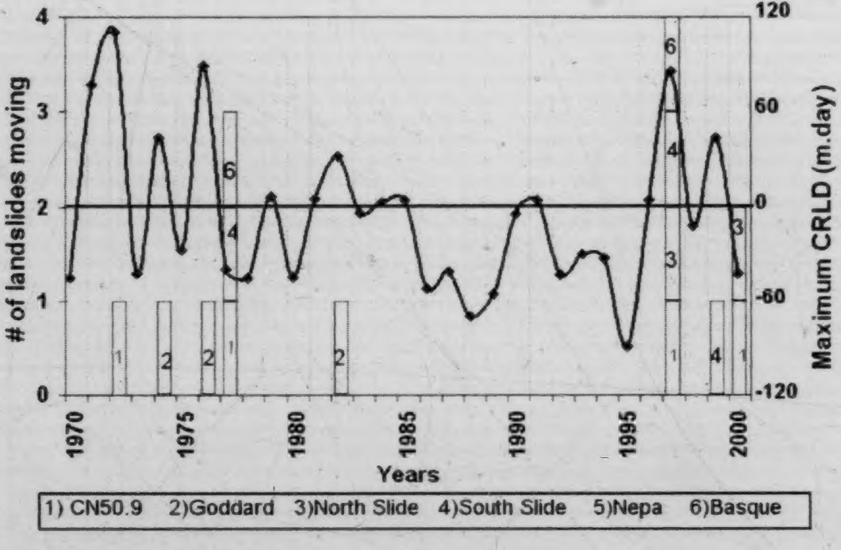

Figure 2. 11. Slide activity versus maximum cumulative Thompson River level difference from average Thompson River level (river data from Kamloops station).

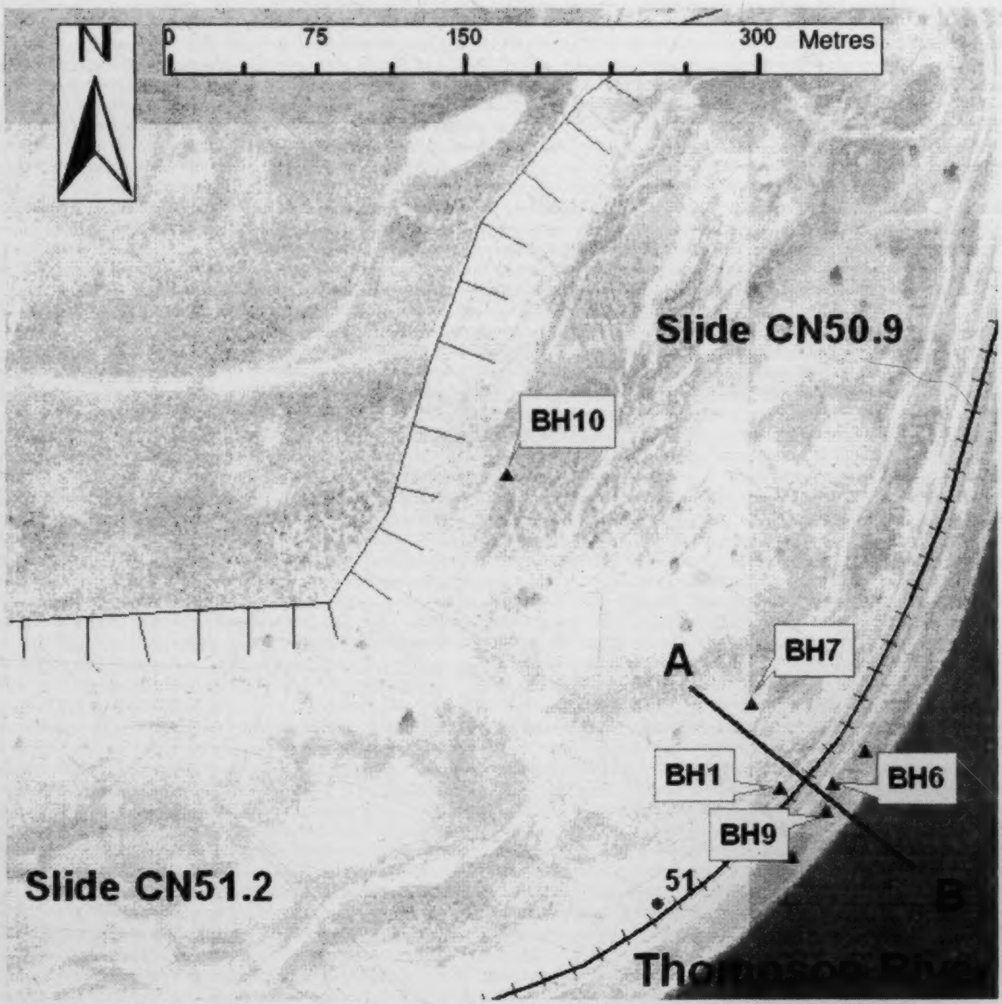
N
0
75
150
300
Metres
Slide CN50.9
BH10
A
BH7
BH1
BH6
BH9
51
B
Slide CN51.2
Thompson River

Figure 2. 12. Slide CN51 plan, the location of the piezometers, and section A-B shown in Figure 2.13.

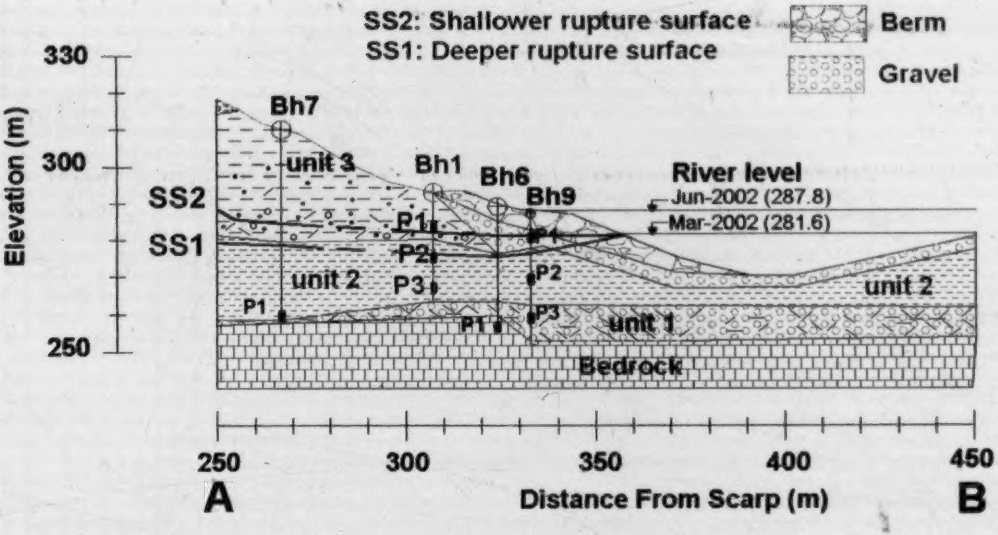
SS2: Shallower rupture surface
SS1: Deeper rupture surface
Berm
Gravel
330
300
250
Elevation (m)
SS2
SS1
Bh7
Bh1
Bh6
Bh9
unit 3
unit 2
unit 1
Bedrock
P1
P2
P3
River level
Jun-2002 (287.8)
Mar-2002 (281.6)
250
300
350
400
450
A
Distance From Scarp (m)
B

Figure 2.13. Piezometers locations at cross-section A-B at the toe of Slide CN51 (see Figure 2. 12 for location).

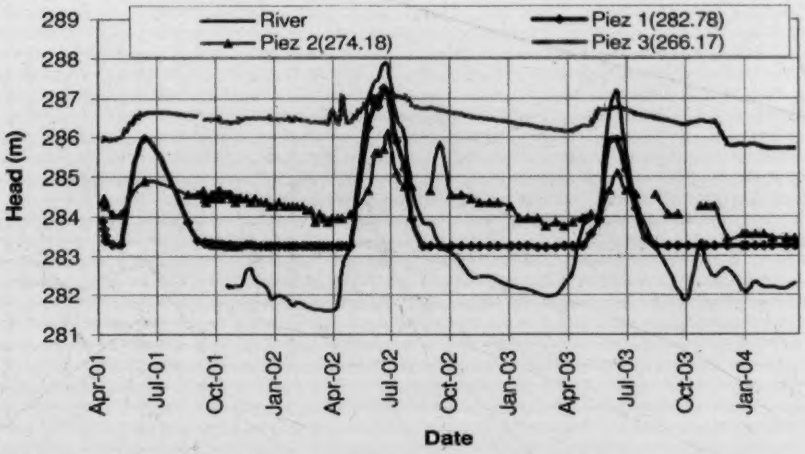

Figure 2.14. Sample responses of piezometers installed at the toe of the slides (Bh1, toe of Slide CN51, see Figs 2.12, 2.13).

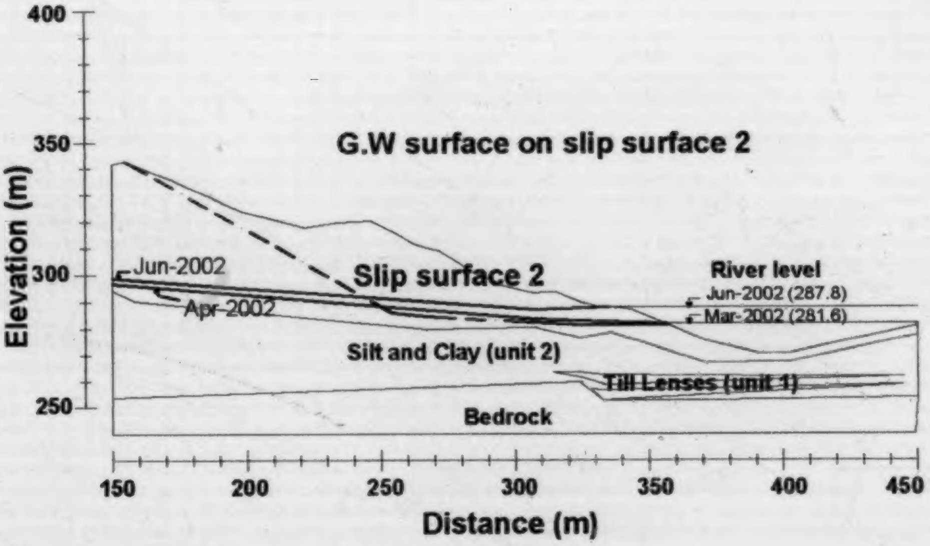

Figure 2.15. Groundwater surfaces for slip surface 2 (shallower slip surface) at the toe of Slide CN51 (see Figure 2.1 for slide location and Figure 2.13 for slip surface location).

Chapter 3

Characteristics of Earth Slides in Ashcroft Area[1]

Large translational landslides with rupture surfaces through glacial lake sediments in glacial valleys are common hazards within river valleys of western Canada (Evans et al., 2005). The sediments deposited in front of glacier advancing up these valleys can have beds of weak plastic clay layers which dictate locations and shapes of the rupture surfaces. When the clay is overconsolidated, the slide initiates by growth of the rupture surface followed by slides that expand the original slide in opposite direction of the movement and result in a multiple retrogressive landslide (Cruden and Varnes, 1996). Previously displaced masses can be reactivated later on these pre-developed rupture surface by seasonal triggers. These retrogressive, reactivated, multiple, translational earth slides may retrogress again in the future.

The Canadian Pacific Railway (CPR) and Canadian National Railway (CN) main rail lines were constructed through the Thompson River Valley in southern British Columbia in 1885 and 1905, respectively. Both have had recurring slope stability problems along 10 km of this valley, south of the town of Ashcroft, British Columbia (Figure 3.1). Two modes of movement are common among the slides in this area: (1)

---

[1] Accepted paper:

A version of this chapter has been published in the Journal of Environmental and Engineering Geoscience. Eshraghian, A., Martin, C.D., and Cruden, D.M. 2007. Complex earth slides in the Thompson River Valley, Ashcroft, British Columbia. Journal of Environmental and Engineering Geoscience, 13: 161-181.

rapid movement of landslides due to propagation of a current rupture surface in opposite direction of the movement (retrogression), or development of a new deeper rupture surface; (2) very slow moving reactivation of landslides on the previously formed rupture surface. The very slow-moving reactivation mode may cause damage to rail lines, whereas the rapid mode has a higher potential for risk to life.

In order to mitigate the risk of these landslides, CPR and CN have conducted geotechnical studies of landslides in the Ashcroft area since the early 1980s. Eleven large translational earth slides are located in this area, the five most active of which have been investigated through subsurface investigation. Data collected for this paper include site investigation results from the 1980s to 2005, laboratory analysis data, geological information, aerial photos of the area, and previous researches. These are stored in a geographical information system (GIS) data base, which has facilitated our study. In this paper, we examine the characteristics of the Ashcroft landslides and in particular the kinematics of the various slides. Before describing the characteristics of each of the active landslides, we outline the geology of the Ashcroft area, describing the Quaternary history in detail. We can then document the properties of the rupture surfaces and the soil units that contain them. We then look at the causes of the movements and finally document what is known of both reactivations and retrogressions of the slides. Our terminology follows Cruden and Varnes (1996).

3.1. GEOLOGY

The Quaternary history and the geology of the area were described by Ryder (1976) and Monger and McMillan (1989). Johnsen and Brennand (2004) examined the Quaternary history in more detail, and Clague and Evans (2003) identified the general stratigraphy of Quaternary sediments in the Thompson River Valley.

The Ashcroft area is part of the Thompson Plateau, a subdivision of the Interior Plateau of British Columbia. The Thompson River flows south (Figure 3.1) and has cut through about 150 m of glacial sediments (Porter et al. 2002). Quaternary sediments occur within the major valleys where deep valley fills have been dissected and terraced by postglacial down-cutting of the trunk rivers. The landslides occurred on the steep walls of an inner valley that formed during the Holocene, when Quaternary sediments filling the broader Thompson River Valley were incised. The valley fill consists dominantly of permeable sediments, the exception being a unit of rhythmically-bedded silt and clay in the Pleistocene sequence (Clague and Evans, 2003). The surficial materials in the area are tills, fluvial, fluvioglacial, lacustrine, and colluvial deposits (Ryder, 1976).

Bedrock of the Ashcroft Formation is exposed at Black Canyon, between South Slide and North Slide (Figure 3.1). The Ashcroft Formation consists of marine argillite, siltstone, sandstone, conglomerate, and minor carbonate of Jurassic age (Nachtigal, 2004b). Boreholes in the South Slide encountered weak, black, dry, stratified, fresh, bedding planes of mudstone and conglomerate inclined at 45 degrees to the core axis (Nachtigal, 2004a). Figure 3.2 shows the contact between the overlying sediments and the Ashcroft Formation, 500 m north of Black Canyon.

3.1.1. Quaternary history of the Ashcroft area

Although the Quaternary sediment fill in the Thompson Valley consists of deposits of three glaciations, most of the Quaternary landforms and surficial materials of the Ashcroft area can be related to the last Fraser Glaciation (Armstrong et al., 1965; Clague and Evans, 2003). During glaciations, ice covered all but the highest peaks of the Coast Mountains and flowed from both the east and west into the Thompson River Valley. In the valley, ice flow was from north to south (Ryder, 1976). Deglaciation occurred by the thinning and stagnation of ice over most of the Ashcroft area. Several phases of Holocene deglaciation can be identified, each represented by characteristic landforms and surficial deposits (Fulton, 1969).

The deposits of the three glacial sequences are separated by unconformities. Figure 3.3 shows the geological succession synthesized from borehole logs and outcrops in scarps and terraces in the Ashcroft area, based on units proposed by Clague and Evans (2003). Johensen and Brennad (2004) estimated the glacial lake bottom elevation at 420 m in Ashcroft. The sediment boundaries should have tilts similar to the glacial lake bottom (1.7 m/km) (Johnsen and Brennand, 2004); so the boundary elevations decreased from north to south as boundaries between bedrock and unit 1, and unit 1 and unit 2 as shown in Figure 3.3. For other boundaries, unconformities changed this pattern.

The oldest exposed sediments are cemented, oxidized, folded and faulted sand and gravel with minor lenses of diamicton (unit 1, Figure 3.3). These sediments were interpreted to be ice-contact materials, deposited against decaying masses of glacier ice at the end of a Pleistocene glaciation of still uncertain age (Clague and Evans, 2003).

The till and the oxidized sand and gravel are overlain by rhythmically-bedded silt and clay of lacustrine or glaciolacustrine origin (unit 2, Figure 3.3). There are up to 45 m of silt and clay couplets, ranging from less than 1 cm to several tens of centimetres thick (Figure 3.4). These sediments may be several hundred thousand years old, and thus of Middle or Early Pleistocene age (Clague and Evans, 2003). Our samples of this unit from boreholes in the South Slide show layers of brown, highly-plastic clay 1 to 20 cm thick between thicker layers of olive-coloured silt (Figure 3.5).

A second glacial sequence (unit 3, Figure 3.3) overlies unit 2. It consists of poorly sorted, inter-tonguing silt, sand, gravel, and diamicton interpreted by Clague and

Evans (2003) as glaciolacustrine. This unit, unlike units 1 and 2, is not significantly weathered (Clague and Evans, 2003) (Figure 3.6).

Sediments deposited during the last (Late Wisconsin or Fraser) glaciation (units 4-7) overlie unit 3. Clague and Evans (2003) identified the Fraser glacial sequence in the Ashcroft area as units 4, 5, 6 and 7. Figure 3.7 shows unit 6 at the South Slide site. At most sections in the area, the Fraser Glaciation sequence is incomplete, consisting of only one or two of the four units 4-7 (Clague and Evans 2003). The authors could only identify unit 6, which is till, in the studied slides (Figure 3.3) in the Ashcroft area, with units 4, 5, and 7 presumably removed by erosion. The Fraser Glaciation sediment sequence (units 4-7) is unconformably overlain by horizontally-bedded, pebble-cobble gravel (unit 8, Figure 3.3) deposited by the Thompson River and its tributaries (Clague and Evans, 2003; Eshraghian et al., 2005a).

3.2. SLIDES IN THE ASHCROFT AREA

There have been 11 large landslides identified in the Ashcroft area. Modern geotechnical studies have been carried out on five of these landslides, shown in Figure 3.1. Table 3.1 gives the areas and volumes of these five most active landslides. For the slides with inclinometers, the volumes are estimated based on rupture surface locations from the inclinometer data, and the ground surface elevation model developed from Light Detection And Ranging (LiDAR) data, using a geographical information system (GIS) program. In the case of slides without inclinometers, the volumes have been estimated using Cruden and Varnes' (1996) formula based on estimated elevation of rupture surfaces and ground surfaces from LiDAR data.

3.2.1. Slide CN50.9 (Slide 1, Figure 3.1)

A view of Slide CN50.9 with three scarps, the CN railway, a toe berm, and the Thompson River is shown in Figure 3.8. The same area with a cross-section position (AB), location of scarps, and a scour hole in the Thompson River bed is shown in plan view in Figure 3.9. There are two minor scarps in the body of the slide. Figure 3.10 shows a cross section through this slide based on ground surface produced from the LiDAR data (vertical resolution of ± 0.25 m) geological information, inclinometer data (from Nachtigal, 2001), borehole information (from Nachtigal, 2001; Pitchard and Baumgard, 2003), modeling of the sliding stages, aerial photos, and site visits. Historic accounts suggest that this slide experienced movement in 1897. The minor scarps are inclined at significantly lower angles than the major scarp. The break in slope on the major scarp is formed by talus. So, the minor scarp surfaces appear older than the major scarp and may represent earlier retrogressions. Therefore, we think the 1897 event likely developed the main scarp and translated the minor scarps.

We hypothesize that Slide CN50.9 has experienced different stages of movement since deglaciation (Figure 3.11). During the first stage, a braided Thompson River started cutting through the glacial sediments after deglaciation. The Thompson River continued its down-cutting until it reached the first weak layer and potential rupture surface (stage 2, Figure 3.11). Progressive failure within this weak layer caused sliding of blocks A and B on the shallower rupture surface. More down-cutting by Thompson River encountered a deeper weak layer (Stage 3, Figure 3.11). This time, movement happened on the deeper rupture surface without forming a new scarp. It caused more horizontal movement by block A and horizontal and vertical movement by block B. This sliding, and also the Thompson River erosion, caused progressive failure on the deeper rupture surface, and the slide was ready for another retrogression (Stage 4, Figure 3.11). The most recent retrogression of Slide CN50.9 happened in September 1897. During this stage, block D moved down on the main scarp, and the rest of the slide material moved horizontally toward the river (Stage 5, Figure 3.11). During this retrogression in the early morning of September 22, 1897, residents of Ashcroft were awakened by loud, thunder-like rumblings (Clague and Evans, 2003). The landslide constricted the Thompson River without completely blocking it (Clague and Evans, 2003). From these reports, we infer that the movement rate during this retrogression was rapid. Following the slide, the Thompson River removed part of the toe of the slide, mainly within block A (stage 6, Figure 3.11).

This slide is now moving on two rupture surfaces as a multiple translational earth slide. The positions of the rupture surfaces were determined by inclinometers installed in boreholes Bh1 and Bh9 (Figure 3.9 and 3.Figure 3.10). The rate of movement differs between inclinometer measurements at boreholes Bh01 and Bh09, on the shallower rupture surface, suggesting possible additional small blocks at the toe part within the R-3 block. The main scarp starts with a 50-degree slope, but some rotation of the ground near the main scarp suggests that the main scarp may be concave. Ground rotation near minor scarps, R2 and R3, is much less than the main scarp, R1.

The profile of the slide surface shows the angle between the line connecting the crown and the tip of the slide and the horizontal, i.e., the travel angle, of 16°. Since 1897, the slide has experienced slow reactivations with different rates of movement. After an acceleration of movement in 1997, an extension to a berm located at the toe of the slope was built for additional protection against river erosion and to provide more support for the toe block (Figure 3.8). There was a 5-metre-deep scour hole in the river bed at the time of the accelerated movement in 1997 (Figure 3.9) (Yaremko, 2002).

The locations of piezometers at the toe of Slide CN50.9 are shown in Figure 3.12. Figure 3.13 shows data from piezometers installed at the toe of Slide CN50.9 in borehole Bh1. Upward gradients in boreholes Bh1, Bh2, and Bh9, caused deeper piezometers to have higher heads. All piezometers respond to changes in the river level, but the shallower the piezometer, the greater the response. The piezometer measurements in borehole Bh1, on the deeper rupture surface, showed 7 to 10 days lag between river-level drops and the subsequent piezometer reduction. The delayed response of pore pressure to river-level changes is seen in piezometer data from borehole Bh9 within 8 to 14 days after the river-level changes. A comparison of piezometers in boreholes Bh1, Bh9, and Bh10 shows that the piezometers at the toe of the slide (boreholes Bh1 and Bh9) respond more to the river level changes than piezometers installed in borehole Bh10 near the main scarp. Also, piezometers installed in Bh10 near the main scarp show a downward gradient in that part of the slide.

These results indicate that the portion near to the scarp, i.e., the slide head, is generally a recharge zone, and the toe is a discharge zone when the Thompson River level is low. On the other hand, when the Thompson River starts rising the water from the river seeps towards the slide mass. However, the river may not stay at these high levels for sufficient time to allow the flow system to reach equilibrium. Therefore, the top part of the impervious rhythmically-bedded silt and clay layer (unit 2) may be more affected by river level changes than the lower part. In the years that the Thompson River stays at high levels for longer periods, the piezometers show the greatest increase in pore-water pressures because the water has more time to seep through the soil mass.

3.2.2. Goddard Slide (Slide 2, Figure 3.1)

The most recent retrogression of the Goddard Slide happened on October 19, 1886 (Stanton 1898). Figure 3.14 shows a digital elevation model (DEM) of the Goddard Slide in a GIS program made from LiDAR data. Four scarps, the CPR rail track, and active erosion locations are visible. Clague and Evans (2003) description of the

19886 retrogression rates suggests that this movement was very rapid (faster than 3 m/min). This slide's reactivations between 1886 and 1982 included reactivations in 1974 (Morgenstern, 1986) and October 1976 (Porter et al., 2002; Morgenstern, 1986; Hawson, 1977). During this period, rates of reactivation were generally slow, in the range of 20 mm/year to 400 mm/year. The rate of reactivation in 1976 reported by Hawson (1977) was 400 mm/year. A much faster reactivation happened between September 22 and September 25, 1982, when the maximum rate of movement was 6 m/hour (Krahn, 1984).

A CPR legal action claimed that irrigation on the terraces above the landslide triggered the 1982 landslide. After the court weighed evidence regarding the volume of irrigation water, efficiency of the irrigation system, evaporation effects, soil texture and its capacity to store water, the soil water content required for healthy crops, lateral movement of groundwater to the slide site, and other possible causes of the landslide, the CPR was not successful in its claim (Wallace, 1987). The CPR appealed against the 1987 decision in 1990, but the case was dismissed (Toy et al., 1990).

The 1982 reactivation was within the original 1886 slide area. Krahn (1984) presented the ground contours before the 1982 slide, in May 1981, and after the 1982 slide, on September 29, 1982, synthesized from aerial photos taken on those dates. From this information, we inferred that there was a main downward movement at the head and upward movement at the toe, while the movement of the main body was sub-horizontal. Figure 3.15 shows the up-turning of bedding sequences of the silt and clay layer at the toe of the Goddard Slide because of the deformation at the toe. Morgenstern's (1986) evidence was that the initial observations revealed that the movements originated at the toe of slope. It was observed that the initial cracks at the toe were in the same locations as the 1976 movements (Morgenstern, 1986). The movement started on September 22, 1982, and continued until September 23, 1982, with a rate of 30 mm/hour. It accelerated to rapid movement (maximum rate 6 m/hour) on September 24, 1982 (Krahn, 1984). Seepage in the vicinity of the main scarp was probably due to perched water in the gravel unit on the terrace (Krahn, 1984). Krahn (1984) also noted a wet area at the middle part of the slide, near boreholes Bh7 and Bh6 (Figure 3.14). This wet area likely developed because of a local high water table. Morgenstern (1986), using aerial photos that span 48 years, estimated the toe erosion rate of the Thompson River bank at the Goddard Slide as between 0.25 and 0.33 m/year.

A cross section through the Goddard Slide is presented in Figure 3.16. The cross-section location, scarp locations, boreholes, the location of a scour hole in the Thompson River bed, and limits of the original 1886 slide and the 1982 slide are shown in Figure 3.14. The layers in Figure 3.16 are based on borehole information, reported by Krahn (1984), and the general geology of the area. None of the boreholes in this slide reached bedrock; so the bedrock depth has been interpolated from the adjacent slides, Slide CN50.9 and South Slide. The 1982 pre-slide ground surface is reproduced from Krahn's (1984) estimate, based on 1981 aerial photos. The main body of the 1982 slide is covered by colluvial material (Figure 3.16), as are the minor scarps (Figure 3.14).

Like other slides in this area, the Goddard Slide is moving on two rupture surfaces as a multiple translational earth slide (Krahn, 1984). The positions of these rupture surfaces were determined by inclinometers installed in boreholes Bh1, Bh2, Bh3, Bh4, and P5 (Figure 3.14). The activity in the 1976 and 1982 slides was within the original 1886 slide (Figure 3.14). Piezometers and inclinometers installed a few days following the 1982 slide, and data from Krahn (1984) and Vanwieren and MacLeod (1988), showed decreasing rates of movement after 1982, which ceased in 1988 in the main part of the slide. The movement was toward the Thompson River. Inclinometer data from borehole Bh1 showed that the major movement occurred on the deeper rupture surface. Inclinometer data from borehole Bh4 showed that, although the rate of movement on the deeper rupture surface was similar to the rate measured in borehole Bh1, the rate of movement on the shallower rupture surface was faster.

Site visits in August 2004 and September 2005 revealed new cracks at the toe between the CPR rail line and Thompson River in blocks R-3 and R-4 (Figure 3.14). Figure 3.17 shows one of these cracks on R-4, near the toe of the slide, where active river erosion is evident (Figure 3.18). Below this, there is a scour hole 6 metres deep in the Thompson River (Figure 3.14) (Krahn 1984).

3.2.3. North Slide (Slide 3, Figure 3.1)

The most recent retrogression of this large slide, in October, 1880, was felt and heard in Ashcroft, where it was thought to be an earthquake (Clague and Evans, 2003). This landslide dammed the Thompson River (Clague and Evans, 2003). The movement rate is estimated as very rapid. Since the 1880 retrogression, the slide has been reactivated at least twice, in 1997 and in 2000 (Porter and Savigny, 2001). Inclinometer measurements, reported by Porter and Savigny (2001), show two rupture surfaces in the highly plastic clay-silt layer (unit 2) at elevation of 264 m and 269 m (Figure 3.3). From a Synthetic Aperture Radar Interferometry (InSAR) map (Kosar et al., 2003), we inferred that the movement in 1997 was extremely slow (slower than 16 mm/year). Porter et al. (2002) reported an average rate of movement of 30 mm/year with a maximum rate of 150 mm/year in the 2000 reactivation. Porter and Savigny (2001) reported that the movement rate on the shallower rupture surface, 55-110 mm/year, was greater than on the deeper rupture surface, 30-45 mm/year. Piezometer data suggest the presence of near-hydrostatic conditions beneath the rail grade, and a slight upward gradient near the toe (Porter and Savigny, 2001). Porter et al. (2002) estimated an average river bank erosion rate of 0.7 m/year for this site. The average travel angle of the landslide is 6°.

3.2.4. South Slide (Slide 4, Figure 3.1)

The most recent retrogression of the South Slide (Figure 3.1) happened before the 1885 construction of the CPR line (Porter et al., 2002), probably in 1881 (Porter and Savigny, 2001). There is no report of the rate of movement during this event. Since then, the slide has experienced reactivations, including those in the winter of 1977 and in the fall of 1997. The 1997 reactivation occurred after a flood that resulted in extensive river erosion and damage to the toe berm built for erosion protection (Figure 3.19). A scour hole had also formed in the Thompson River bed below this slide (Figure 3.19). During these reactivations, the smaller part of the toe, Block R-3, was moving faster. An InSAR map (Kosar et al., 2003) indicated that 16 mm of ground movement occurred between August 1997 and August 1998. From past experiences of slides in this area, most of this movement would have occurred in the fall of 1997. Using this data, we estimated the movement in fall 1997 to be very slow (rate between 16 mm/year and 1.6 m/year). Since the repair of the river erosion protection berm in 1998, the rate of movement has decreased. Slope inclinometer measurements indicated a maximum rate of movement of 4 mm/year during the first three months of 2005 (B. J. Nachtigal, personal communication, 2005)

The cross-section line AB, scarps, and other features are shown in a 3-dimensional view of the South Slide (Figure 3.19). Borehole information reported by Nachtigal (2004a, 2004b) was used for making cross section AB shown in Figure 3.20. More scarps may be present at the toe, within block 3; however, they would be covered by the rail-line fills. Bedrock and unit 1 elevations are defined by borehole Bh6 (Figure 3.19), not shown in this cross section, which reached mudstone. The R-3 block is the most active block. This slide is moving on two rupture surfaces. Based on inclinometer data reported by Nachtigal (2004b), the shallower rupture surface is at an elevation of 273 m elevation and the deeper rupture surface is at an elevation of 264 m. Porter and Savigny (2001) reported that the movement rate on the shallower rupture surface during the year 2000 was 110 mm/year, compared to a movement rate of 50 mm/year on the deeper rupture surface in the same year.

3.2.5. Basque Slide (Slide 5, Figure 3.1)

The Basque Slide is south of the South Slide (Figure 3.1). Its most recent retrogressions happened before the CPR railway construction in 1885. Everard and Savigny (1998) reported new cracks in the Basque site, which probably developed in 1997 at the time of the large flood (Figure 3.21). More recent cracks have been discovered north of the Basque Slide site between CPR mileage 55 and CN mileage 57 (Figure 3.1) which may be evidence of developing new slide at this location (C. Bunce personal communication, 2005).

Four boreholes were drilled in the Basque Slide near the cracks discovered in 1997 (Figure 3.21) (Everard and Savigny 1998). A 3-dimensional view of the Basque Slide is shown in Figure 3.21, and the geological cross section AB is shown in Figure 3.22. The bedrock elevation shown in Figure 3.22 was assumed to be similar to that of the South Slide site.

3.3. RUPTURE SURFACES AND SOIL PARAMETERS

The surfaces of rupture of these slides are in clay beds in unit 2 (Figure 3.3). These highly plastic, overconsolidated clay layers are sandwiched between layers of clayey silt. Table 3.2 shows the range and average of soil parameters for samples taken from this unit at different landslides. Porter et al. (2002) reported values similar to Table 3.2 for these material indices.

As the slides are moving along pre-existing surfaces of rupture, the controlling Mohr-Coulomb parameters are residual parameters. Residual friction angles for this material can be estimated from their average indices using Stark and Eid's (1994) correlation. In Table 3.2, the average residual friction angle, φ_r, is between 11° and 15° in different slides (residual cohesions are assumed to be zero). Keegan et al. (2003) used residual friction angles between 9° and 11° for this material in their analyses for Slide CN50.9. Nachtigal's (2004b) back analyses of the South Slide and Basque Slide indicated a residual friction angle of 12.9° and 12.8° for the rupture surface's material in unit 2 for these slides.

We collected samples of the shear zone from South Slide boreholes (boreholes 1, 5, and 6 in Figure 3.19) for direct shear tests, Atterberg Limit tests, and particle-size-distribution analyses. We took separate specimens from the highly plastic brown clay seam and the olive clayey silt in these samples. The results of tests on these specimens are compared with results from previous soil tests shown in Table 3.2. The earlier results encompass the range of the new tests results. Previous results may reflect samples of both the thin highly plastic clay layers and the clayey silt layers in tests. The direct shear tests were done with normal effective stress within the range of expected effective stresses in the slides. The peak friction angle and cohesion of the highly plastic brown clay from the direct shear tests are estimated respectively as 16° and 10 kPa. The peak friction angle and cohesion of olive clayey silt material from the direct shear tests are estimated respectively as 23° and 25 kPa.

Two scanning electron microscope (SEM) photographs of the brown-clay-layer rupture surface and of the silty clay layers for the South Slide are shown in Figure 3. 23. As can be seen in this figure, the brown clay specimen has a high clay content. X-ray fluorescence (energy dispersive x-ray micro fluorescence) tests on samples from the brown clay layer on the rupture surface show that the dominant elements in these samples are Al, Fe, Ca, and Mg. Considering the range of clay fraction (82-87%), liquid limit (67-70%), plastic limit (30-33%), activity (0.45-0.49), liquid index (0.45-0.49), and residual friction angle (12.8-13°), the clay minerals are in the range of non-swelling clay types (probably illite).

Skempton (1969) found a correlation between the liquidity index and effective overburden pressure (or overburden material thickness) for normally consolidated clay sediments. Considering relatively small changes in the volume of a clayey material during unloading, the water content after unloading the material can be considered close to water content before unloading, at the end of deposition of material. Therefore, the Skempton's correlation can be used for estimating the overburden material thickness of overconsolidated clays and their overconsolidation ratios (OCRs). The OCRs were found using Skempton's approach on the samples taken from the undisturbed part of the rhythmically bedded silt and clay layer (unit 2). The results show that this unit is highly overconsolidated with an OCR ranging between 5 and 20.

After inputting all of the information from slide inclinometers, borehole logs, geological study of the area, and site visits into a geographical information system, it became clear that all of the studied slides are sliding on more than one surface of rupture. These surfaces of rupture are in the rhythmically-bedded glaciolacustrine silt and clay unit (unit 2 in Figure 3.3). The surfaces of rupture are at different elevations in different landslides (Figure 3.3). The average elevation difference between shallower and deeper rupture surfaces in each slide is 6.5 m. Table 3.3 shows the elevations of the rupture surfaces for the slides in which inclinometers have been installed. As shown in Table 3.3, the elevations of the deeper rupture surfaces decrease toward the South by about 12 m, and the elevations of the shallower rupture surfaces decrease toward the south by about 9 m. This is in agreement with the general tilting of the glacial lake bottom found by Johnsen and Brennand (2004). So sliding may be occurring on the same weak layers throughout the area.

3.4. LANDSLIDE CAUSES

Popescu (1994) divided landslide causes into two main categories: preparatory causal factors, which change a slope from stable to marginally stable, and triggering causal factors, that cause active instability. More than one preparatory factor may bring a stable slope to the marginally stable stage and then a trigger can cause movement.

3.4.1. Triggering causes

The average rainfall in the area has been increasing since the 1920s from about 150 mm/year to 240 mm/year (Porter et al., 2002). Despite this rainfall increase, no correlation between slide movements and short-term or long-term rainfall has been found (Eshraghian et al., 2005a). Turning then to the level of the Thompson River, consider the Thompson River level for two different years (1981 and 1982) and the average Thompson River level shown in Figure 3.24. As can be seen in Figure 3.24, the level of the Thompson River during 1982 was significantly above normal, and in that year Goddard Slide disrupted the CPR operations at the end of September (Krahn, 1984).

Eshraghian et al. (2005a, 2005b) examined the levels of the Thompson River and slide movements from 1970 to 2000. Data prior to 1970 are sparse. They presented a correlation between the daily river level difference from the average level, cumulated over the whole year, CRLD, and the years in which the slides were active, active years. All of the movements used for finding the correlation (Eshraghian et al., 2005a) were reactivations of the slides, and no case of retrogression of the main scarp was seen during this period. Therefore, we conclude that the main trigger for reactivation of these slides is the above-average Thompson River discharge.

Clague and Evans (2003) suggested "irrigation of the bench lands above the river, especially in the late 1800s, introduced large amounts of water into the valley fill.

High pore pressures probably developed locally at the top of the rhythmically bedded silt-clay unit, triggering large landslides". They added "although high pore pressures generated by irrigation-related groundwater recharge probably triggered most of the historical landslides in the Ashcroft area, the fundamental causes are geological". According to Clague and Evans (2003) there is a possibility of increasing pore water pressures in the silty gravel layer (unit 1 in Figure 3.3) above the bedrock and under the rhythmically bedded silt and clay layer (unit 2 in Figure 3.3). Piezometers at the toe of Slide CN50.9 and the South Slide show an upward hydraulic gradient from unit 1 toward the Thompson River at the toe. Porter and Savigny (2001) also reported an upward hydraulic gradient at the toe of the North Slide. Eshraghian et al. (2005a, 2005b) showed that the changes in the river level had the largest impact on the piezometers in the toe of Slide CN50.9, and the largest impact on slope stability occurred when the river remained high for a long period and then retreated, effectively causing a drawdown effect on the slope toe blocks.

3.4.2. Preparatory Causes

The drop in the stage of Thompson River following floods, drawdown, is a trigger of the reactivation mode of movement for the slides with toe erosion protection. River erosion can be another trigger of the reactivation mode of the slides without toe erosion protection, but there are other processes and conditions that act as preparatory factors to bring these earth slides to the marginally stable stage.

The stratigraphy of the valley fill predisposes it to movement. Disturbance by overriding ice or early slope movements may have created pre-sheared discontinuities that predisposed these units to failure (Clague and Evans, 2003). The rapid down-cutting of valleys during deglaciation resulted in rebound, and the weakness thus generated along the flat-lying bedding results in a planar rupture surface for slope movement (Cruden et al., 1989). This can be a reason for having translational earth slides in the Thompson River Valley too.

There is a 5-m scour hole in the Thompson River bed in front of Slide CN50.9. Hydraulic analyses of the Thompson River in Slide CN50.9 site by Yaremko (2002) showed 30% higher velocity in the river flow just upstream of the scour-hole location. Another 6-m-deep scour hole can be seen in Thompson River bottom profiles made by Krahn (1984) from echo-sounding surveys in October 1982 and October 1983 in front of the Goddard Slide following the 1982 movement. There is no measurement of the rate of river-bed down-cutting, but the higher flow velocity in the vicinity of the scour holes might cause continued extension of these holes. These scour holes are signs of ongoing down-cutting by the Thompson River in the study area. If the river down-cutting encounters another clay layer similar to the highly-plastic brown clay layers that the current rupture surfaces are located in, slides may occur on new rupture surfaces. From previous experience, these slides are likely to be rapid to extremely rapid.

Krahn (1984) reported river-bank erosion at the toe of the Goddard Slide (Figure 3.14). Morgenstern (1986) estimated a toe erosion rate between 0.25 and 0.33 m/year for the Goddard Slide. At Slide CN50.9 and South Slide river bank erosion was effectively stopped by protection. River bank erosion can produce over-steepened toe blocks at the river bank, and their failure and removal by the river flow can lead to more retrogression of the slides due to toe unloading. This can also lead to rapid to very rapid movements following a new retrogression or movement on new a deeper rupture surfaces.

Both river down-cutting and river bank erosion processes have been acting since deglaciation, but neither of them have developed enough since the early 1900's to initiate retrogression of the earth slides. These processes need time to develop and remove material deposited in this section of the river by previous earth slides or material carried by the river from upstream. Even if they are not severe enough to trigger retrogressions, they still can create marginal stability of the slide toe, which can be triggered later to a reactivation mode of movement by a rapid drop in the river level, river drawdown.

3.5. MOVEMENT BEHAVIOUR

Hungr et al. (2005) suggested that "the best means of assessing a landslide's potential for catastrophic motion is to compare it with similar case histories whose failures have already taken place". The slides in the Ashcroft area are moving on rupture surfaces within the same geological unit, and probably on the same seams of highly plastic clay, so past movement behavior of these landslides can give insights into their future movement.

There are two modes of movement common among the landslides in this area. The first mode is rapid to very rapid movement, which results from growth of an existing rupture surface by retrogression or by sliding on a new deeper rupture surface after enough river down-cutting. The second mode is reactivation of the slide on a previously-developed rupture surface without retrogression. Table 3.4 gives a summary of movements of the most active slides in this area.

3.5.1. Retrogression Movement

Retrogression, by extension of an existing rupture surface or movement on a new deeper rupture surface, can cause much faster movements than reactivation. Slide CN50.9, Goddard Slide, and South Slide slid at rapid to very rapid rates during the late 1800s, which we speculate was due to this mode of movement. The possibility of slide retrogression on glaciolacustrine material appears to be higher when the average landslide slope angle is larger than the rupture surface material's residual friction angle, φ_r (Keegan et al., 2003). Comparing average residual friction angles, φ_r, for slides (Table 3.2) and their travel angles (Table 3.4) helps to recognize the relative possibility of this mode of movement in the area. This comparison shows that the travel angles of Slide CN50.9 and the Basque Slide are larger than the residual friction angle of the material in these two slides, and that the travel angle of South Slide is equal to its residual friction angle. For these slides the possibility of retrogression is higher than for other slides in this area.

The Thompson River still has 10 to 15 m of highly-plastic clay-silt material of unit 2 to cut through (Figures Figure 3.10, Figure 3.16, Figure 3.20, and Figure 3.22). Two current rupture surfaces are separated by about 6 m in this unit in different slide locations (Table 3.3). It is possible for the Thompson River to encounter another weak layer during this down-cutting process. If this happens, a new deeper block may slide on this new rupture surface. The time to this mode of failure depends on the rate of river down-cutting and the location of the possible weak layer. Stanton (1898, page 16) suggested that slides happened in the early 1800's, and then not until the late 1800's. Thus, if the river flow regime has not changed significantly since the 1800's, it is possible to estimate approximate time need to develop new deeper rupture surfaces within the study area. The period needed to develop new deeper rupture surfaces is the period needed to remove the displaced material deposited in the river by previous slides and to allow enough down-cutting to reach another high concentration of highly plastic clay layer in the glacial sediment. Because, the average elevation differences between two current rupture surfaces is 6.5 metre (Table 3.3), this time period might be of the order of a century. Considering the lack of irrigation activity in the early 1800s, Stanton's (1898) suggestion might be considered another reason to believe that the main triggers of these slides were natural.

3.5.2. Reactivation Movement

The other mode of movement is the reactivation of the slides. Generally, the rates of movement of the slides in this mode are very slow with higher movement rate during late summer and fall. The movement on the main rupture surface (the deeper rupture surface) measured in borehole Bh1 (Figure 3.10) of Slide CN50.9 is shown in Figure 3.25. Acceleration begins when the Thompson River level and groundwater head on the rupture surface drop. The movements follow drops in the groundwater head, after a period of almost constant groundwater head or increasing head (from piezometer data in borehole Bh1). The average pore pressure ratio, r_u, during drawdown on the deeper slip surface, calculated from Bh1 and Bh10 at each movement period, and the rate of movement in that period are shown in Table 3.5. There is a nonlinear correlation between the rate of movement and the average groundwater head during each drawdown period (Figure 3.26).

We measured the change of travel angle for the Goddard Slide due to the 1982 slide activity. The Goddard Slide had a travel angle of 14.5°, slightly lower than its residual friction angle (Table 3.2), before the 1982 movement. In 1982, it decreased to 13.7° due to 15 m movement towards the Thompson River. Although there was no retrogression of the 1886 main scarp, the displaced material advanced towards the Thompson River to a more stable geometry. The 1982 slide was within the main body of the original 1886 slide (Figure 3.14), and it included the same area that had been reactivated in the 1976 movement. The maximum rate of movement during sliding was 6 m/hour (Krahn, 1984), much faster than the rates for the other reactivated slides (Slide CN50.9, South Slide and North Slide) and also for its previous reactivations in 1974 and 1976. It was slower than the rate of movement of this slide during its last retrogression in 1886, estimated to have been very rapid (Table 3.4). The contrast between the rate of movement of the 1982 slide and other slide reactivations may be explained by particular causal factors acting during 1982 sliding.

The slide occurred in September 1982, at the end of the Thompson River drawdown period for that year. In 1982, the Thompson River had higher than average discharge (Figure 3.24). There is no toe erosion protection at the Goddard Slide; therefore, river erosion might have had an important effect in starting movement. The report of initial movement at the toe (Morgenstern, 1986) supports this idea. Krahn (1984) reported seepage from the scarp of the slide after the 1982 slide and also piezometers in borehole Bh10 (Figures Figure 3.14 and Figure 3.16) suggested a perched water table in unit 8 (Figure 3.16) in the terrace above the Goddard slide. Photographs taken after the slide (Krahn, 1984) showed a wet area at the middle of the slide (Figure 3.14), suggesting a high local water table in the slide mass. Aerial photos taken in 1981 before the 1982 slide, show that the head of the slide was connected to the gravel unit in the terrace above the slide; therefore, it had access to the perched water table in this unit (Figure 3.16).

During the first 2 days of the Goddard 1982 reactivation, the rate of movement was relatively slow, 25 mm/hour; the rate changed to rapid movement by the night of September 24, 1982 (Krahn 1984). Probably, the slide was marginally stable, and toe erosion by the Thompson River caused a slow reactivation of the slide during the first 2 days of movement. During this period, cracks developed in the displaced mass. Martin et al. (1984) showed the effect of rainfall infiltration in cracks on the acceleration of a slow moving slide. Because of the high water table and access to a perched water table at the Goddard Slide scarp, the newly developed cracks in the Goddard Slide may have filled with water, and the rate of movement may have increased to a rapid state. Once movement increased, the geometry of the slide changed, and the water supply from the perched water table became disconnected from the head of the slide. This combination of change of geometry to more stable geometry and drainage of cracks may have reduced the rate of movement. The movement finally ceased on September 25, 1982.

3.6. CONCLUSIONS

Slides in the Ashcroft area moved rapidly in the late 1800s, the result of retrogressions of existing rupture surfaces or movements on new deeper rupture surfaces. Today, these slides are reactivated, retrogressive, multiple, very slow to extremely slow moving (rate of movement slower than 1.6 m/year), translational, earth slides. The main movements occur through the non-swelling clay layers in the rhythmically-bedded silt and clay glacial sediment (unit 2) on more than one rupture surface. These rupture surfaces follow the weakest layers in unit 2. There is evidence to suggest that these weak layers may be continuous through all the slides examined.

The movement frequency in the area and our analysis of the sliding mechanism show that the main triggers for recent slide movements are river level changes. A drawdown mechanism after periods of high flow may significantly contribute to the slide movements during reactivations of these slides with river erosion protection, Slide CN50.9 and South Slide. On the other hand, reactivations of slides without toe erosion protection are more likely due to changes of toe geometry by river erosion. Study of the acceleration behaviours of slides during their reactivations shows the significance of average groundwater pressure on rupture surfaces during drawdown periods.

The possibility of rapid to very rapid movement (rate between 1.8 m/hr and 5 m/sec) due to retrogression of the slides with a travel angle higher than the residual friction angle of the rupture surface should be considered. Thompson River down-cutting may expose deeper, weak clay layers, which in turn may lead to new rapid movements of the slides. The rate of movement during reactivation is very slow (slower than 1.6 m/year), but there is a possibility of rapid reactivation (rate between 1.8 m/hr and 3 m/min) of the slides if the slide mass is wet and has access to water to fill cracks.

3.7. REFERENCES

Armstrong, J. E., Crandell, D. R., Easterbrook, D. J., and Noble, J. B. 1965. Late Pleistocene stratigraphy and chronology in southwestern British Columbia and western Washington. Geological Society America Bulletin, **76**: 321-330.

Clague, J. J., and Evans, S. G. 2003. Geological framework of large historic landslides in Thompson River Valley, British Columbia. Environmental and Engineering Geoscience, **9**: 201-212.

Cruden, D. M., Tedder, K.H., and Thomson, S. 1989. Setbacks from the crests of slopes along the North Saskatchewan River Valley. Canadian Geotechnical Journal, 26: 64-74.

Cruden, D. M., and Varnes, D. J. 1996. Landslide types and processes. In Landslides: Investigation and Mitigation. Edited by Turner, A.K., Schuster, R.L.,. Transportation Research Board, Special report 247. pp. 36-75.

Eshraghian, A., Martin, C. D., and Cruden, D. M. 2005a . Landslides in the Thompson River Valley between Ashcroft and Spence's Bridge, British Columbia. In Proceedings of the International Conference on Landslide Risk Management, Vancouver, Canada, May 31 to June 4, 2005. pp. 437-446.

Eshraghian, A., Martin, C. D., and Cruden, D. M. 2005b . Earth slide movements in the Thompson River Valley, Ashcroft, British Columbia. In Proceedings of the 58th Canadian Geotechnical Conference, Saskatoon, Saskatchewan, Canada, September 18-21, 2005.

Evans, S. G., Cruden, D. M., Bobrowsky, P. T., Guthrie, R. H., Keegan, T. R., Liverman, D. G. E., and Perret, D. 2005. Landslide risk assessment in Canada; a review of recent developments. In Proceedings of the International Conference on Landslide Risk Management, Vancouver, Canada, 31 May- 3 June 2005. A.A. Balkema. pp. 351-434.

Everard, K.A., and Savigny, K.W. 1998. Geotechnical assessment of the Nepa cross-over. Report to Canadian Pacific Railway, Thompson Subdivision, Calgary, Alberta. Bruce Geotechnical Consultants Inc., Vancouver, British Columbia. 32 p.

Fulton, R. J. 1969. Glacial Lake History, Southern Interior Plateau, British Columbia. Geological Survey of Canada, Paper 69-37.

Hawson, H.H. 1977. Slide area, mile 50.6 Thompson Subdivision. Report to Canadian Pacific Railway, Calgary, Alberta. Golder Association, Kamloops, British Columbia. 10 p.

Hungr, O., Corominas, J., and Ebehardt, E. 2005. Estimating landslide motion mechanism, travel distance and velocity. In Proceedings of The International Conference on Landslide Risk Management, Vancouver, Canada, 31 May - 3 June. A.A. Balkema. pp. 99-128.

Johnsen, T. F., and Brennand, T. A. 2004. Late-glacial lakes in the Thompson Basin, British Columbia: paleogeolography and evolution. Canadian Journal of Earth Science, **41**: 1367-1383.

Keegan, T., Abbot, B., Cruden, D., Bruce, L., and Pritchard, M. 2003. Railway ground hazard risk scenario: River erosion: Earth-slide. In Proceedings of the 3rd Canadian Conference on Geotechnique and Natural Hazards, Edmonton, Alberta, 9-10 June, 2003. Canadian Geotechnical Society. pp. 269-277.

Kosar, K., Revering, K., Keegan, T., Black, K., and Stewart, L. 2003. Use of spaceborne InSAR to characterize ground movements along a rail corridor and open pit mine. In Proceedings of the 3rd Canadian Conference on Geotechnique and Natural Hazards, Edmonton, Alberta, 9-10 June, 2003. Canadian Geotechnical Society. pp. 177-184.

Krahn, J. 1984. Geotechnical evaluation of the Goddard Landslide. Report to Canadian Pacific Railway, Vancouver Division, Thompson Subdivision. EBA Engineering Consultants Ltd, Report 306-0950. 26 p.

Martin, R.L., Williams, D.R., Balanko, L.A., and Morgenstern, N.R. 1984. The Grierson Hill slide, Edmonton, Alberta. In Proceedings of 37th Canadian Geotechnical Conference: Canadian case histories - landslides. Toronto, Ont. Canadian Geotechnical Society, pp. 125-133.

Monger, J.W.H., and McMillan, W.J. 1989. Geology, Ashcroft, British Columbia. Geological Survey of Canada. Map 42-1989, sheet 1, scale 1:250000.

Morgenstern, N. R. 1986. Goddard landslide of September, 1982, summary of the opinion of Norbert R. Morgenstern. Report prepared for court between Canadian Pacific Limited and Highland Valley Cattle Company Limited. Supreme Court of British Columbia, Vancouver registry No. C841694. 16 p.

Nachtigal, B.J. 2001. Ashcroft 51 landslide: September 2001 instrumentation installations. Report to Canadian National Railway, Edmonton, Alberta. Bruce Geotechnical Consultants Inc., Kamloops, British Columbia. 15 p.

Nachtigal, B.J. 2004a. Thomson 52.80 westcap geotechnical investigations, Volume 2. Report to Canadian Pacific Railway, Calgary, Alberta. Bruce Geotechnical Consultants Inc., Kamloops, British Columbia. 100 p.

Nachtigal, B.J. 2004b. Thompson 52.80 westcap geotechnical investigations, Volume 3. Report to Canadian Pacific Railway, Calgary, Alberta. Bruce Geotechnical Consultants Inc., Kamloops, British Columbia. 90 p.

Pitchard, M., and Baumgard, A. 2003. Ashcroft 51 landslide: June 2003 instrumentation installations. Report to Canadian National Railway, Edmonton, Alberta. Bruce Geotechnical Consultants Inc., Vancouver, British Columbia. 30 p.

Popescu, M. E. 1994. A suggested method for reporting landslide causes. Bulletin of the International Association of Engineering Geology, **50**: 71-74.

Porter, M., and Savigny, K.W. 2001. Geotechnical evaluation of the North Slide - Mile 51.7 Thompson Subdivision. Report to Canadian Pacific Railway, Thompson subdivision. Bruce Geotechnical Consultants Inc., Vancouver, British Columbia. 70p.

Porter, M. J., Savigny, K. W., Keegan, T. R., Bunce, C. M., and MacKay, C. 2002. Controls on stability of the Thompson River landslides. In Proceedings of the 55th Canadian Geotechnical Conference: Ground and Water: Theory to Practice, Niagara Falls, Ontario, 20-23 October 2002. Canadian Geotechnical Society. pp. 1393-1400.

Ryder, J. M. 1976. Terrain inventory and Quaternary geology, Ashcroft, British Columbia, Geological Survey of Canada, Ottawa.

Skempton, A. W. 1969. The consolidation of clays by gravitational compaction. Journal of the Geological Society, **125**: 373-407.

Stark, T. D., and Eid, H. T. 1994. Drained residual strength of cohesive soils. Journal of Geotechnical Engineering, **120**: 856-871.

Stanton, R. B. 1898. The great land-slides on the Canadian Pacific Railway in British Columbia. Proceedings of the Institution of Civil Engineers, **132**: 1-48.

Toy, J.A., Hollinrake, J.A., and Taggart, J.A. 1990. Canadian Pacific Ltd. versus Highland Valley Cattle Company Limited. British Columbia Court of Appeal, Vancouver, B.C.J. No. 1860.

Vanwieren, R., and MacLeod, N.R. 1988. Goddard Slide Mile 50.4 Thompson River subdivision, Report 0306-34170. Report to Canadian Pacific Railway, Vancouver Division, Thompson Subdivision. EBA Engineering Consultants Ltd. 10 p.

Wallace, J. 1987. Reason for Judgment: Canadian Pacific Ltd. versus Highland Valley Cattle Company. In the Supreme Court of British Columbia, Vancouver, Vancouver registry number C841694, B.C.J. No. 218.

Yaremko, E. K. 2002. Thompson River, MP 50.9, Ashcroft Subdivision assessment of flow hydraulics, enlarged berm. Report to Canadian National Railway, Edmonton, Alberta. Norhtwest Hydroulic Consultants ltd. (NHC), Edmonton, Alberta. 20 p.

Table 3.1. Volumes and areas of the five active landslides (Figure 3.1)

Landslide	Area (ha)	Volume (Mm^3)
1) CN50.9	15.1	3.3[a]
2) Goddard	9.7	2.0[a]
3) North Slide	58.7	21.4[a]
4) South Slide	27.5	9.0[a]
5) Basque	5.8	1.8[b]

[a] Estimated using a GIS program

[b] Approximated from Cruden and Varnes (1996) formula

Table 3.2. Soil parameters of glaciolacustrine unit (unit 2) at the Thompson River valley

Slide Name	Clay (%)	Liquid Limit (LL) (%)	Plastic Limit (PL) (%)	Plasticity Index (PI) (%)	Water Content (%)	Activity [f]	Liquidity Index [g]	φ_r (°)
1) CN50.9[a]	(48-80)[e]	(66-79)	(22-29)	(44-50)	30	(0.63-0.92)	0.1	11[c]
	59	73	26	47		0.77		
2) Goddard[a]	(30-60)	(45-65)	(22-27)	(20-43)	(21-31)	(0.67-0.72)	(0.1-0.3)	15[c]
	45	56	25	31	28	0.69	0.18	
3) North Slide[a]	(80-84)	(48-85)	(24-34)	(24-54)	(27-43)	(0.58-0.67)	(0.12-0.27)	12[c]
	81	72	29	43	36	0.6	0.18	
4) South Slide[a]	(18-88)	(40-99)	(23-29)	(17-76)	(17-39)	(0.5-0.9)	(-1.1-0.49)	15[c]
	47.3	58	24	35	27	0.77	0.02	
South Slide[b]	(82-87)	(67-76)	(30-33)	(37-43)	(45-47)	(0.45-0.49)	(0.34-0.40)	(12.8-13.1)
(Clay seam)	84.5	71.5	31.5	40	46	0.47	0.37	13.0[d]
South Slide[b]	(33-34)	(41-42)	(23-23)	(18-19)	(30-36)	(0.55-0.56)	(0.40-0.71)	(23.9-31.2)
(Silt)	33.5	41.5	23	18.5	33	0.55	0.55	27.5[d]
5) Basque[a]	(32-60)	(40-69)	(19-27)	(21-42)	(14-34)	(0.6-0.7)	(-0.3-0.11)	15[c]
	48	55	24	31	21	0.65	-0.12	

[a] Laboratory data from Nachtigal (2001), Krahn (1984), Porter and Savigny (2001), Nachtigal (2004a), and Everard and Savigny (1998)

[b] Sample tested at University of Alberta

[c] Residual friction angle from Stark and Eid's correlation (Stark and Eid 1994)

[d] Residual friction angle from direct shear test conducted by authors

[e] numbers in parentheses are ranges of the data

[f] Plasticity Index/ % Clay

[g] (in-situ water content – Plastic Limit)/ Plasticity Index

Table 3.3. Surface of rupture elevations in different slides

Landslide	River Level (m) [a]	Deeper Rupture Surface Elev. (m)	Shallower Rupture Surface Elev. (m)
1) CN50.9	282.6	275.7	280.9
2) Goddard	275.8	270.6	278.1
3) North Slide	273.2	264.2	269.4
4) South Slide	269.2	263.7	272.7

[a] . River level at the site in May 2003 based on LiDAR data at that date.

Table 3.4. Summary of slide movements in the Ashcroft area

Landslide	Most recent retrogression[a]	Retrogression movement rate [a]	Number of Reactivations (1970-2000)	Reactivation movement rate [b] (mm/year)	Higher reactivation movement rate rupture surface	Travel angle (°)
1) CN50.9	September 22, 1897	Rapid	4	3-20	Deeper	16
2) Goddard	October 19, 1886	Very rapid	3	20-400[c]	Shallower	14
3) North Slide	October 14, 1880	Very rapid	2	10-110	Shallower	6
4) South Slide	Pre 1885	No information	3	4-35	Shallower	13
5) Basque	Pre 1897	No information	2	3-15	Deeper	17

[a] Estimated from evidence reported by Clague and Evans (2003) and Porter et al. (2002)

[b] Estimated from inclinometer data and InSAR data by Kosar et al. (2003)

[c] Rate of movement during summer 1982 was much higher than this range (6 m/hour)

Table 3. 5. Average pore pressure ratio (r_u) and rate of movement at each movement period for the deeper rupture surface of Slide CN50.9

Period	$r_{u(average)}$[a]	Movement rate (mm/year)
(8-Apr.-2001) to (15-Feb.-2002)	0.213	3.4
(15-Feb.-2002) to (1-Jul.-2002)	0.204	0.5
(1-Jul.-2002) to (15-Dec.-2002)	0.218	4.2
(15-Dec.-2002) to (1-Jul.-2003)	0.203	0.9
(1-Jul.-2003) to (1-Nov.-2003)	0.210	2.7
(1-Nov.-2003) to (1-Mar.-2004)	0.198	0.3

[a] average pore pressure ratio on the deeper rupture surface during the drawdown period calculated from piezometric elevation in boreholes Bh1 and Bh10

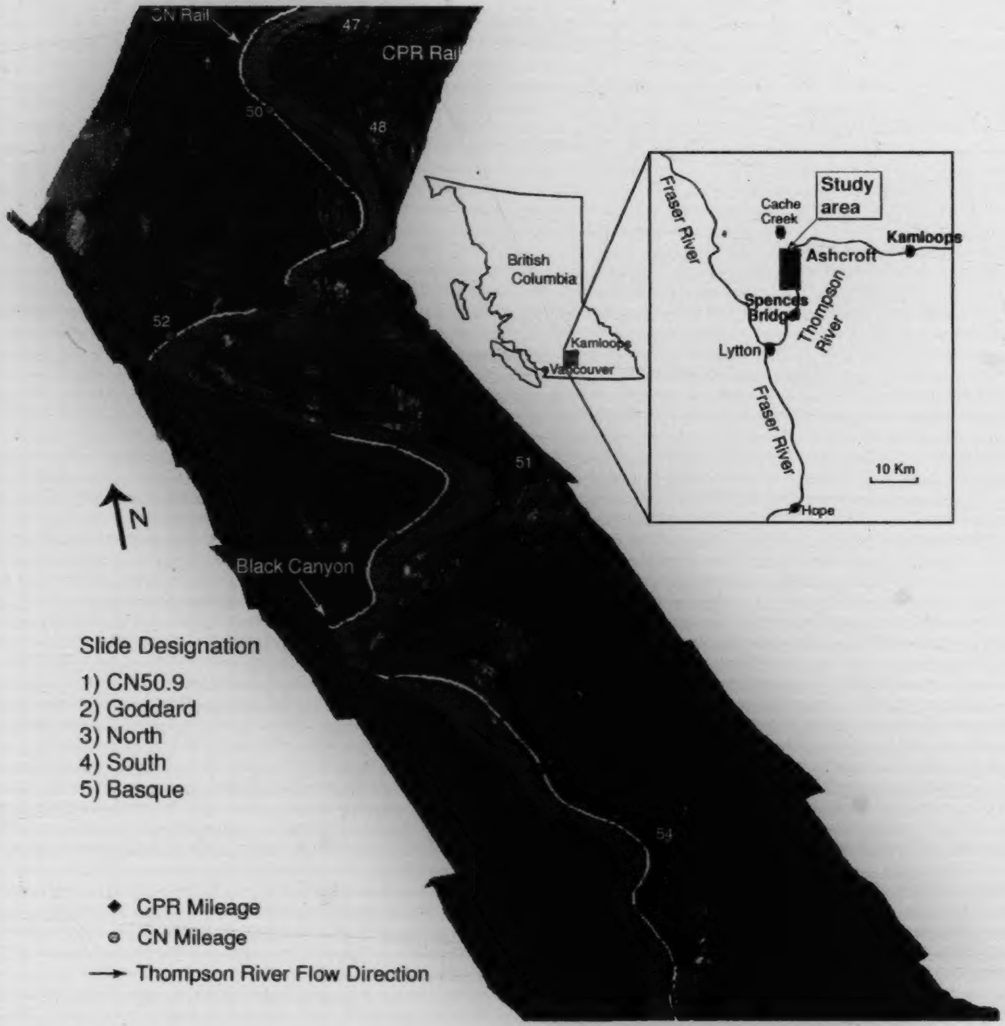
CN Rail
47
CPR Rail
50
48
52
51
Black Canyon
54
N
Slide Designation
1) CN50.9
2) Goddard
3) North
4) South
5) Basque
◆ CPR Mileage
● CN Mileage
→ Thompson River Flow Direction
British Columbia
Kamloops
Vancouver
Fraser River
Study area
Cache Creek
Ashcroft
Kamloops
Spences Bridge
Thompson River
Lytton
Fraser River
10 Km
Hope

Figure 3.1. Landslides south of Ashcroft, BC, between 50° 10′ to 50° 20′ N and 121° 15′ to 121° 20′ W.

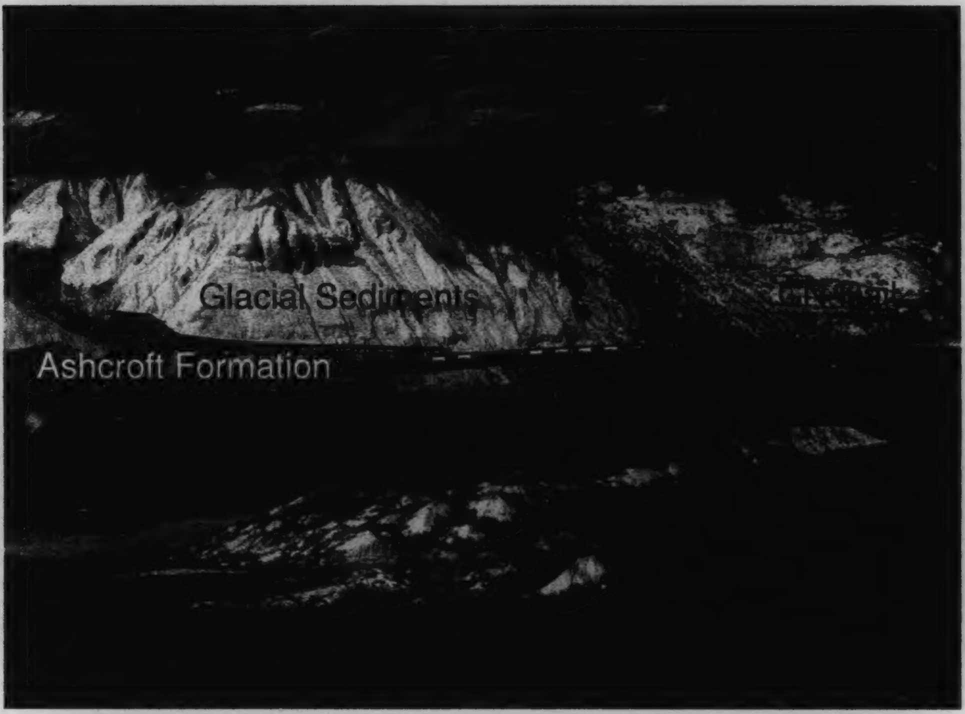
Glacial Sediments
Ashcroft Formation

Figure 3.2. Contact between the overlying sediments and the Ashcroft Formation (marine argillite, siltstone, sandstone, conglomerate, and minor carbonate of Jurassic age) at CN mileage 54 (see Figure 3.1 for location).

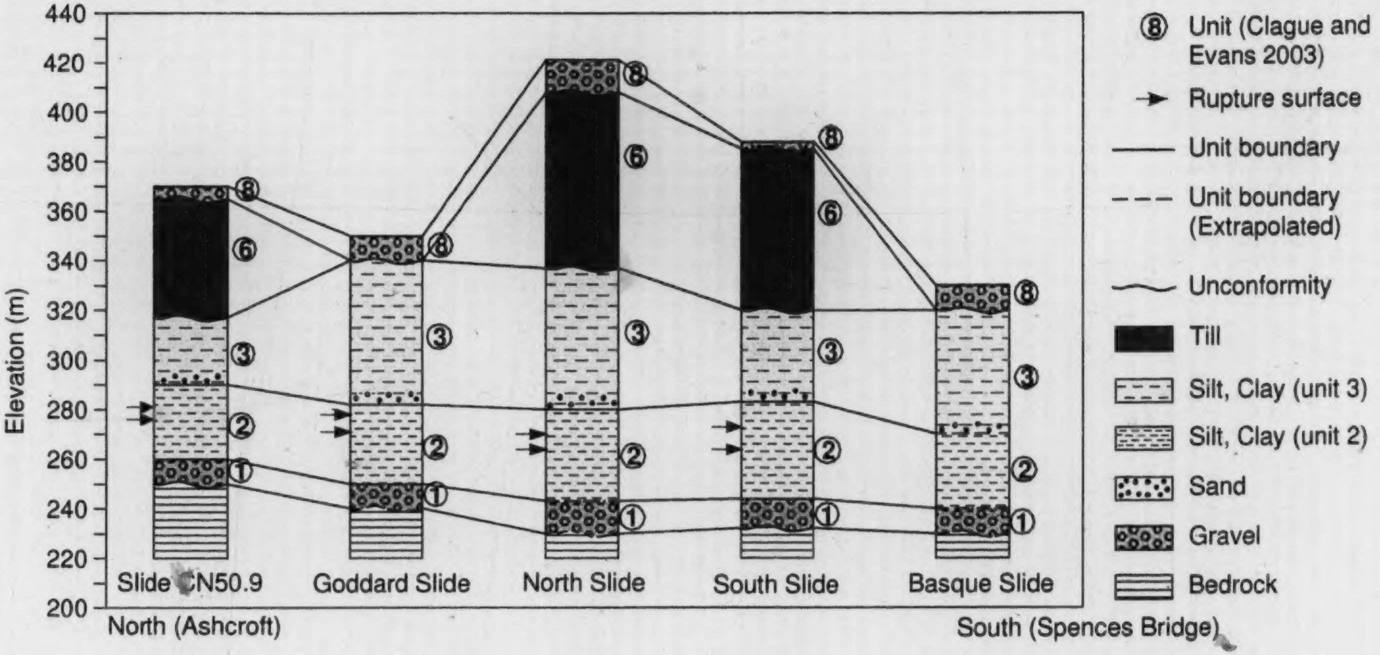
Elevation (m)
440
420
400
380
360
340
320
300
280
260
240
220
200
Slide CN50.9
Goddard Slide
North Slide
South Slide
Basque Slide
North (Ashcroft)
South (Spences Bridge)
⑧
⑥
③
②
①
⑧ Unit (Clague and Evans 2003)
Rupture surface
Unit boundary
Unit boundary (Extrapolated)
Unconformity
Till
Silt, Clay (unit 3)
Silt, Clay (unit 2)
Sand
Gravel
Bedrock

Figure 3.3. Geological units in the earth slides and highland terraces in Ashcroft area (the horizontal distance is not to scale)

Figure 3.4. Silt and clay layers in unit 2, at the Goddard Slide toe (Figure 3.1).

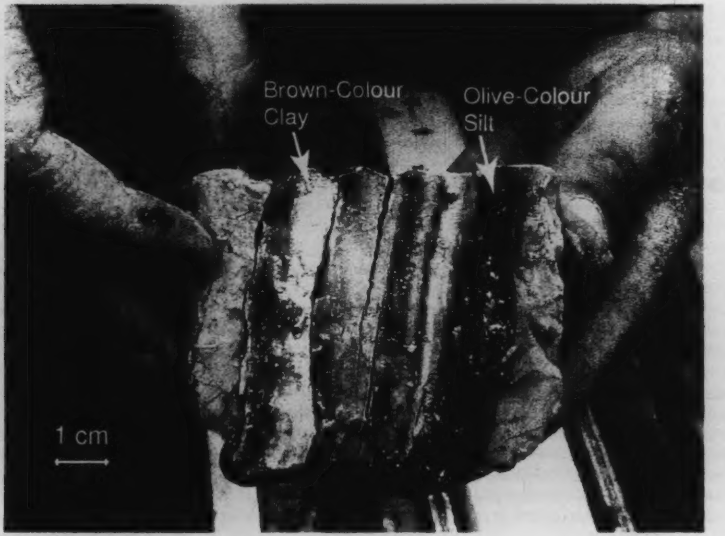

Brown-Colour Clay
Olive-Colour Silt
1 cm

Figure 3.5. Sample of silt-clay layer, unit 2, from a borehole at South Slide (Figure 3.1).

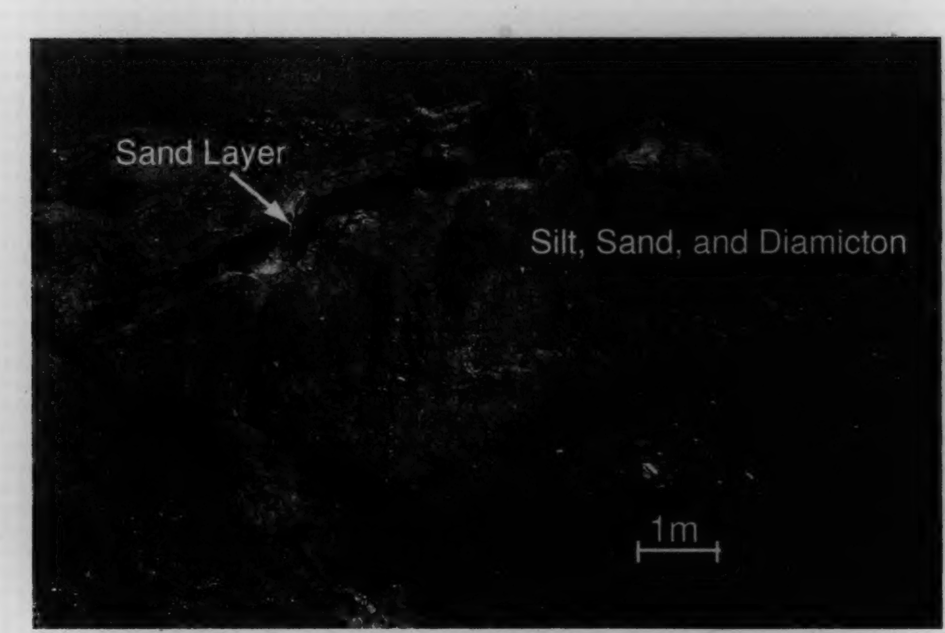
Sand Layer
Silt, Sand, and Diamicton
1m

Figure 3.6. Sand, silt, and diamicton of unit 3 at Goddard Slide scarp (Figure 3.1).

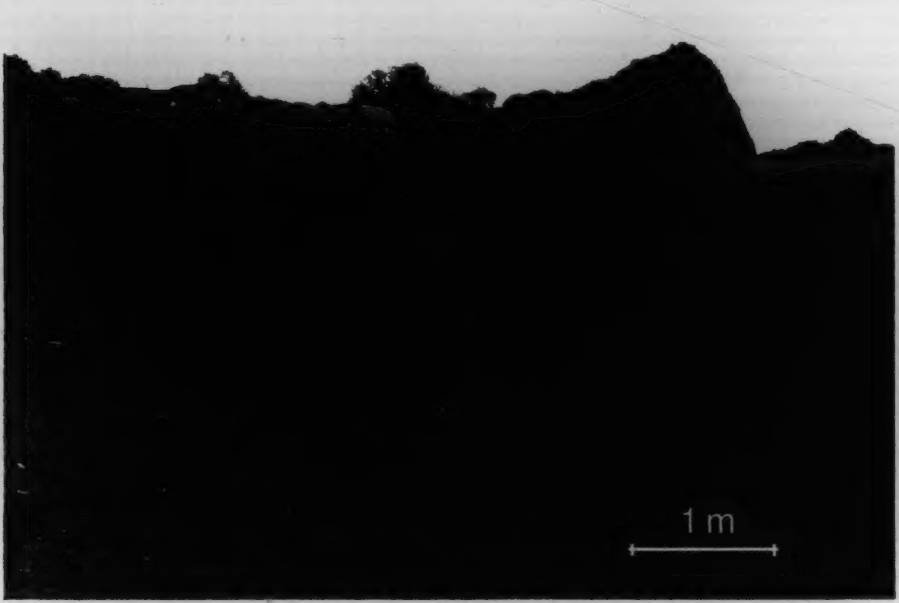

Figure 3.7. Silt, clay, and diamicton (till) unit 6 at South Slide scarp (Figure 3.1).

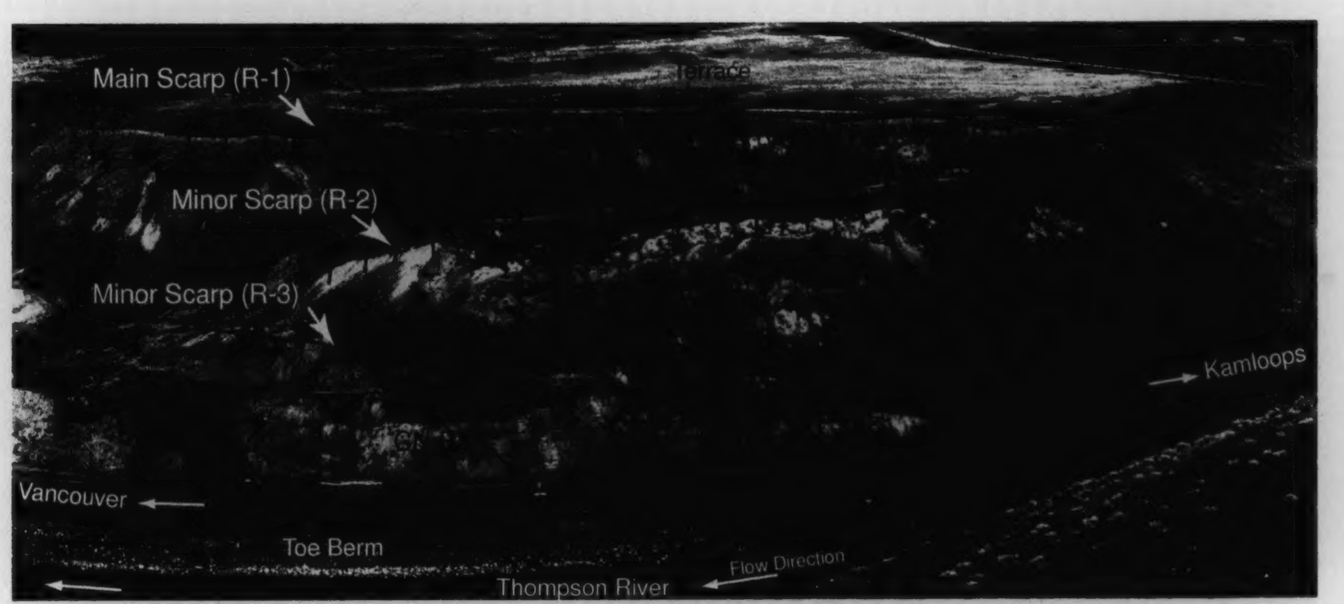
Main Scarp (R-1)
Terrace
Minor Scarp (R-2)
Minor Scarp (R-3)
Kamloops
Vancouver
Toe Berm
Flow Direction
Thompson River

Figure 3.8. A view from the east of Slide CN50.9 with its three scarps, CN track, Thompson River, and toe berm (Figure 3.1)(the slide wide is 600 m at the river level)

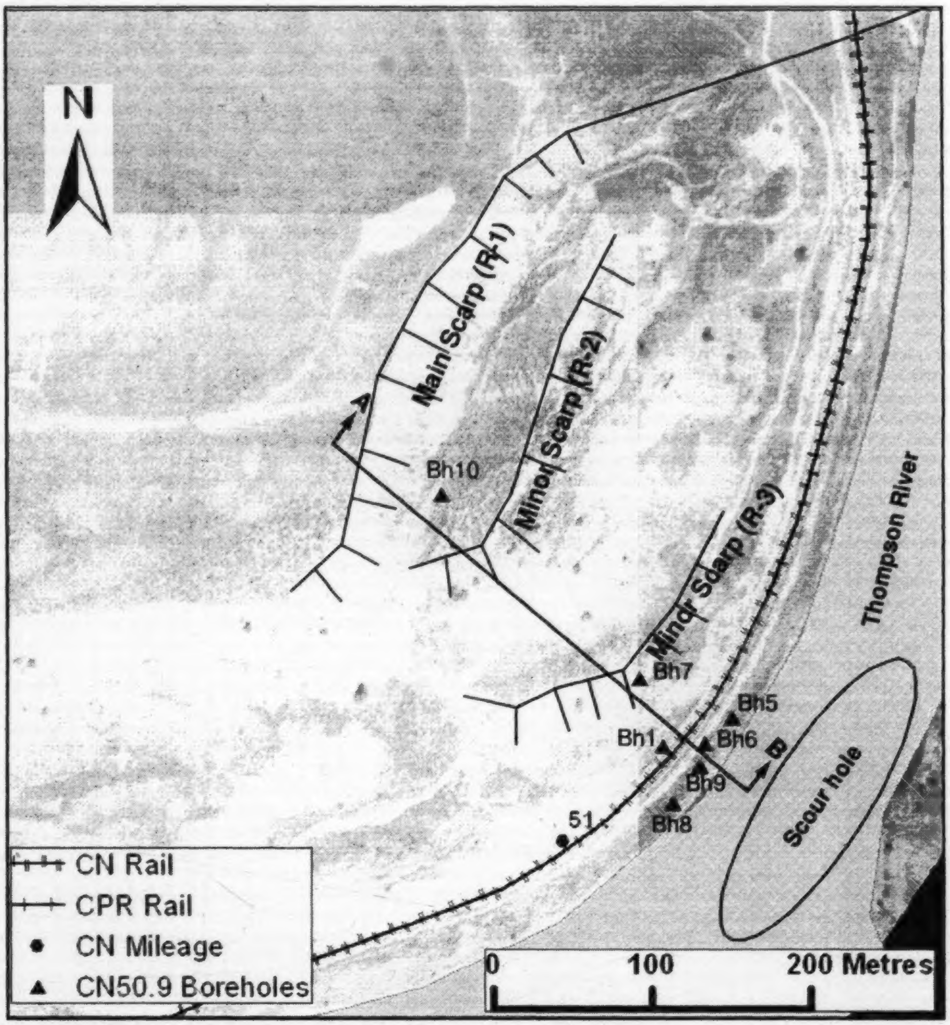
N
Main Scarp (R-1)
Minor Scarp (R-2)
Minor Scarp (R-3)
Thompson River
A
B
Bh10
Bh7
Bh5
Bh1
Bh6
Bh9
Bh8
51
Scour hole
CN Rail
CPR Rail
CN Mileage
CN50.9 Boreholes
0
100
200 Metres

Figure 3.9. A plan view of Slide CN50.9 showing the cross-section line, scarps, and borehole positions.

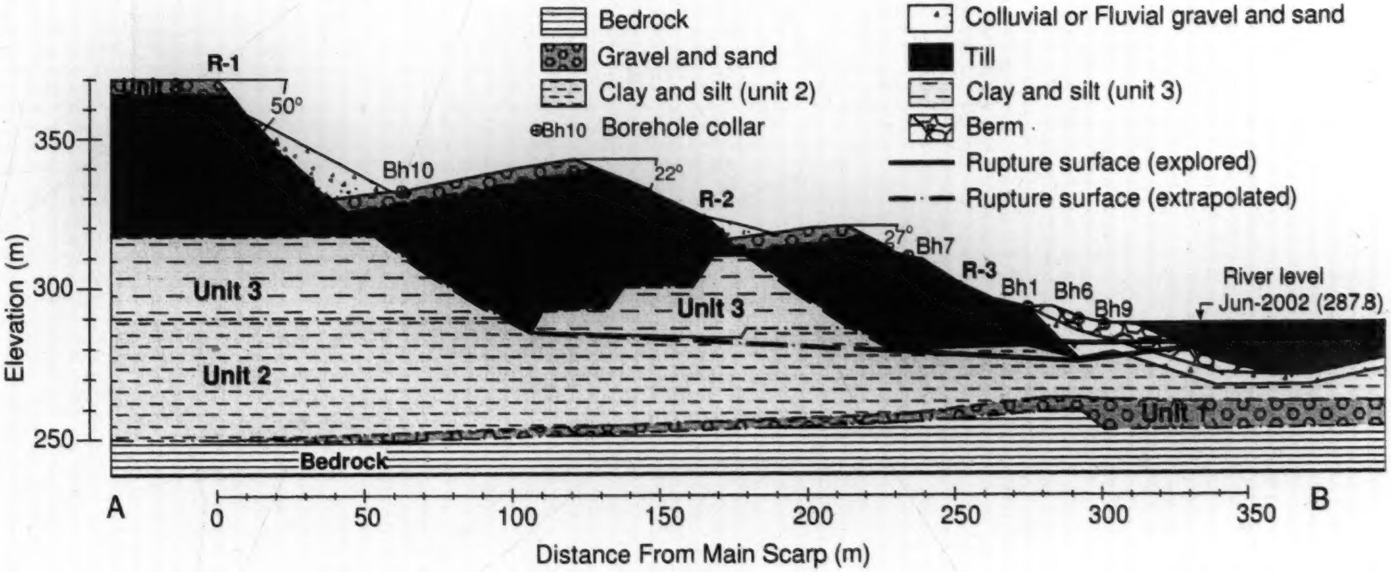
Bedrock
Gravel and sand
Clay and silt (unit 2)
Bh10 Borehole collar
Colluvial or Fluvial gravel and sand
Till
Clay and silt (unit 3)
Berm
Rupture surface (explored)
Rupture surface (extrapolated)
R-1
50°
Bh10
22°
R-2
27°
Bh7
R-3
Bh1
Bh6
Bh9
River level
Jun-2002 (287.8)
Unit 3
Unit 3
Unit 2
Unit 1
Bedrock
Elevation (m)
350
300
250
A
B
0
50
100
150
200
250
300
350
Distance From Main Scarp (m)

Figure 3.10. Cross section through Slide CN50.9 showing rupture surfaces, stratification, and borehole locations (see Figure 3.10 for cross-section position).

Stage	Simplified Cross-section	Description
1	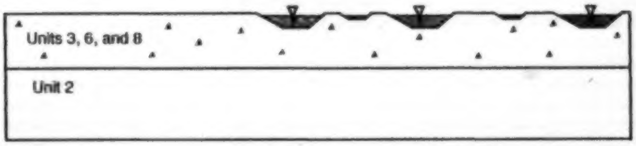 Units 3, 6, and 8 Unit 2	Post-glaciation Stage: Braided river started cutting through the glacial sediments
2	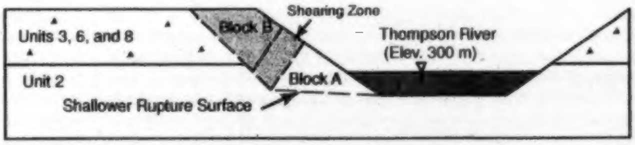 Shearing Zone Block B Units 3, 6, and 8 Thompson River (Elev. 300 m) Unit 2 Block A Shallower Rupture Surface	Pre-Slide Stage: The Thompson River down-cutting reached the first weak layer in the glacial sediments. Blocks A and B were ready to move on this weak layer which was the shallower rupture surface.
3	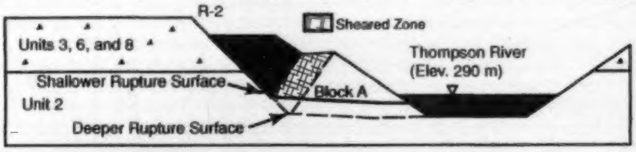 R-2 Sheared Zone Units 3, 6, and 8 Thompson River (Elev. 290 m) Shallower Rupture Surface Block A Unit 2 Deeper Rupture Surface	Retrogression on the Shallower Rupture Surface: Blocks A and B slid on the shallower rupture surface. More Thompson River down-cutting through glacial sediments reached another weak layer in this material.
4	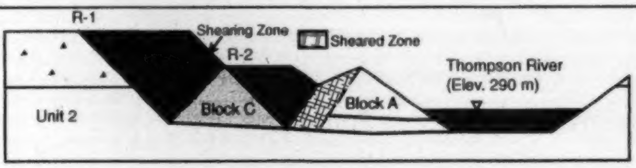 R-1 Shearing Zone Sheared Zone R-2 Thompson River (Elev. 290 m) Block A Unit 2 Block C	Sliding on the Deeper Rupture Surface: More sliding, without retrogression, happened on the deeper rupture surface. The slide is ready for more retrogression on the deeper rupture surface.
5	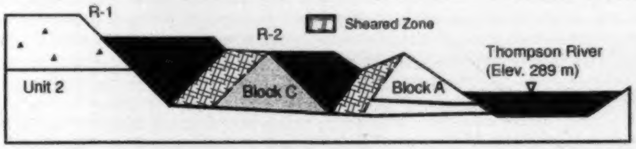 R-1 Sheared Zone R-2 Thompson River (Elev. 289 m) Unit 2 Block C Block A	Retrogression on the Deeper Rupture Surface: September 1897, Blocks C and D sliding on the deeper rupture surface caused retrogression from main scarp. Toe material moved toward the Thompson River.
6	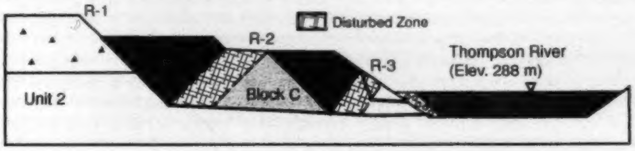 R-1 Disturbed Zone R-2 R-3 Thompson River (Elev. 288 m) Unit 2 Block C	Current Situation: Most of the toe material (Block A) has eroded by the Thompson River. A berm has been built at toe for protection against more toe erosion.

Figure 3.11. Simplified sliding process since deglaciation at Slide CN50.9 (Figure 3.1).

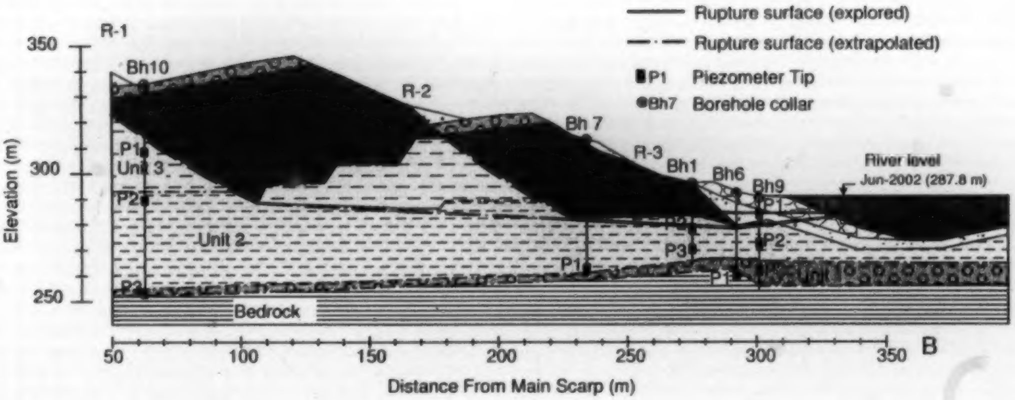
Rupture surface (explored)
Rupture surface (extrapolated)
P1 Piezometer Tip
Bh7 Borehole collar
R-1
R-2
R-3
Bh10
Bh 7
Bh1
Bh6
Bh9
River level
Jun-2002 (287.8 m)
P1
P2
P3
Unit 3
Unit 2
Unit 1
Bedrock
Elevation (m)
350
300
250
50
100
150
200
250
300
350
B
Distance From Main Scarp (m)

Figure 3.12. Piezometer locations at Slide CN50.9.

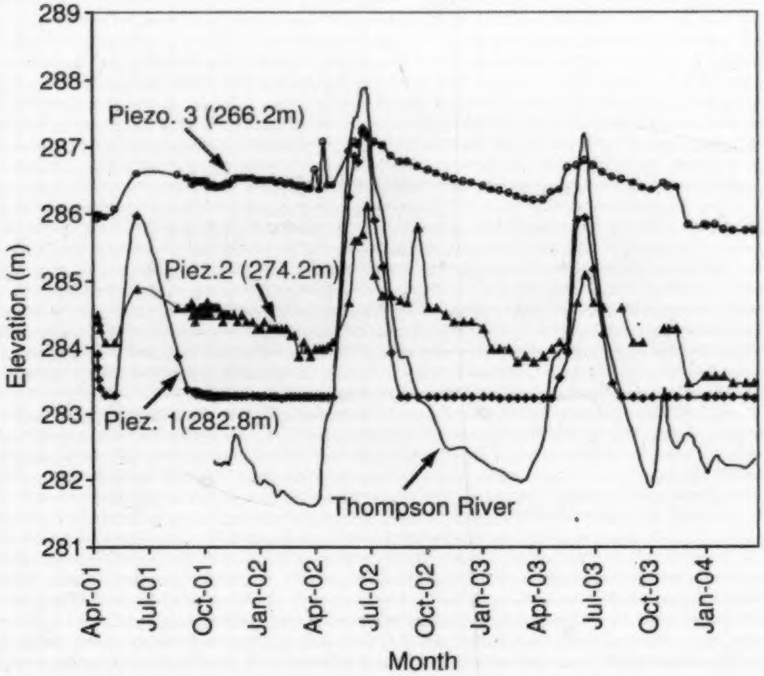

Figure 3.13. Responses of piezometers installed in Borehole Bh1 at the toe of Slide CN50.9 (see Fig. 3.12 for location of Borehole Bh1)

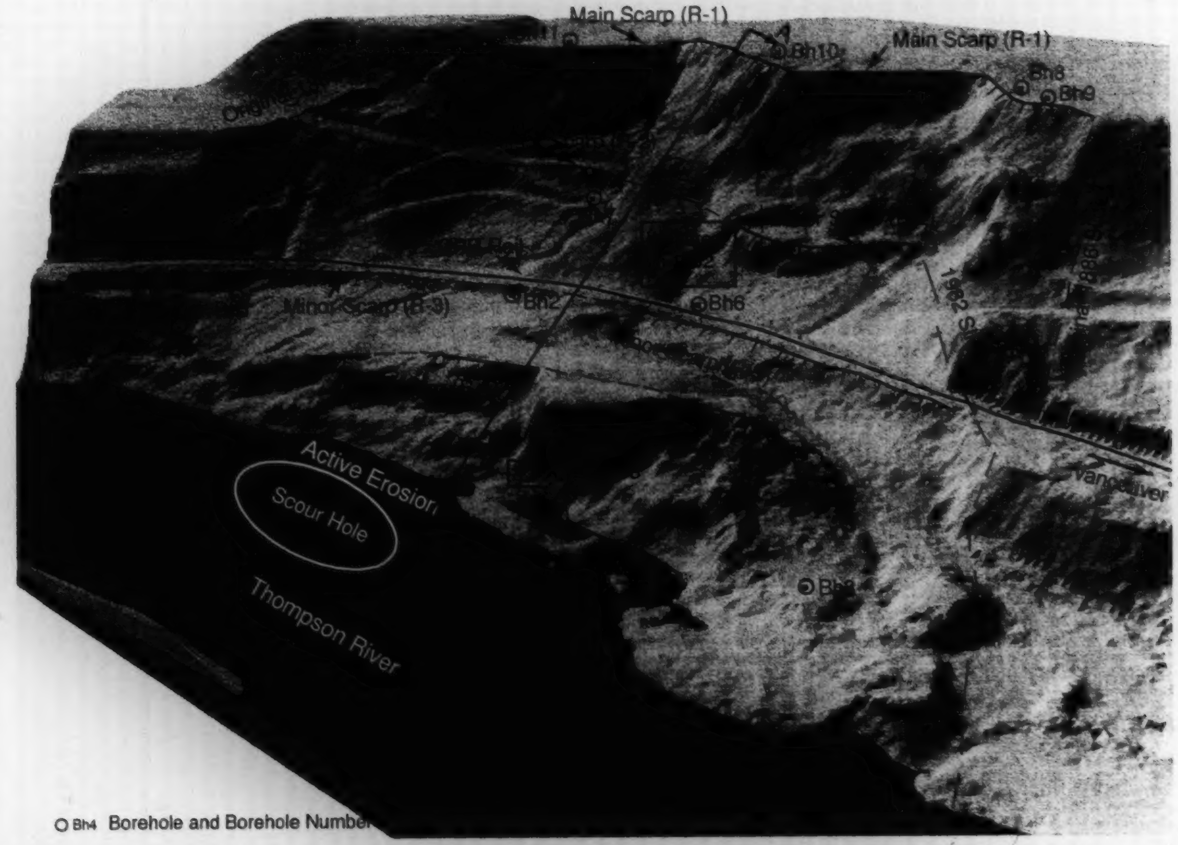
Main Scarp (R-1)
Bh10
Main Scarp (R-1)
Bh8
Bh9
1982 S
Bh6
Bh2
Minor Scarp (R-3)
Active Erosion
Scour Hole
Thompson River
Vancouver
Bh3
Bh4 Borehole and Borehole Number

Figure 3.14. A digital elevation model of the Goddard Slide looking from the southwest showing four scarps, borehole locations, CPR rail line, a scour hole in the Thompson River bed, wet area after 1982 reactivation of the slide area, and limits of 1886 retrogression and 1982 reactivation. At river level the slide is 400m wide.

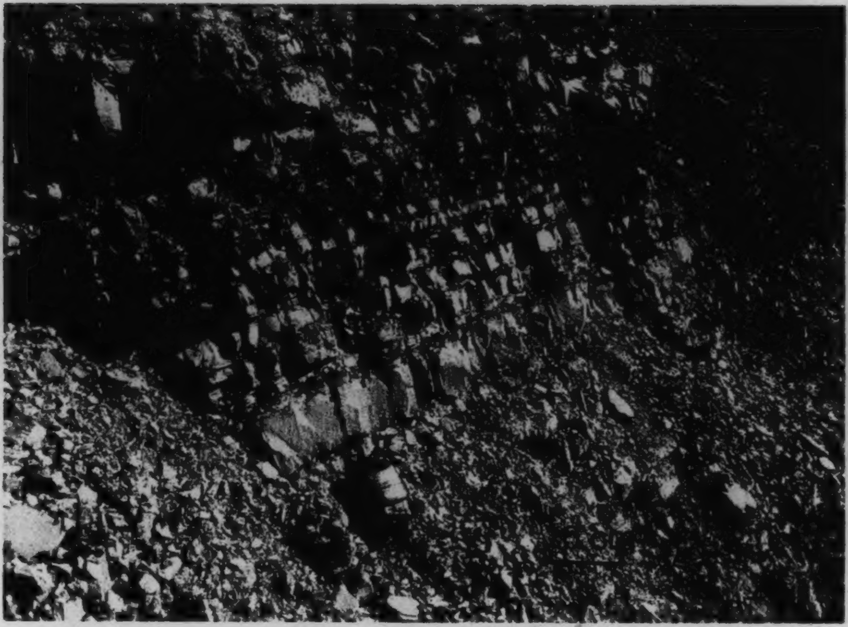

Figure 3.15. Bedded sequence showing the northeast (into the slope) dipping beds at the toe of the Goddard Slide bulging up (See Figure 3.14 for location).

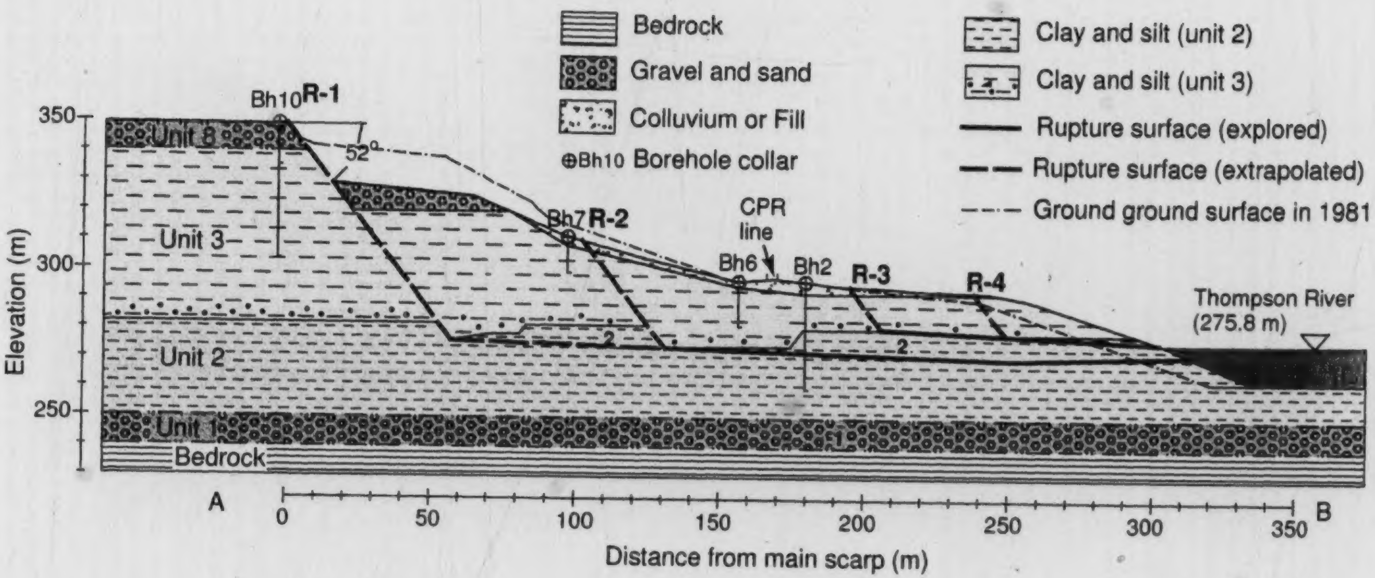
Bedrock
Gravel and sand
Colluvium or Fill
⊕Bh10 Borehole collar
Clay and silt (unit 2)
Clay and silt (unit 3)
Rupture surface (explored)
Rupture surface (extrapolated)
Ground ground surface in 1981
Bh10
R-1
52°
Bh7
R-2
CPR line
Bh6
Bh2
R-3
R-4
Thompson River (275.8 m)
Unit 8
Unit 3
Unit 2
Unit 1
Bedrock
2
1
A
B
350
300
250
Elevation (m)
0
50
100
150
200
250
300
350
Distance from main scarp (m)

Figure 3.16. Cross section after the Goddard 1982 Slide and surface profile before the Goddard 1982 Slide.

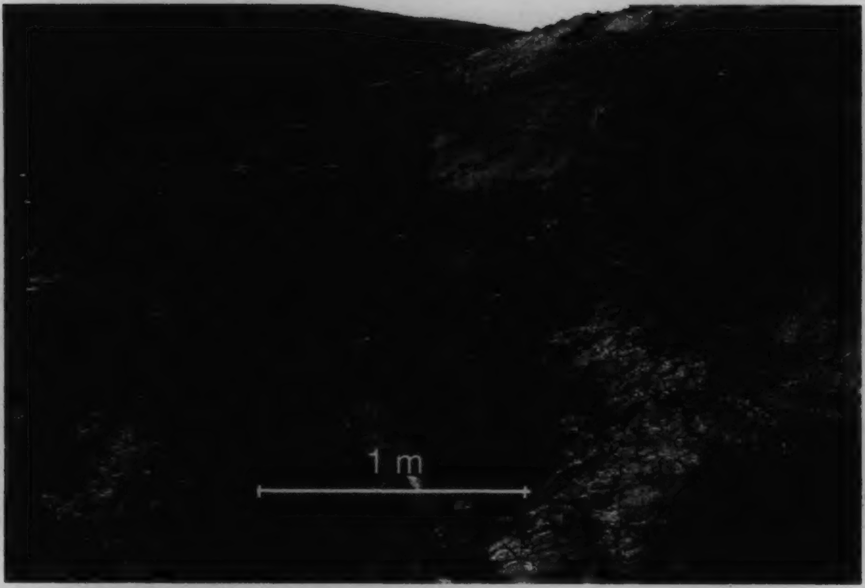

Figure 3.17. New cracks developing at the toe of the Goddard slide observed in May 2005 (probably developed in fall 2004).

Flo
Directio
Thompson

Figure 3.18. Cracks at the Goddard Slide toe resulted from Thompson River erosion.

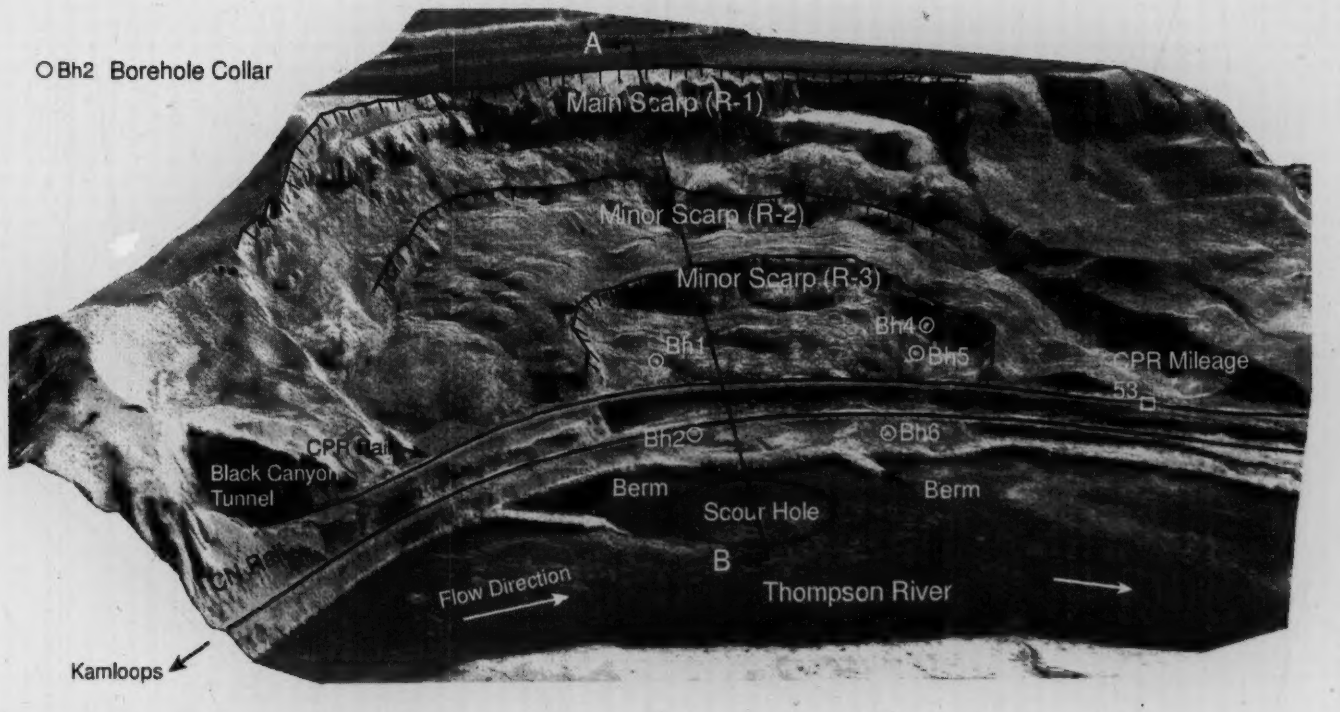
○ Bh2 Borehole Collar
A
Main Scarp (R-1)
Minor Scarp (R-2)
Minor Scarp (R-3)
Bh1
Bh4
Bh5
CPR Mileage
53
Bh2
Bh6
CPR Rail
Black Canyon Tunnel
Berm
Scour Hole
Berm
B
CN Rail
Flow Direction
Thompson River
Kamloops

Figure 3.19. View of the South Slide from the west with its three scarps, CN and CPR rail lines, borehole locations, a scour hole in the Thompson River bed, and the Black Canyon tunnel. At river level the slide is 700 m wide.

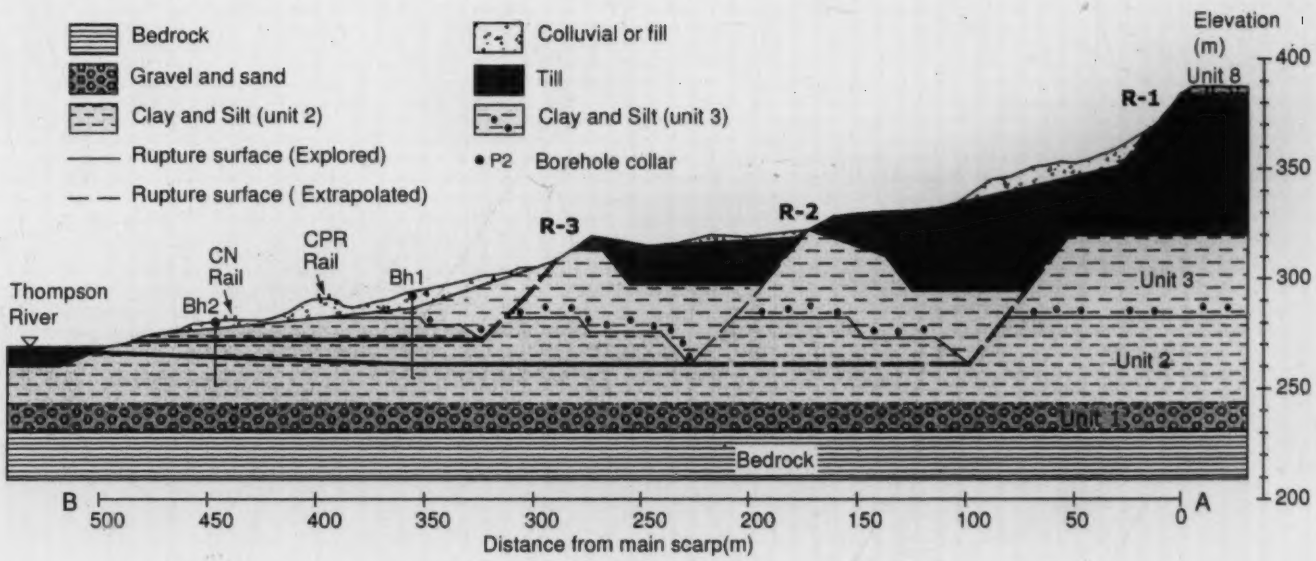
▤ Bedrock
▦ Gravel and sand
▨ Clay and Silt (unit 2)
—— Rupture surface (Explored)
— — Rupture surface (Extrapolated)
▧ Colluvial or fill
■ Till
▨ Clay and Silt (unit 3)
• P2 Borehole collar
Elevation (m)
400
350
300
250
200
Unit 8
R-1
R-2
R-3
Unit 3
Unit 2
Unit 1
Bedrock
Thompson River
CN Rail
CPR Rail
Bh2
Bh1
B
A
500
450
400
350
300
250
200
150
100
50
0
Distance from main scarp(m)

Figure 3.20. Cross section through the South Slide.

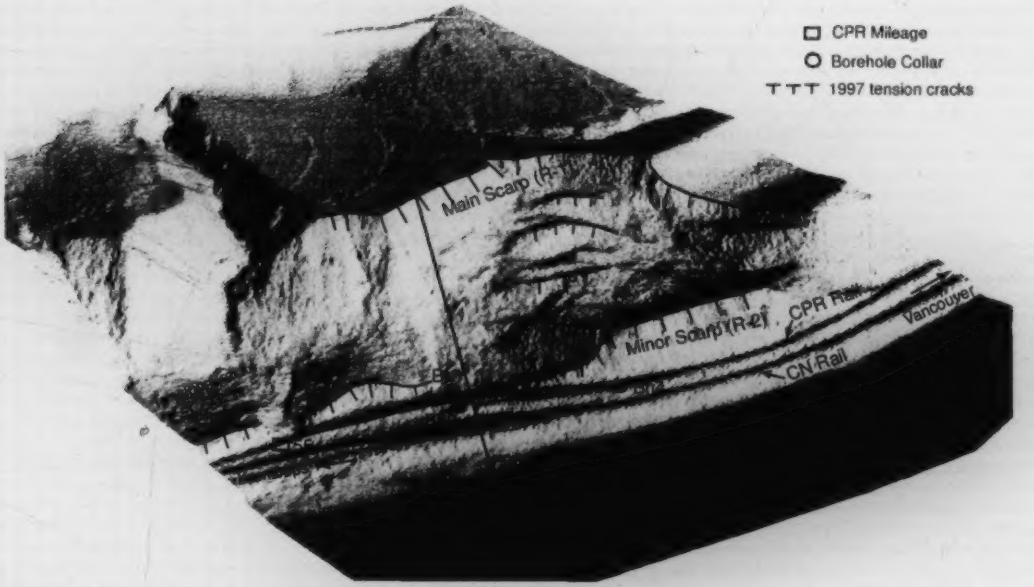
□ CPR Mileage
○ Borehole Collar
┬┬┬ 1997 tension cracks
Main Scarp (R-
Minor Scarp (R-2)
CPR Rail
CN Rail
Vancouver

Figure 3.21. A 3-dimensional view of the Basque Slide from the northwest. At river level the slide is 350 m wide.

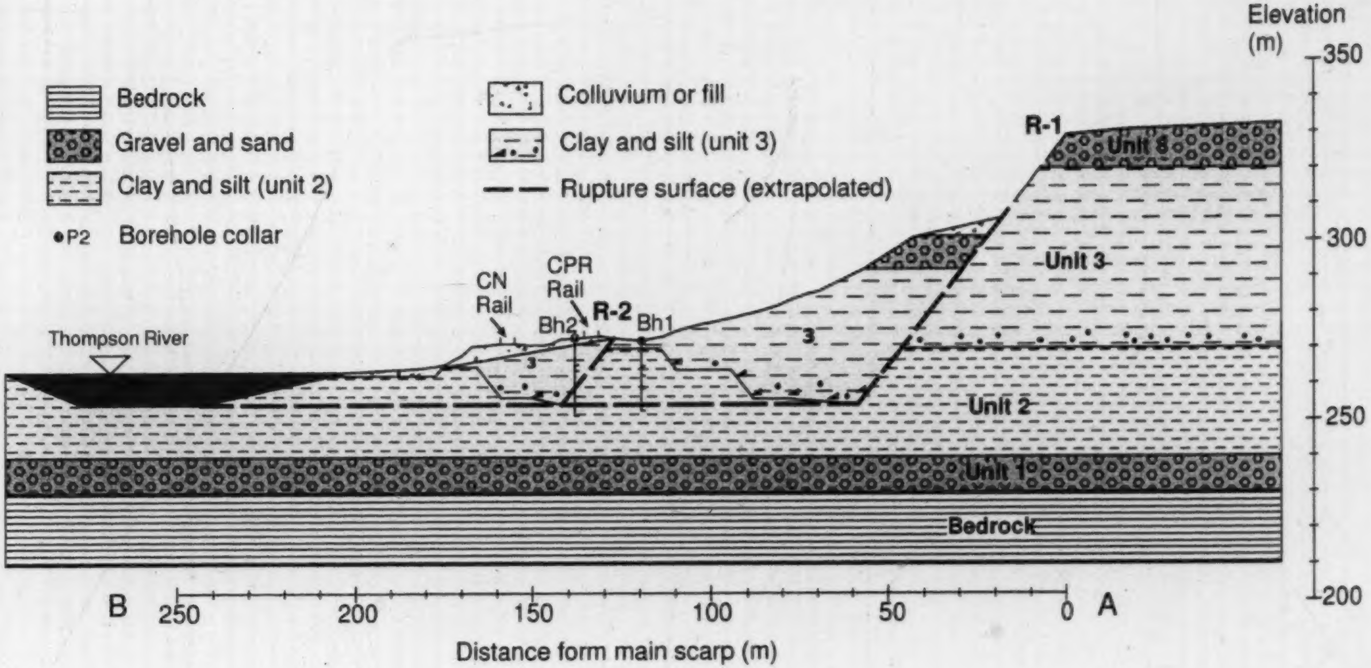
Bedrock
Gravel and sand
Clay and silt (unit 2)
•P2 Borehole collar
Colluvium or fill
Clay and silt (unit 3)
Rupture surface (extrapolated)
Elevation (m)
350
300
250
200
R-1
Unit 6
Unit 3
3
Unit 2
Unit 1
Bedrock
CN Rail
CPR Rail
R-2
Bh2
Bh1
Thompson River
B
A
250
200
150
100
50
0
Distance form main scarp (m)

Figure 3.22. Cross section through the Basque Slide.

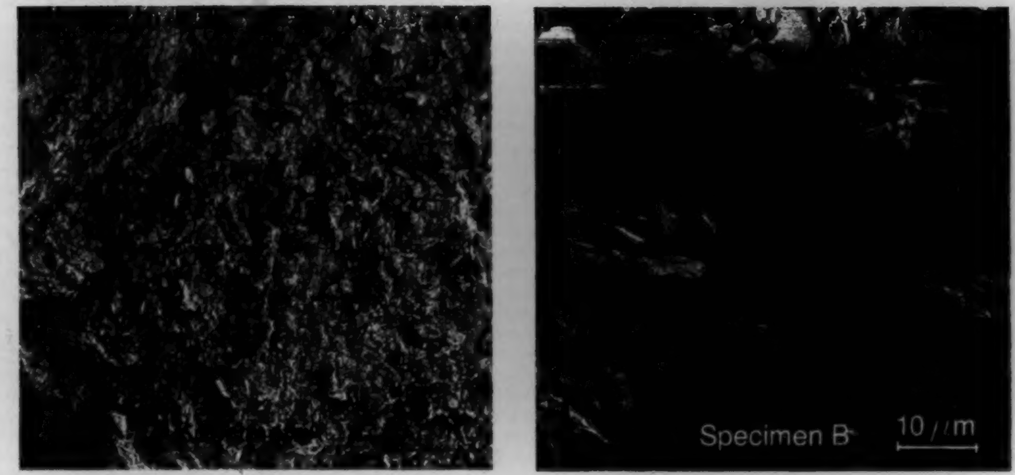

Figure 3. 23. SEM photographs of Sample A, the plastic brown clay layer forming the shear zone of the South Slide, and Sample B, the silty clay layer at South Slide.

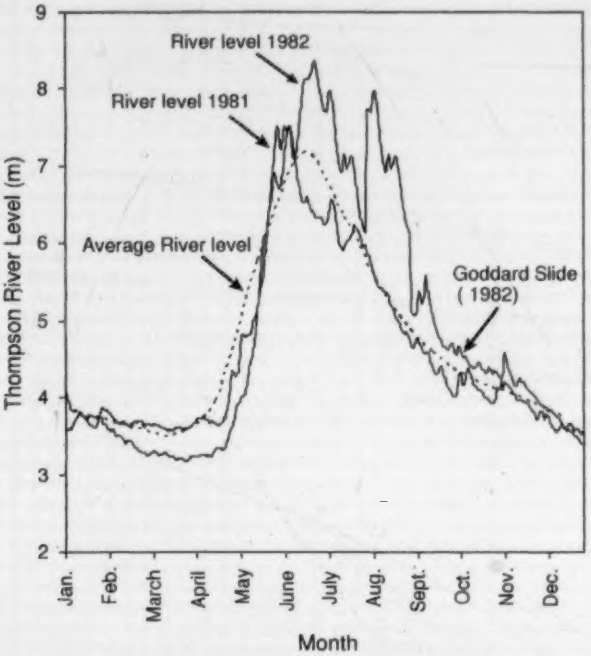

Figure 3.24. Comparison of the Thompson River level in an active year (1982) and non-active year (1981) with the average flow for 1911 to 2000.

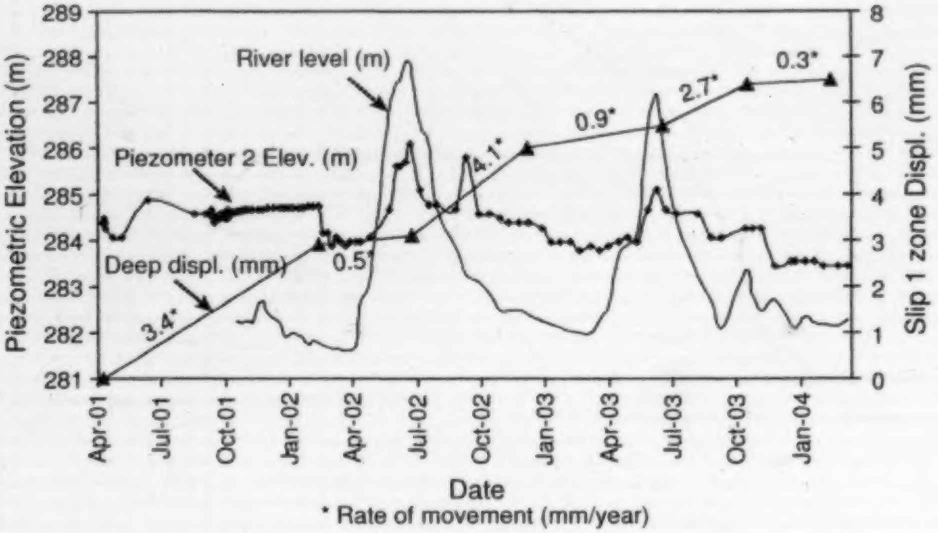

Figure 3.25. Thompson River level, groundwater level and movement rate on the deeper rupture surface in Slide CN50.9 between April 2001 and January 2004.

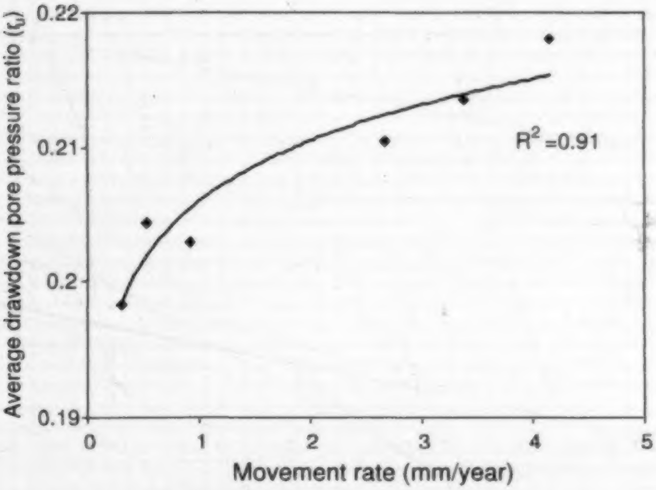

Figure 3.26. Relationship between movement rate of Slide CN50.9 and pore-pressure ratio for the deeper rupture surface during reactivation.

Chapter 4

Movement Triggers and Mechanisms of the Earth Slides in the Thompson River Valley[1]

4.1. INTRODUCTION

Large translational landslides are common hazards within river valleys of western Canada. Slides in the Peace River Lowlands in Saskatchewan (Miller and Cruden 2002), Little Smoky River Valley in Alberta (Thomson and Hardy 1975, and Brooker and Peck 1993), North Saskatchewan River Valley in Alberta (Martin et al. 1984, Pennell 1969), South Saskatchewan River Valley in Saskatchewan (Haug et al. 1977, Yoshida and Krahn 1985, Christiansen and Sauer 1984), Nichola River Valley in Merritt, British Columbia (Chin et al. 1984), Muddy Lake near town of Unity in Saskatchewan (Richardson 1984), Battle River Valley in Alberta (Thomson and

---

[1] Submitted paper:

A version of this chapter has been submitted for publication to Canadian Geotechnical Journal. Eshraghian, A., Martin, C.D., Morgenstern, N.R., Movement triggers and mechanisms of two earth slides in the Thompson River Valley, British Columbia, Canada.

Published paper:

Part of this chapter has been published in the 59th Canadian Geotechnical Conference, October 2006, Vancouver, British Columbia. Eshraghian, A., Martin, C.D., and Morgenstern, N.R., 2006. Groundwater and movements of earth slides in the Thompson River Valley.

Tweedie 1978, Cruden et al. 1995), and Chilliwack River Valley in British Columbia (Fletcher et al. 2002) are examples of these large translational landslides.

River down-cutting since the last glaciation has often left benches of glacial sediments and relatively deep and steep river valleys. This relatively rapid river down-cutting caused valley rebound and recurring retrogressive translational sliding within these valleys (Evans et al. 2005). The benches in these valleys are often used for agricultural, residential, and recreational activities, while the transportation corridors are relegated to the steeper portions of the valleys of the down-cutting rivers. As the rivers within these valleys continue their down-cutting, the transportation routes (highways and railways) within these valleys are exposed to the ongoing landslide activity associated with this down-cutting. The Thompson River Valley in British Columbia and associated landslides exemplify this process.

Canadian Pacific Railways (CPR) and Canadian National Railways (CN) constructed their main rail lines through the Thompson River Valley in southern British Columbia in 1885 and 1905, respectively. Since then the importance of this valley has grown as a major transportation corridor for Western Canada. Since the construction of the rail lines, both railway companies have had problems with eleven large translational earth slides within a 10-kilometre length of their rail lines south of Ashcroft between Kamloops and Spence's Bridge (Figure 4.1). Rail lines can tolerate relatively slow small movements as routine track maintenance can adjust for these deflections. However, while these landslides today are normally slow moving, rapid to very rapid movements that have blocked the Thompson River have occurred in the past (Clague and Evans, 2003).

These slides have been studied since the late 1800s (Stanton, 1898). More recently, Ryder (1976) described the geology of the area and Monger and MacMillan (1989) examined the Ashcroft formation bedrock. Furthermore, Clague and Evans (2003) summarized the general stratigraphy of the Quaternary sediments in the Thompson

River Valley. CPR and CN have conducted geotechnical investigations of the landslides in the Ashcroft area since the early 1980s. Eshraghian et al. (2005a) showed that the main movement trigger is the Thompson River rather than human activities or rainfall.

The Thompson River is a large river with a five-million-hectare drainage basin upstream of the study area. The average flow, in a normal year, ranges from 230 m^3/sec in January to a maximum 2650 m^3/sec in June when snow melt is most active. The average yearly flow is 24460 Mm^3/year. Eshraghian et al. (2005a) showed that the observed instability of the slides in the Thompson River Valley correlated with the years when the Thompson River flows were elevated above the average flows for longer than normal periods. They found a correlation between the maximum cumulative river level difference from the average river level (maximum CRLD) and years with slide movement (Figure 4.2). Figure 4.2 does not contain a complete history of the correlation between the slide movement and the CRLD for the Thompson River. Only the slides where the rate of movement has been noticeable have been documented and, therefore; Figure 4.2 can only be considered partially complete. It is not obvious how periods of sustained river flows above normal flows changes the stability and movement pattern of these slides. Without such an understanding it is difficult for the railways to develop a risk strategy for managing the deformations associated with these slides.

In this paper, two sample slides in this area, Slide CN50.9 and the Goddard Slide (Figure 4.1), are examined to assess the effect of the river on the movement of the slides. Slide CN50.9 was selected because of its effective river erosion protection that has been repaired and extended in place since 2001 (Tim Keegan, personal communication 2006), while the Goddard Slide was selected to examine the effect of continuous toe erosion by the river. First, the site investigation data, geological information, and historical movement records of the slides are presented. Then for each slide, the groundwater system within the slide body is reproduced by a transient seepage analysis, and the result is compared with the available piezometric data for the site. The modeled groundwater systems are then used to examine the stability of the slides and the stability analysis results are compared with the in-situ inclinometer data and the historical movement records. Finally, based on the stability analyses, the kinematics and deformation patterns of the earth slides and the river effects on their stability are discussed.

4.2. GEOLOGY AND MOVEMENT HISTORY

The Ashcroft area is part of the Thompson Plateau, a subdivision of the Interior Plateau. Quaternary sediments fill the deep pre-glacial valley (Porter et al. 2002). The Thompson River flows south and has down-cut through about 150 metres of these glacial sediments (Porter et al. 2002). Fulton (1969) described the general glaciation in this area, and Johnsen and Brennand (2004) studied the development of two narrow (width to length ratio of ~3:100) late-glacial, ice-dammed lakes within the Thompson Basin.

Clague and Evans (2003) divided the general stratigraphy of the glacial sediments in the Thompson River Valley into eight units. These sediments are the result of three glacial sequences and are separated by unconformities (Clague and Evans 2003). Moreover, Eshraghian et al. (2007) synthesized the geological succession for the slides in the Ashcroft area based on units proposed by Clague and Evans (2003). Figure 4.3 shows the stratification within the two sample slides.

The slides in the Ashcroft area are moving on two rupture surfaces in clay beds of highly plastic overconsolidated clay sandwiched between layers of clayey silt in a glaciolacustrine clay-silt unit or are in contact with this unit and units above it (Figure 4.3). Eshraghian et al. (2007), using Geographical Information System (GIS) technology, concluded that the rupture surfaces in each slide were likely within the same weak glacial sediments that formed in the glacial lakes. Samples, taken from this unit at different locations, show average plasticity indices in the range from 31% to 47% and plastic limits in the range from 24% to 29%. The average activities of these samples ranged from 0.6 to 0.79, and their average liquid limits ranged from 55% to 73% (Eshraghian et al., 2007). Porter et al. (2002) reported similar values for the material indices.

Eshraghian et al. (2007) tested samples of the clay-silt unit from the South Slide (see Figure 4.1), in direct shear tests. They tested the clay beds, silt beds, and mixture of clay and silt beds in the clay-silt sequences separately in direct shear tests with vertical effective stress within the range of the overburden pressure on the slides' rupture surfaces. The peak friction angle and the cohesion of the highly plastic brown clay was found to be 16° and 10 (kPa), respectively, and its residual friction angle was 13° with zero cohesion. The residual friction angle of olive clayey silt material was reported as 23° with peak friction angle of 23° and peak cohesion of 25 (kPa), while samples with a mixture of silt and clay showed a peak friction angle of 18° and a peak cohesion of 25 (kPa). These parameters were used for estimating the strength of the undisturbed and disturbed material in the slides examined in this paper.

Using the movement classification proposed by Cruden and Varnes (1996), the translational slides in the Ashcroft area are in a reactivation stage and moving extremely slowly (slower than 16 mm/year) on two rupture surfaces. Table 4.1 presents a summary of the movements of Slide CN50.9 and the Goddard Slide. In the following sections these slides are examined to assess the effect of the Thompson River on the slide movements and stability.

4.3. SLIDE WITH EFFECTIVE RIVER EROSION PROTECTION (SLIDE CN50.9)

Slide CN50.9 is protected against river erosion by a toe berm which was built in late 1970s (Keegan personal communication, 2006). Four main translational blocks are moving on two rupture surfaces within the clay-silt glaciolacustrine sequence (Eshraghian et al. 2007). The most recent retrogression of this slide, which likely developed the main scarp and translated the minor scarps in a rapid movement, happened in 1897 (Table 4.1). Since its last retrogression, this slide has been reactivated many times (Eshraghian et al. 2005a). After the slide accelerated in 1997, an extension to the existing toe berm was constructed to provide more protection against river erosion and more support for the toe blocks (Figure 4.4). A bathymetric survey of the river in 2000 showed that a 5-m-deep scour hole had developed, suggesting that the geometry of the river in the vicinity of the slide can change from year to year (Yaremko 2002), a sign of the on-going river down-cutting at this site.

4.3.1. Instrumentation

Eleven piezometers were installed in five boreholes at Slide CN50.9 (Figure 4.5-B). Eight of these piezometers are shown in Figure 4.5-B, and three more were installed in Borehole Bh10 near the main scarp (Figure 4.5-A). Sample piezometric responses, for the period of 2001 to 2004, are shown in Figure 4.6. These piezometric data show an upward gradient at the toe, boreholes Bh9 and Bh1, and a downward gradient at the main scarp, borehole Bh10. This result suggests that the recharge zone is located at the slide head, and the discharge zone is located at the slide toe. Moreover, the smaller changes in the deeper piezometer elevations imply that the Thompson River level fluctuation effect on the groundwater system decreased with depth. For the piezometer installed in the same soil unit and approximately at the same level (P2 in borehole Bh9 and P3 in borehole Bh1), the greater the horizontal distance of the piezometer is from the toe, the smaller the change in the elevation heads and the smaller the response to the Thompson River level fluctuations. Thus, the Thompson River affects the groundwater system mainly at the shallower portion of the toe.

The data from the five inclinometers installed in boreholes Bh1, Bh3, Bh5, Bh8, and Bh9 available since April 2001, show extremely slow movement on the two rupture surfaces (see Figure 4.5 for inclinometer locations). The movement on the deeper rupture surface was continuous with a movement rate less than 5 mm/year, while the movement on the shallower rupture surface was occasional and even slower than the deeper rupture surface movement. The movement on the deeper rupture surface was found to accelerate when the Thompson River level started to fall from its peak level (Figure 4.7-A). On the other hand, the movement on the shallower rupture surface, as recorded by the inclinometer in borehole Bh1, was occasional and in each year happened at discrete periods in July, August and September with maximum rate of 1.5 mm/year (Figure 4.7-B).

4.3.2. Groundwater System Modeling

The data from the piezometers gave an approximation of the groundwater system, but the complete groundwater system and its change with the Thompson River level fluctuations were required to study the effect of the river on the stability of the slides. In this section we describe the transient seepage analyses that were conducted using SEEP/W to evaluate the impact of the Thompson River on the groundwater system.

In the Thompson River Valley groundwater system, the Thompson River level fluctuation, rainfall infiltration on the slide's crown terrace, and rainfall infiltration on the slopes of the slide are the main contributors to the system. The Thompson River level changes more than 6 m in a normal year; however, the Thompson River fluctuation in flood years can be up to 8 m. The Thompson River is the boundary condition acting on the slide toe while the rainfall infiltration is the boundary condition acting on the slope as well as on the terrace above the slope (crown terrace). Precipitation infiltration through the fluvial gravel and the sand unit at the slide crown terrace (Figure 4.5-A) and on the slope itself recharge the groundwater system.

The average annual precipitation in the Ashcroft area is 240 mm/year (Porter et al. 2002). The slides in the Ashcroft area are relatively deep (the average depth of the rupture surface is 40 m); consequently, rain storms in this arid environment cannot significantly change the groundwater system in the slide mass. Therefore, in our seepage analyses, constant infiltration boundary conditions on the slide crown terrace and on the slope itself were assumed. On the other hand, considering the complex geology and stratigraphy with layers of different hydraulic conductivities adjacent to the river, the Thompson River level changes may make complex groundwater flow systems within the slide mass. Modelling the groundwater system response to the Thompson River level fluctuation required carrying out a transient seepage analysis with variable head boundary conditions on the river bank.

4.3.2.1. Procedure

The Thompson River level fluctuation cycle from March 22, 2002 to November 17, 2002 was used to analyse Slide CN50.9's groundwater system in 2002. In the first step for the transient groundwater system analysis, steady state seepage was modeled for the slide with the minimum Thomson River level (281.6 m) at the beginning of the study cycle (on March 22, 2002). The steady state seepage was modeled with constant precipitation on both the slide slope and its terrace. From Chanasyk's (1986) report, the infiltration of the annual precipitation through the Goddard Slide crown terrace (Figure 4.1) was estimated to be 8% which is also considered appropriate for Slide CN50.9, since the material in the Goddard Slide site and Slide CN50.9 site is similar. Considering the non-horizontal surface of the slope, less infiltration was assumed for the slope compared to that for the horizontal crown terrace. A surface flux of 4.5×10^{-10} m/s (6% of mean annual precipitation) was assumed on the slope to reach the best agreement between piezometer records and model result.

Slide CN50.9's crown terrace is more gravely than the Goddard Slide's crown terrace. Through trial and error, to match the minimum piezometer data (starting of the river level cycle) from borehole Bh10 at the head, a 13% infiltration of annual rainfall (rather than 8% infiltration in the Goddard Slide's crown terrace) was required through Slide CN50.9's crown terrace. It means a surface flux of 1.0×10^{-9} m/s. At Slide CN50.9, the crown terrace at an elevation of 420 metre extends 1200 metre back from the main scarp of the slide.

Material properties were estimated from the grain-size analysis reported by Eshraghian et al. (2005b) and similar materials reported in the literature. The selected values of the hydraulic conductivities were adjusted during the steady state seepage analyses to match the predicted heads with the heads measured by the piezometers during the starting date of the river level cycle (minimum Thompson River level). Table 4.2 shows the final conductivities used for the seepage analyses of both slides, Slide CN50.9 and the Goddard Slide. Because these materials are generally laminated, the vertical hydraulic conductivity is less than the horizontal hydraulic conductivity. Pauls et al. (1999) and Kelly et al. (1995) used k_v/k_h between 0.2 and 0.5 for the disturbed landslide material in their analyses. Considering the disturbance of this material due to the previous slide movement, the ratio of the vertical to the horizontal hydraulic conductivity (k_v/k_h) was assumed to be 0.5. The hydraulic conductivity changes with soil suction, which also had to be considered in steady state seepage analysis. Figure 4.8 shows the hydraulic conductivity versus soil suction based on grain size analysis, used for the till unit in Slide CN50.9. Also, a 2-m thick sand layer was assumed at the toe at contact between clay-silt and till units to model horizontal sand layer at the toe.

In the second step of our groundwater system analysis, the steady state seepage analysis result from the minimum Thompson River level was used as the starting point for the transient analysis during the river level fluctuation cycle. In the transient analysis, the transient seepage for Slide CN50.9 during the period March 2001 to November 2002 was modeled in 10-day time increments. In this analysis, the same infiltration boundary conditions used in the steady state analyses were used again not only on the slope but also on the crown terrace. However, in the transient analyses, a variable head boundary function was used to model the Thompson River level fluctuation at toe. The material hydraulic conductivity was assumed to be the same for both the steady state and transient analyses. In the transient seepage analysis, not only the material hydraulic conductivity functions, but also the material soil storage functions are required. The soil storage functions were defined based on the material database in the literature and the coefficient of volume change, m_v, 1×10^{-7} (m^2/kN), from a consolidation test. The results from the transient analyses were compared with the response of the installed piezometers, and from this comparison the soil storage functions and conductivities were adjusted to reach the best agreement between the model response and the piezometric field response. Figure 4.8 shows the storage function for the glacial till unit at Slide CN50.9 in transient seepage analysis that provided the best fit to the field data.

4.3.2.2. Results

The result of the steady state analysis for the minimum 2002 Thompson River level is shown in Figure 4.9. This result is in agreement with the minimum piezometer reading from the piezometers installed in Slide CN50.9 (Table 4.3).

The transient seepage analysis shows a change in the groundwater system and seepage direction with the Thompson River level fluctuations mostly within 100 metres from the slide toe, i.e. at one-third of the total length of the slide (Figure 4.10). This finding is in agreement with the smaller changes in the piezometric elevation for the piezometers installed in borehole Bh10 (Figure 4.5-A) compared to the piezometric elevation changes in the piezometers installed at the toe (Figure 4.6). When the river level is at its minimum, the seepage direction at the slide toe is from the slide body toward the river and when the river level starts rising, the seepage direction at the slide toe changes from the river toward the slide body, and the groundwater table rises as well (Figure 4.10-A). At the maximum river level, the seepage direction at the toe is still toward the slide body (Figure 4.10-B). As soon as the drawdown begins, the groundwater table starts lowering, and the water stored in the parts previously under the groundwater table is distributed within the slide body (Figure 4.10-C). This process creates a complex groundwater system after drawdown starts. The seepage direction gradually changes toward the river within two to three weeks after the drawdown starts. The seepage direction remains toward the river till the end of the river drawdown period (Figure 4.10-D).

A sample of the calculated elevation heads in Slide CN50.9's piezometer locations is shown in Figure 4.11. The calculated response at the location of piezometer P1 and the piezometric measurements for piezometer P1 in borehole Bh1 (Figure 4.5-B) are compared in Figure 4.12. Although the measured piezometric data of piezometer P1 in borehole Bh1 are more sensitive to the river level fluctuation, the model's general response is in agreement with the data.

4.3.3. Stability Analyses

The results from the groundwater model were used as input for stability analyses of Slide CN50.9 in order to understand the movement mechanisms of the slide. The change in the factor of safety was calculated based on the change in the groundwater system determined from the transient seepage analyses, change of pressure on the slide toe with river level fluctuation, and the change in the slide's toe geometry because of the toe berm construction.

4.3.3.1. Procedure

Slide CN50.9 is protected against river bank erosion by a toe berm. Stability analyses were conducted for 25 stages of river level changes (10-day intervals) within the period of March 2002 to November 2002. The reactivation was investigated by analysing four reactivation blocks R-1, R-2, R-3, and R-4 (see Figure 4.5). The retrogression on the deeper rupture surface (Figure 4.5) was also analysed.

The surface topography was reproduced from a 2-metre by 2-metre mesh of LiDAR data (taken in 2003) which had a vertical resolution of ± 0.2 metre. The locations and shapes of the two rupture surfaces were defined based on the movement data from the inclinometers installed in the boreholes and the shear disturbance and slickensides in the samples from boreholes without inclinometers. Most of the length of these two rupture surfaces is within clay-silt glaciolacustrine material (Figure 4.5).

Eshraghian et al. (2005b) estimated the residual friction angle of the clay-silt material in the Ashcroft slides from the index property of this material and by using Stark and Eid's (1994) correlation. The residual material properties for the other layers were estimated based on their index properties, grain-size distributions, and the results of the direct shear tests on the clay and silt layers in the South Slide (see Figure 4.1 for slide location). The soil properties used in the stability analysis of both the Slide CN50.9 and the Goddard Slide are shown in Table 4.4.

These material properties were used with the Morgenstern and Price (1965) method of slices for calculating the factor of safety for each of the four blocks in Slide CN50.9. At each stage, the change of the river's supporting force at the toe was modelled by the pressure on the river bank, and the groundwater system was imported from the transient seepage at that stage. Therefore, the changes in the blocks factors of safety were caused by changing the pore pressure in the slide mass and changing the Thompson River's supporting load at the slide toe.

In order to investigate the possibility of more main scarp retrogression on the deeper rupture surface, a future retrogressed block in the undisturbed material was assumed (see Figure 4.5 for location). The movement of the retrogression block was assumed to occur on the deeper rupture surface. The material in the new growth part of the rupture surface was assumed to be undisturbed and the peak parameters (Table 4.4) were used in the stability analyses for this portion of the rupture surface while the residual parameters were used for the old existing part of the rupture surface.

4.3.3.2. Results

The effects of the river level fluctuation during March 2002 to November 2002 on the stability of Slide CN50.9's four reactivation blocks are presented in Figure 4.13. The factor of safety of the reactivation blocks changes as the river level changes (Table 4.5). This change is maximum for the smaller toe block on the shallower rupture surface, R-3.

In 2001, the toe berm at Slide CN50.9 was extended to improve stability. Based on information presented by Nachtigal (2001), an average width of 5 metres was used for this berm in the stability analysis. The transient seepage analysis and stability analysis for the cross section without this new berm were repeated to investigate its effect on stability (Figure 4.14). This toe berm affected mainly toe blocks, block R-3 and block R-4. The toe berm construction improved the factor of safety of block R-4, R-3, R-2, and R-1 by 19%, 11%, 3%, and 1% respectively.

To investigate more possible retrogression in Slide CN50.9, a new retrogression block was defined by assuming a 50-metre retrogression from the current main scarp on the deeper rupture surface (Figure 4.5). The minimum factor of safety of this new block for the year 2002 Thompson River level fluctuation cycle was calculated to be 1.2.

4.4. SLIDE WITHOUT EFFECTIVE RIVER EROSION PROTECTION (THE GODDARD SLIDE)

The Goddard Slide is one of the slides in the Ashcroft area without toe erosion protection. A Digital Elevation Model (DEM) of the Goddard Slide created from LiDAR data and displayed in a GIS program, is shown in Figure 4.15. The most recent retrogression of this slide happened on October 19, 1886 (Stanton 1898). Since its 1886 retrogression, this slide has reactivated many times including reactivations in 1974, October 1976, and September 1982 (Hawson 1977, Morgenstern 1986, Krahn 1984 and Porter et al. 2002). While the rates of these reactivations were generally very slow (Table 4.1), a rapid reactivation occurred between September 22 and September 25, 1982, when the estimated maximum rate of movement was 6 m/hour (Krahn 1984).

The 1982 reactivation was a translational movement within the original 1886 slide area with a main downward movement at the head and upward movement at the toe. The movement started on September 22, 1982 and continued until September 23, 1982 with a moderate rate (maximum rate of 30 mm/hour), and then accelerated to a rapid movement on September 24, 1982 (Krahn 1984). The cross section of the Goddard Slide in Figure 4.16 shows the pre-1982 reactivation and post-1982 reactivation geometries. The pre-1982 ground surface was reproduced from Krahn's (1984) estimation based on 1981 aerial photos.

4.4.1. Instrumentation

The data from the ten piezometers installed in the Goddard boreholes after the 1982 reactivation are shown in Figure 4.17. The piezometers at the toe (P3 and P4) show seasonal changes with the Thompson River level fluctuation. In contrast, the piezometers at the middle of the slide body (P2, P6, and P7) do not show changes with the Thompson River level fluctuation. The elevation heads in piezometers P6 and P7, at the middle of the slide body and within the silt, sand, and diamicton unit, were generally increasing after the 1982 reactivation. This increase might be the result of the water table adjusting to the new geometry after the 1982 reactivation. The changes in head recorded by piezometers installed in the crown terrace are given in Figure 4.17-B. Inspection of these piezometers show no significant seasonal changes and a downward gradient suggesting the crown terrace is the recharge area for the slide mass.

A few days after the 1982 reactivation, inclinometers were installed in boreholes Bh1, Bh2, Bh3, Bh4, and Bh5 (Figure 4.15). The data from these inclinometers showed that the movement rate decreased after the 1982 reactivation and the movement finally ceased in 1987 except some part of the toe near to the river (within block R-4) (MacLeod and Thomas 1987).

4.4.2. Groundwater System Modelling

4.4.2.1. Procedure

The same procedure used in the Slide CN50.9 groundwater modelling was followed in modelling the Goddard Slide's groundwater system. During the 1982 reactivation, the slide geometry changed because of 15 metres of movement toward the Thompson River (Figure 4.16). This movement changed the groundwater system within the slide body. Therefore, the groundwater system was modeled for the pre-1982 reactivation and the post-1982 reactivation geometry (during the most extreme flood event in 1997).

In order to model Goddard's groundwater system prior to the 1982 reactivation, first, the steady state seepage was modeled with the minimum Thompson River level at the beginning of the study cycle (275.4 m, on January 1, 1982). 4.5×10^{-10} m/s (6% of mean annual precipitation) was assumed for the infiltration on the slope, the same infiltration that had been used for Slide CN50.9. The infiltration of the annual precipitation on the crown terrace was assumed to be 8% of mean annual precipitation, which was inferred from Chanasyk's (1986) report.

The material properties used in the seepage analyses are shown in Table 4.2. The same ratio of the vertical to the horizontal hydraulic conductivity (k_v/k_h) used in Slide CN50.9's groundwater analysis (0.5) was used for the Goddard Slide as well.

In the next step, the period from January 1982 to December 1982 was selected for the transient seepage analysis which was carried out in 20-day increments with variable boundary conditions at river bank to model the river level fluctuation. The same steps and material properties used in the 1982 seepage analysis were followed to model the Goddard Slide's groundwater system during the 1997 flood which is the highest flood since the last reactivation of the slide in 1982. There have been no significant changes in the slide geometry and profile since 1982 unless erosion at toe based on examination of aerial photos. Hence, the detailed geometry provided by 2003 LiDAR data was used for the post-1982 geometry groundwater modelling with corrections for small toe erosion between 1997 and 2003 (2 m) (Figure 4.16).

4.4.2.2. Results

Before the 1982 reactivation, the colluvial gravel and sand at the Goddard Slide head was connected to the fluvial gravel and sand unit at the crown terrace (Figure 4.16). The result of the groundwater system modeling at the time of the maximum Thompson River level (280.6 m) in 1982 is shown in Figure 4.18-A. This result shows a perched water table in the fluvial gravel and sand material at the Goddard Slide crown terrace and also in the colluvial gravel and sand material at the head. The groundwater table at the middle part of the slide body was close to the ground surface. This result is in agreement with Krahn's (1984) reporting of seepage from the head scarp and from the wet area at the middle part of the slide (Figure 4.15) after the 1982 reactivation.

Like Slide CN50.9, the Goddard Slide had mainly an 80-metre length of the slide toe affected by the Thompson River level fluctuations. No piezometric data are available prior to the 1982 reactivation. Therefore, the validity of this seepage analysis result cannot be confirmed, but evidence of high groundwater after the 1982 reactivation, seepage from the post-1982 reactivation main scarp (Krahn 1984), and the downward gradients in the crown terrace and upward gradient at the toe given by the post-reactivation piezometer data (Figure 4.17) suggest general agreement with the modeling results.

The result of the groundwater system modeling for the Goddard Slide after the 1982 reactivation, with the 1997 geometry and maximum river level, is shown in Figure 4.18-B. The modeling result shows the change in the groundwater system because of the Thompson River level fluctuation in 1997.

The nearest piezometers to the cross section are shown in Figure 4.18-B. From the groundwater model, the elevation heads of piezometers P2 and P7 are 293.2 metres and 303.7 metres, which are reasonably close to the piezometric measurements after the 1982 reactivation (P2=290.7 m and P7=304 m in Figure 4.17). The elevation head of piezometer P10, estimated by the groundwater model, is 314 metres, which is lower than the piezometer data (P10=319 m in Figure 4.17).

The main difference between the pre-1982 reactivation groundwater system and the post-1982 reactivation groundwater system is the change in the extent of the perched water at the head of the slide. In the pre-1982 groundwater system (Figure 4.18-A), the perched water table is within both the crown terrace fluvial and the slide head colluvial, which was connected to the crown terrace, while, in the 1997 groundwater system (Figure 4.18-B), the perched water table is within only the slide crown terrace. This change is because of the slide head detachment from the crown terrace after the 1982 reactivation.

4.4.3. Stability Analyses

The Goddard Slide has no river erosion protection. The stability analyses of this slide provided an opportunity to investigate the river erosion effect on the stability of the slides without toe erosion protection in the Ashcroft area. The results of the groundwater modeling were used to model the changes in the stability of Goddard's translational blocks with its toe erosion and the river level fluctuation.

4.4.3.1. Procedure

The procedure used in the stability analyses of Slide CN50.9 was followed in the stability analyses of the Goddard Slide. The Goddard Slide pre-1982 stability was analysed for the pre-1982 reactivation geometry (Figure 4.16) with the Thompson River level and groundwater system changes from February 1982 to November 1982 in 20-day intervals. Because of slide's previous movements in 1976, it was assumed that open cracks with depth of 6 metres existed at the toe within blocks R-4 and R-5 before the 1982 reactivation. To analyse the post-1982 reactivation stability, the Goddard Slide stability during the 1997 flood was analysed with the post-1982 geometry (1997 geometry) in 20-day intervals from January 1997 to December 1997.

Like Slide CN50.9, strengths for the Goddard Slide materials were also estimated from index properties, direct shear tests, and similar material tested in adjacent slides in the study area where their rupture surfaces pass through the same geological units. The material properties used in the stability analyses of the Goddard Slide are shown in Table 4.4.

4.4.3.2. Results

The results from the stability analysis are shown in Figure 4.19. Figure 4.19-A shows the effect of the Thompson River level fluctuations on the pre-1982 reactivation conditions and Figure 4.19-B shows the results of the stability analysis for the post-1982 reactivation conditions in 1997 during the highest Thompson River CRLD (difference from average river level) after the 1982 reactivation.

Morgenstern (1986) examined the aerial photo record for the period 1928 to 1976 and estimated that the average rate of erosion at the Goddard Slide was as high as 0.33 m/year. It is reasonable to assume that the majority of this erosion occurs during flood years. Morgenstern (1986) suggested that a reactivation of the Goddard Slide occurred in 1976, although the rate of movement was very slow. If we assume that the amount of river erosion between 1976 and 1982 was approximately 2 metres (6 years times 0.33 m/year), it is possible to assess the impact of river erosion on the stability of the pre-1982 reactivation geometry. This was accomplished by adding 2 metres of material to the pre-1982 cross-sectional width at the toe. The stability analysis showed that an increased length of 2 metres of additional material at the toe would improve the stability of block R-1 by 0.5% (compared to the 1.5% change caused by the river level fluctuation effect for this block).

To assess the potential for possible future retrogression of the Goddard Slide with current geometry, a new retrogression block was defined by assuming a 50-metre retrogression from the current main scarp on the deeper rupture surface (Figure 4.16). This new block's minimum factor of safety for the 1997 Thompson River flood was 1.2.

4.5. SUMMARY OF SLIDE KINEMATICS AND DEFORMATION PATTERNS

4.5.1. Slide CN50.9

Slide CN50.9 toe is protected against river erosion; therefore, the Thompson River mainly affects stability by changing the pore pressure on the rupture surface. In addition, during periods of rapid rise in the river level, the river also provides a temporary supporting effect at the toe. However, once the river level drops, a rapid drawdown condition is also created. As expected, from Table 4.5, it can be seen that the changes in the levels of the Thompson River has the greatest effect on the smallest of the reactivation blocks with the shallower rupture surface.

The inclinometer data from borehole Bh1 (Figure 4.7) at Slide CN50.9 toe (Figure 4.5) show a small movement of 0.5 mm of block R-3 on the shallower rupture surface between July 2002 and November 2002. No movement in block R-3 occurred during the remainder of 2002. The stability analysis (Figure 4.13) shows that block R-3 was marginally stable in 2002, with the factor of safety lower than 1.08 between mid-June 2002 and August 2002, which was the period of the small movement recorded by the inclinometers.

The field measurements at Slide CN50.9 (Figure 4.7) indicate extremely slow continuous movement on the deeper rupture surface with maximum movement rate of 4.1 mm/year. This movement accelerates during the river's drawdown period. The results of stability modeling (Figure 4.13) showed that the factor of safety for the middle block, R-2, was always below unity and its movement accelerates during the drawdown period which may be related to the change in seepage direction. During a rise in the river level, the seepage direction is toward the slide mass (Figure 4.10), but as soon as drawdown begins, the seepage direction reverses and the seepage force is now in the movement direction toward the river. This condition persists until the excess pore pressure comes to equilibrium with the new river levels. The results of stability analysis show that during the study period in 2002, block R-2 was always unstable, but block R-1 was stable. These results imply that only movement in the vicinity of the toe should be recorded on the deeper rupture surface. This is supported by the fact that no movements or new cracks were recorded at borehole Bh10 on the deeper rupture surface in the vicinity of the main scarp (Figure 4.5), but that continuous movement on the deeper rupture surface was recorded in borehole Bh1 (Figure 4.7) located near the toe.

The toe berm 2001 extension improved the stability of Slide CN50.9 (Figure 4.14). Despite this improvement in the blocks' stability after toe berm construction, the factor of safety for block R-2 remained below unity, which is consistent with the extremely slow continuous movements being recorded on the deeper rupture surface. The berm construction improved the stability of block R-3 on the shallower rupture surface. It reduced the period of reactivation on the shallower rupture surface but did not halt occasional extremely slow movements on this rupture surface. The berm construction also improved the stability of block R-4, on the deeper rupture surface. After the 1997 reactivation, tension cracks were visible at the toe (Nachtigal 2001) (Figure4). The stability analysis show that block R-4 was unstable before berm extension and was stabilized by the berm construction (Figure 4.14). This is consistent with no new cracks developing at the toe.

In the reactivation mode, the river level fluctuations affect the stability of deeper blocks and the shallower blocks differently. The factor of safety of the shallower block, block R-3, decreases in response to the increases in the Thompson River level (Figure 4.13). The minimum factor of safety for block R-3 occurred three weeks after the maximum river level was reached. This period is when the seepage direction at the toe was redirected to the movement direction (Figure 4.15). On the other hand, the factor of safety of the deeper blocks, block R-2 and block R-1, increases as the Thompson River rises. The maximum factor of safety for block R-1 and block R-2 occurs a few days after the maximum Thompson River level and then decreases as drawdown occurs. This response is almost opposite to the response in the shallower block (block R-3). The increase in the pore pressure from rising water levels is greater for the shallower block than for the deeper blocks. Therefore, the river's supporting effect plays the main role in changing the stability of the deeper blocks. Whenever the river level is rising, the river's supporting effect increases, but the pore pressure increase during this period is not as significant on the deeper rupture surfaces (Figure 4.11). The effect of river fluctuation on the shallower block (block R-3) is due mainly to increasing the pore water pressure on the shallower rupture surface. The higher hydraulic conductivity of the material at the toe increases the pore pressure response on the shallower rupture surface to the river level fluctuation, and, therefore, also increases the effect of river level fluctuation on the toe block stability.

Our stability analysis showed a minimum factor of safety of 1.2 for the retrogressive block on the deep rupture surface. Therefore, if the current berm can prevent river bank erosion at this site, more retrogression at this site is unlikely.

4.5.2. The Goddard Slide

Stability analysis of the pre-1982 Goddard Slide (Figure 4.19) shows that while toe blocks on the shallower rupture surface were stable during 1982, blocks R-1 and R-4, on the deeper rupture surface, were marginally stable at the beginning of year 1982. At the time of 1982 rapid reactivation the factor of safety of the entire slide, block R-1, was 1.04 and the factor of safety of toe block, R-4, reduced to unity (Figure 4.19-A). The 1982 slide was contained within the main body of the original 1886 slide (Figure 4.15) and it included the same area that had been reactivated in 1976. Morgenstern (1986) reported that the 1982 movement started from the toe and later changed to a rapid reactivation. It is likely that in the first stage of reactivation, only the toe block R-4 was moving and this triggered the movement of the marginally stable main block R-1. While the reduction in the factor of safety of block R-1 was only 1.5% in 1982, this reduction was coincident with the rapid reactivation of the main part of the Goddard Slide which occurred on September 22, 1982. From our analysis, the reduction in the factor of safety to near unity resulted from a combination of both the continuous river erosion and increased pore pressure on the slide rupture surface associated with the changes in the levels of the Thompson River.

If we assume that the same processes of river erosion and river level fluctuation have been acting on the Goddard slide since its last retrogression in 1886, it is likely that the factor of safety of the slope has changed significantly since 1886. Terzaghi (1950) suggested a gradual decrease in the factor of safety of a natural slope as a function of time. Figure 4.20 illustrates a similar decrease in the factor of safety for the Goddard Slide caused by river erosion. Such a process, which is visibly active today, was likely responsible for the gradual destabilization of the Goddard Slide by the Thompson River. In both 1976 and 1982, the Thompson River flow was higher than average (Figure 4.2). It is likely that the Goddard Slide was also marginally stable in 1976 (Figure 4.20), but the amount of river erosion was less extensive; and therefore, the very slow movement was limited to the toe.

The 1982 reactivation started as a slow movement at the toe, but changed to a rapid reactivation of the whole slide within a few days (Morgenstern 1986). Krahn (1984) noted that the pre-1982 groundwater table was near the ground surface and our analyses showed a perched water table in both the slide's head and crown terrace (Figure 4.18-A). During the 1982 reactivation of the Goddard Slide, new cracks were observed in the slide body (Morgenstern 1986). It is likely that the slow movement started in the unstable block at the toe, block R-4, which made conditions favourable for the movement that occurred in the larger block, R-1. This process opened cracks within the slide body. It is likely that these cracks became filled with water from the perched water table. The additional forces from these water-filled cracks may have been sufficient to trigger the accelerated movement. This is similar to the mechanism which Martin et al. (1984) suggested for the acceleration of the Grierson Hill slide. Once movement increased, the slide geometry changed, the water supply from the perched water table became disconnected from the crown terrace perched water table, and the cracks drained. This combination of the change to a more stable geometry and the drainage of the cracks reduced the rate of movement. Since the 1982 reactivation, there has been no movement in the main body of Goddard Slide, even during the 1997 Thompson River flood but slow movements at the toe still persist. This observation is in agreement with the results of the stability analysis for the post-1982 reactivation conditions which showed that all blocks except block R-4 were stable in 1997 with the unstable block R-1 in the pre-1982 analysis, now with a factor of safety of approximately 1.2 (Figure 4.19-B). The improvement in stability since the 1982 reactivation results from a flatter slope geometry (see Figure 4.16). However, the toe of the Goddard Slide (block R-4) remains unstable as tension cracks are readily observed (see Figure 4.15 for tension crack location).

Our analysis suggests that the stability of the Goddard Slide was marginal prior to 1982. The combinations of elevated river levels and river erosion in 1982 made the reactivation possible. Because the Goddard Slide has no protection against toe erosion, the erosion rates estimated by Morgenstern (1986) of 0.33 m/year are likely to continue. More erosion may bring the currently stable Goddard Slide to the marginally stable stage, but the reactivation is likely to be very slow, because the perched water table is no longer connected to the slide's crown terrace. Site visits in August 2004 and September 2005 revealed new tension cracks in blocks R-4 at the toe between the CPR rail line and the Thompson River (Figure 4.21). While it is clear that active erosion is taking place, the new tension cracks further from the river bank are more likely the result of translational movement of toe block R-4. The railway track maintenance crews have not reported any track deflections since 1982 (Chris Bunce, personal communication 2005). Therefore, these toe movements are likely restricted to the tip of the slide within block R-4.

The stability analyses suggest that, with the current condition of the Goddard Slide, fluctuations in the Thompson River levels are unlikely to trigger a retrogression. However, with time the erosion at the toe could gradually reduce the stability. Eventually, this erosion when combined with elevated river levels may create the conditions for a new retrogression.

4.6. CONCLUSIONS

The slides in the Ashcroft area are reactivated, retrogressive, multiple, very slow to extremely slow moving, translational, earth slides. These slides moved rapidly in the late 1800s during their most recent retrogressions on two rupture surfaces which followed the weakest layers in the clay-silt glaciolacustrine sediments in this area.

The main trigger for the movement of these slides is associated with the Thompson River, which can affect the stability of these slides in three ways: (1) by changing the water pressure on their rupture surfaces as the river level fluctuates, (2) by changing the supporting pressure on toes of the slides, and (3) by altering the slide geometry by river bank erosion. The relative importance of each of these effects depends on the river erosion protection system in place, the dimensions of the blocks, the depth and shape of the rupture surface, and the amount of river level fluctuation. The seepage analysis of the two slides in the Ashcroft area shows that the groundwater system changes are mainly restricted to within 100 metres of the slides' toes. Therefore, the pore pressure changes on the rupture surfaces occur mainly on the blocks within the immediate vicinity of the slides' toes. When a slide is not protected against river erosion, river toe erosion may change the geometry of the slide and destabilize the blocks. Toe berm construction appears to significantly improve the stability of the toe blocks by minimising the effects of river erosion and preventing the development of new tension cracks.

From the stability analysis and the movement records of the slides in the Ashcroft area, it can be concluded that extremely slow reactivation of the blocks starts when the factor of safety approaches 1.1 or less. While generally the rate of movement during reactivation is very slow, rapid reactivation of the slides may occur if the slide mass is wet and the tension cracks are filled with water.

Through out this thesis, factors of safety and movement rates have been used to characterize the stability of the slides investigated. It is recognized that there is no correlation between the factor of safety determined from limit equilibrium analysis and the movement rates. The correlations in this paper are entirely empirical and cannot be transferred to other sites.

4.7. REFERENCES

Brooker, E.W., and Peck, R.B. 1993. Rational design treatment of slides in overconsolidated clays and clay shales. Canadian Geotechnical Journal, 30: 526-544.

Chanasyk, D.S. 1986. Goddard landslide of September, 1982, summary of the opinion of David S. Chanasyk. Report prepared for court between Canadian Pacific Railway Limited and Highland Valley Cattle Company Limited. Supreme Court of British Columbia, Vancouver registry No. C841694.

Chin, B.G., Wightman, A., Lo, R.C., and Stewart, W.P. 1984. Case history of a landslide in lacustrine soils. *In* Proceedings of the 37th Canadian Geotechnical Conference. Toronto, Ontario. Canadian Geotechnical Society, pp. 75-84.

Christiansen, E.A., and Sauer, E.K. 1984. Landslide styles in the Saskatchewan River plain: a geological apprisal. *In* Proceedings of the 37th Canadian Geotechnical Conference. Toronto, Ontario. Canadian Geotechnical Society, pp. 35-48.

Clague, J.J., and Evans, S.G. 2003. Geological framework of large historic landslides in Thompson River Valley, British Columbia. Environmental and Engineering Geoscience, 9: 201-212.

Cruden, D.M., Tedder, K.H., and Thomson, S. 1989. Setbacks from the crests of slopes along the North Saskatchewan River Valley. Canadian Geotechnical Journal, 26: 64-74.

Cruden, D.M., Thomson, S., Kim, H.J., and Peterson, A.E. 1995. The Edgerton landslides. Canadian Geotechnical Journal, 32: 989-1001.

Cruden, D. M., and Varnes, D. J. 1996. Landslide types and processes. In Turner, A.K., Schuster, R.L. (Editors), *Landslides: Investigation and Mitigation.* Transportation Research Board, Special report 247. pp. 36-75.

Eshraghian, A., Marin, C.D., and Cruden, D.M. 2005a. Landslides in the Thompson River Valley between Ashcroft and Spence's Bridge, British Columbia. *In* Proceedings of the International Conference on Landslide Risk Management. Vancouver, Canada, May 31 to June 4, 2005. Edited by: O. Hungr, R. Fell, R. Couture, and E. Eberhardt, London, Balkema, pp. 437-446.

Eshraghian, A., Martin, C.D., and Cruden, D.M. 2005b. Earth slide movements in the Thompson River Valley, Ashcroft, British Columbia. *In* Proceedings of the 58th Canadian Geotechnical Conference. Saskatoon, Saskatchewan, Canada, September 18-21, 2005. Canadian Geotechnical Society.

Eshraghian, A., Martin, C.D., and Cruden, D.M. 2007. Complex earth slides in the Thompson River Valley, Ashcroft, British Columbia. Journal of Environmental and Engineering Geoscience, 13: 161-181.

Evans, S.G., Cruden, D.M., Bobrowsky, P.T., Guthrie, R.H., Keegan, T.R., Liverman, D.G.E., and Perret, D. 2005. Landslide risk assessment in Canada; a review of recent developments. *In* Proceedings of the International Conference on Landslide Risk Management. *Edited by* O. Hungr, R. Fell, R. Couture, and E. Eberhardt. Vancouver, Canada. 31 May- 3 June 2005. A.A. Balkema, pp. 351-434.

Fletcher, L., Hungr, O., and Evans, S.G. 2002. Contrasting failure behaviour of two large landslides in clay and silt. Canadian Geotechnical Journal, 39: 46-62.

Fulton, R.J. 1969. Glacial Lake History, Southern Interior Plateau, British Columbia. Geological Survey of Canada, Paper 69-37.

Haug, M.D., Sauer, E.K., and Fredlund, D.G. 1977. Retrogressive slope failure at Beaver Creek, South of Saskatoon, Saskatchewan, Canada. Canadian Geotechnical Journal, 14: 288-301.

Hawson, H.H. 1977. Slide area, mile 50.6 Thompson Subdivision. Report to Canadian Pacific Railway, Calgary, Alberta. Golder Association, Kamloops, British Columbia.

Johnsen, T.F., and Brennand, T.A. 2004. Late-glacial lakes in the Thompson Basin, British Columbia: paleogeolography and evolution. Canadian Journal of Earth Science, 41: 1367-1383.

Kelly, A.J., Sauer, E.K., Christiansen, E.A., Barbour, S.L., and Widger, R.A. 1995. Deformation of the Deer Creek bridge by an active landslide in clay shale. Canadian Geotechnical Journal, 32: 701-724.

Krahn, J. 1984. Geotechnical evaluation of the Goddard Landslide, Report 306-0950. Report to Canadian Pacific Railway, Vancouver Division, Thompson Subdivision. EBA Engineering Consultants Ltd.

MacLeod, N.R., and Thomas, M.B. 1987. Goddard Landslide, Thompson Subdivision Mile 50.4, Report 306-34170. Report to Canadian Pacific Railway, Vancouver Division, Thompson Subdivision. EBA Engineering Consultants Ltd. Calgary.

Martin, R.L., Williams, D.R., Balanko, L.A., and Morgenstern, N.R. 1984. The Grierson Hill slide, Edmonton, Alberta. *In* Proceedings of the 37th Canadian Geotechnical Conference: Canadian case histories - landslides. Toronto, Ont. Canadian Geotechnical Society, pp. 125-133.

Martin, R.L., Williams, D.R., Balanko, L.A., and Morgenstern, N.R. 1984. The Grierson Hill slide, Edmonton, Alberta. *In* Proceedings of the 37th Canadian Geotechnical Conference: Canadian case histories - landslides. Toronto, Ont. Canadian Geotechnical Society, pp. 125-133.

Miller, B.G.N., and Cruden, D.M. 2002. The Eureka River landslide and dam, Peace River lowlands, Alberta. Canadian Geotechnical Journal, 39: 863-878.

Monger, J.W.H., and McMillan, W.J. 1989. Geology, Ashcroft, British Columbia, Map 42-1989, sheet 1, scale 1:250,000. Geological Survey of Canada.

Morgenstern, N.R. 1986. Goddard landslide of September, 1982. Report prepared for court between Canadian Pacific Railway Limited and Highland Valley Cattle Company Limited. Supreme Court of British Columbia, Vancouver registry No. C841694.

Morgenstern, N.R., and Price, W.E. 1965. The analysis of the stability of general slip surfaces. Geotechnique, 15: 74-93.

Nachtigal, B.J. 2001. Ashcroft 51 landslide: September 2001 instrumentation installations. Report to Canadian National Railway, Edmonton, Alberta. Bruce Geotechnical Consultants Inc., Kamloops, British Columbia.

Pauls, G.J., Sauer, E.K., Christiansen, E.A., and Widger, R.A. 1999. A transient analysis of slope stability following drawdown after flooding of a highly plastic clay. Canadian Geotechnical Journal, 36: 1151-1171.

Pennell, D.G. 1969. Residual strength analysis of five landslides. Ph.D thesis, University of Alberta, Edmonton, Alberta.

Porter, M.J., Savigny, K.W., Keegan, T.R., Bunce, C.M., and MacKay, C. 2002. Controls on stability of the Thompson River landslides. *In* Proceedings of the 55th Canadian Geotechnical Conference: Ground and Water: Theory to Practice. Niagara Falls, Ontario. 20-23 October, 2002. Canadian Geotechnical Society, pp. 1393-1400.

Richardson, N.W. 1984. Muddy lake, Saskatchewan, site investigation and analysis. *In* 37th Canadian Geotechnical Conference: Canadian case histories - landslides. Toronto, Ont. Canadian Geotechnical Society, pp. 167-180.

Ryder, J.M. 1976. Terrain inventory and Quaternary geology, Ashcroft, British Columbia. Paper 74-49. Geological Survey of Canada, Ottawa.

Stanton, R.B. 1898. The great landslides on the Canadian Pacific Railway in British Columbia. Proceedings of the Institution of Civil Engineers, 132: 1-48.

Stark, T.D., and Eid, H.T. 1994. Drained residual strength of cohesive soils. Journal of Geotechnical Engineering, 120: 856-871.

Terzaghi, K. 1950. Mechanism of landslides. In Engineering Geology (Berkey) Volume. The Geological Society of America, New York. 83-123.

Thomson, S., and Hardy, D.W. 1975. The Little Smoky landslide. Canadian Geotechnical Journal, 12: 379-392.

Thomson, S., and Tweedie, R.W. 1978. The Edgerton landslide. Canadian Geotechnical Journal, 15: 510-521.

Yaremko, E.K. 2002. Thompson River, MP 50.9, Ashcroft Subdivision assessment of flow hydraulics, enlarged berm. Report to Canadian National Railway, Edmonton, Alberta. Northwest Hydraulic Consultants ltd. (NHC), Edmonton, Alberta.

Yoshida, R.T., and Krahn, J. 1984. Movement and stability analysis of the Beaver Creek landslide. *In* 37th Canadian Geotechnical Conference: Canadian case histories - landslides. Toronto, Ont. Canadian Geotechnical Society, pp. 223-231.

Table 4.1. Summary of the slide movements.

Landslide	Most Recent Retrogression	Retrogression Movement Rate	Most Recent Reactivation	Reactivation Rate (mm/year)	Travel angle [c] (°)
1) CN50.9	1897	Rapid	Active	3-20	16
2) Goddard	1886	Very rapid	1982	20-400[b]	14

---

[a] Estimated from Clague and Evans' (2003) and Porter et al.'s (2002) movement descriptions.

[b]. Rate of the 1982 Goddard reactivation was much faster with a maximum rate of 6 m/hour (Krahn 1984).

[c] The angle between the line from slide tip to slide crown and horizontal surface (Cruden and Varnes 1996).

Table 4.2. Material properties used in groundwater modeling of the slides in Ashcroft area.

Landslide	Soil Unit and Type	K_{sat} (cm/sec)
Slide CN50.9	Fluvial and Berm, Gravel and Sand	2.3×10^{-3}
	Glacial Till	4.6×10^{-4}
	Glaciolacustrine Silt, Sand and Gravel	8.1×10^{-5}
	Glaciolacustrine Clay-Silt	1.8×10^{-9}
	Glaciofluvial Sand and Gravel	1.2×10^{-6}
Goddard Slide	Fluvial Gravel and Sand	6.8×10^{-4}
	Glaciolacustrine Silt, Sand, and Gravel	8.1×10^{-6}
	Glaciolacustrine Clay-Silt	7.0×10^{-7}
	Glaciofluvial Sand and Gravel	3.5×10^{-4}

Table 4.3. Comparing the result of steady state seepage analysis and the minimum piezometric head of piezometers installed in Slide CN50.9.

Borehole	Piezometer	Type	Tip Elevation (m)	Measured Head (m)	Predicted Head (m)
Bh1	P1	Stand Pipe	282.8	283.3	282.1
	P2	Pneumatic	274.2	284.0	283.7
	P3	Stand Pipe	266.2	286.4	285.8
Bh9	P1	Stand Pipe	281.2	281.8	281.7
	P2	Pneumatic	269.0	283.6	283.9
	P3	Stand Pipe	259.3	286.9	287.0
Bh10	P1	Pneumatic	289.6	302.2	301.8
	P2	Pneumatic	253.4	293.0	291.0

Table 4.4. Residual and peak strengths used in the stability analyses.

Material	Property	Slide CN50.9		Goddard Slide	
		Residual	Peak	Residual	Peak
Silt, sand, and diamicton	φ′ (°)	25	25	22	24
	c′ (kPa)	0	25	0	25
	γ (kN/m^3)	19	19	19	19
Clay-silt	φ′ (°)	11	16	16	16
	c′ (kPa)	0	12	0	12
	γ (kN/m^3)	19	19	19	19
Till	φ′ (°)	26	26	NA	NA
	c′(kPa)	0	50	NA	NA
	γ (kN/m^3)	18	18	18	18
Fluvial	φ′ (°)	24	NA	NA	NA
	c′(kPa)	0	NA	NA	NA
	γ (kN/m^3)	18	NA	NA	NA
Berm	φ′ (°)	30	NA	NA	NA
	c′(kPa)	0	NA	NA	NA
	γ (kN/m^3)	18	NA	NA	NA

Table 4.5. Change in the Factor of Safety for the reactivation blocks in Slide CN50.9 during year 2002.

Block	Minimum F.S.	Maximum F.S.	F.S. Change (%)
R-1	1.31	1.32	1.1
R-2	0.92	0.95	2.9
R-3	1.05	1.25	19.3
R-4	1.12	1.29	15.4

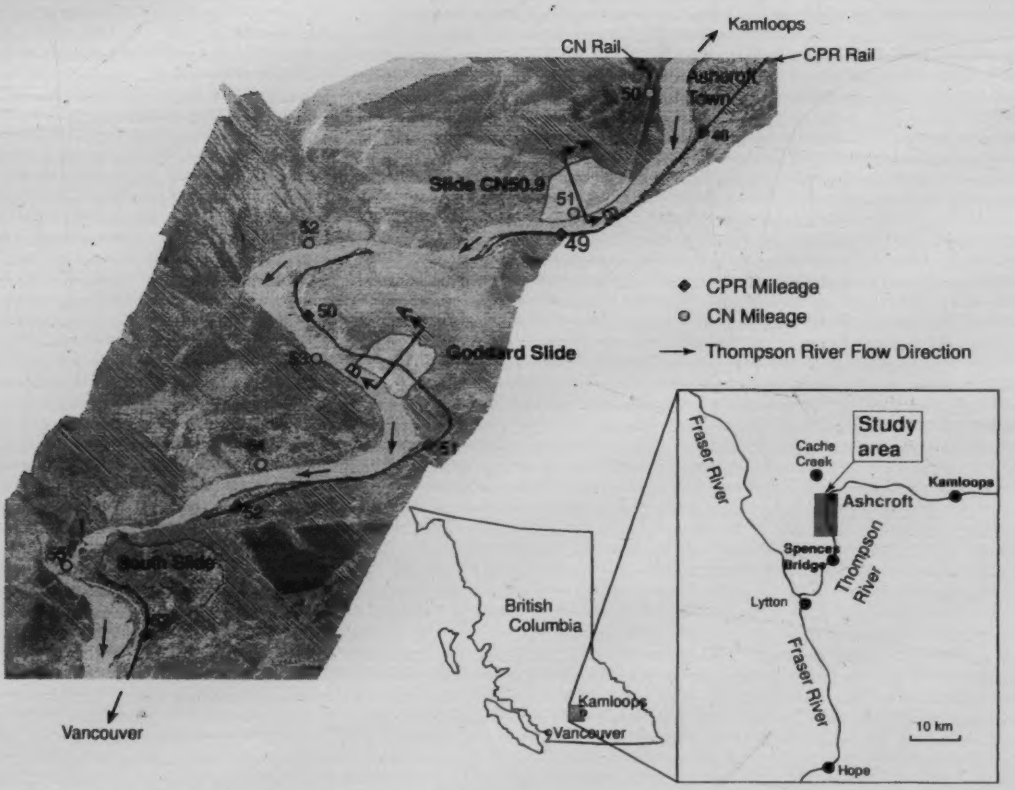
Kamloops
CN Rail
CPR Rail
Ashcroft Town
50
Slide CN50.9
51
49
52
50
53
51
52
South Slide
Goddard Slide
Vancouver
◆ CPR Mileage
○ CN Mileage
→ Thompson River Flow Direction
British Columbia
Kamloops
Vancouver
Fraser River
Cache Creek
Study area
Ashcroft
Kamloops
Spences Bridge
Thompson River
Lytton
Fraser River
10 km
Hope

Figure 4.1. Study area south of Ashcroft, BC, between 50° 10′ to 50° 20′ N and 121° 15′ to 121° 20′ W in a view from south showing the location of the Goddard Slide and Slide CN50.9.

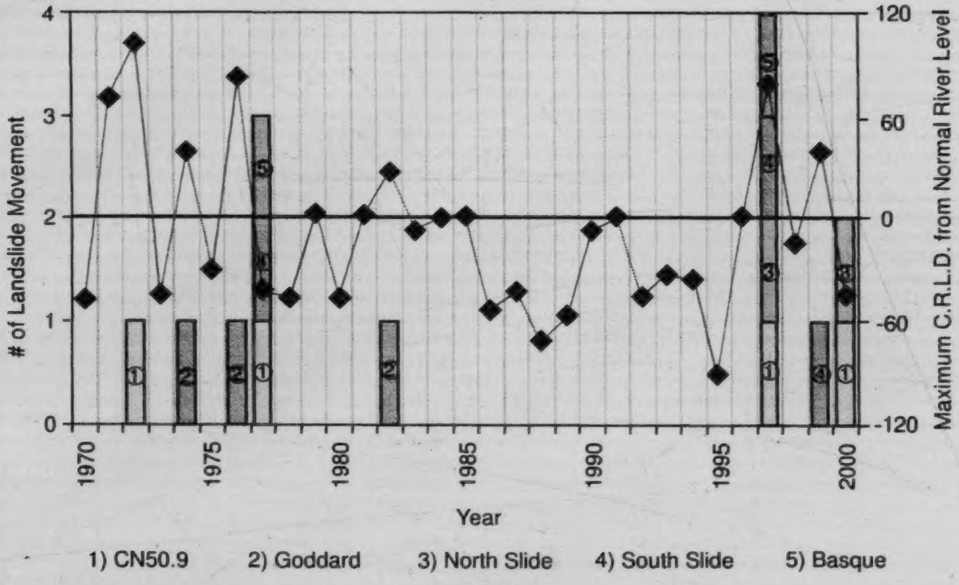

Figure 4.2. Correlation between the annual Thompson River's maximum Cumulative River Level Difference from its normal river level and slides in Ashcroft area with a noticeable increase in their rate of movement.

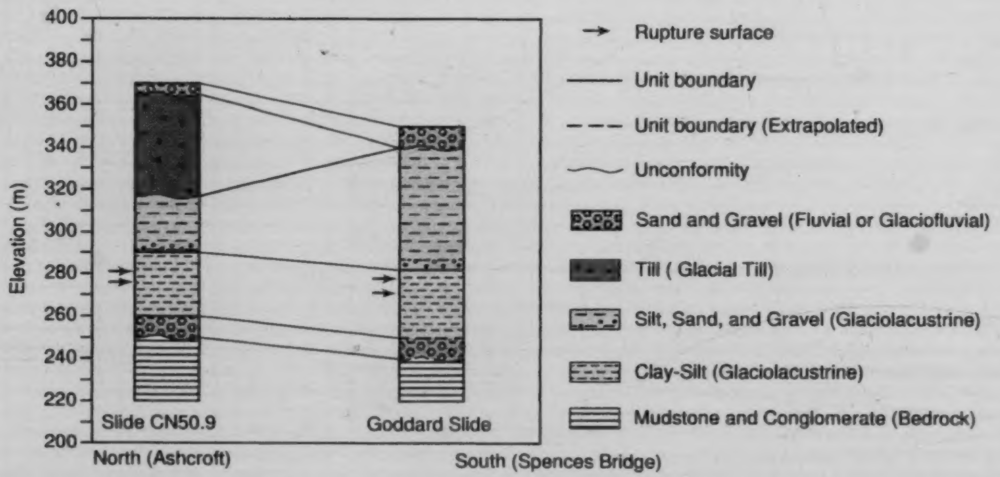

Elevation (m)
400
380
360
340
320
300
280
260
240
220
200
Slide CN50.9
Goddard Slide
North (Ashcroft)
South (Spences Bridge)
Rupture surface
Unit boundary
Unit boundary (Extrapolated)
Unconformity
Sand and Gravel (Fluvial or Glaciofluvial)
Till (Glacial Till)
Silt, Sand, and Gravel (Glaciolacustrine)
Clay-Silt (Glaciolacustrine)
Mudstone and Conglomerate (Bedrock)

Figure 4.3. Geological units in Slide CN50.9 and the Goddard Slide (the horizontal distance is not to scale).

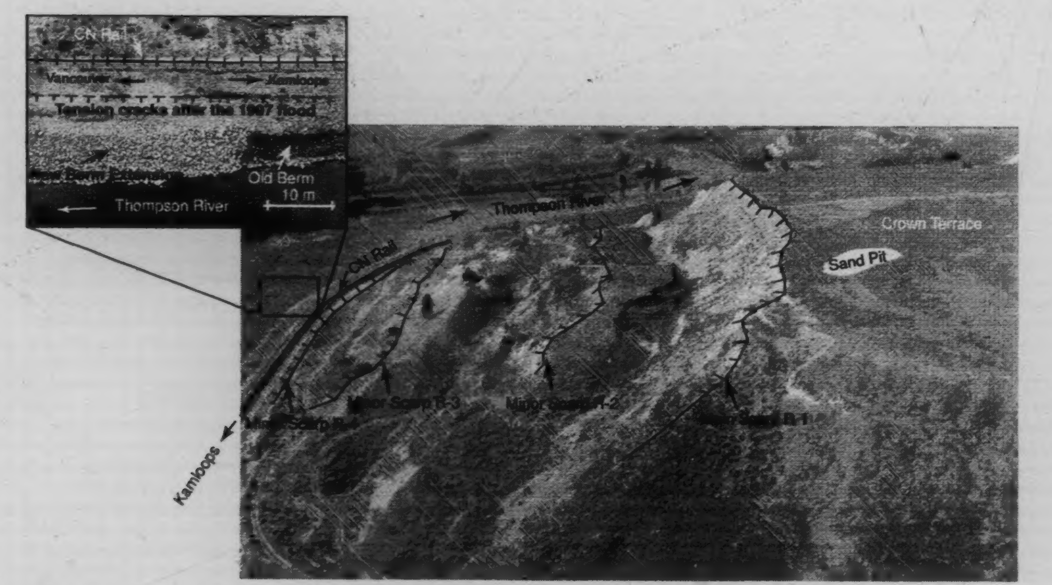
CN Rail
Vancouver
Kamloops
Tension cracks after the 1997 flood
Old Berm
10 m
Thompson River
Thompson River
CN Rail
Crown Terrace
Sand Pit
Minor Scarp R-3
Minor Scarp R-2
Major Scarp R-1
Minor Scarp R-4
Kamloops

Figure 4.4. A view from north to Slide CN50.9 shows its crown terrace, four scarps, CN rail, and old and new extension toe berms at toe. (Photograph by T. Keegan).

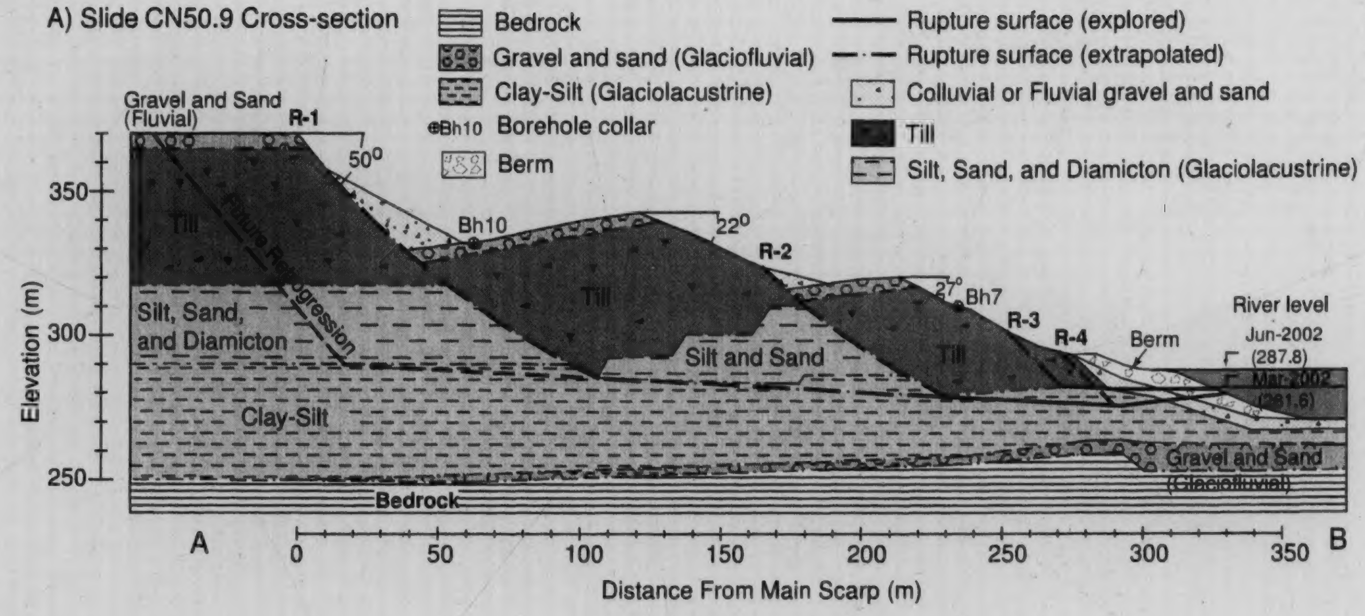
A) Slide CN50.9 Cross-section
Bedrock
Gravel and sand (Glaciofluvial)
Clay-Silt (Glaciolacustrine)
Bh10 Borehole collar
Berm
Rupture surface (explored)
Rupture surface (extrapolated)
Colluvial or Fluvial gravel and sand
Till
Silt, Sand, and Diamicton (Glaciolacustrine)
Gravel and Sand (Fluvial)
R-1
50°
Bh10
22°
R-2
27°
Bh7
R-3
R-4
Berm
River level
Jun-2002 (287.8)
Mar-2002 (281.6)
Till
Till
Till
Future Retrogression
Silt, Sand, and Diamicton
Silt and Sand
Clay-Silt
Gravel and Sand (Glaciofluvial)
Bedrock
Elevation (m)
350
300
250
A
B
0
50
100
150
200
250
300
350
Distance From Main Scarp (m)

Figure 4.5A. Slide CN50.9 cross section showing the rupture surfaces, stratification, and borehole (see Figure 1 for cross-section line)

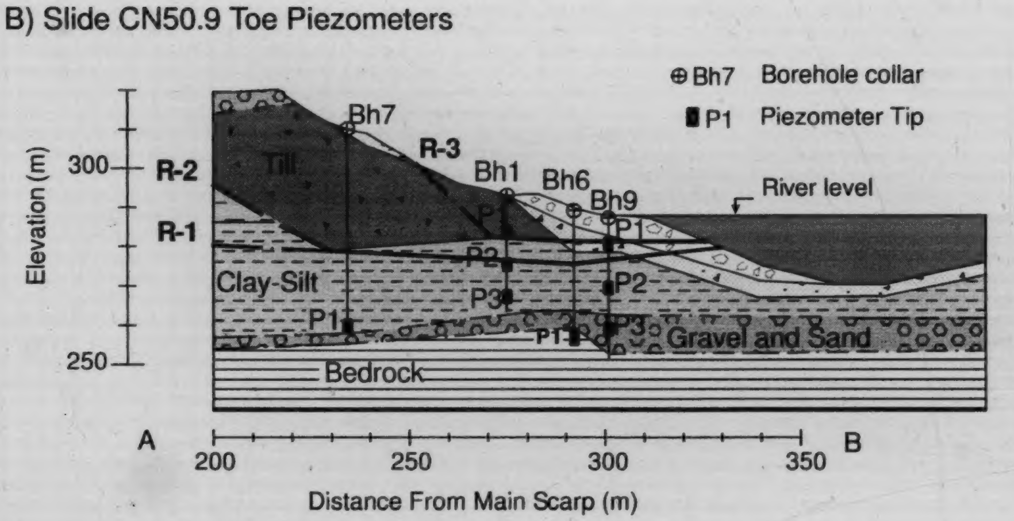
B) Slide CN50.9 Toe Piezometers

⊕ Bh7 Borehole collar
▮ P1 Piezometer Tip
River level
Elevation (m)
300
250
R-2
R-1
R-3
Till
Clay-Silt
Gravel and Sand
Bedrock
Bh7
Bh1
Bh6
Bh9
P1
P2
P3
P1
P2
P3
P1
P2
P3
P1
A
B
200
250
300
350
Distance From Main Scarp (m)

Figure 4.5.B. Piezometers installed at the Slide CN50.9 toe.

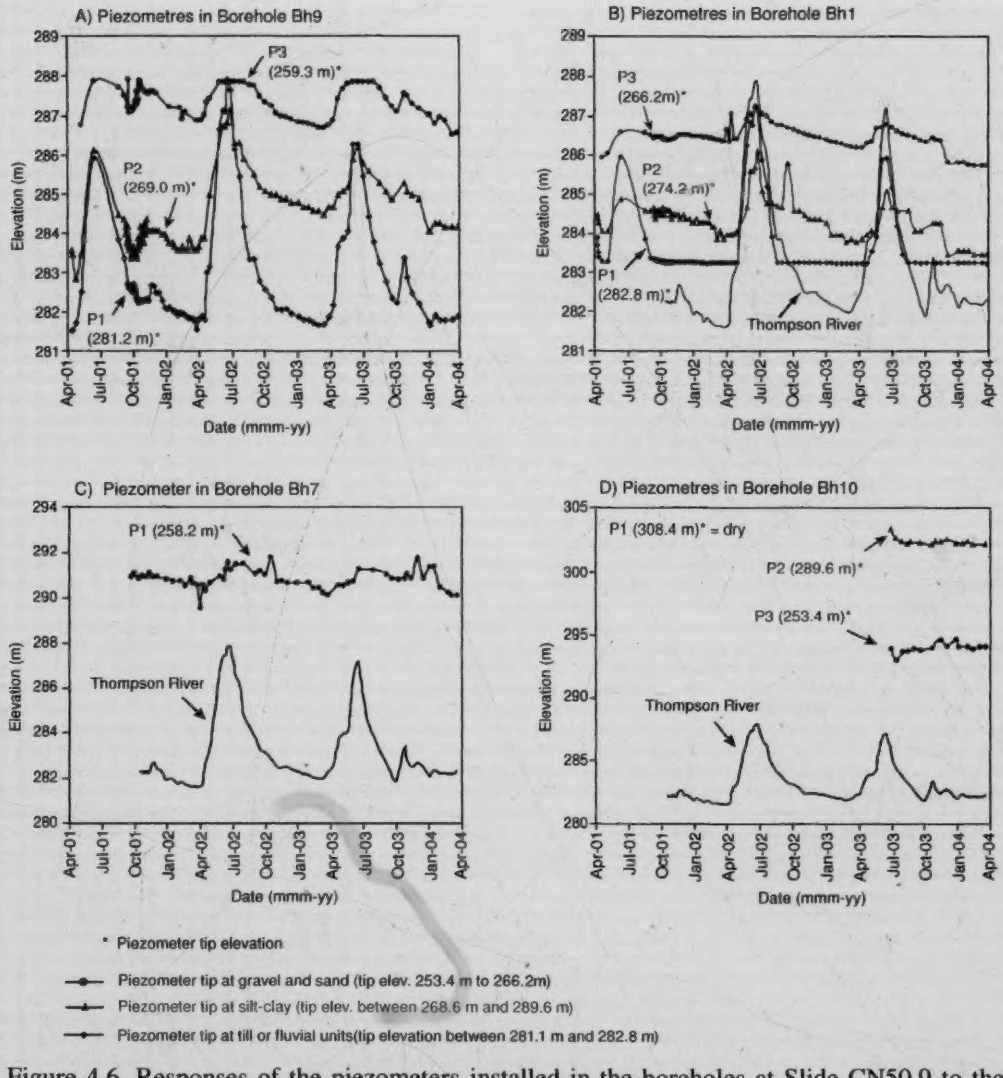

Figure 4.6. Responses of the piezometers installed in the boreholes at Slide CN50.9 to the Thompson River level changes. Elevation head of piezometer P1 in borehole Bh1 is equal to the river level (data from Tim Keegan, personal communication 2005).

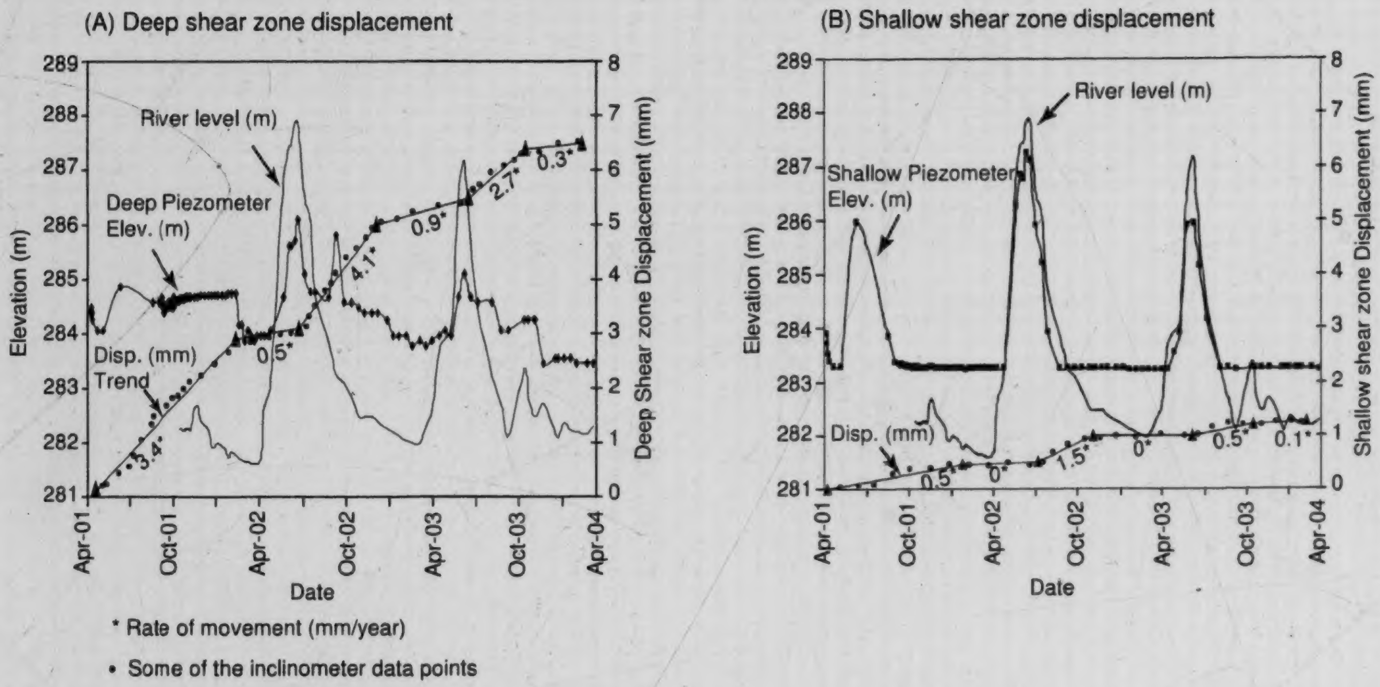

Figure 4.7. Slide CN50.9 movement versus rupture surface pore pressure changes with the Thompson River level fluctuation measured in borehole Bh1 (A) on the deeper rupture surface, (B) on the shallower rupture surface (the flat portion of the shallow piezometer in (B) reflects elevation of the tip).

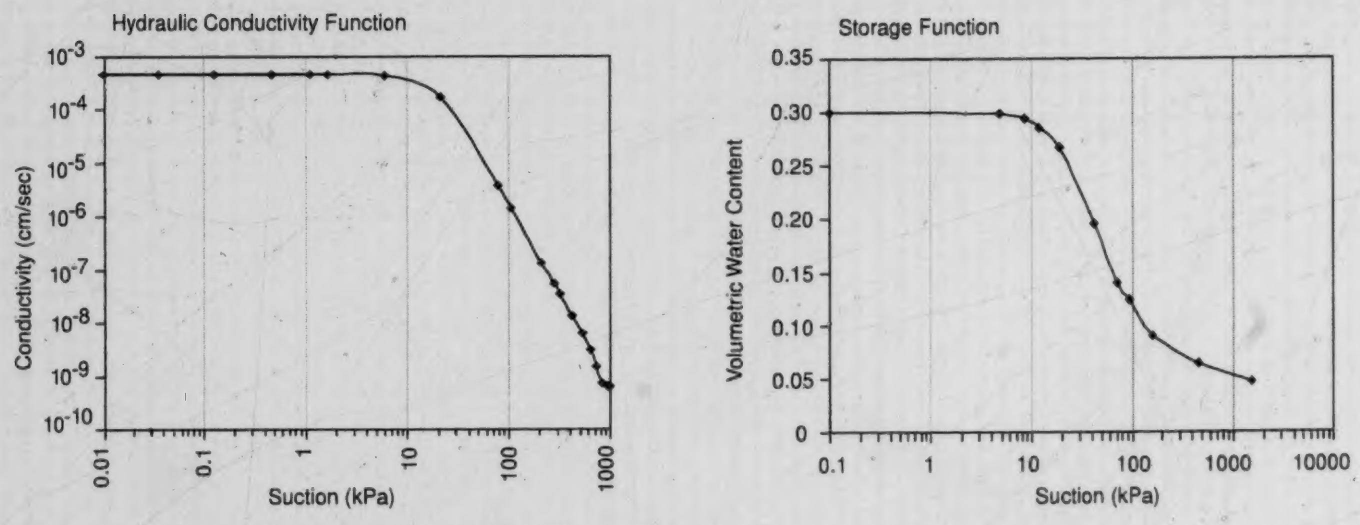

Figure 4.8. Hydraulic conductivity function and storage function for glacial till in Slide CN50.9.

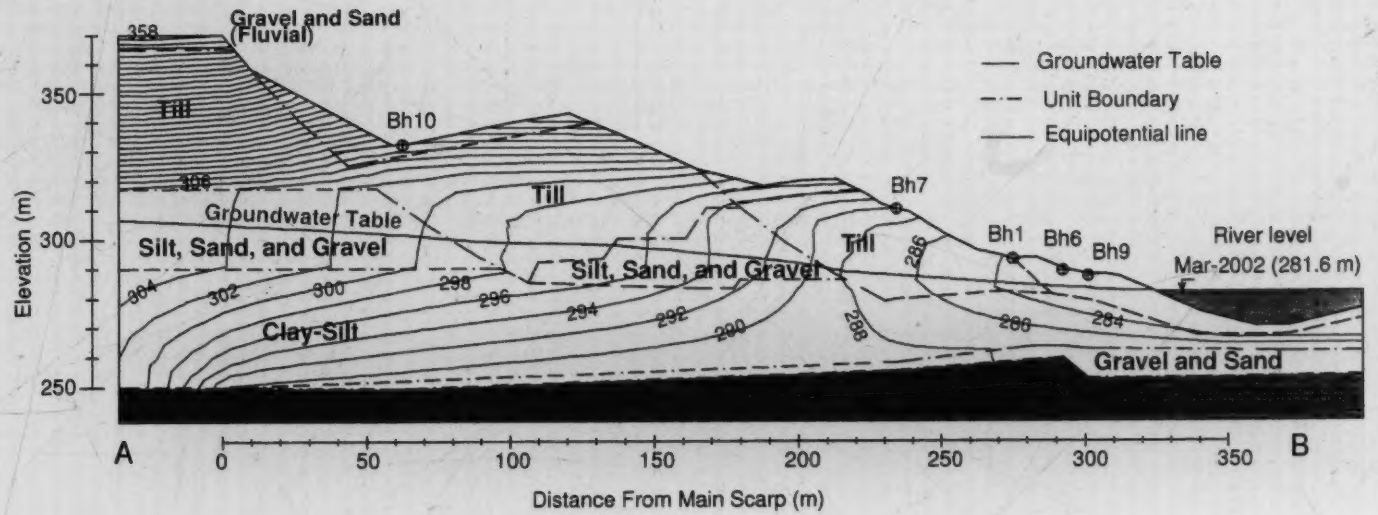
358
Gravel and Sand (Fluvial)
Till
306
Bh10
Groundwater Table
Silt, Sand, and Gravel
Till
Silt, Sand, and Gravel
Bh7
Till
286
Bh1
Bh6
Bh9
River level
Mar-2002 (281.6 m)
304
302
300
298
296
294
292
290
288
286
284
Clay-Silt
Gravel and Sand
Groundwater Table
Unit Boundary
Equipotential line
Elevation (m)
350
300
250
A
B
0
50
100
150
200
250
300
350
Distance From Main Scarp (m)

Figure 4.9. Groundwater system in Slide CN50.9 calculated for the minimum Thompson River level.

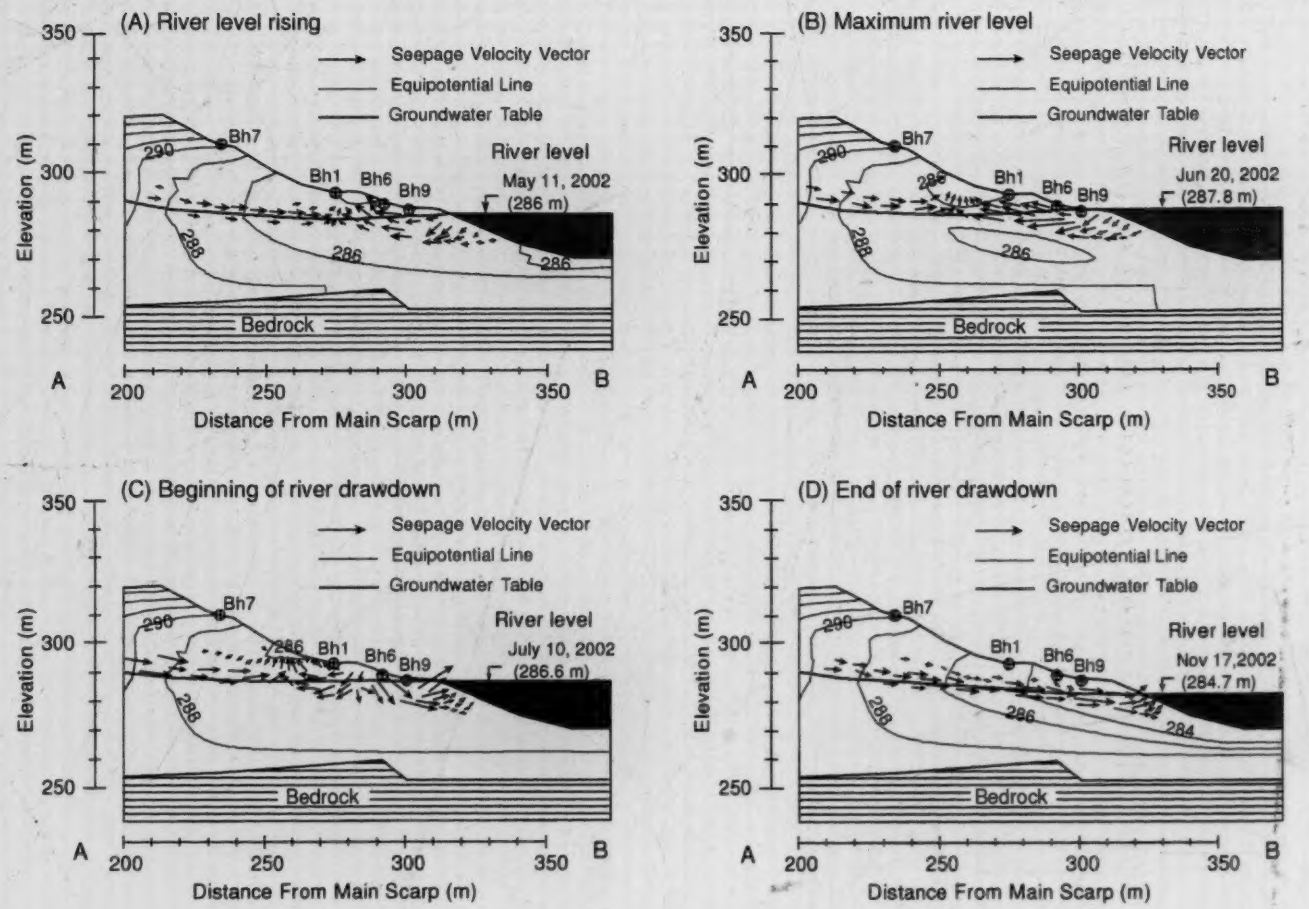
(A) River level rising
Seepage Velocity Vector
Equipotential Line
Groundwater Table
River level
May 11, 2002
(286 m)
Bh7
Bh1
Bh6
Bh9
290
288
286
286
Bedrock
Elevation (m)
350
300
250
A
B
200
250
300
350
Distance From Main Scarp (m)
(B) Maximum river level
Seepage Velocity Vector
Equipotential Line
Groundwater Table
River level
Jun 20, 2002
(287.8 m)
Bh7
Bh1
Bh6
Bh9
290
288
286
286
Bedrock
Elevation (m)
350
300
250
A
B
200
250
300
350
Distance From Main Scarp (m)
(C) Beginning of river drawdown
Seepage Velocity Vector
Equipotential Line
Groundwater Table
River level
July 10, 2002
(286.6 m)
Bh7
Bh1
Bh6
Bh9
290
288
286
Bedrock
Elevation (m)
350
300
250
A
B
200
250
300
350
Distance From Main Scarp (m)
(D) End of river drawdown
Seepage Velocity Vector
Equipotential Line
Groundwater Table
River level
Nov 17,2002
(284.7 m)
Bh7
Bh1
Bh6
Bh9
290
288
286
284
Bedrock
Elevation (m)
350
300
250
A
B
200
250
300
350
Distance From Main Scarp (m)

Figure 4.10. Change of groundwater system and seepage velocity vectors at Slide CN50.9 toe modeled by a transient seepage analysis for 2002.

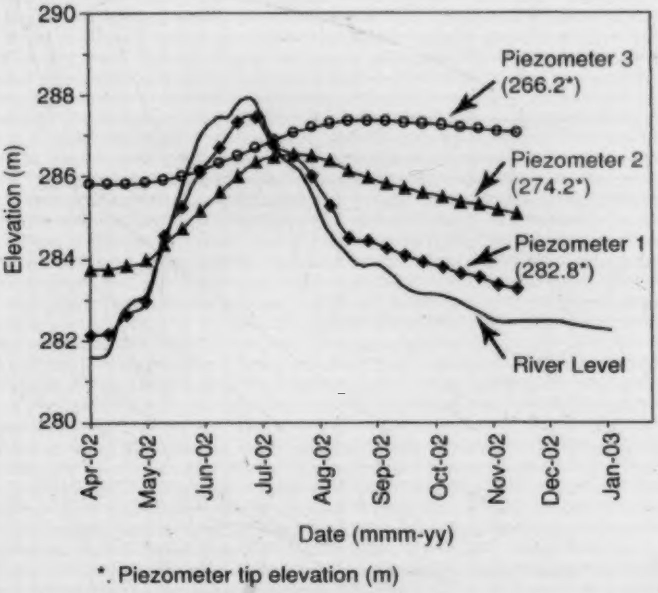

Figure 4.11. Change of elevation head at the location of piezometers installed in borehole Bh1 (see Figure 4.5-B) from the transient seepage analysis.

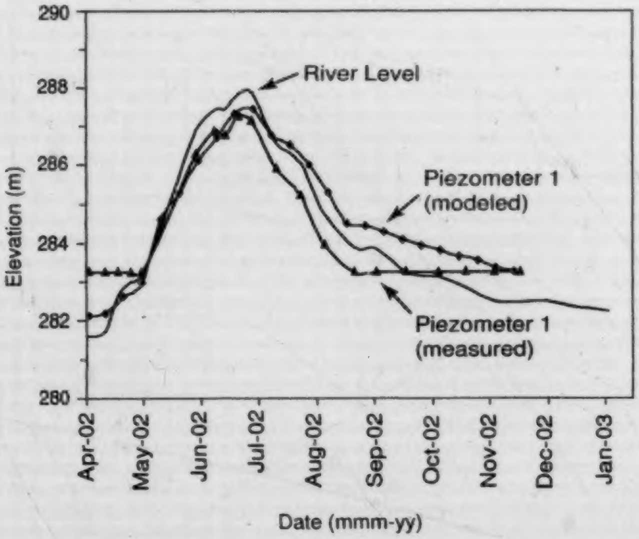

Figure 4.12. Comparison between modeled and real response of piezometer P1 in borehole Bh1 (Figure 4.5-B). The flat portion in the measured piezometer response reflects the piezometer tip elevation at 282.8 m.

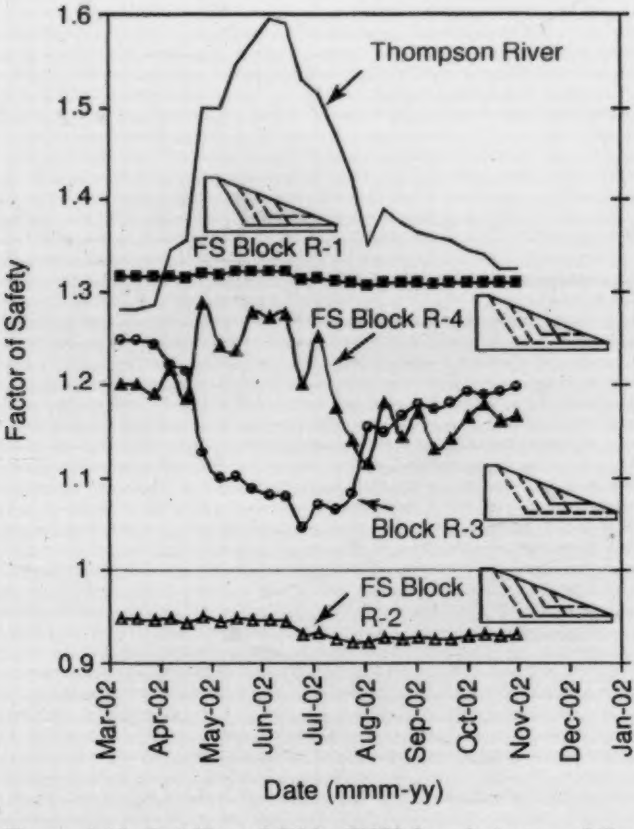

Figure 4.13. Stability of Slide CN50.9 and change of Factor of Safety with the Thompson River levels measured in 2002 (a normal year with a maximum CRLD close to zero).

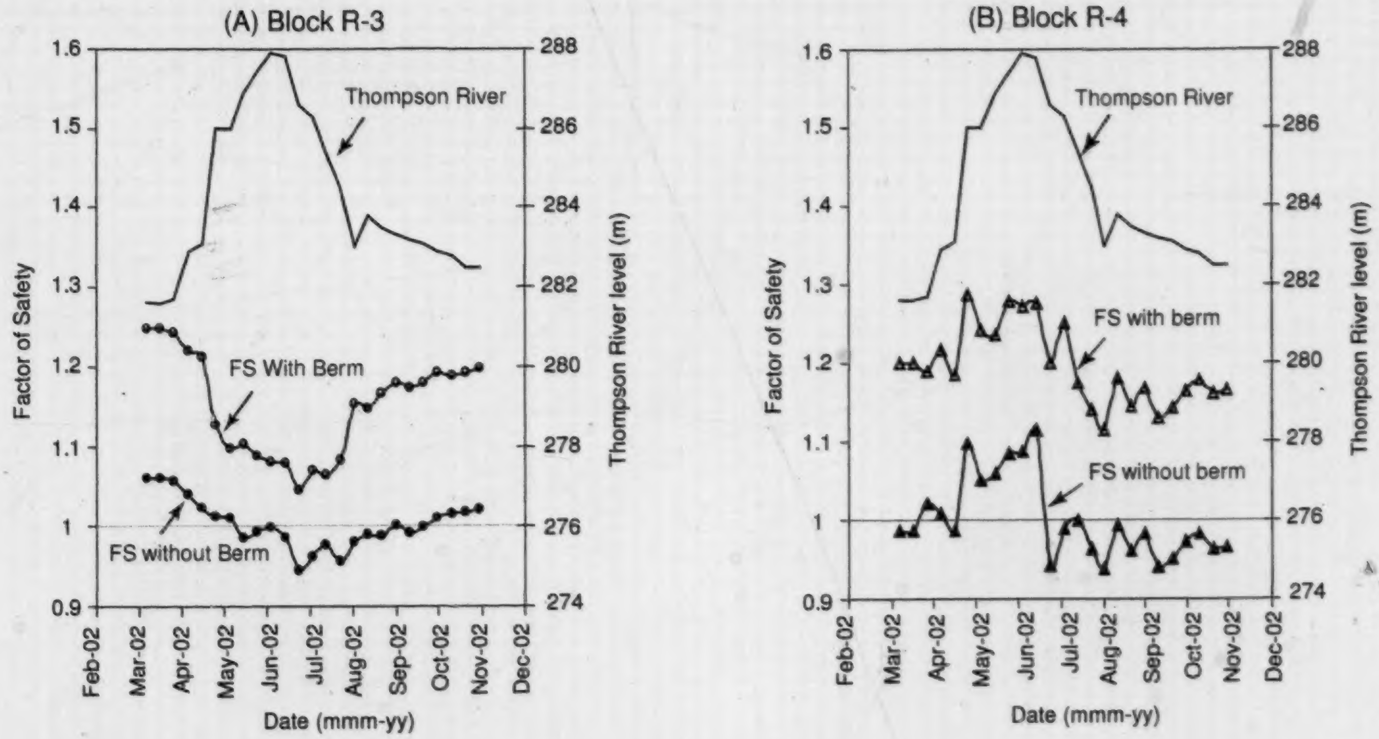

Figure 4.14. Effect of the toe berm construction on the stability of toe blocks, block R-3 and block R-4, with the 2002 Thompson River level fluctuation cycle.

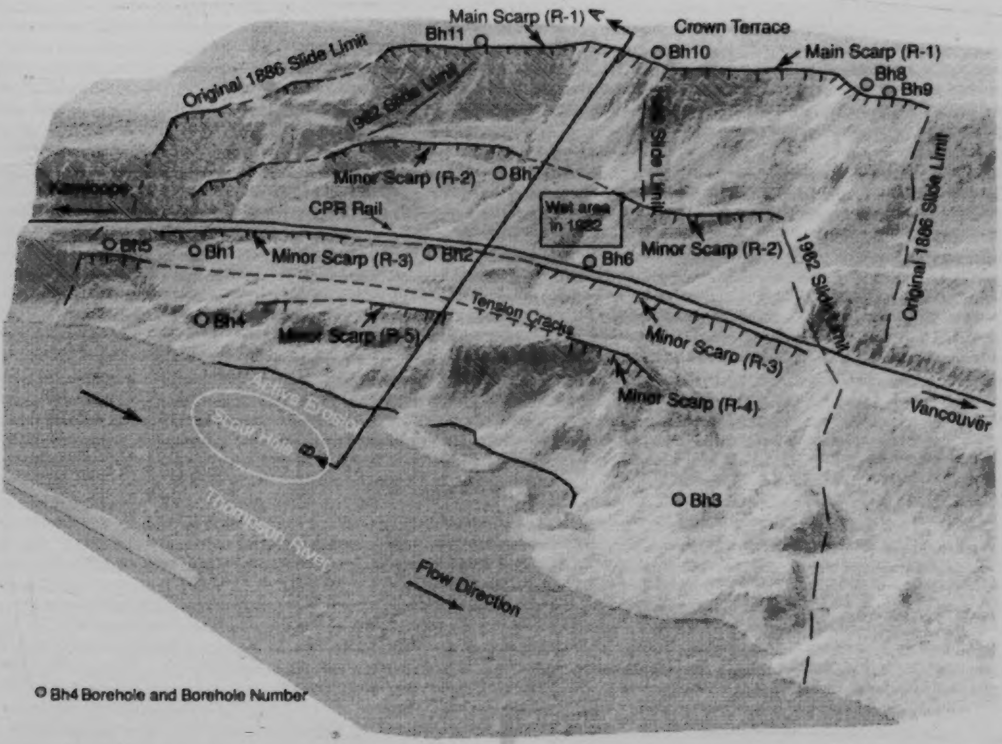
Main Scarp (R-1)
Crown Terrace
Bh11
Bh10
Main Scarp (R-1)
Bh8
Bh9
Original 1886 Slide Limit
1982 Slide Limit
Slide Limit
Original 1886 Slide Limit
Minor Scarp (R-2)
Bh7
Kamloops
CPR Rail
Wet area in 1982
Minor Scarp (R-2)
Bh5
Bh1
Minor Scarp (R-3)
Bh2
Bh6
1982 Slide Limit
Tension Cracks
Bh4
Minor Scarp (R-5)
Minor Scarp (R-3)
Minor Scarp (R-4)
Vancouver
Active Erosion
Scour Hole
Bh3
Thompson River
Flow Direction
Bh4 Borehole and Borehole Number

Figure 4.15. A digital elevation model of the Goddard Slide, looking from the south-west and showing five scarps, borehole locations, the CPR rail line, a scour hole in the Thompson River bed, the seepage locations after the 1982 reactivation at the slide area, and the limits of the 1886 retrogression and 1982 reactivation. At the river level, the slide is 400m wide.

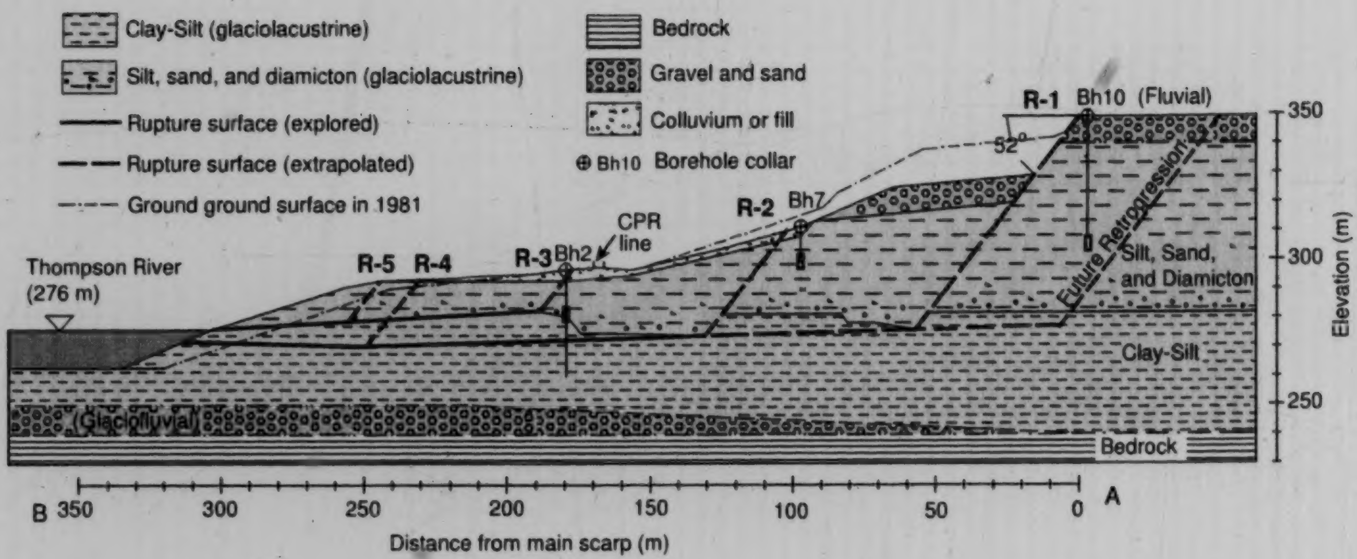

Clay-Silt (glaciolacustrine)
Silt, sand, and diamicton (glaciolacustrine)
Rupture surface (explored)
Rupture surface (extrapolated)
Ground ground surface in 1981
Bedrock
Gravel and sand
Colluvium or fill
Bh10 Borehole collar
Thompson River
(276 m)
R-5
R-4
R-3
Bh2
CPR
line
R-2
Bh7
R-1
Bh10
(Fluvial)
52°
Future Retrogression
Silt, Sand,
and Diamicton
Clay-Silt
(Glaciofluvial)
Bedrock
350
300
250
Elevation (m)
B
350
300
250
200
150
100
50
0
A
Distance from main scarp (m)

Figure 4.16. Cross section after the Goddard 1982 reactivation showing borehole and piezometer locations, ground profile before the Goddard 1982 reactivation, the CPR rail line, five translational blocks, and the stratigraphy of the slide (see Figure 1 and Figure 15 for location of the section).

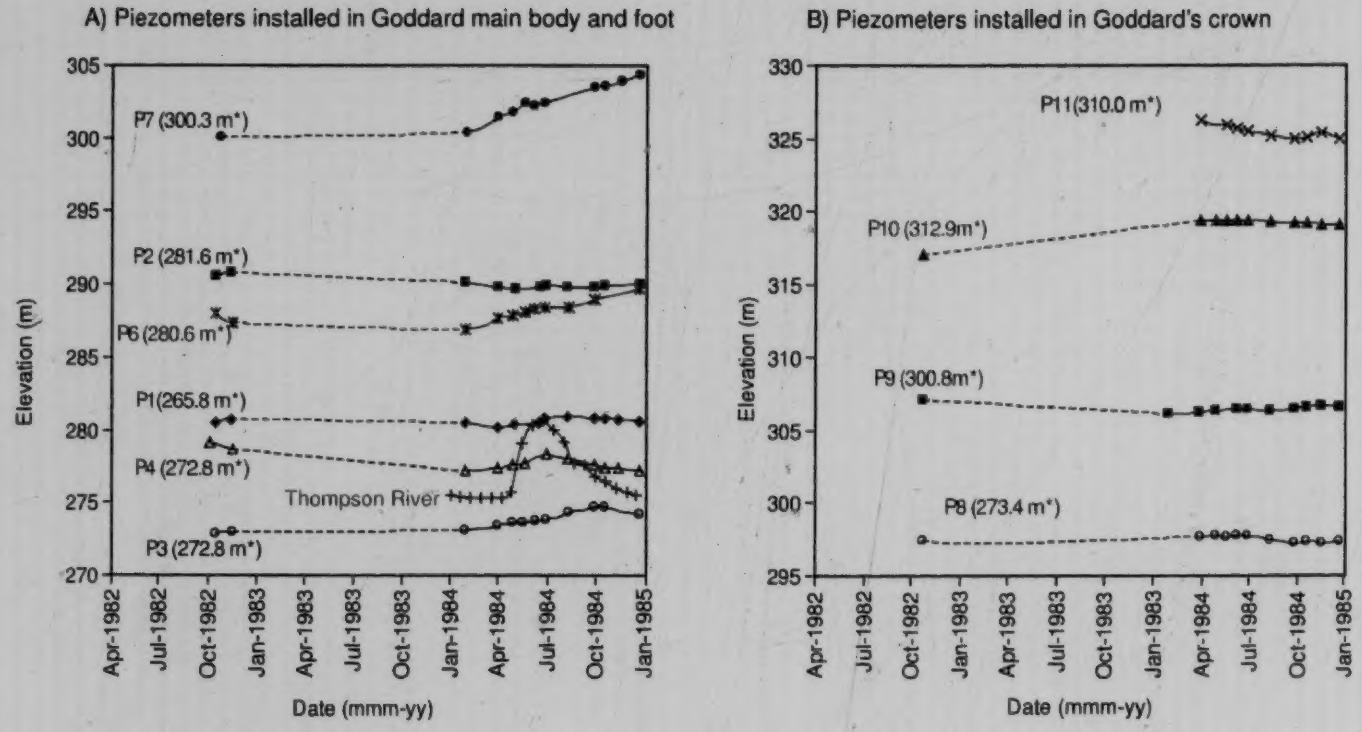

* Piezometer's tip elevation (m)

Figure 4.17. Data from piezometers installed in the Goddard Slide post-reactivation: (A) main body and foot and (B) crown. The frequent readings were stopped in 1985

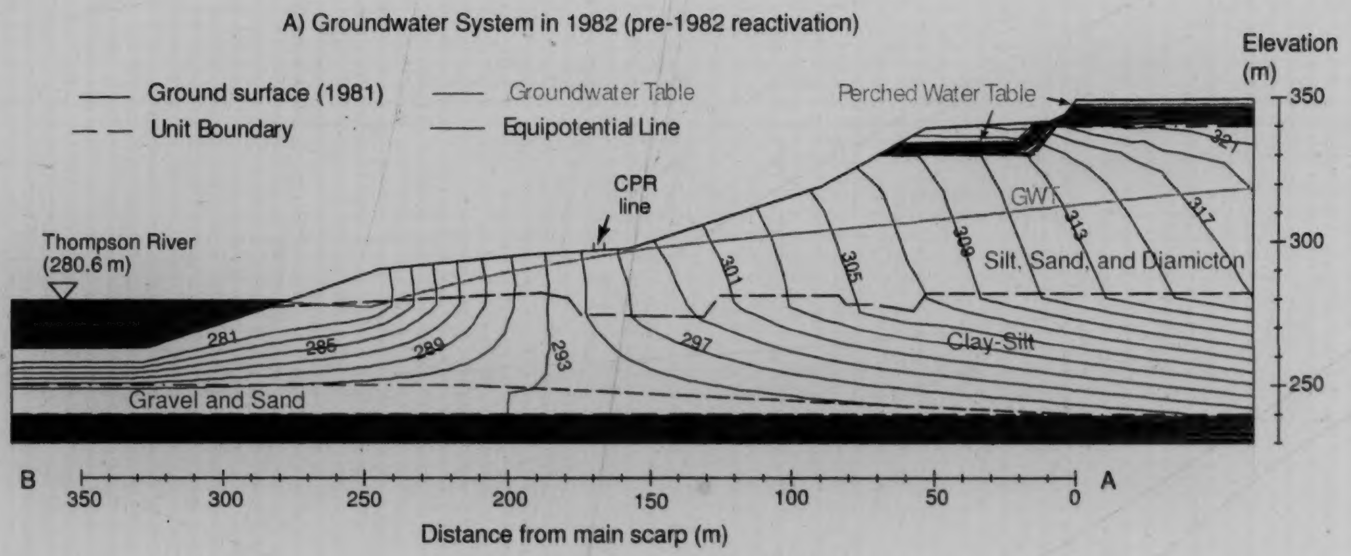
A) Groundwater System in 1982 (pre-1982 reactivation)
Ground surface (1981)
Unit Boundary
Groundwater Table
Equipotential Line
Perched Water Table
Elevation (m)
350
300
250
CPR line
Thompson River (280.6 m)
321
317
313
309
305
301
297
293
289
285
281
GWT
Silt, Sand, and Diamicton
Clay-Silt
Gravel and Sand
B
A
350
300
250
200
150
100
50
0
Distance from main scarp (m)

Figure 4.18A. Groundwater system modeled for the Goddard Slide during the maximum Thompson River level in 1982 (before the 1982 reactivation)

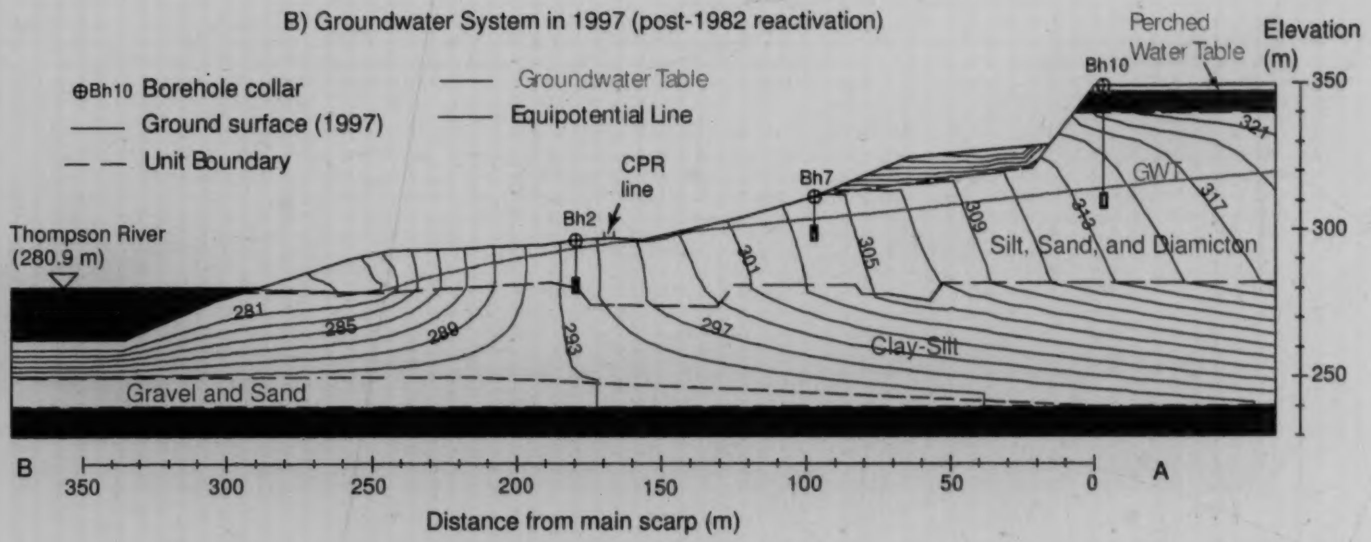

B) Groundwater System in 1997 (post-1982 reactivation)

⊕Bh10 Borehole collar
Ground surface (1997)
Unit Boundary
Groundwater Table
Equipotential Line
CPR line
Thompson River (280.9 m)
Bh2
Bh7
Bh10
Perched Water Table
Elevation (m)
350
300
250
GWT
321
317
313
309
305
301
297
293
289
285
281
Silt, Sand, and Diamicton
Clay-Silt
Gravel and Sand
B
A
350
300
250
200
150
100
50
0
Distance from main scarp (m)

Figure 4.18.B. Groundwater system modeled for the Goddard Slide during the maximum Thompson River level in 1997 (after the 1982 reactivation).

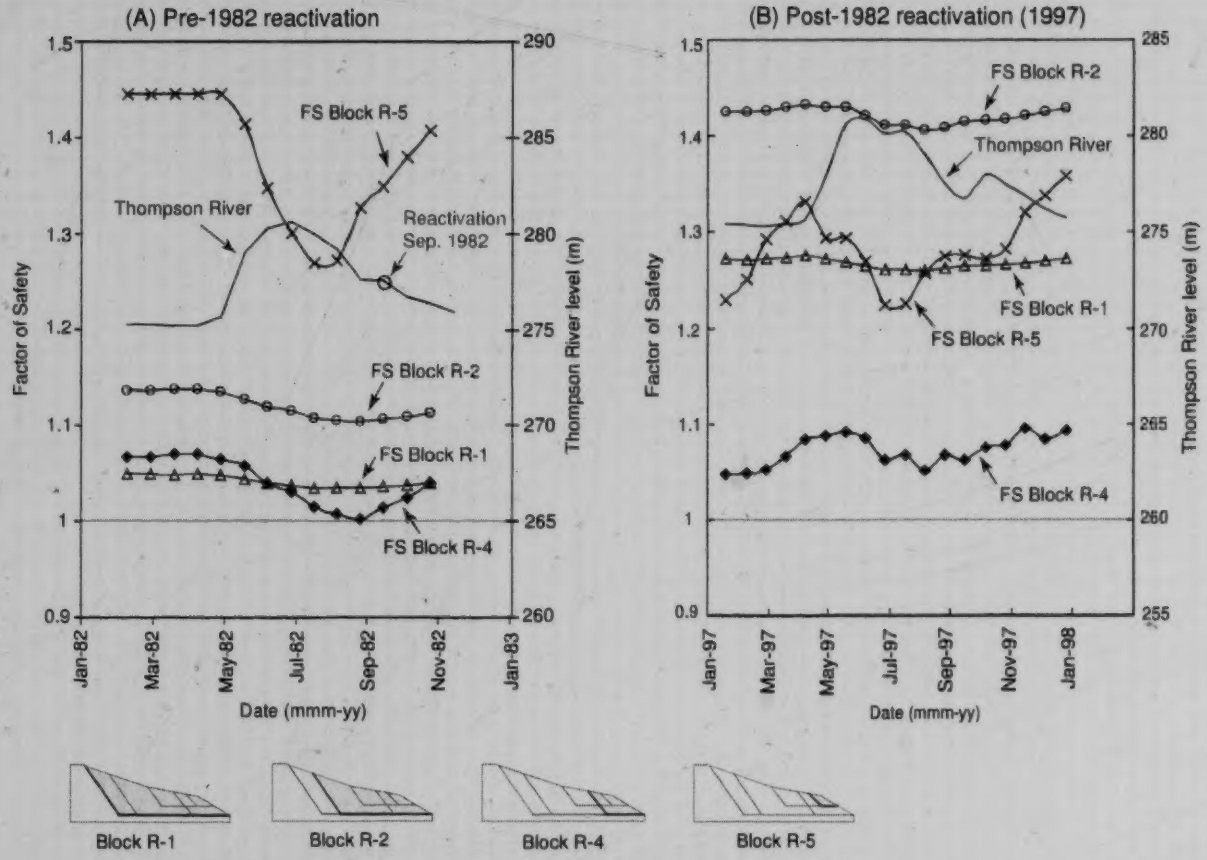

Figure 4.19. Change in the Goddard Slide factor of safety with the Thompson River fluctuation: (A) Pre-1982 reactivation geometry in 1982 and (B) Post-1982 reactivation geometry in 1997.

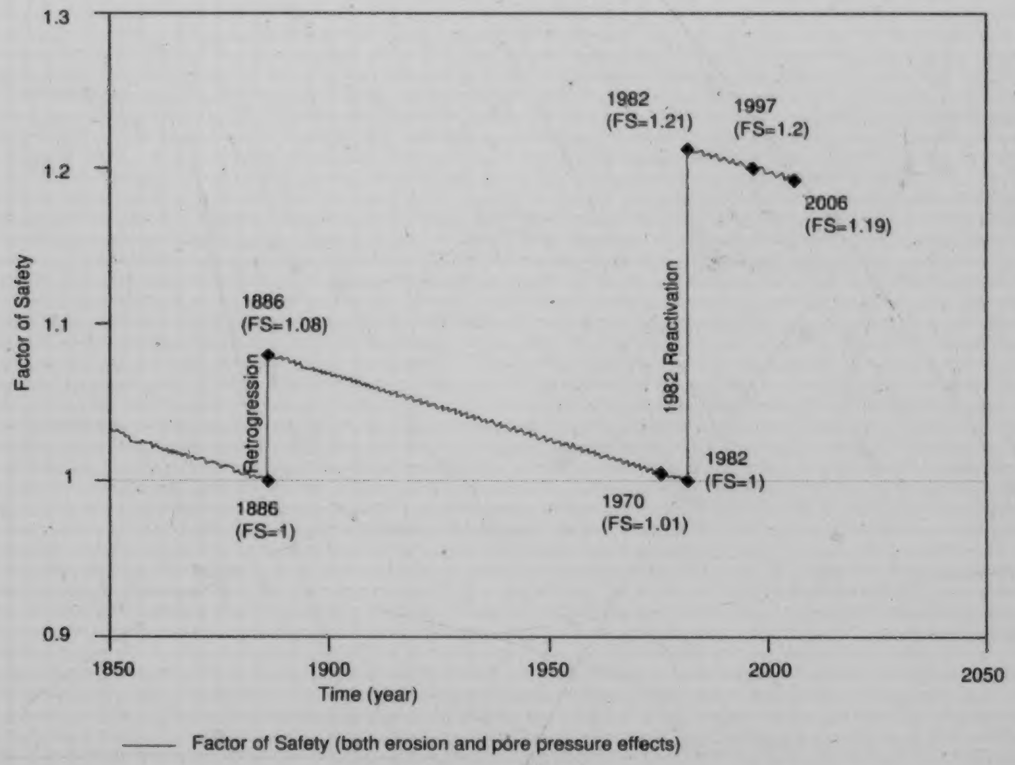

Figure 4.20. Change of factor of safety of the Goddard Slide within last 150 years.

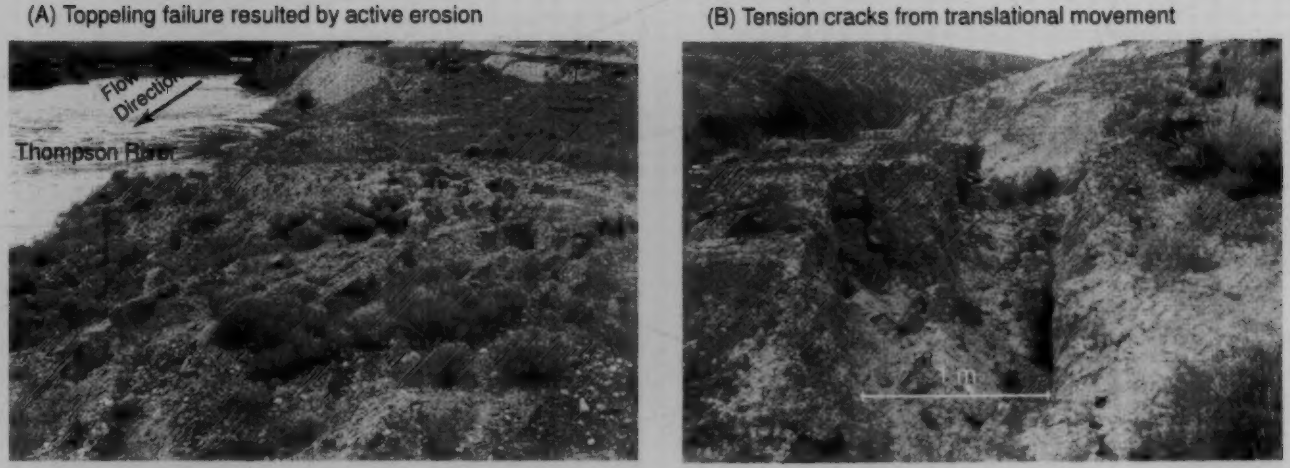

(A) Toppeling failure resulted by active erosion

(B) Tension cracks from translational movement

Figure 4. 21. Cracks at the Goddard Slide toe (A) resulted from toe erosion by the Thompson River at the active erosion site (see Figure 4.15 for location), and (B) resulted from the toe block (block R-4) translational movement (see Figure 4.15 for tension crack location).

Chapter 5

A Review of Movements of Reactivated Translational Earth Slides[1]

Sixty case histories of slow-moving reactivated translational earth slides were examined, and their movement behaviour analysed. The objective was to find correlations between slope and soil parameters and the movement rates of reactivated translational earth slides. The information regarding slope parameters, soil parameters, triggers, and the slide movement rates are summarized. Table 5.1 presents the general information for the earth slides.

5.1. CAUSAL FACTORS

Table 5.2 presents the causal factors for the reactivation of the studied landslides, including their trigger and preparatory factors. Figure 5.1 shows the relative frequency of triggers among the studied slides. As this figure shows that human activity, cut and fill, causes 30 % of the slides' reactivations while natural triggers (rainfall, river erosion, and river draw down) are responsible for 70 % of the reactivations.

---

[1] A version of this paper has been submitted to the 60th Canadian Geotechnical Conference for publication. Eshraghian, A., Martin, C.D., Morgenstern, N.R., 2007. A review of pore-pressure-induced reactivation of translational earth slides.

Rainfall triggers slides by pore pressure increase, filling cracks, and loading on slides due to ponding. Filling, toe cuts, and river erosion trigger slides by changing the geometry of slides. River drawdown is a special trigger which causes reactivation by decreasing the river's supporting force at the toe followed by an increase in the pore pressure in the slide mass.

5.2. PORE-PRESSURE-INDUCED ACCELERATION

The movement rates of the earth slides in the Ashcroft area appear to be sensitive to the pore pressures on their rupture surfaces. Therefore, this study focused on slides whose reactivation movement rates were directly sensitive to the rupture surfaces' pore pressure changes, including slides triggered by rainfall and river drawdown.

In order to conduct a complete study of these slides' movement behaviours, information regarding the geometry, soil properties, and rates of movement were needed. Although most slides triggered by rainfall are caused by increased pore pressure on their rupture surfaces, and, therefore, their reactivation rate is directly sensitive to the pore pressure changes on their rupture surfaces, not enough information was available to do a complete study of all these cases. Among the 30 cases triggered by rainfall and river drawdown, only 17 slides showing rate sensitivity to the pore pressure changes on the slides rupture surfaces had enough information to allow for a detailed study. Table 5.3 provides a list of slides, showing the sensitivity of their rate of movement to change of pore pressure on their rupture surface.

In order to study movement behaviour of a slide, information about the slide's geometry, material property, and previous movement rates is essential.

5.2.1. Geometry

Information regarding the slopes' geometry is presented in Table 5.4. This table presents the slides' dimensions, maximum and average depth of the rupture surfaces, travel angle of the slides, and dip angles of the rupture surface.

5.2.2. Soil Properties

The next essential parameters needed to analyze slides are the properties of the soil on the slides' rupture surfaces. The main information needed is the soil type, index properties, and residual friction angle of the material on the slides' rupture surfaces. Table 5.5 presents the material information for rupture surfaces of the 17 studied slides. Whenever the residual friction angle of the material on the rupture surface was not available, Stark and Eid's (1994) correlation was used to estimate the material's residual friction angle.

5.2.3. Rate of Movement

The rate of movement of the studied slides changed with the pore pressure on the rupture surface. These changes were shown by changes in the slide pore pressure ratio (r_u). In some cases, only two points of the movement behaviour curve of the slide were available, which were usually the pore pressure ratio at the starting of movement and the pore pressure ratio at one other specific rate after the movement started. In some cases, more points of movement behaviour were available and helped to define the movement curve for the rate changes with the pore pressure ratio in more detail.

Movement rate versus the corresponding pore pressure ratio for the studied slides is shown in Table 5.6. In cases with enough information, three points of the rate pore pressure ratio curve are presented, but in cases with limited information, only two points are presented.

5.3. MOVEMENT BEHAVIOUR

The 17 studied slides in the previous section show acceleration when the pore pressure on the slides' rupture surfaces increases. Figure 5.2 shows the changes of the movement rate versus the pore pressure ratio on the rupture surface for a few of the studied slides. As the figure shows, the slides differ in the pore pressure at the time of their movement starts and how they accelerate with changes in the pore pressure ratio after starting movement. All curves show a non-linear relationship between the pore pressure increases and the rate of movement increases.

In order to compare the movement behaviours of the slides, these slides' movement curves had to be compared with each other. Figure 5.3 shows a typical rate versus the pore pressure on the rupture surface changes, the movement behaviour curve, of a reactivated translational earth slide (the Anali-Paty slide). As this figure shows, the rate increases nonlinearly with an increase in the pore pressure ratio (r_u) on the slide rupture surface. When the horizontal scale (movement rate axes) is changed to square root rate axes the movement behaviour curve changes to a straight line (Figure 5.3). Therefore, the slides' non-linear movement behaviour curve can be expressed by Equation 5.1. This equation can be changed to a linear equation (Equation 5.2), which is equivalent to a linear movement behaviour on square root rate axes.

$$v = (a.r_u + b)^2 \qquad \text{(Equation 5.1)}$$

$$\sqrt{v} = (a.r_u + b) \qquad \text{(Equation 5.2)}$$

The intersection of the movement behaviour line in the square root rate axis gives a pore pressure ratio equivalent to the zero rate of movement (r_{u0}) (pore pressure at the start of movement), and the slope of this line shows how the slide accelerates after starting the movement. Figure 5.4 shows more slides' movement behaviour lines on the square root rate axes. This figure shows that r_{u0} for each slide differs from the others and that acceleration with a change in r_u (slope of the line) after movement starts for each slide also differs from that of the other slides. Slides with flatter lines show more increase in rate with the same amount of increase in r_u. Table 5.7 gives the intersection (r_u at the time of movement initiation, r_{uo}) and slope of the movement line on the square root rate axes for the studied slides.

5.3.1. Correlation for the start of reactivation

When studying a slide with possibility for reactivation, we are interested in predicting the movement initiation and at the movement rate. In this section, the conditions for starting the slide's reactivation are studied.

Because the acceleration in the studied slides depends on the pore pressure ratio on the slide's rupture surfaces, the discussion in this section focuses on finding a correlation between the pore pressure ratio at the start of the movement (r_{u0}) and the slides' geometry and soil characteristics. Figure 5.5 shows the change of the starting pore pressure ratio (r_{u0}) with the slides' slope and soil parameters. As this figure shows, r_{u0} increases with the increase in the ratio of the residual friction angle over the summation of the travel angle and rupture surface dip angle. This finding means that an increase in the residual friction angle has a stabilizing effect on the slide's reactivation and that an increase in the travel angle and rupture surface dip angle has a destabilizing effect.

On the other hand, a slide's geometry and soil characteristics, residual friction angle, travel angle, and rupture surface dip are the same parameters that define Factor of

Safety of a slide. Therefore, it is expected to find a correlation between the slide's Factor of Safety and r_{u0}. Using the geometry and material information from the references for the studied slides, Factor of Safety of these slides were calculated for the time of starting the movement. Figure 5.6 shows the correlation between the slides' Factor of Safety at the starting reactivation and r_{u0}. As this figure shows, whatever the starting reactivation pore pressure ratio (r_{u0}) is, the movement always starts with a Factor of Safety close to unity. In fact, in most cases some movement can be expected with a Factor of Safety under 1.1.

5.3.2. Correlation for rate of reactivation movement

In order to obtain a complete picture of the movement behaviour of a slide prone to reactivation, the next step after finding the correlation for the start of reactivation is to predict the rate of reactivation.

The acceleration after the movement starts depends on the slope of the trend line of the movement rate on the square root rate axes. If this slope is high for a slide, more increase in the pore pressure ratio will be needed to increase the rate compared to that needed for a slide with a lower slope for the movement behaviour line in the square root rate axes. The acceleration of slides during reactivation actually behaves opposite to the slope of their trend line on the square root rate movement axes. Therefore, we call the inverse of the slope of the movement rate trend line on the square root rate axes the Acceleration Factor (AF). A slide with a lower slope of movement rate trend line on the square root rate axes will accelerate more easily than other slides, and its AF will be higher.

The first attempt was to try to find a correlation between the AF and the same parameters governing the start of the movement (Factor of Safety). Figure 5.7 shows no correlation between the Factor of Safety at the movement initiation and the AF. Therefore, after the movement starts, how it continues does not have anything to do with the Factor of Safety, and other factors should govern the acceleration of slides. Thus just because a slide with a specific Factor of Safety is reactivated at a specific rate does not mean that another slide with the same Factor of Safety will move at the same rate.

The material on the slide's rupture surface should play a significant role in the acceleration of that slide with a change in the pore pressure on the rupture surface. The plasticity index (PI) of the material on the slide's rupture surface reflects the mineralogy and clay content of the clay material. Therefore, plasticity index was selected as the parameter which shows the material property on a slide's rupture surface. Figure 5.8 shows the AF versus the plasticity index of the material on the slides' rupture surface. Again, no clear correlation is observed between AF and plasticity index, but a closer look at this graph reveals an important point: some cases have similar plasticity indexes but different AF. Table 5.8 compares four slides with similar material on their rupture surface (similar Plasticity Indexes) but different AFs. As this table shows, the AF of the shallower slides is greater than that of the deeper ones. Therefore, another important parameter for the acceleration of slides is the slides' depth. With a decrease in the average slide depth, the possibility of rapid movement increases.

Therefore, the effects of both the slide depth and the material property on the slide rupture surface have to be considered to understand a slide's acceleration behaviour. In order to consider these effects, another parameter was defined by multiplying the slide's average depth and Plasticity Index of the material on the slide's rupture surface. Figure 5.9 shows the change in the AF versus the result of multiplying the slide's depth and the slide's material Plasticity Index. This figure shows a decrease in the AF with this multiplication. This result means that this new parameter actually shows how ductile the slide mass can be; therefore, the result of multiplying the slide's depth and the slide's material plasticity index was called Ductility Factor (DF)

(Equation 5.3). With an increase in the Ductility Factor (DF), the slide's Acceleration Factor (AF) decreases.

Ductility Factor= PI(%) × Average Depth (m) (Equation 5.3)

5.4. DISCUSSION

Considering the rough data that were used, the correlations for the start of the reactivation and the acceleration of the slide movement are satisfactory. It was found that the slide reactivation always started with a Factor of Safety near unity, but that the movement acceleration after the movement initiation depended on other factors. Two factors affecting the slides' reactivation rate after the movement started were the materials on the slides' rupture surfaces and the slides' average depth.

The Plasticity Index (PI) was selected as an indicator of the material property on the slides' rupture surface. It was found that with an increase in the Plasticity Index, the slides will be more ductile and the movement rate was less likely to accelerate compared to slides with a lower Plasticity Index and a similar average depth. The Plasticity Index is a parameter which shows the range of the water content that put a soil in a plastic state.

In almost all the studied cases, the material on the rupture surface was overconsolidated fine-grain material (silt, clay, or clayshale). During shearing, overconsolidated materials dilate and absorb water. Therefore, the water content of the material on the slides' rupture surfaces increases when enough water is available (as was the case here). As the water content increases from the soil's plastic limit toward the soil's liquid limit (LL), the material behaves more fluid-like with less viscosity. If the water content passes the liquid limit, the soil's viscosity will drop dramatically and might significantly affect the slide's movement rate. If the plasticity index is high enough, an increasing in the water content during shearing will likely cause the soil to stay relatively near to its plastic limit and vice versa. This result probably explains why slides with a higher Plasticity Index have a lower rate of movement with the same changes in the pore pressure ratio (r_u), and, therefore, a lower Acceleration Factor (AF) than the slides with a lower PI. A study of the liquidity index (LI) could probably support this conclusion, but not enough information about the water content of the slides' shear zone materials was available and measuring this water content was difficult, because as soon as the movement rate decreased, the shear zone material started consolidating and losing water; therefore, the water content dropped.

The other parameter affecting the rate of the reactivation movement is the average depth of the slide's rupture surface. When the pressure on the rupture surface's materials increases, they become more ductile in shear tests such as the triaxial test. With an increase in the pressure on the materials on rupture surface their ability to dilate decreases. Thus, they are less likely to absorb water and increase their liquidity index during shearing. Therefore, their viscosity does not decrease, and the rate of movement does not increase. Therefore, the slide will have less Acceleration Factor (AF) and behaves in a more ductile fashion.

Also, with a decrease in the pressure on a slide's rupture surface, the shear zone thickness increases (Picarelli et al. 2004), and instead of having a concentrated slip surface, the slide is more likely to have thicker rupture zone during shearing. Therefore, a shear strain in a shallower slide's thicker shear zone will cause more movement compared to that in the thinner shear zone of a deeper slide. The result will be a higher rate of movement in the shallower slide. This difference is shown by the higher AF for a shallower slide compared to the AF for a deeper slide.

5.5. CONCLUSIONS

This study of the reactivated translational earth slides' movement behaviour had two main results. First, the reactivation was found to start with the Factor of Safety near unity. In fact, movement could be expected with a Factor of Safety less than 1.1. Second, the movement rate acceleration depended on the Plasticity Index of the material on the slide's rupture surface and the average stress on the rupture surface (the slide's average depth).

A slide's movement behaviour depends on the slide's Ductility Factor (DF) which is the result of multiplying the slide's depth and Plasticity Index of the material on the slide's rupture surface. The effect of the slide's DF on movement behaviour after the start of the reactivation can be explained by the slide's rupture surface material dilation during shearing.

A higher stress on a slide's rupture surface decreases the slide's dilation ability and reduces the possibility of increases in the material's Liquidity Index. Thus, the viscosity of the material on the rupture surface may decrease less. The higher stress on a slide's rupture surface also decreases the shear zone thickness, and, therefore, a specific shear strain produces less movement and a lower rate of movement for deeper slides. With a higher Plasticity Index for the slide rupture surface material, the dilation during shearing causes less increase in the liquidity index; therefore, less decrease in the material's viscosity occurs. The result will be a slower reactivation and a lower Acceleration Factor (AF).

5.6. REFERENCES

Barton, B., and Thomson, R.I. 1984. Studies of the water balance in a rapidly degrading soil cliff. In Proceedings of the Fourth International Symposium on Landslides. Toronto, Ontario. 16-21 September 1984. Toronto, Vol.1, pp. 355-361.

Baum, R.L., and Reid, M.E. 1995. Geology, hydrology, and mechanics of a slow-moving, clay-rich landslide, Monolulu, Hawaii. Reviews in Engineering Geology, 10: 79-105.

Bertini, T., Cugusi, F., D-Elia, B., and Rossi-Doria, M. 1984. Climate conditions and slow movments of colluvial covers in central Italy. In Proceedings of the Fourth International Symposium on Landslides. Toronto, Ontario. 16-21 September 1984. Toronto, Vol.1, pp. 367-376.

Brooker, E.W., and Peck, R.B. 1993. Rational design treatment of slides in overconsolidated clays and clay shales. Canadian Geotechnical Journal, 30: 526-544.

Buccolini, M., and Sciarra, N. 1996. The Caramanico landslide (Abruzzo, Italy). In Proceedings of the Seventh International Symposium on Landslides, 17-21 June 1996. Tronheim, Norway. 17-21 June 1996. A.A. Balkema, Rotterdam, Brookfield, Vol.2, pp. 661-666.

Canuti, P., Focardi, P., Garzonio, C.A., Rodolfi, G., and Zanchi, C. 1984. Analysis of the dynamic of a mass movement on silty clayey lacustrine deposits in north-central Italy (Mugello, Tuscany). In Proceedings of the Fourth International Symposium on Landslides. Toronto, Ontario. 16-21 September 1984. Toronto, Vol.1, pp. 391-397.

Chandler, M.P., and Huchinson, J.N. 1984. Assesment of relative slide hazard within a large pre-existing coastal landslide at Ventor, Isle of Wight. In Proceedings of the Fourth International Symposium on Landslides. Toronto, Ontario. Toronto, Vol.2, pp. 517-522.

Chin, B.G., Wightman, A., Lo, R.C., and Stewart, W.P. 1984. Case history of a landslide in lacustrine soils. In Proceedings of the 37th Canadian Geotechnical Conference. Toronto, Ontario. Canadian Geotechnical Society, pp. 75-84.

Christiansen, E.A. 1983. The Denholm landslide, Saskatchewan, Part I: Geology. Canadian Geotechnical Journal, 20: 197-207.

Christiansen, E.A., and Sauer, E.K. 1984. Landslide styles in the Saskatchewan River plain: a geological apprisal. In Proceedings of the 37th Canadian Geotechnical Conference. Toronto, Ontario. Canadian Geotechnical Society, pp. 35-48.

Clifton, A.W., Krahn, J., and Fredlund, D.G. 1981. Riverbank instability and development control in Saskatoon. Canadian Geotechnical Journal, 18: 95-105.

Clifton, A.W., Yoshida, R.T., and Chursinoff, R.W. 1984. Regina Beach, a town on a landslide. In Proceedings of the 37th Canadian Geotechnical Conference: Canadian case histories - landslides. Toronto, Ontario. Canadian Geotechnical Society, pp. 85-94.

Corominas, J., Moya, J., Ledesma, A., Rius, J., Gili, J.A., and Lloret, A. 1999. Monitoring of the Valcebre landslide, eastern Pyrenees, Spain. In International Symposium on Slope stability Engineering. Edited by N. Yagi, T. Yamagami, and J. Jiang. Japan. 8-11 November, 1999. A.A. Balkema, Rotterdam, Brookfield, Vol.2, pp. 1239-1244.

Cruden, D.M., Thomson, S., Kim, H.J., and Peterson, A.E. 1995. The Edgerton landslides. Canadian Geotechnical Journal, 32: 989-1001.

Cruden, D.M., Lu, Z.-Y., and Thomson, S. 1997. The 1939 Montagneus River landslide, Alberta. Canadian Geotechnical Journal, 34: 799-810.

Cruden, D.M., Peterson, A.E., Thomson, S., and Zabeti, P. 2002. Thirty-five years of activiry at the Lesueur landslide, Edmonton, Alberta. Canadian Geotechnical Journal, 39: 266-278.

Eckel, B.F., Sauer, E.K., and Christiansen, E.A. 1987. The Petrofka landslide, Saskatchewan. Canadian Geotechnical Journal, 24: 81-99.

Eigenbrod, K.D., and Morgenstern, N.R. 1971. A slide in cretaceous bedrock at Devon, Alberta. In International Conference on Stability in Open Pit Mining, 1971. Edited by C.O. Brawner and V. Milligan. Vancouver. Society of Mining Engineers of the American Institution of Mining, New York, pp. 223-238.

Eshraghian, A., Martin, C.D., and Cruden, D.M. 2005a. Landslides in the Thompson River Valley between Ashcroft and Spence's Bridge, British Columbia. In Proceedings of the International Conference on Landslide Risk Management. Vancouver, Canada. May 31 to June 4, 2005, pp. 437-446.

Eshraghian, A., Martin, C.D., and Cruden, D.M. 2005b. Earth slide movements in the Thompson River Valley, Ashcroft, British Columbia. In Proceedings of the 58th Canadian Geotechnical Conference. Saskatoon, Saskatchewan, Canada. September 18-21, 2005.

Esser, A.J. 1996. Case study of a landslide in heavily overconsolidated lacustrine clay. In Proceedings of the Seventh International Symposium on Landslides, 17-21

June 1996. Tronheim, Norway. 17-21 June 1996. A.A. Balkema, Rotterdam, Brookfield, Vol.2, pp. 707-714.

Gerber, G.E., Tweedie, R.W., Bean, S., Thomson, S., and Eisenstain, Z. 1993. Stability of the north slope and portal at the Edmonton Light Rail Transit crossing of the North Saskatchewan River. Canadian Geotechnical Journal, 30: 12-21.

Gillon, M.D., Riley, P.B., Halliday, G.S., and Lilley, P.B. 1992. Movement history and infiltration Cairnmuir landslide NZ. In Proceedings of the Sixth International Symposium on Landslides, 10-14 February 1992. Christchurch, New Zealand. 10-14 Februarry 1992. A.A. Balkema, Rotterdam, Brookfield, pp. 103-109.

Gottardi, G., and Tonni, L. 1999. An investigation on the stability of two adjacent slope movements. In International Symposium on Slope stability Engineering. Edited by N. Yagi, T. Yamagami, and J. Jiang. Japan. 8-11 November, 1999. A.A. Balkema, Rotterdam, Brookfield, Vol.2, pp. 1211-1216.

Hardy, R.M., Clark, J.I., and Stepanek, M. 1980. A summary of case histories spanning thirty years of slope stabilization in Calgary, Alberta. In Slope Stability Problems in Urban Areas: Specialty Conference. Toronto, Canada. April 21-22, 1980.

Haug, M.D., Sauer, E.K., and Fredlund, D.G. 1977. Retrogressive slope failure at Beaver Creek, South of Saskatoon, Saskatchewan, Canada. Canadian Geotechnical Journal, 14: 288-301.

Kelly, A.J., Sauer, E.K., Christiansen, E.A., Barbour, S.L., and Widger, R.A. 1995. Deformation of the Deer Creek Bridge by an active landslide in clay shale. Canadian Geotechnical Journal, 32: 701-724.

Kelly, A.J., Antunes, P.J., Vu, H.Q., Clifton, A.W., and Widger, R.A. 2005. Analysis of multiple landslide blocks on a highway crossing of the Frenchman River Valley, Saskatchewan. In Proceedings of the 58th Canadian Geotechnical Conference. Saskatoon, Saskatchewan. Canadian Geotechnical Society.

Kelly, A.J., Antunes, P.J., Vu, H.Q., Clifton, A.W., Widger, R.A., and King, G.L. 2005. Retrogressive landslide near Ptince Albert, Saskatchewan: a case history. In Proceedings of the 58th Canadian Geotechnical Conference. Saskatoon, Saskatchewan. Canadian Geotechnical Society.

Krahn, J., Jonson, R.F., Fredlund, D.G., and Clift, A.W. 1979. A highway cut failure in cretaceous sediments at Maymont, Saskatchewan. Canadian Geotechnical Journal, 16: 703-715.

Krahn, J., and Weimer, N.F. 1984. The W.I.D landslide. In 37th Canadian Geotechnical Conference: Canadian case histories - landslides. Toronto, Ont. Canadian Geotechnical Society, pp. 209-215.

Lokin, P., Petrice, M., Vasic, M., and Sakovic, S. 1996. Landslide along the Danube Bank at Novi Sad, Yugoslavia. In Proceedings of the Seventh International Symposium on Landslides, 17-21 June 1996. Tronheim, Norway. 17-21 June 1996. A.A. Balkema, Rotterdam, Brookfield, Vol.2, pp. 803-808.

Longworth, T.I. 1992. Investigation, monitoring, and emergency remedial works at the La Butte landslide, Mauritius. In Sixth International Symposium on Landslides. Edited by D.H. Bell. Christchurch. A.A. Balkema, Rotterdam, Brookfield, Vol.3, pp. 1593-1602.

Martin, R.L., Williams, D.R., Balanko, L.A., and Morgenstern, N.R. 1984. The Grierson Hill slide, Edmonton, Alberta. In 37th Canadian Geotechnical Conference:

Canadian case histories - landslides. Toronto, Ont. Canadian Geotechnical Society, pp. 125-133.

Miller, B.G.N., and Cruden, D.M. 2002. The Eureka River landslide and dam, Peace River lowlands, Alberta. Canadian Geotechnical Journal, 39: 863-878.

Misfeldt, G.A., Sauer, E.K., and Christiansen, E.A. 1991. The Hepburn landslide: An interactive slope-stability and seepage analysis. Canadian Geotechnical Journal, 28: 556-573.

Nakamura, H. 1984. A landslide, its movement mechanism and control works. In Fourth International Symposium on Landslides. Toronto, Ont. Toronto, pp. 155-159.

Oyagi, N., Makio, H., and Mori, S. 1996. Landslide structure and control works at Nashitani landslide, Wakayama Pretecture, Japan. In Eight International Conference and Field Trip on Landslides. Edited by J. Chacon, C. Irigaray, and T. Frenandez. Granada, Spain. 27-28 September, 1996. A.A. Balkema, Rotterdam, Brookfield.

Pauls, G.J., Sauer, E.K., Christiansen, E.A., and Widger, R.A. 1999. A transient analysis of slope stability following drawdown after flooding of a highly plastic clay. Canadian Geotechnical Journal, 36: 1151-1171.

Pennell, D.G. 1969. Residual strength analysis of five landslides. Ph.D thesis, University of Alberta, Edmonton, Alberta.

Picarelli, L., Urciuoli, G., and Russo, C. 2004. Effect of groundwater regime on the behaviour of clayey slopes. Canadian Geotechnical Journal, 41: 467-484.

Richardson, N.W. 1984. Muddy Lake, Saskatchewan, site investigation and analysis. In 37th Canadian Geotechnical Conference: Canadian case histories - landslides. Toronto, Ont. Canadian Geotechnical Society, pp. 167-180.

Sauer, E.K. 1983. The Denholm landslide, Saskatchewan, Part 2: Analysis. Canadian Geotechnical Journal, 20: 208-220.

Sauer, E.K., and Christiansen, E.A. 1985. A landslide in till near Warman, Saskatchewan, Canada. Canadian Geotechnical Journal, 22: 195-204.

Sauer, E.K., and Christiansen, E.A. 1987. The Denholm landslide, Saskatchewan, Canada: an update. Canadian Geotechnical Journal, 24: 163-168.

Sauer, E.K., Egeland, A.K., and Christiansen, E.A. 1993. Compression Characteristics and index properties of tills and intertill clays in southern Saskatchewan, Canada. Canadian Geotechnical Journal, 30: 257-275.

Skempton, A.W., Leadbeater, A.D., and Chandler, R.J. 1989. The Mam Tor landslide, north Derbyshire. Philosophical Transactions of the Royal Society of London. Series A, Mathematical and Physical Science, 329(1607): 503-547.

Thomson, S., and Hardy, D.W. 1975. The Little Smoky landslide. Canadian Geotechnical Journal, 12: 379-392.

Thomson, S., and Tweedie, R.W. 1978. The Edgerton landslide. Canadian Geotechnical Journal, 15: 510-521.

Thomson, S., and Kjartanson, B.H. 1985. A study of delayed failure in a cut slope in stiff clay. Canadian Geotechnical Journal, 22: 285-297.

Tommasi, P., Pellegrini, P., Boldini, D., and Ribacchi, R. 2006. Influence of rainfall regime on hydraulic conditions and movement rates in the overconsolidated clayey slope of the Ovieto hill (central Italy). Canadian Geotechnical Journal, 43: 70-86.

Tonnetti, G., and Angeli, M.G. 1984. Geological kinematical and developing features of some landslides in Plio-Pleistocene clayey sediments of the Adriatic Hilly Region in Italy. In Proceedings of the Fourth International Symposium on Landslides. Toronto, Ont. Toronto, Vol.2, pp. 221-226.

Watts, C.R., and Macfarlane, D.F. 1996. Engineering geology of the Cairnmuir landslide, New Zealand. In Proceedings of the Seventh International Symposium on Landslides, 17-21 June 1996. Tronheim, Norway. 17-21 June 1996. A.A. Balkema, Rotterdam, Brookfield, Vol.2, pp. 931-936.

Wedage, A.M. 1995. Influence of rate effects on the residual strengths of moving slopes. Ph.D thesis, University of Alberta, Edmonton.

Wilson, S.D., and Mikkelsen, P.E. 1978. Field instrumentation. In Landslides, analysis and control: Transportation Research Board, Special Report 176. National Academy of Science, Washington D.C. pp. 112-138.

Yoshida, R.T., and Krahn, J. 1984. Movement and stability analysis of the Beaver Creek landslide. In Proceedings of the 37th Canadian Geotechnical Conference: Canadian case histories - landslides. Toronto, Ont. Canadian Geotechnical Society, pp. 223-231.

Yoshida, R.T., and Krahn, J. 1985. Movement and stability analysis of the Beaver Creek landslide, Saskatchewan, Canada. Canadian Geotechnical Journal, 22: 277-285.

Table 5.1. Studied cases of reactivated translational earth slides.

Case	Name	Location	References
1	Denholm	North Battleford, Saskatchewan, Canada	Sauer (1983), Christiansen (1983), Sauer and Christiansen (1987), Christiansen and Sauer(1984)
2	Little Smoky	Little Smoky Bridge, Central Alberta, Canada	Thomson and Hardy (1975), Brooker and Peck (1993)
3	Maymont	Maymont Bridge, Saskatchewan, Canada	Krahn et al.(1979), Christiansen and Sauer (1981)
4	Hepburn	North Saskatchewan River Valley, Saskatchewan	Misfeldt et al. (1991)
5	Lesueur	North East Edmonton, Alberta, Canada	Cruden et al.(2002), Pennell (1969)
6	Edgerton North	48km north of Waimwright, Alberta, Canada	Thomson and Tweedie (1978), Cruden et al. (1995)
7	Edgerton South	48km northern of Waimwright, Alberta, Canada	Thomson and Tweedie(1978), Cruden et al. (1995)
8	Edgerton East	48km northern of Waimwright, Alberta, Canada	Thomson and Tweedie (1978), Cruden et al. (1995)
9	Beaver Creek	South of Saskatoon, Saskatchewan, Canada	Haug et al.(1977), Yoshida and Krahn(1985), Christiansen and Sauer (1984), Yoshida and Krohn (1984)
10	Saskatoon 13th street	13th street, Saskatoon, Saskatchewan, Canada	Clifton et al. (1981)
11	Nutana Collegiate	Saskatoon, Saskatchewan, Canada	Clifton et al. (1981)
12	Saskatoon 18th street	18th street, Saskatoon, Saskatchewan, Canada	Clifton et al. (1981)
13	Warman	10km North of Saskatoon, Saskatchewan, Canada	Sauer and Christiansen (1985), Sauer et al. (1993), Christiansen and Sauer (1984)
14	Whitemud freeway	Edmonton, Alberta, Canada	Thomson and Kjartanson (1985)

Table 5.1 Continued.

Case	Name	Location	References
15	LRT Portal	Edmonton, Alberta, Canada	Gerber et al. (1993)
16	Rycroft (Saddle River Slide)	Saddle River, near Rycroft, Alberta, Canada	Cruden et al. (1993), Miller and Cruden (2002)
17	Montagneuse River	West of Peace River, Montagneuse River	Cruden et al. (1997)
18	Seattle Freeway	Seattle washington, U.S	Brooker an Peck (1993)
19	Bismarck Bridge	Missouri River, U.S	Brooker and Peck(1993)
20	Smith Bridge	Athabasca River at Smith, Alberta, Canada	Brooker and Peck (1993)
21	Dunvegan Creek Slide	Peace River at Dunvegan, Northern Alberta, Canada	Brooker and Peck(1993), Miller and Cruden (2002), Pennell (1969)
22	Swan Hills Oil Field	Peace River, Taylor, British Columbia, Canada	Brooker and Peck(1993)
23	Savery Creek	North of Colorado,Central Wyoming, U.S	Brooker and Peck(1993)
24	Peace River Bridge	Peace River, Taylor, British Columbia, Canada	Brooker and Peck(1993)
25	Grierson Hill Slide	North Saskatchewan Valley, Edmonton, Alberta, Canada	Martin et al.(1984), Pennell (1969)
26	Merritt	Nicola River Valley, Merritt, British Columbia, Canada	Chin et al. (1984)
27	Regina Beach	Regina Beach, Saskatchewan, Canada	Clifton et al. (1984)
28	WID	Irrigation Canal, Bow River, Calgary, Alberta, Canada	Krahn and Weimer (1984), Hardy et al. (1980)

Table 5.1 Continued.

Case	Name	Location	References
29	Muddy Lake	10 km south of Town of Unity, Saskatchewan, Canada	Richardson (1984)
30	Petrofka	Petrofka Bridge, North Saskatchewan River, Saskathewan, Canada	Eckel et al. (1987)
31	Eureka	Eureka River, Peace River Lowlands, Canada	Miller and Cruden (2002)
32	Alani-Paty	Manou Valley, Honolulu, Hawaii	Baum and Reid (1995)
33	Fort Benton	Burlington Northern Rail, Wetern Montana, U.S	Wilson and Mikkelsen (1978)
34	Caramanico	Caramanico, Terme, Abruzzo, Italy	Buccolini and Sciarra (1996)
35	Chagrin	Chagrin River, Northern Ohio, U.S	Esser (19996)
36	Sloboda Bridge	Sloboda Bridge, Danube bank at Novisad, Yogoslavia	Lokin et al. (1996)
37	Cairnmuir	Lake Dunstan, Upstream of Clyde Dam, New Zealand	Watts and Macfarlane (1996), Gillon et al. (1992)
38	Devon	Highway 60, North Saskatchewan Valley, Edmonton, Alberta	Eigenbrod and Morgenstern (1971)
39	La Butte	Port Louis, Maritius Iland	Longworth (1992)
40	Montegranaro	Adriatic Hilly Region, Italy	Tonnetti and Angeli (1984)
41	Montappone	Adriatic Hilly Region, Italy	Tonnetti and Angeli (1984)
42	Castignano	Adriatic Hilly Region, Italy	Tonnetti and Angeli (1984)
43	Monturano	Adriatic Hilly Region, Italy	Tonnetti and Angeli (1984)
44	Ventor	Town of Ventor, Southern coast of Isle of Wight, Britain	Chandler and Huchinson (1984)

Table 5.1 Continued.

Case	Name	Location	References
45	Corniglio	Corniglio Village, near Parma, Northern Apennines, Italy	Gottardi and Tonni (1999)
46	Vallcebre	140 km North of Barcelona, Eastern Pyrenees, Spain	Corominas et al. (1999)
47	San Matino	Hilly Piedmont belt of the Abruzzi Adriatic, Italy	Bertini et al. (1984)
48	Mishitani	Mishitani River, Wakayama prefecture, Kii Peninsula, Western Japan	Oyagi et al. (1996)
49	CN50.9 (Deep block)	CN rail, Ashcroft, British Columbia, Canada	Eshraghian (2005), Keegan et al. (2003)
50	South Slide (Toe block)	CPR Rail, Ashcroft, British Columbia, Canada	Eshraghian (2005)
51	Mam Tor	North Derbyshire	Wedage (1995), Skempton et al. (1989)
52	San Martino	Central Italy	Picarelli et al. (2004), Bertini et al. (1984)
53	Deer Creek	North Saskatchewan River, Saskatchewan	Kelly et al. (1995)
54	Carrot River	East-central saskatchewan	Pauls et al. (1999)
55	Sarukuyoji	Japan	Nakamura (1984)
56	Fagna Slide	Mugello valley, north-central italy	Canuti et al. (1984)
57	highcliff	christchun\rch bay, hampshire, UK	Barton and Thomson (1984)
58	Porta Cassia	Town of Ovieto, Central Italy	Tommasi et al. (2006)
59	Frenchman	Frenchman River Valley, Shaunavon, Saskatchewan	Kelly et al. (2005)
60	Prince Albert	North Saskatchewan River, west of Prince Albert, Saskatchewan	Kelly et al. (2005)

Table 5. 2. Causal factors of studied, reactivated, translational, earth slides.

Case	Name	Trigger	Preparatory Factors
1	Denholm	River erosion	NA
2	Little Smoky	River erosion	NA
3	Maymont	Toe cut	NA
4	Hepburn	River erosion	Artesian pressure at toe
5	Lesueur	River erosion	Fill at head
6	Edgerton North	Rainfall	NA
7	Edgerton South	Rainfall	NA
8	Edgerton East	Rainfall	NA
9	Beaver Creek	River Erosion	Rainfall
10	Saskatoon 13th Street	Rainfall	Surficial water
11	Nutana Collegiate	Rainfall	Surficial water
12	Saskatoon 18th Street	Rainfall	Surficial water
13	Warman	Rainfall	NA
14	Whitemud freeway	Toe cut	NA
15	LRT Portal	Toe cut and tunnelling	NA
16	Rycroft	River erosion	NA
17	Montagneuse River	Rainfall	NA
18	Seatle Freeway	Toe cut	NA
19	Bismarck Bridge	Toe cut	NA
20	Smith Bridge	Toe cut	River down cut
21	Dunvegan Creek Slide	fill	Toe cut
22	Savery Creek	Rainfall	NA
23	Peace River Bridge	River erosion	NA
24	Savery Creek	Rainfall	River erosion + water pipe damaged
25	Gierson Hill Slide	Rainfall	Filling
26	Merritt	Rainfall	NA

Table 5.2 Continued

Case	Name	Trigger	Preparatory Factors
27	Regina Beach	Rainfall	River erosion + toe cut
28	WID	Rainfall	NA
29	Muddy Lake	Fill	NA
30	Petrofka	Artesian G.W (rainfall)	NA
31	Eureka	River down cutting	River erosion, high GWT
32	Alani-Paty	Rainfall	NA
33	Fort Benton	NA	NA
34	Caramanico	Rainfall	River erosion
35	Chagrin	River erosion	NA
36	Sloboda Bridge	River erosion	NA
37	Cairnmuir	Rainfall	Perched W.T, construction
38	Devon	Toe cut	NA
39	La Butte	Rainfall	NA
40	Montegranaro	Rainfall	NA
41	Montappone	Rainfall	NA
42	Castignano	Rainfall	River erosion
43	Monturano	Rainfall	NA
44	Ventor	Rainfall	NA
45	Corniglio	Rainfall	Earthquake
46	Vallcebre	Rainfall	NA
47	San Matino	Rainfall	NA
48	Mishitani	Rainfall	NA
49	CN50.9 (Deep)	Drawdown	River erosion
50	South Slide (Toe)	Drawdown	River erosion
51	Mam Tor	Rainfall	NA
52	San Martino	Rainfall	NA
53	Deer Creek	Rainfall	NA
54	Carrot River	Rainfall	NA
55	Sarukuyoji	Rainfall	Snow weight
56	Fagna Slide	Rainfall	NA
57	highcliff	Rainfall	NA
58	Porta Cassia	Rainfall	NA
59	Frenchman	Fill	NA
60	Prince Albert	River erosion	Poor drainage

Table 5.3. List of studied slides show rate sensitivity to pore pressure changes on their rupture surfaces with enough information for detailed movement behaviour study.

#	Case	Name	References
1	1	Denholm	Sauer (1983), Christiansen (1983), Sauer and Christiansen (1987), Christiansen and Sauer(1984)
2	7	Edgerton South	Thomson and Tweedie(1978), Cruden et al. (1995)
3	15	LRT Portal	Gerber et al. (1993)
4	26	Merritt	Chin et al. (1984)
5	27	Regina Beach	Clifton et al. (1984)
6	28	WID	Krahn and Weimer (1984), Hardy et al. (1980)
7	32	Alani-Paty	Baum and Reid (1995)
8	37	Cairnmuir	Watts and Macfarlane (1996), Gillon et al. (1992)
9	46	Vallcebre	Corominas et al. (1999)
10	49	CN50.9 (Deep)	Eshraghian (2005), Keegan et al. (2003)
11	50	South Slide (toe)	Eshraghian (2005)
12	51	Mam Tor	Wedage (1995), Skempton et al. (1989)
13	52	San Martino	Picarelli et al. (2004), Bertini et al. (1984)
14	53	Deer Creek	Kelly et al. (1995)
15	55	Sarukuyoji	Nakamura (1984)
16	56	Fagna	Canuti et al. (1984)
17	58	Ovieto	Tommasi et al. (2006)

Table 5.4. Information on geometry of the slides

Name	Volume (Mm^3)	Max. Depth (m)	Ave. Depth (m)	Travel Angle (°)	Rupture Surface Dip (°)
1) Denholm	83.3	100	75	4.6	0
2) Edgerton South	0.7	30	17	9.5	4
3) LRT Portal	0.07	25	15	16.7	0
4) Merritt	0.01	12	7	15.6	2
5) Regina Beach	4.1	35	25	5.5	1.5
6) WID	0.04	25	15	19	0
7) Alani-Paty	0.09	12	10.5	7.6	7.5
8) Cairnmuir	3.15	70	40	20.1	17
9) Vallcebre	6.5	50	22	13.0	10
10) CN50.9	3.3	60	40	16.5	2.7
11) South Slide	1	35	30	13	0.7
12) Mam Tor	2.63	35	30	12	7
13) San Martino	1.3	26	22	11.5	8
14) Deer Creek	9	70	50	6.8	0
15) Sarukuyoji	0.04	8	5	12	10
16) Fagna	0.04	5.5	4.5	8	6
17) Ovieto	10	18	17	10	5.5

Table 5.5. Information on material properties of rupture surfaces.

Name	Soil type	C.F. (%)	L.L. (%)	P.L. (%)	P.I. (%)	φ_r (°)
1) Denholm	Montmorillonite clay	>50	77.8	30.5	47.3	8
2) Edgerton South	Bentonite clay shale	>50	126	25	101	8
3) LRT Portal	Bentonite clay	>50	300	50	250	8
4) Merritt	Clay	45	70	25	45	14
5) Regina Beach	Bentonite clay shale	45	135	35	100	8
6) WID	Clay seam	70	31.5	21.5	10	9
7) Alani-Paty	Silty clay	>50	101	47	54	11
8) Cairnmuir	Sandy silty clay	45	55	22	33	18
9) Vallcebre	Clayey siltstone	45	60	30	30	20
10) CN50.9	Clay	80	79	29	50	10
11) South Slide	Clay	80	71	31	40	12.5
12) Mam Tor	Mudstone	35	53	28	25	14
13) San Martino	Silty clay	50	82.5	25.3	57	17
14) Deer Creek	Clay shale	55	80	25	55	6.5
15) Sarukuyoji	Clay	>50	82.5	25.3	57	17
16) Fagna	Silty clay	70	65	29	36	9.6
17) Ovieto	Clay	>50	53	28	25	17

Table 5.6. Rate versus pore pressure on rupture surface changes for 17 studied slides.

Name	Maximum Rate		Minimum Rate		Intermediate Rate	
	Rate (mm/yr)	r_u	Rate (mm/yr)	r_u	Rate (mm/yr)	r_u
1) Denholm	14.4	0.49	6	0.45	NA	NA
2) Edgerton South	168	0.14	108	0.11	NA	NA
3) LRT Portal	20	0.24	0	0.03	NA	NA
4) Merritt	3000	0.39	0	0.23	360	0.26
5) Regina Beach	120	0.41	20	0.37	NA	NA
6) WID	120	0.28	0	0.27	70	0.277
7) Alani-Paty	900	0.28	10	0.18	180	0.23
8) Cairnmuir	20	0.115	0	0.105	2	0.109
9) Vallcebre	60	0.39	10	0.375	NA	NA
10) CN50.9	3.4	0.213	0.3	0.198	2.7	0.21
11) South Slide	35	0.35	0	0.28	NA	NA
12) Mam Tor	1200	0.47	150	0.43	NA	NA
13) San Martino	130	0.46	3.7	0.42	37	0.447
14) Deer Creek	4.3	0.413	0.5	0.401	NA	NA
15) Sarukuyoji	1825	0.41	0	0.35	NA	NA
16) Fagna	860	0.43	0	0.3	340	0.38
17) Ovieto	23	0.483	3	0.47	NA	NA

Table 5.7. Slope of movement line in root rate axes and r_{u0}.

Name	r_{u0}	Slope of root rate movement trend-line
1) Denholm	0.377	0.0297
2) Edgerton South	0	0.0117
3) LRT Portal	0.03	0.047
4) Merritt	0.219	0.003
5) Regina Beach	0.34	0.0062
6) WID	0.27	0.0009
7) Anali-Paty	0.173	0.0037
8) Cairnmuir	0.105	0.0022
9) Vallcebre	0.365	0.0033
10) CN50.9	0.192	0.0114
11) South Slide (toe)	0.28	0.0285
12) Mam Tor	0.408	0.0018
13) San Martino	0.416	0.0041
14) Deer Creek	0.395	0.0088
15) Sarukuyoji	0.35	0.0014
16) Fagna	0.30	0.0044
17) Ovieto	0.463	0.0042

Table 5.8. Different Acceleration Factor (A.F.) for the slides with similar material on their rupture surfaces.

Name	Plasticity Index (PI) (%)	Acceleration Factor (A.F.)	Average Slide Depth (m)
Denholm	47.3	33.7	75
CN50.9	50	87.7	40
Anali-Paty	54	270.3	7.6
Sarukuyoji	57	714.3	5

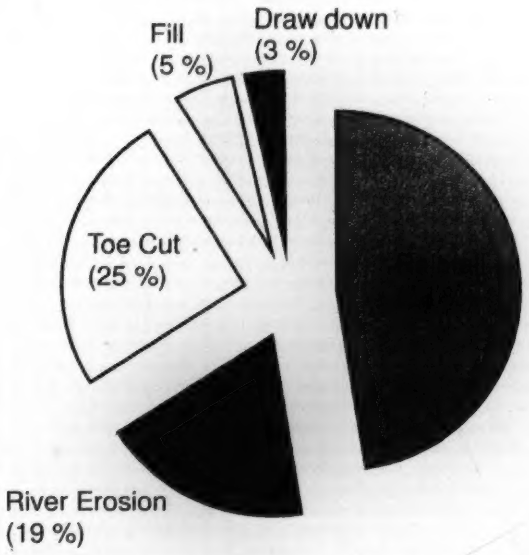

Figure 5.1. Relative frequency of reactivation triggers of studied translational earth slides.

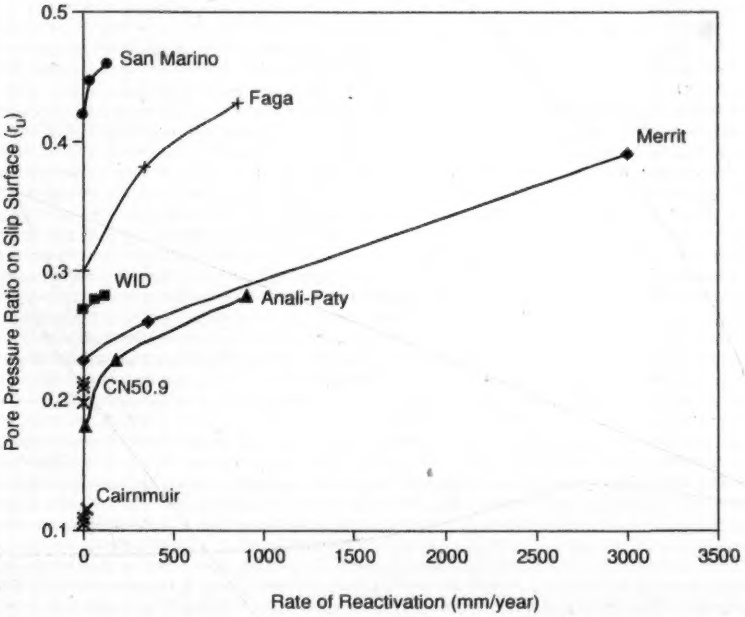

Figure 5.2. Movement acceleration with pore pressure ratio (ru) increasing on the slides' rupture surfaces.

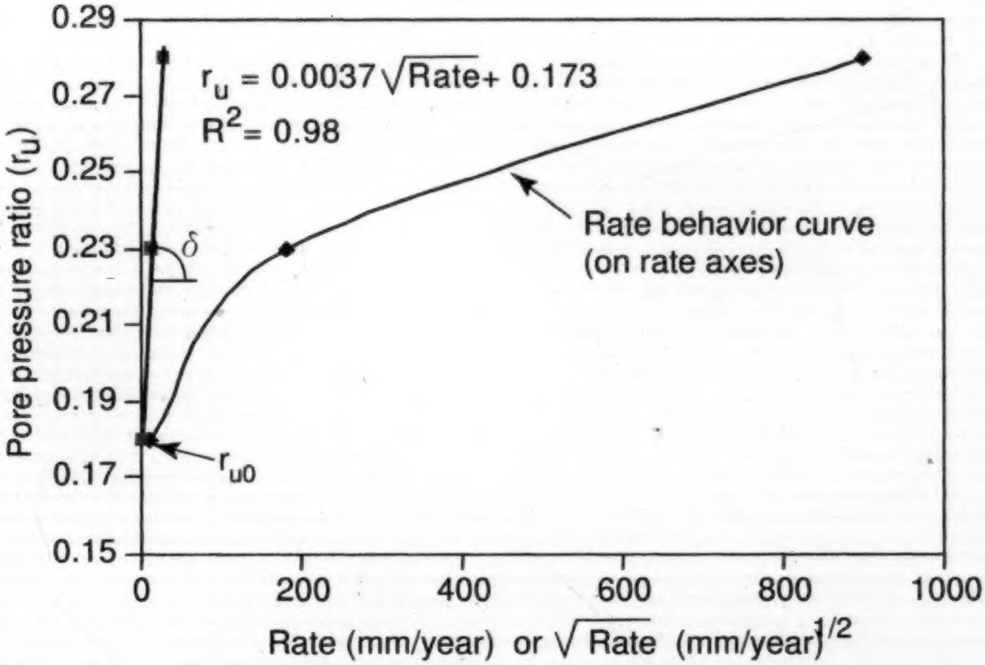

Figure 5.3. Anali-Paty movement acceleration curve in rate axes and Anali-paty movement acceleration line in square root rate axes.

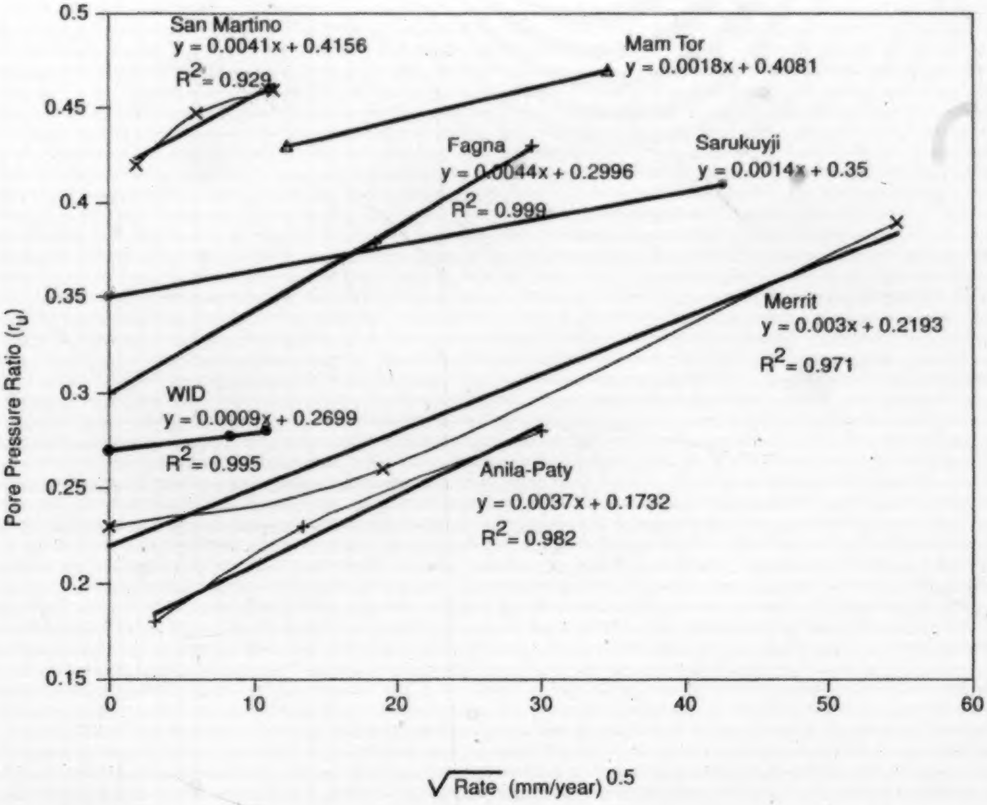

Figure 5.4. Pore pressure ratio (r_u) versus square root rate movement line of some of the slides.

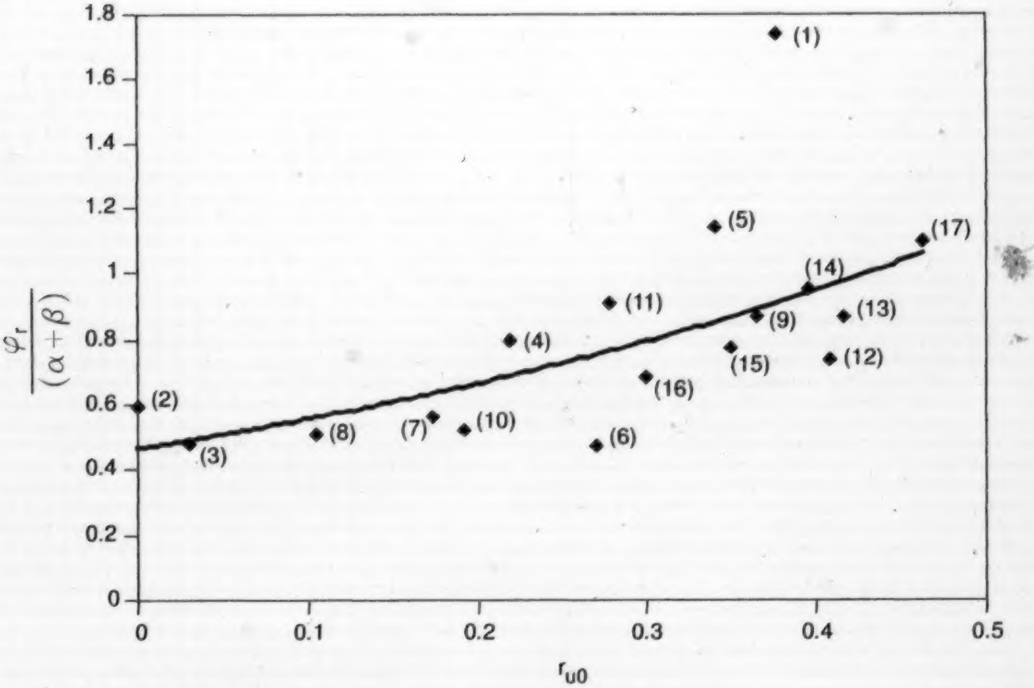

φ_r: Residual friction angle of material on rupture surface

α: Travel Angle

β: Rupture surface dip angle

(1): Case number

Figure 5.5. Change of r_{u0} with slide's geometry and material property characteristics.

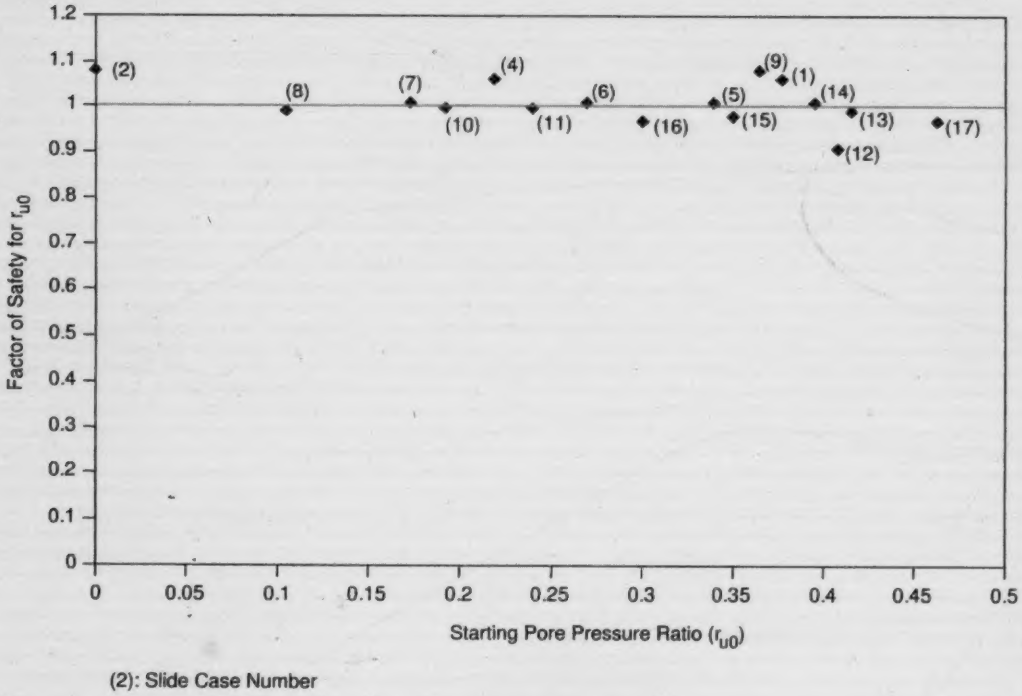

Figure 5.6. Factor of Safety for starting the slides' reactivation.

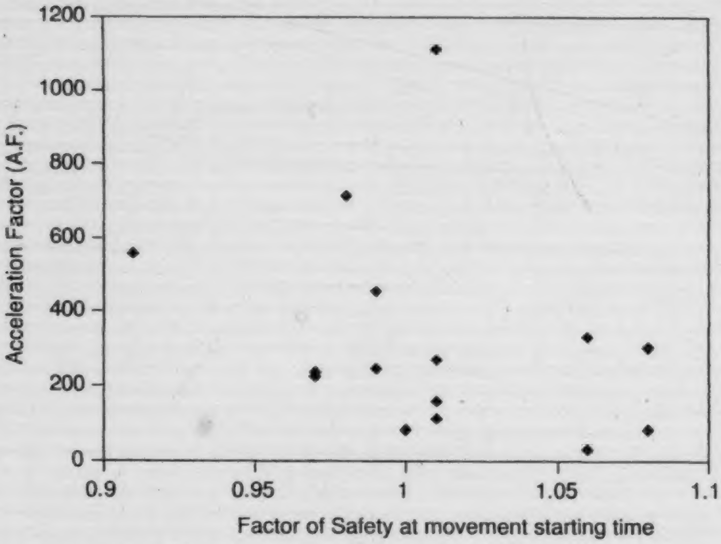

Figure 5.7. Acceleration Factor versus Factor of Safety at the time of starting the slides' reactivation.

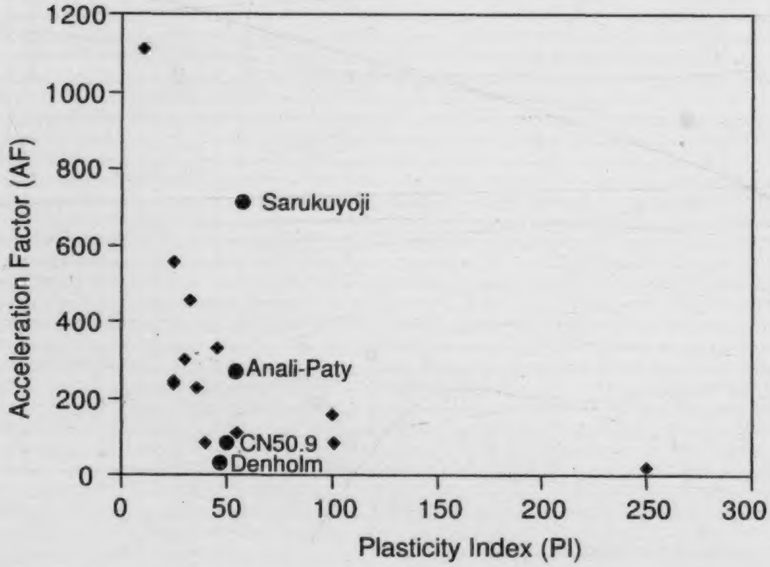

Figure 5.8. Acceleration Factor (A.F.) versus plasticity index (PI) of material on rupture surface.

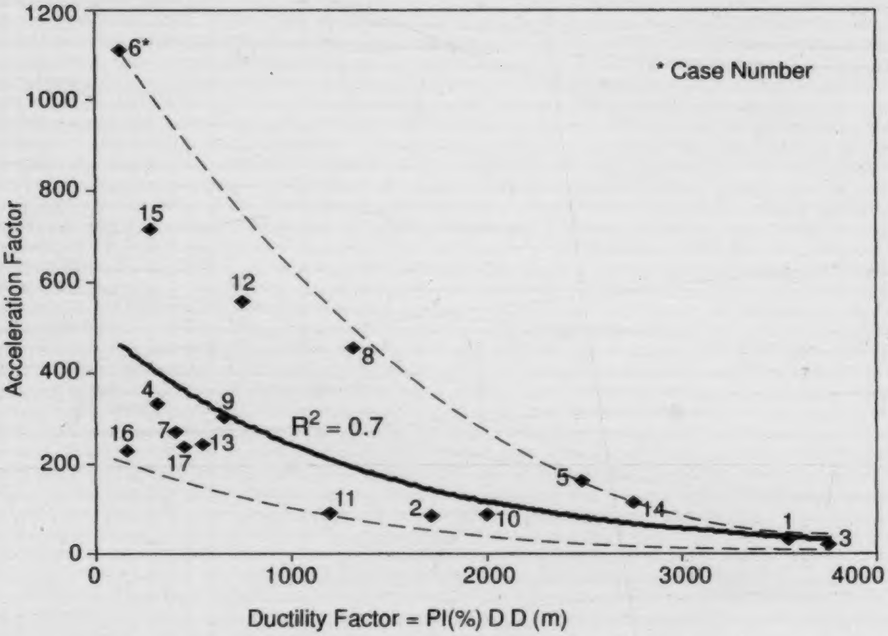

Figure 5.9. Acceleration Factor (A.F.) versus Ductility Factor.

Chapter 6

Hazard Analysis of an Active Earth Slide in the Thompson River Valley, Ashcroft, British Columbia[1]

6.1. INTRODUCTION

Risk analysis involves calculating the risk after scope definition, hazard analysis, and consequence analysis (Fell et al. 2005). Landslide hazard analysis includes characterizing the danger of a slide in terms of type, size, velocity, location, travel distance, pre-failure deformations, and failure mechanics, and the corresponding frequency of sliding (Picarelli et al. 2005). A landslide hazard analysis usually involves an analysis of likelihood that a slide will occur within a given period of time based on the geology, slope gradient, elevation, geotechnical properties, vegetation cover, weathering, and drainage pattern (Lacasse and Duzgun, 2006). Examples of quantitative hazard analysis for specific landslides are rare in the literature, and basically assume a stable or failed slope with a specific post-failure movement rate (El-Ramly, 2001) and El-Ramly et al. (2003 and 2006). On the other hand, the post-failure movement rate of an earth slide may be in the range of extremely slow to rapid (Hungr et al. 2005). Because the consequence of movements may be closely related to the rate of movement, the hazard analysis of the danger of an earth slide should consider the probability of different post-failure movement rates. The probabilities of different movement rate may later be used to define the different levels of vulnerability or damage required in risk analysis.

---

[1] Submitted paper:

A version of this chapter has been submitted for publication to Canadian Geotechnical Journal. Eshraghian, A., Martin, C.D., Morgenstern, N.R., 2007. Hazard analysis of an active earth slide in the Thompson River Valley, Ashcroft, British Columbia, Canada.

The Canadian railway industry has been exposed to ground hazards, including earth slides, ever since their first transcontinental line was constructed in the late 1800s (Bunce et al. 2005). In particular, the 10-kilometre length of the Canadian Pacific Railway (CPR) and Canadian National Railway (CN) lines passing through the Thompson River Valley, south of Ashcroft, south-central British Columbia, Canada (Figure 6.1) has had stability problems with 11 large translational earth slides. Although the landslides in this area today are normally slow-moving, rapid to very-rapid movements, which have blocked the Thompson River in some cases, have occurred in the past (Clague and Evans, 2003). Rail lines can tolerate relatively slow small movements, but rapid movements may endanger passenger and railway workers. Therefore, a hazard analysis framework is required that considers the different possible post-failure movement rates.

These slides have been studied since the late 1800s, when Stanton (1898) provided the results of the first known study. Ryder (1976) described the geology of the area, and Monger and MacMillan (1989) described the surficial geology and bedrock. Furthermore, Clague and Evans (2003) clarified the general stratigraphy of the Quaternary sediments in the Thompson River Valley. In order to reduce the risk from these slides, Canadian railway companies have initiated a risk-management program for the Ashcroft slides since 2002 (Bunce et al. 2005). As part of this program, Eshraghian et al. (2005a) showed that the main trigger for the movement is the Thompson River rather than human activities or rainfall. Eshraghian et al. (2005b) investigated the effect of the Thompson River level changes on the movements of a sample landslide in this area, Slide CN50.9 (Figure 6.1). Eshraghian et al. (2007) further examined the characteristics of the Ashcroft landslides and the kinematics of the various slides. Eshraghian et al. (submitted) analysed two sample slides in this area, including Slide CN50.9, (Figure 6.1) to assess the effect of the river on slide movements.

In this paper, a quantitative hazard analysis in a new framework that considers the different post-failure movement rates is carried out using Slide CN50.9. First, a review of the slide and trigger (the Thompson River) characteristics is presented. Then, a probabilistic stability analysis using the material and trigger uncertainties is conducted on the sample landslide. Subsequently, other uncertainties from the groundwater modeling and toe erosion are added to the probabilistic slope stability results. In the next step, by using the frequency of the trigger (the Thompson River flood), the probabilistic stability analyses, and previous experiences of the slide movement rates, different rate frequencies for each reactivation block and a new retrogression block within the slide body are calculated. Finally, a threshold warning flood is suggested based on the movement rate frequency analyses to limit the reactivation movement rate to slow.

6.2. BACKGROUND

6.2.1. Landslide Characterization

Slide CN50.9, like other slides in Ashcroft area, is a reactivated translational earth slide. Eshraghian et al. (2007) identified four reactivation blocks (Figure 6.2), one on the shallower rupture surface and three on the deeper rupture surface, within the clay-silt glaciolacustrine unit in Slide CN50.9. They also considered that a retrogression block might result from the extension of the deeper rupture surface from the current main scarp and assumed the same translational mechanism for this possible future retrogressive failure. The current slide has an area of 15.1 hectares and a volume of

3.3 million cubic metres. Table 6.1 presents the estimated volumes and areas for each defined block at this site.

Eshraghian et al. (submitted) showed that the main trigger for the movement of these slides is associated with the Thompson River, which can affect the stability of the slide blocks in three ways: (1) by changing the water pressure on their rupture surfaces with the river level fluctuation, (2) by changing the river's supporting pressure on the slide toe with the changes of river level, i.e., a rapid drawdown scenario, and (3) by altering the slide geometry due to river bank erosion. The relative importance of each of these effects depends on the river erosion protection system in place, the dimensions of the blocks, the depth and shape of the rupture surface, and the amount of river level fluctuation. Slide CN50.9 is protected against river erosion by a toe berm built originally in the late 1970's and extended in 2001. Therefore, the river erosion effect is limited but still should be considered for extreme flood events which may wash away the existing toe berm. The drawdown mechanism acts on all the blocks but will have more effect on the toe blocks than on the larger, deeper blocks.

The rate of movement for the reactivation blocks (blocks R-1, R-2, R-3, and R-4) differs from the retrogressive block's movement rate. Hungr et al. (2005) suggested three possible means to estimate if a landslide can change to a rapid landslide: (1) judgment, based on experience and comparison with the precedents, (2) an empirical approach, based on monitoring, and (3) a numerical approach, based on limit equilibrium or stress-strain analysis. In this paper, a combination of judgment and the empirical approach is used for estimating the rates of movement.

6.2.1.1. Reactivation Movement Rate

When the records of the previous movements are available, the best means of assessing a landslide's movement rate is to compare its current condition with its condition during previous movements, as long as its geometry and material properties have not changed significantly. Previous movement monitoring at this site showed that the reactivation blocks generally move extremely slowly or very slowly unless extra forces due to water filling the cracks cause rapid reactivation (Eshraghian et al. 2007). Based on movement measurements and comparing them with the Factor of Safety calculated from material properties selected from borehole samples, the reactivations triggered by the Thompson River drawdown have started with a Factor of Safety less than 1.1 (Eshraghian et al. 2006). The measurements from eleven piezometers and five inclinometers installed in Slide CN50.9 since 2001 provided information about the changes in the reactivation movement rate with groundwater system changes (Eshraghian et al. submitted).

The inclinometer and piezometric data recorded between 2001 and 2004 for block R-2 on the deeper rupture surface showed a non-linear correlation between the pore pressure ratio and the movement rate during the drawdown period (Figure 6.3). In the case of the shallower reactivation block (R-3), not enough movement data were available to produce a specific movement correlation for the reactivation on the shallower rupture surface. However, given the similarity between the materials on the two rupture surfaces, and also given previous experience with translational slide movements, the correlation between the rate of movement and the pore pressure ratio for the shallower block is also likely to be non-linear. Therefore, a similar formula used for the movement correlation on the deeper rupture surface was used again for the movement correlation on the shallower rupture surface. In order to explain the similarity between the two correlations, both correlations for block R-2 and block R-3 are shown on the square root rate horizontal axes in Figure 6.3. Bonnard and Glastonbury (2005) showed a similar non-linear correlation for the rate of movement and Factor of Safety of 5 earth flow and debris slides. In their study, the movement correlations were linearised by using a logarithmic horizontal scale. The Factor of Safety changes linearly with the pore pressure ratio if the geometry does not change. Therefore, the Bonnard and Glastonbury (2005) correlation is quite similar to the linear correlation between the pore pressure ratio and movement rate on the horizontal square root rate scale presented here.

Eshraghian et al. (2007) showed that these slides have the potential for a rapid reactivation. If these slides have access to water to fill the tension cracks previously opened by slow reactivation, rapid reactivation may happen. At Slide CN50.9, the head colluvial material is detached from the fluvial material at the slide crown, a potential source of water, and therefore there is little potential for a rapid reactivation of block R-1 (Figure 6.2). The other way to access water for filling tension cracks and to change the reactivation rate is through the Thompson River itself. If toe erosion causes movement of the toe block and opens the cracks, and then the Thompson River level rises enough to overflow the toe berm and cover the slide toe, the river may fill the cracks with water, so that during drawdown, the rate of movement may change to a rapid movement. In 1997, some new cracks developed at the toe of Slide CN50.9 between elevation 287.5 m and 289 m within block R-4 (Nachtigal 2001). Therefore, it was assumed that block R-4 could start a rapid reactivation when the Thompson River level exceeds 291 m, or high enough to fill cracks at the toe. This level would be expected within the return period of more than 500 years. Krahn (1984) reported a maximum rate of 6 metres per hour for Goddard Slide's reactivation in this area. In our analysis, it was assumed that when the Thompson River discharge is higher than its 500-year return period yearly discharge, the reactivation movement rate may change to rapid movement.

6.2.1.2. Retrogression Movement Rate

According to Picarreli et al. (2005), in the first-time failure of landslides within overconsolidated clays, the peak velocity usually ranges between rapid and moderate, and the rate of movement depends on either the slope morphology (inclination of the slip surface) or the physical and mechanical properties of soil on their rupture surfaces. The velocity of the soil mass in a first-time slide depends on the Generalized Brittleness Index defined by D'Elia et al. (1998) (Picarelli et al., 2005). According to Hungr et al. (2005), one of the ways to assess the potential for catastrophic motion is to compare the landslide movement rate with similar case histories that have already failed.

Eshraghian et al. (2007) showed that all previous slide retrogressions or movements within the undisturbed material in the Ashcroft area have been rapid to very rapid (with rates between 1.8 m/hr and 5 m/sec). In our analysis, based on the previous movement experienced in the area, we assume that significant creep movement may start when the Factor of Safety is less than 1.1 and that very rapid failure can occur if the Factor of Safety drops to less than unity.

6.2.2. Trigger Characterization (Thompson River)

The Thompson River is a large river with a five-million-hectare drainage basin upstream of the study area. The average flow calculated from data for the last 35 year, in a normal year, ranges from 230 m^3/sec in January to a maximum of 2650 m^3/sec in June when snow melt is most active. The average yearly flow is 24460 Mm^3/year. Eshraghian et al. (2005a) showed that the observed instability of the slides in the Thompson River Valley correlated with the years when the Thompson River flows were elevated above the average flows for longer than normal periods.

6.2.2.1. The Thompson River Discharge

The Thompson River flow data have been available for a station near Spence's Bridge (Figure 6.1) since 1911, when they were first recorded by Environment Canada. Because no main tributary joins the Thompson River between Ashcroft and Spence's Bridge, and the rainfall in the area adds relatively little to the main river discharge between these two locations, the data from station at Spence's Bridge were used for estimating the Thompson River flow at Ashcroft. Figure 6.4 shows the yearly discharge for the Thompson River at the Spence's Bridge river level station between 1951 and 2003. While the yearly discharge trend line between 1951 and 2003 shows a relatively small increase in trend, the yearly discharge trend line from 1970 to 2003 shows a clear increase in the yearly discharge trend. The yearly discharge trend line shows an increase in the discharge trend from 23520 Mm3 in 1970 to 25390 Mm3 in 2003 (an 8% increase in the yearly discharge trend within 34 years). Not only was the yearly discharge trend line increasing, but also more extreme fluctuations occurred between 1970 and 2003. Porter et al. (2002) also reported an increase in the precipitation trend in the Kamloops area, north of Ashcroft between 1900 and 2000(Figure 6.1). These more noticeable changes in both the river level and precipitation in the study area may reflect a changing climate in the region. Bunce et al. (2005) suggested using the last 30-year data sample to identify the effect of climate change trends on the severity of the mid-to-long return-period events.

In order to consider the more extreme Thompson River discharge due to climate change since the 1970's, only the river discharge data from 1970 to 2003 were used to evaluate the river flood return periods. Different probabilistic distributions were evaluated and the lognormal distribution (Figure 6.5) provided the best fit to the data.

The yearly Thompson River discharge can be estimated for a specific cumulative descending probability from the fitted lognormal distribution shown in Figure 6.5.

Therefore, for each future Thompson River flood return period, a discharge value can be defined. The Thompson River yearly discharge data from 1970 to 2003 showed an increase of 8% in the yearly discharge mean within 34 years (0.235 %/year). Therefore, it was assumed that the Thompson River yearly discharge trend would increase on average by 11.8% within the next 100 years (the design life of the project). Table 6.2 presents the results of considering this average increase in the Thompson River yearly discharge trend related to the return period.

6.2.2.2. The Thompson River Level

Eshraghian et al. (2006) showed that a drawdown mechanism may have contributed to reactivation of the slides in the Ashcroft area during high river flows. The maximum Thompson River discharge at the Spence's Bridge river level station normally happens during the summer period, but the exact date may vary from year to year. Using the average discharge for each day gives a slightly lower peak flow compared to that of a regular normal year. In order to obtain a more realistic average Thompson River discharge, the peak discharges of years were put on each other, and then the 165 days before and 200 days after the day with the maximum discharge in each year was assumed as the river cycle for that specific year. Then the average discharge for each day was calculated. The end results of the calculation of the average Thompson River discharge after using the methods with and without peak date correction are compared in Figure 6.6. Although both methods of calculating the average Thompson River discharge gave the same total yearly discharge (24424 Mm^3 in the peak date correction case versus 24458 Mm^3 in the method without peak date correction), it was found that the average river discharge obtained by using the peak date correction method was a better representative of a normal year's discharge. The increase in the average peak discharge calculated by using peak date corrections compared to the average peak discharge calculated without using peak date correction is 14%.

The next step was to establish a correlation between the Thompson River level and the discharge at Slide CN50.9. The river level at Slide CN50.9 was recorded from October 2001 until December 2003 (data from Brian Nachtigal and Tim Keegan, personal communications, 2004). Because no main tributary joins the river between the station at Spence's Bridge and the Slide CN50.9's site at Ashcroft (Figure 6.1), it was decided to use the Thompson River discharge at Spence's Bridge and the river level data from the Slide CN50.9's site to find a correlation between the river discharge and river level at Slide CN50.9 (Figure 6.7). This correlation was also used to determine the river level at Slide CN50.9 for different discharge return periods.

The correlation between the Thompson River discharge at the Spence's Bridge river station and the Thompson River level at the Slide CN50.9 site was used to calculate the daily river level at Slide CN50.9. It was assumed that for each day, the Thompson River discharge increased with the same ratio at which the yearly discharge increased compared to the average river discharge for that specific return period (this ratio is shown in Table 6.2). After obtaining the daily river discharge at Slide CN50.9, using the correlation between the Thompson River discharge and the Thompson River level at Slide CN50.9, the river level was calculated for each river discharge return period (Figure 6.8).

6.2.2.3. Probability of River Flood in the Railway Lifetime

An important temporal consideration in risk assessment is the time period of interest (Roberds 2005). The likelihood of at least one case of a specific flood occurring during a particular time period increases with the length of that time period. The relationship between the frequency (f) of a specific flood and the probability (P) of its happening in a particular time period of interest (the design life of the project) (r) can be expressed as

$$P = 1 - (1 - f)^r \qquad (1)$$

The frequency (f) is the inverse of the return period (T). The probability of different flood return periods is higher for the interest period (the design life of the railway), 100 years in this analysis, compared to its probability of happening without considering the railway's lifetime (Table 6.3 and Figure 6.9). A correlation exists between the Thompson River flood return period and the Thompson River discharge (Figure 6.10); therefore, the probability of different Thompson River discharges can be calculated for the design lifetime of the railway in the study area.

6.3. PROBABILISTIC STABILITY ANALYSES

6.3.1. Seepage Analyses

Eshraghian et al. (2006, submitted) presented transient seepage analysis results for Slide CN50.9 for the 2002 Thompson River level fluctuation cycle. They used constant infiltration boundary conditions on both the slide crown terrace and slope and a changing head boundary condition at the slide toe to represent the Thompson River level fluctuations. They compared the computed results with the measured piezometric data recorded in boreholes. Their results were in general agreement with the measured piezometric data (Figure 6.11). The same procedure and material properties (Table 6.4) used by Eshraghian et al. (2006) were also used to analyse the transient seepage system in Slide CN50.9 for each river yearly discharge return period. Later, these transient modeled groundwater systems were used as input for the deterministic and probabilistic stability analyses for each return period.

6.3.2. Deterministic Stability Analyses

The Factors of Safety of Slide CN50.9 translational blocks change with the river level and amount of erosion at toe. The material properties for the deterministic stability analyses were determined from index property tests and Stark and Eid's (1994) correlation, direct shear tests on clay and silt beds in the clay-silt deposit, and grain-size distributions (Table 6.5). These material properties and the deterministic stability analyses method are described in Eshraghian et al. (submitted).

Figure 6.12 shows the changes in the Factor of Safety for the four reactivation blocks in Slide CN50.9 and the retrogression block, obtained by using the Thompson River level fluctuation cycle for a 2-year discharge return period. These analyses show that the minimum factor of safety of the retrogressive block (block B-5) and main reactivation block (R-1) occurs as the river level returns to its normal level. The minimum Factor of Safety of block R-2 on the current deep rupture surface occurs on the 255th day of the river level cycle (August or September); the minimum Factor of Safety of the toe block on the shallower rupture surface (block R-3) occurs on the 185th day of the river level cycle (June or July); and the minimum Factor of Safety of the toe block on the deeper rupture surface (block R-4) occurs on the 265th day of the river level cycle (September).

6.3.3. Material Uncertainties

The soil property uncertainty depends on the inherent soil variability, the degree of equipment and procedural control maintained during site investigation, and the precision of the correlation model used to relate the field measurement to the design soil property (Phoon and Kulhawy 2003). The total variability of a measured property is a summation of the variations in trend, the inherent variability, and the measurement error (Phoon and Kulhaway 1999).

Phoon and Kulhaway (1999) considered the inherent soil variability as a random field, which can described by the coefficient of variation (COV) and the scale of fluctuation. They suggested the probable ranges of the soil coefficients of variation

(COV) to be used in the absence of site-specific data or where the data are too limited for meaningful statistical analyses.

In our analysis, Phoon and Kulhawy's (1999) suggestions for inherent variability were used for quantifying the inherent soil parameter uncertainty, but for cases with higher measurement errors (tests or estimations containing more judgments), a higher COV was used compared to the inherent variability alone to account for higher measurement and judgmental errors (Table 6.6). Then triangular distributions for the soil parameters were defined by using the standard deviation calculated from the total estimated COV and with 1.5σ from the mean value in each side of the mean (Figure 6.13) which gives relatively realistic range for material properties.

Another statistical parameter needed to describe the inherent soil variability is the autocorrelation distance or scale of fluctuation, which indicates the distance within which the property values show a relatively strong correlation (El-Ramly et al. 2002). The main part of Slide CN50.9's rupture surface is sub-horizontal. Phoon and Kulhawy (1999) suggested using a horizontal scale of fluctuation in the range of 40-60 m, while El-Ramly et al. (2003) suggested using a horizontal scale of fluctuation in the range of 40-80 m. Therefore, in this probabilistic slope stability analysis, the horizontal scale of fluctuation was assumed to be 60 m.

6.3.4. Sensitivity Analyses

The rupture surfaces of Slide CN50.9 pass through different materials, and each material has its own soil parameter distribution. The relative significance of the input variables on the Factor of Safety output was assessed through sensitivity analyses. The result of the sensitivity analyses was useful in identifying the most critical variables in the analyses and helped in deciding which critical soil parameters should be considered in the probabilistic stability analyses. Table 6.7 shows the results of the sensitivity analyses of the five translational blocks in Slide CN50.9. Given these results, it was decided to define all the parameters shown for the reactivation blocks (blocks R-1, R-2, R-3, and R-4) in Table 6.7 as variable parameters for the probabilistic stability analyses. Only the five most effective soil parameters were defined variable for the retrogression block (B-5) to reduce the number of samples in the probabilistic stability analyses.

The probabilistic stability analyses of the reactivation blocks (blocks R-1, R-2, and R-3) with four variable soil parameters, required 300,000 iterations while the probabilistic stability analyses of the retrogression block (block B-5) with five variable soil parameters required 600,000 iterations to obtain enough confidence in calculated reliability index and the probability of a Factor of Safety less than unity.

6.3.5. Results of Probabilistic Stability Analyses

Factor of Safety distribution of each block for each discharge return period of Thompson River was calculated from the probabilistic stability analysis (Figure 6.14) by Monte Carlo method. The probability of the Factor of Safety being less than a specific amount for each block could be assessed from these distributions. Eshraghian et al. (submitted) showed that the movement threshold of the reactivation blocks in Ashcroft area could occur with a Factor of Safety lower than 1.1 and that the block movement rate depended on the pore pressure ratio on the rupture surface. Therefore, the main results of the probabilistic stability analyses for the reactivation blocks were (1) the change in the probability of the Factor of Safety being less than 1.1 with the yearly river discharge and (2) the change in the pore pressure ratio with the yearly river discharge at the time of the minimum Factor of Safety (Figure 6.15 and Figure 6.16).

In this analysis, it was assumed that the creep movement of the retrogression block may start with a Factor of Safety of less than 1.1. Therefore, the change of probability of the block Factor of Safety being less than 1.1, at the time of the minimum Factor of Safety, with the river discharge was one of the main results of the probabilistic stability analysis for retrogression block (Figure 6.17). It was assumed that the movement can change to rapid if the Factor of Safety drops under unity. The analysis showed that the probability of Factor of Safety less than unity for the retrogression block was changing slightly with the river discharge and was between 0.25% and 0.37% with average probability of 0.29%.

6.3.6. Uncertainties in Results of the Probabilistic Stability Analyses

6.3.6.1. Groundwater Modeling Uncertainty

The groundwater system for each yearly discharge return period of Thompson River was calculated by using a seepage program and the results used in the deterministic and probabilistic stability analysis. Although the general results of the groundwater modeling were relatively close to the measured piezometer responses, differences always exist between predicted and measured piezometric responses because of model and geological uncertainties. Eshraghian et al. (submitted) compared the measured piezometric responses and the piezometric responses predicted by the groundwater model for the Thompson River level fluctuation cycle in 2002 which was a normal year (close to the river discharge of the 2-year return period). There was an average difference of 0.6 metres between the predicted and measured responses for the 8 piezometers installed in Slide CN50.9. In order to consider this uncertainty in the analyses, it was assumed that the maximum difference between the predicted and measured average piezometric responses could be as high as 0.65 metres. Then the probabilistic stability analyses conducted for the groundwater table 0.65 metres higher and 0.65 metres lower than the current modeled groundwater table from the transient seepage analysis. Table 6.8 gives the range of changes in the probabilistic stability analysis for the maximum and minimum errors in the groundwater system predicted by seepage analyses.

6.3.6.2. Toe Erosion Uncertainty

The other main issue related to the stability of the slide is the possibility of river erosion at the slide toe. A toe erosion berm was originally built in the late 1970s at the toe of Slide CN50.9 to protect the toe against river erosion (T. Keegan, personal communication, 2006). This berm was extended in 2001 (Naghtigal 2001), and since then, no major toe erosion has occurred. The experience with toe erosion protection with the other slides in this area (the South Slide was reported by Eshraghian et al., 2007), suggests that if, during a flood, the river overflows the erosion protection berm, the berm might be either damaged or destroyed. The top of the toe berm at Slide CN50.9 is located at an elevation of 287 metres, and it was assumed that with the maximum river level elevation above 289.5 metres, the overtopping flood could start the toe erosion at Slide CN50.9. This erosion could increase with higher floods (Figure 6.18). Because of the uncertainty imbedded in this assumption, the possibility of different amounts of erosion appearing in the probabilistic stability analysis results had to be considered. Therefore, a range was defined between the maximum and minimum toe erosion around the mean. The probabilistic stability analyses with the maximum, minimum, and average toe erosion amounts for each of the discharge return periods of Thompson River provided a range of uncertainty to include in the stability analyses due to the erosion (Table 6.9).

6.3.6.3. Total Uncertainty

Main sources of uncertainty in the results of probabilistic stability analyses are the material uncertainty, the Thompson River level uncertainty, the pore water pressure uncertainty, and the toe erosion uncertainty. The uncertainties resulting from the approximations in the geometry, location of the rupture surfaces, and the fitted trend line on the results of the probabilistic stability analyses were found to be minor compared to the four main sources of uncertainties. For example, the average possible changes in the probability of the factor of safety being less than 1.1 (P(F.S<1.1)) introduced by the trend line fit on the data (shown in Figure 6.15) for blocks R-1, R-2, R-3, R-4, and B-5 are, respectively, 0.008%, 0.015%, 1.25%, 2.22%, and 0.069%. These changes, compared to the changes introduced by pore pressure and toe erosion uncertainties (Table 6.9 and Table 6.8), are negligible.

The uncertainty in the material properties and the Thompson River level are already considered in the probabilistic stability analyses. A trend line was defined for the result of probabilistic analysis. In order to consider the uncertainties from the groundwater modeling and toe erosion in the results, a triangular distribution function is defined around the trend line of the probabilistic stability analyses results and between the upper limits and lower limits of possible results (which defines the possible range of results around the trend line without considering the uncertainties in the groundwater modeling and toe erosion) (Figure 6.19). Because the ground water uncertainty is larger than uncertainty from toe erosion, the upper and lower limits around the trend of the probabilistic slope stability analyses results were defined by adding half of the uncertainty from the toe erosion to the uncertainty from the groundwater modelling (Table 6.10).

6.4. PROBABILITY OF DIFFERENT MOVEMENT RATES

In the previous sections, the probability of the Factor of Safety of each block being less than the threshold for the onset of movement was examined. The next step was to calculate the movement rate and movement rate classes defined by Cruden and Varnes (1996) for each block. The software program @Risk was used to define the probability distributions and sample them using a Latin Hypercube sampling method. Figure 6.20 shows the flowchart followed for these calculations and the following summarises the steps completed in calculating the probability of different rates of movement for each block.

1) In the first step, a Thompson River discharge return period was selected by sampling from its probability distribution for the design life period of railway (100 years) from Figure 6.9.
2) Then the Thompson River yearly discharge for this selected return period was calculated by using the correlation between the return period and the Thompson River discharge (Figure 6.10). This is the maximum Thompson River yearly discharge which can happen during the design life time (100 years).
3) Because the start of movement occurs with a Factor of Safety being less than 1.1, the probability of the Factor of Safety less than 1.1 was calculated from the correlation between Factor of Safety and the Thompson River yearly discharge resulting from probabilistic stability analyses (Figure 6.15 or Figure 6.17).
4) The probability of the Factor of Safety being less than 1.1 (starting the movement) calculated in step 4 was estimated only by considering the uncertainties in the river discharge and material properties. In order to consider the uncertainty from groundwater modeling and amount of toe erosion, a new triangular probability function was defined using total uncertainty numbers given in Table 6.10 (a sample shown in Figure 6.19) and sampled.

5) The probability of movement was estimated by adding the uncertainty calculated from step 4 to the probability of the Factor of Safety less than 1.1 calculated in step 3.

6) The probability of no movement for a selected return period and calculated discharge was estimated from the probability of the Factor of Safety less than 1.1 calculated in previous step.

7) Although we calculated the probability of movement and probability of no movement in previous steps for a specific block, the block may move or not move. The choosing of witch depends on their probability. This is like sampling from a discrete probability function with two choices: movement and no movement. In this step, a discrete probability distribution, called movement happen function, is defined with two choices, movement or no movement with their probability as defined in steps 5 and 6.

8) Sampling from the movement happen function gives either no movement; the rate of movement is zero, or movement. If the result of sampling from movement happens function is no movement, the movement rate is zero and the program goes to step 17 (end of loop). If the result of sampling from the movement happen function is movement, the next step will be followed to calculate the block movement rate.

9) If the movement happens, the method for calculating the rate of movement will depend on the type of block. If it is a reactivation block,

there are movement correlations available which can be used for calculating the movement rate (Figure 6.3). If the block is a retrogression block, the rate of movement will be calculated from previous movement experience which can be creep or very rapid movement.

10) If the block is a reactivation block, first the pore pressure ratio on the rupture surface is calculated from correlation with the river discharge (Figure 6.16).
11) Then the condition for rapid reactivation is checked. This mode of movement is possible for the toe block R-4 with high Thompson River level with the river yearly discharge of 500 years or higher and toe crack developed after erosion.
12) Even if all these conditions exist, still there is uncertainty in the occurrence of rapid reactivation as there is no data for this type of movement at the toe. Therefore, a discrete function is defined with two possible outcomes of rapid reactivation and slow reactivation which each has equal probability of happening (50% each). Sampling from this discrete function defines if, for this specific loop, the movement will be rapid reactivation or slow reactivation.
13) If rapid reactivation does not happen, the rate of movement will be calculated from the correlation between pore pressure ratio and rate of movement (Figure 6.3).

14) For the retrogression block, it is assumed that the general failure with very rapid rate will happen with a Factor of Safety less than unity, but a creep movement, with slow movement, can start with factor of safety less than 1.1. Therefore, in this step probability of Factor of Safety less than unity is probability of very rapid retrogression and probability of Factor of Safety between 1.1 and 1 is probability of creep movement (which is slow). The probability of Factor of Safety less than 1 and between 1.1 and 1 are calculated in this step from Figure 6.17.

15) For the retrogression block, after movement initiation, there are possibilities of extremely rapid movement with general failure (Factor of Safety less than 1), otherwise the movement is slow creep movement (with Factor of Safety between 1 and 1.1). Therefore, creep happening function, a discrete probability function, is defined with two choices of general failure and creep movement. Their probability depends on the probability of the Factor of Safety less than 1 and Factor of Safety between 1 and 1.1 which calculated in previous step.

16) In this step for the retrogression block, sampling from the creep happening function gives two possible outcomes: (1) slow creep movement, and (2) general sliding in undisturbed material which is very rapid from previous experience. Sampling from this function defines the movement rate class for the retrogression block.

17) After calculating the block rate of movement for the selected return period, this step checks if enough iteration has been done to define the probability of movement distribution or not. If the maximum number of iteration is reached, the loop will stop. If enough samples have not occurred, the program will go to step 1 and start the loop again. The maximum number of iterations used in the analyses was 500,000.
18) The result of all iterations is used to define the distribution for the block rate of movement. If the block is a reactivation block, first a distribution for the block movement rate is calculated and then the probability of different movement classes are calculated (extremely slow, very slow, etc.). If the block is a retrogression block, only the probability of movement classes can be calculated.

The result of calculating the probability of movement for reactivation blocks is a movement probability distribution (Figure 6.21) which shows the probability distribution of different movement rates over the design life time of the project. Because of the uncertainty imbedded in the calculation of frequency of movement rate and also insensitivity of the risk to small changes in rate of movement, it was decided to report the result in the form of probability of different movement rate classes. From the movement rate distribution histograms, the probability of each movement rate class (based on Cruden and Varnes, 1996 definition) for each reactivation block was calculated for the design life time of the railway (100 years) (Figure 6.22). For the retrogression block, block B-5, the vast range of movement rate, from zero to a few metres per second, and lack of detailed measured movement during retrogression did not allow defining a complete movement rate histogram in the way that was done for reactivation blocks. Instead the probability of movement classes for the design life time of the railway (100 years) was calculated (Figure 6.23).

The calculated probability of movement rates and movement classes are for the design lifetime of the project (100 years). This frequency of each movement rate class for each reactivation and retrogression block is presented in Table 6.11. Very slow movements (slower than 1.6 m/year) may cause serviceability problems and need continual repairing but would not normally incur risk to loss of life. The risk of loss of life may result from very rapid movement of retrogression block (B-5) and from rapid movement of the toe reactivation block (R-4).

The rapid reactivation of block R-4 needs two conditions, first development of toe cracks; second those cracks should be filled by the elevated river level water. The possibility of filling cracks by the river water starts with the Thompson River discharge return period of 500 years (i.e. the Thompson River yearly discharge of 45092 Mm3/year with maximum level of 291 m). Also, because the mechanism of this rapid reactivation contains uncertainty, it is assumed that if these conditions occur the probability of a rapid reactivation will be 0.5. The probability of very rapid movement of block B-5 is not noticeably sensitive to the Thompson River discharge. Therefore, there are not safe thresholds of the Thompson River discharge that denote a change to very rapid retrogression of this retrogression block. El-Ramly et al. (2003) suggested the probability of failure of 2×10^{-2} as the limit of safe slopes. Comparing this limit, the probability of very rapid retrogression of block B-5 is in acceptable range. A more detailed risk analysis that considers the movement consequences for assessing the risk to life because of the very rapid movement of the retrogression block would be helpful.

6.5. CONCLUSIONS

The hazard analysis for five blocks of Slide CN 50.9, as an active landslide in Ashcroft area, gives the distribution of movement rate and the probability of different possible classes of movement rate for each of these blocks. This analysis showed that although the reactivation blocks R-1 and R-2 on the deeper rupture surface and block R-3 on the shallower rupture surface will probably move slowly during the design lifetime of the project (100 years), their rapid movement is unlikely. On the other hand there is a relatively high probability (0.11) of rapid reactivation of the toe block R-4 on the deeper rupture surface. This rapid reactivation may be the result of developing toe cracks after toe erosion and extra forces by filling water from the elevated Thompson River. The rapid reactivation of the toe block may occur with the Thompson River discharge return period of 500 years which is equivalent to a yearly discharge of 45092 Mm^3/year with the maximum river level of 291 m. The probability of very rapid failure of the retrogression block, blocks B-5, is lower than 2×10^{-2} (0.3×10^{-2}) and therefore seems to be safe. A detail risk analysis may help in evaluating the risk to life because of this very rapid movement. Constant toe berm inspection and repair may eliminate the conditions for very rapid retrogression by securing the toe block because of eliminating the possibility of developing cracks at toe.

The analyses of this sample active translational earth slide in Ashcroft area with toe erosion protection highlights the process of hazard analysis for an active landslide. The movement rate was calculated using previous movement records for this slide and the other slides in this area. This hazard analysis resulted in the probability of movement rate classes which can be used in a risk analysis that considers all risks, e.g., risk to life, property damage, and service interruptions, depending on the formulation of the risk analysis.

6.6. REFERENCES

Bonnard, C. and Glastonbury, J. 2005. Risk assessment for very large natural rock slopes. In Proceedings of the International Conference on Landslide Risk Management. Edited by O. Hungr, R. Fell, R. Couture, and E. Eberhardt. Vancouver, Canada. 31 May - 3 June. A.A. Balkema, Vol.1, 335-349.

Bunce, C.M., Martin, C.D., and Abbott, B. 2005. An overview of the Canadian railway ground hazard research program. In Proceedings of the International Conference on Landslide Risk Management. Edited by O. Hungr, R. Fell, R. Couture, and E. Eberhardt. Vancouver, Canada. 31 May - 3 June. A.A. Balkema, Supplementary Volume, on CD-ROM.

Clague, J.J., and Evans, S.G. 2003. Geological framework of large historic landslides in Thompson River Valley, British Columbia. Environmental and Engineering Geoscience, 9: 201-212.

Cruden, D.M., and Varnes, D.J. 1996. Landslide types and processes. In Landslides Investigation and Mitigation: Special report 247. National Research Council (U.S.). Transportation Research Board. 36-75.

D-Elia, B., Picarelli, L., Leroueil, S., and Vaunat, J. 1998. Geotechnical characterisation of slope movements in structurally complex clay soils and stiff jointed clays. Rivista Italiana di Geotechnica, 32: 5-47.

El-Ramly, H. 2001. Probabilistic analyses of landslide hazards and risk: bridging theory and practice. Ph.D thesis, University of Alberta, Edmonton.

El-Ramly, H., Morgenstern, N.R., and Cruden, D.M. 2002. Probabilistic slope stability analysis for practice. Canadian Geotechnical Journal, 39: 665-683.

El-Ramly, H., Morgenstern, N.R., and Cruden, D.M. 2003. Probabilistic stability analysis of a tailing dyke on presheared clay-shale. Canadian Geotechnical Journal, 40: 192-208.

El-Ramly, H., Morgenstern, N.R., and Cruden, D.M. 2006. Lodalen slide: a probabilistic assessment. Canadian Geotechnical Journal, 43: 956-968.

Eshraghian, A., Martin, C.D., and Cruden, D.M. 2005a. Landslides in the Thompson River Valley between Ashcroft and Spence's Bridge, British Columbia. In Proceedings of the International Conference on Landslide Risk Management. Vancouver, Canada. May 31 to June 4, 2005b. London, Balkema, 437-446.

Eshraghian, A., Martin, C.D., and Cruden, D.M. 2005b. Earth slide movements in the Thompson River Valley, Ashcroft, British Columbia. In Proceedings of the 58th Canadian Geotechnical Conference. Saskatoon, Saskatchewan, Canada. September 18-21, 2005. Canadian Geotechnical Society.

Eshraghian, A., Martin, C.D., and Morgenstern, N.R. 2006. Groundwater and movements of earth slides in the Thompson River Valley. In 59th Canadian Geotechnical Conference. Vancouver, B.C. Canadian Geotechnical Society.

Eshraghian, A., Martin, C.D., and Morgenstern, N.R. 2007. Effect of the Thompson River on the stability of the South Slide, Ashcroft, British Columbia, Canada. In First North American Landslide Conference. Vail, Colorado. June 3-8.

Eshraghian, A., Martin, C.D., and Cruden, D.M. 2007. Complex earth slides in the Thompson River Valley, Ashcroft, British Columbia. Environmental and Engineering Geoscience. 13:161-181.

Eshraghian, A., Martin, C.D., and Morgenstern, N.R. submitted 2007. Movement triggers and mechanisms of two earth slides in the Thompson River Valley, British Columbia, Canada. Canadian Geotechnical Journal.

Fell, R., Ho, K.K.S., Lacasse, S., and Leroi, E. 2005. A framework for landslide risk assessment and management. In Proceedings of the International Conference on Landslide Risk Management. Edited by O. Hunger, R. Fell, R. Countre, and E. Eberhardet. Vancouver, Canada. 31 May- 3 June 2005.

Hungr, O., Corominas, J., and Ebehardt, E. 2005. Estimating landslide motion mechanism, travel distance and velocity. In Proceedings of the International Conference on Landslide Risk Management. Edited by O. Hunger, R. Fell, R. Couture, and E. Eberhardt. Vancouver, Canada. 31 May - 3 June. A.A. Balkema, Vol.1, 99-128.

Krahn, J. 1984. Geotechnical evaluation of the Goddard Landslide, Report 306-0950. Report to Canadian Pacific Railway, Vancouver Division, Thompson Subdivision. EBA Engineering Consultants Ltd.

Lacasse, S., and Duzgun, S. 2006. An integrated framework for risk assessment of slopes. In the Proceedings of the 59th Canadian Geotechnical Conference. Vancouver, British Columbia, Canada. October 1-4, 2006. Canadian Geotechnical Society.

Monger, J.W.H., and McMillan, W.J. 1989. Geology, Ashcroft, British Columbia. Geological Survey of Canada, Map 42-1989, sheet 1, scale 1:250,000.

Nachtigal, B.J. 2001. Ashcroft 51 landslide: September 2001 instrumentation installations. Report to Canadian National Railway, Edmonton, Alberta. Bruce Geotechnical Consultants Inc., Kamloops, British Columbia.

Phoon, K., and Kulhawy, F.H. 1999. Characterization of geotechnical variability. Canadian Geotechnical Journal, 36: 612-624.

Phoon, K., and Kulhawy, F.H. 2003. Evaluation of model uncertainties for reliability-based foundation deign. In Proceedings of the 9th International Conference on Applications of Statistics and Probability in Civil Engineering. Edited by A.D. Kiureghian, S. Madanat, and J.M. Pestana. San Fransisco, California, USA. July 6-9. Millpress Roterdam Netherlands, Vol.2, 1351-1356.

Picarelli, L., Oboni, F., Evans, S.G., Mostyn, G., and Fell, R. 2005. Hazard characterization and quantification. In Proceedings of the International Conference on Landslide Risk Management. Edited by O. Hungr, R. Fell, R. Couture, and E. Eberhardt. Vancouver, Canada. 31 May- 3 June 2005, 27-61.

Porter, M.J., Savigny, K.W., Keegan, T.R., Bunce, C.M., and MacKay, C. 2002. Controls on stability of the Thompson River landslides. In Proceedings of the 55th Canadian Geotechnical Conference: Ground and Water: Theory to Practice. Edited by D. Stolle, A.R. Piggott, and J.J. Crowder. Niagara Falls, Ontario. 20-23 October, 2002. Canadian Geotechnical Society, 1393-1400.

Roberds, W. 2005. Estimating temporal and spatial variability and vulnerability. In Proceedings of the International Conference on Landslide Risk Management. Edited by O. Hungr, R. Fell, R. Couture, and E. Eberhardt. Vancouver, Canada. 31 May - 3 June. A.A. Balkema, Vol.1, 129-157.

Ryder, J.M. 1976. Terrain inventory and Quaternary geology, Ashcroft, British Columbia. Geological Survey of Canada, Ottawa.

Stanton, R.B. 1898. The great landslides on the Canadian Pacific Railway in British Columbia. Proceedings of the Institution of Civil Engineers, 132: 1-48.

Stark, T.D., and Eid, H.T. 1994. Drained residual strength of cohesive soils. Journal of Geotechnical Engineering, 120: 856-871.

Terzaghi, K. 1950. Mechanism of landslides. In Application of Geology to Engineering Practice. Geological Society of America, New York. 83-123.

Table 6.1. Dimension of translational blocks in Slide CN50.9.

Block	Maximum Depth (m)	Width (m)	Length (m)	Area (ha)	Volume (Mm^3)
R-1 (main reactivation block on deeper rupture surface)	38	600	320	15.1	3.3
R-2 (reactivation on deeper rupture surface)	30	500	160	6.3	1.3
R-3 (toe reactivation on shallower rupture surface)	15	300	70	1.6	0.2
R-4 (toe reactivation on deeper rupture surface)	15	300	50	1.2	0.1
B-5 (retrogression on deeper rupture surface)	38	650	370	18.9	4.7

Table 6.2. Return periods of the Thompson River yearly discharge.

Return Period (Year)	Ascending Probability (%)	Q_1* (Mm^3)	Q † (Mm^3)	Q/Q_{mean}=24458 (Mm^3)
2	50	23842	26728	1.093
5	80	27679	30565	1.25
10	90	30108	32994	1.35
20	95	32372	35258	1.44
50	98	35236	38122	1.56
100	99	37352	40238	1.65
200	99.5	39447	42333	1.73
500	99.8	42206	45092	1.84
1000	99.9	44298	47184	1.93

* Yearly discharge without trend change effect

† Yearly discharge with trend change effect

Table 6.3. Probability of different Thompson River flood return periods in the designed lifetime of the railway (100 years).

Return Period (year)	Discharge (Mm^3/year)	Frequency (1/year)	Probability (in 100 year)
2	26728	0.5	1
5	30565	0.2	1
10	32994	0.1	0.999
20	35258	0.05	0.994
50	38122	0.02	0.867
100	40238	0.01	0.634
200	42333	0.005	0.394
500	45092	0.002	0.181
1000	47184	0.001	0.095

Table 6.4. Soil properties used in seepage analyses

Soil type	K_{sat} (cm/sec)	Volumetric Water Content at Saturation
Sand and gravel (berm)	2.31×10^{-3}	0.3
Till	4.63×10^{-4}	0.3
Silt, sand, diamicton	8.10×10^{-5}	0.42
Clay-silt	1.16×10^{-9}	0.35
Glaciofluvial	1.16×10^{-6}	0.23

Table 6.5. The material properties used in Slide CN50.9's deterministic stability analyses

Material	γ (kN/m^3)	c' (kPa)	φ' (°)
Till $_{residual}$	18	0	26
Silt and Sand $_{residual}$	19	0	25
Clay-Silt $_{residual}$	19	0	11
Fluvial $_{residual}$	18	0	24
Berm $_{residual}$	18	0	30
Till $_{undisturbed}$	18	50	26
Silt and Sand $_{undisturbed}$	19	30	25
Clay-Silt $_{undisturbed}$	19	10	11

Table 6.6. Definitions of the variability in soil parameters used in probabilistic slope stability analysis

Soil	Parameter	Source *	Mean	COV$_{inherent}$ (%)	COV$_{total}$ (%)	σ
Till	$\varphi'_{r(disturbed)}$	G.S	26	10	15	3.9
Till	$\varphi'_{(undisturbed)}$	G.S	26	10	16	4.16
Till	$c'_{(undisturbed)}$	G.S	50	20	25	12.5
Silt & Sand	$\varphi'_{r(disturbed)}$	I.P and G.S.	25	14	16	4.0
Silt & Sand	$\varphi'_{(undisturbed)}$	G.S	25	14	17	4.25
Silt & Sand	$c'_{(undisturbed)}$	G.S.	25	20	25	6.25
Clay-Silt	$\varphi'_{r(disturbed)}$	I.P, G.S. and D.S.	11	18	19	2.09
Clay-Silt	$\varphi'_{(undisturbed)}$	D.S. and G.S.	11	18	20	2.2
Clay-Silt	$c'_{(undisturbed)}$	D.S. and G.S.	10	20	25	2.5
Fluvial	$\varphi'_{r(disturbed)}$	G.S.	24	14	17	4.08
Berm	$\varphi'_{r(disturbed)}$	G.S.	30	10	15	4.5

* Source of estimation (G.S.= Grain Size Analyses, I.P.= Index Property, D.S.= Direct Shear test)

Table 6.7. Sensitivity of blocks' factor of safety to change in soil parameters

Block	Soil Parameter	Standard Deviation (σ)	Min. F.S change with material change *	Min. F.S change (%)
R-1	Till $\varphi'_{r(\text{disturbed})}$	3.9	0.036	2.9
	Silt and sand $\varphi'_{r(\text{disturbed})}$	4.0	0.144	11.8
	clay-silt $\varphi'_{r(\text{disturbed})}$	2.09	0.293	25.7
	Fluvial $\varphi'_{r(\text{disturbed})}$	4.08	0.004	0.3
R-2	Till $\varphi'_{r(\text{disturbed})}$	3.9	0.01	1.1
	Silt and sand $\varphi'_{r(\text{disturbed})}$	4.0	0.137	16.2
	clay-silt $\varphi'_{r(\text{disturbed})}$	2.09	0.178	21.8
	Fluvial $\varphi'_{r(\text{disturbed})}$	4.08	0.004	0.3
R-3	Till $\varphi'_{r(\text{disturbed})}$	3.9	0.167	16.5
	clay-silt $\varphi'_{r(\text{disturbed})}$	2.09	0.118	11.6
	Fluvial $\varphi'_{r(\text{disturbed})}$	4.08	0.086	8.3
R-4	Till $\varphi'_{r(\text{disturbed})}$	3.9	0.117	10.8
	clay-silt $\varphi'_{r(\text{disturbed})}$	2.09	0.166	15.3
	Fluvial $\varphi'_{r(\text{disturbed})}$	4.08	0.115	10.6
B-5	clay-silt $\varphi'_{r(\text{disturbed})}$	2.09	0.218	20.5
	Fluvial $\varphi'_{r(\text{disturbed})}$	4.08	0.002	0.2
	Till $\varphi'_{(\text{undisturbed})}$	4.16	0.059	5.1
	Till $c'_{(\text{undisturbed})}$	12.5	0.029	2.5
	Silt and sand $\varphi'_{(\text{undisturbed})}$	4.25	0.084	7.4
	Silt and sand $c'_{(\text{undisturbed})}$	6.25	0.009	0.8
	Clay-silt $\varphi'_{(\text{undisturbed})}$	2.2	0.059	5.1
	Clay-silt $c'_{(\text{undisturbed})}$	2.5	0.004	0.3

* Change of minimum factor of safety with change of material property within one standard deviation (σ) each side of material property's mean

Table 6.8. Range of changes in the probability of Factor of Safety being less than 1.1 (P(FS<1.1)) by uncertainty in the groundwater system modeling for each of the four blocks in Slide CN50.9.

Block	$P(F.S.<1.1)_{GWmean}$ - $P(F.S<1.1)_{GWmin}$ (%)	$P(F.S<1.1)_{GWmax}$ - $P(F.S<1.1)_{GWmean}$ (%)	Average changes (%)
R-1	0.1	0.2	0.15
R-2	0.37	0.20	0.29
R-3	19	19.1	19.0
R-4	27.0	28.0	27.5
B-5	1.3	2.1	1.7

Table 6.9. Range of changes in the probability of Factor of Safety being less than 1.1 (P(FS<1.1)) by uncertainty in the amount of toe erosion in each of the five blocks in Slide CN50.9

Block	$P(F.S.<1.1)_{max. erosion}$ - $P(F.S<1.1)_{min. erosion}$ (%)	Average Changes from $P(F.S<1.1)_{mean erosion}$ (%)
R-1	0.05	0.03
R-2	0.04	0.02
R-3	8.56	4.28
R-4	14.22	7.11
B-5	0.35	0.18

Table 6.10. Definition of the total uncertainty of the probabilistic stability analysis results' trend line based on uncertainties in groundwater modeling and toe erosion

Block	Uncertainty in P(F.S<1.1) from		Total uncertainty in P(F.S<1.1) (%)
	Groundwater modeling (%)	Toe erosion (%)	
R-1	0.15	0.03	0.17
R-2	0.29	0.02	0.30
R-3	19.0	4.28	21.14
R-4	27.5	7.11	31.06
B-5	1.7	0.18	1.79

Table 6.11. Probability of the blocks' different movement rate classes in the design lifetime of the project (100 years)

Block	No Movement	Extremely Slow	Very Slow	Rapid	Very Rapid
R-1	0.998	0.002	0	0	0
R-2	0.002	0.765	0.233	0	0
R-3	0.127	0.031	0.842	0	0
R-4	0.138	0.0	0.752	0.110	0
B-5	0.960	0	0.037	0	0.003

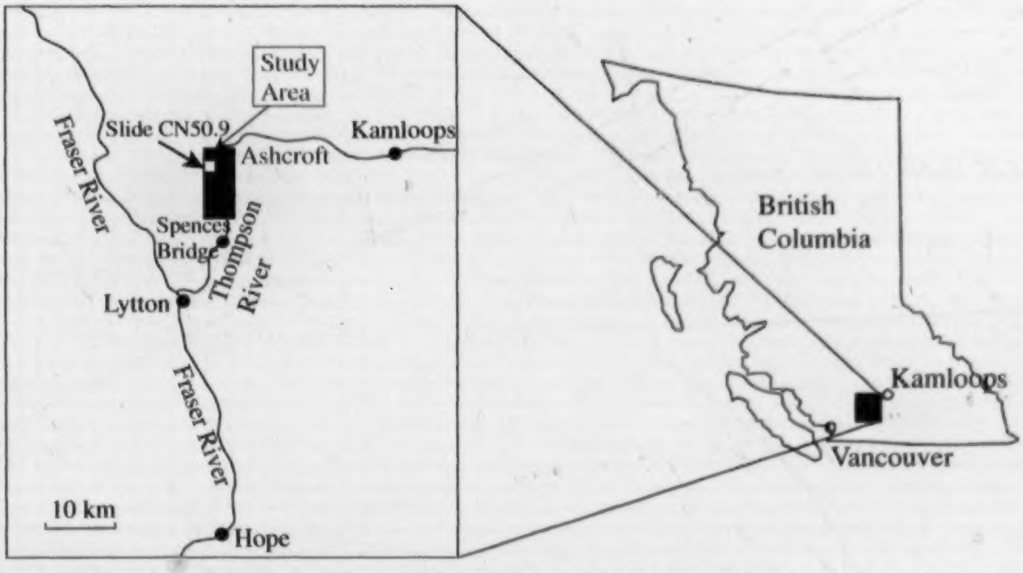
Study Area
Slide CN50.9
Kamloops
Ashcroft
Fraser River
Spences Bridge
Thompson River
Lytton
Fraser River
10 km
Hope
British Columbia
Kamloops
Vancouver

Figure 6. 1. Slide CN50.9 in study area south of Ashcroft, British Columbia, between 50° 10′ to 50° 20′ N and 121° 15′ to 121° 20′ W.

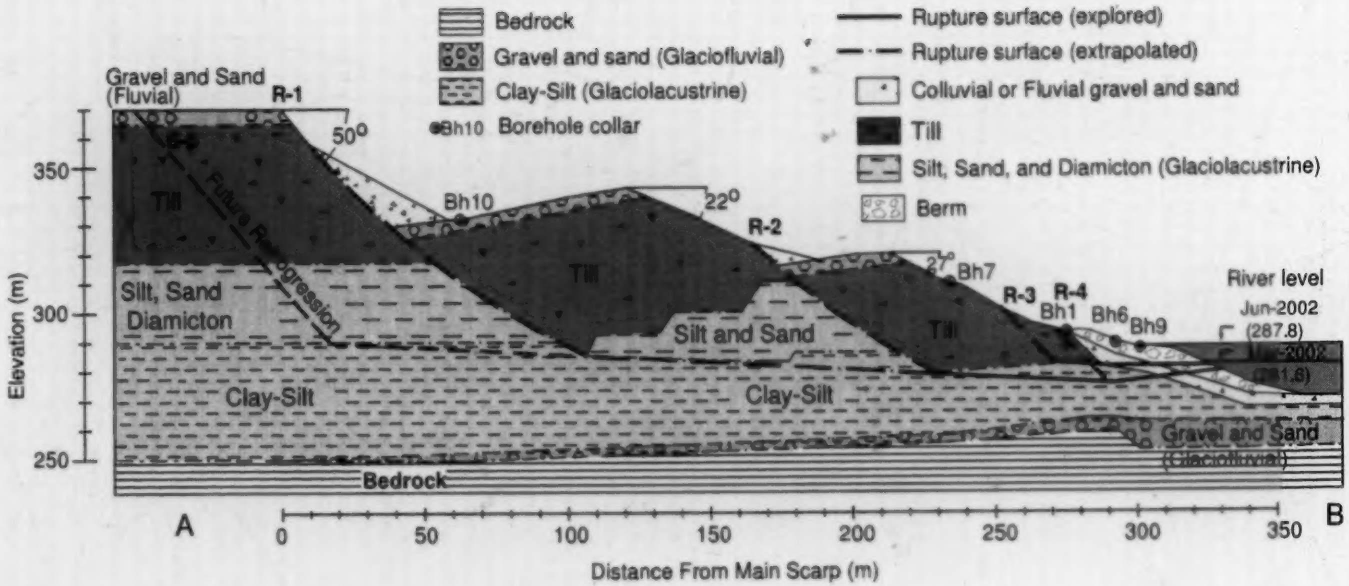
Bedrock
Gravel and sand (Glaciofluvial)
Clay-Silt (Glaciolacustrine)
Bh10 Borehole collar
Rupture surface (explored)
Rupture surface (extrapolated)
Colluvial or Fluvial gravel and sand
Till
Silt, Sand, and Diamicton (Glaciolacustrine)
Berm
Gravel and Sand (Fluvial)
R-1
50°
Bh10
22°
R-2
27°
Bh7
R-3
R-4
Bh1
Bh6
Bh9
River level
Jun-2002
(287.8)
Till
Future Retrogression
Till
Till
Silt, Sand Diamicton
Silt and Sand
Clay-Silt
Clay-Silt
Gravel and Sand (Glaciofluvial)
Bedrock
Elevation (m)
350
300
250
A
B
0
50
100
150
200
250
300
350
Distance From Main Scarp (m)

Figure 6.2. Slide CN50.9 cross section showing the rupture surfaces, stratification, boreholes, four reactivation blocks, and a retrogression block.

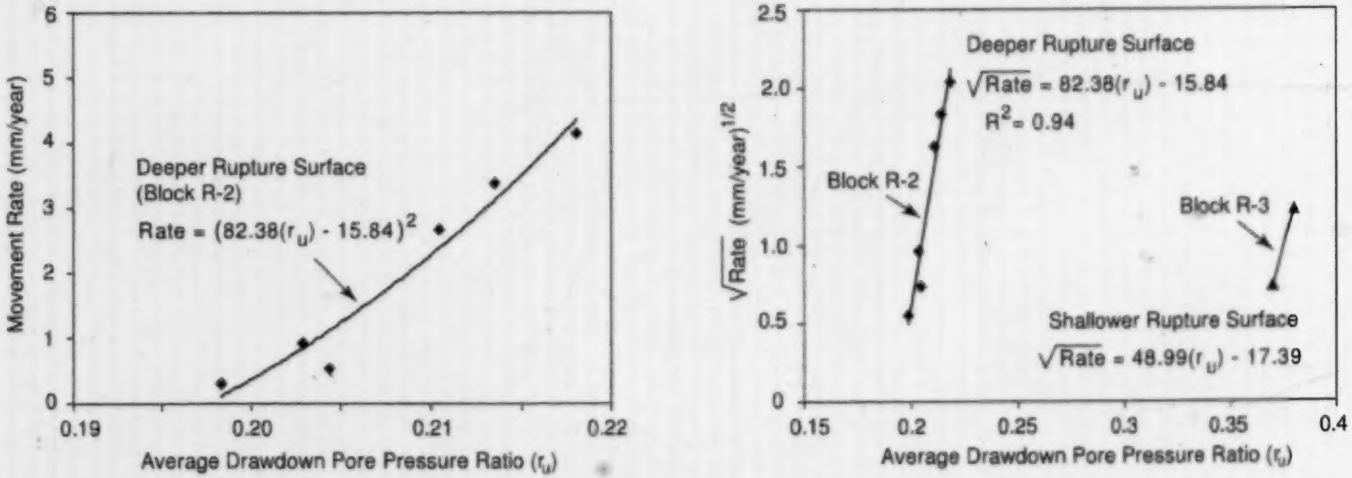

Figure 6.3. Correlation between pore pressure ratio during drawdown period and movement rate for reactivation blocks.

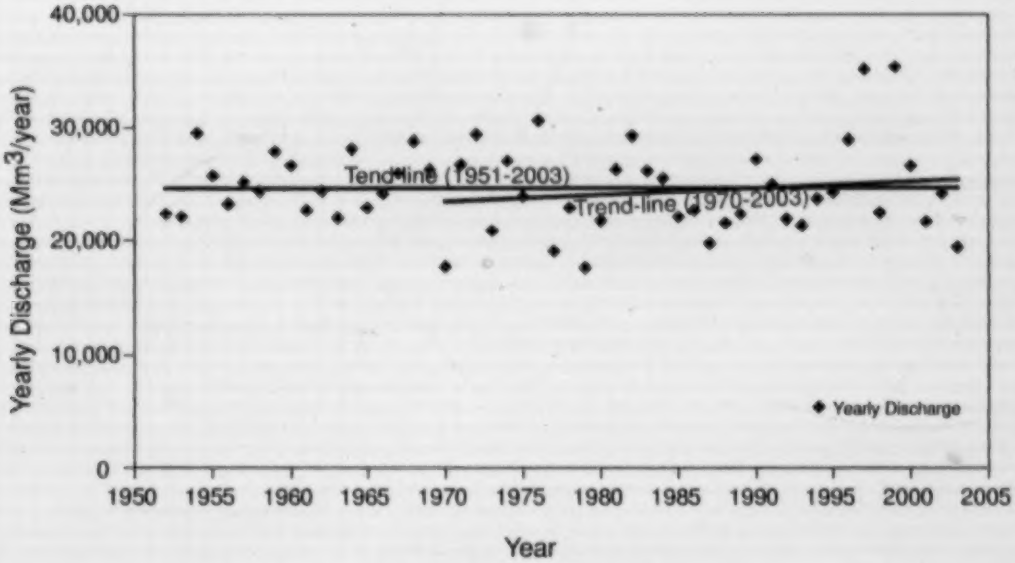

Figure 6.4. Increase in the trend line of the yearly discharge of Thompson River since 1970s.

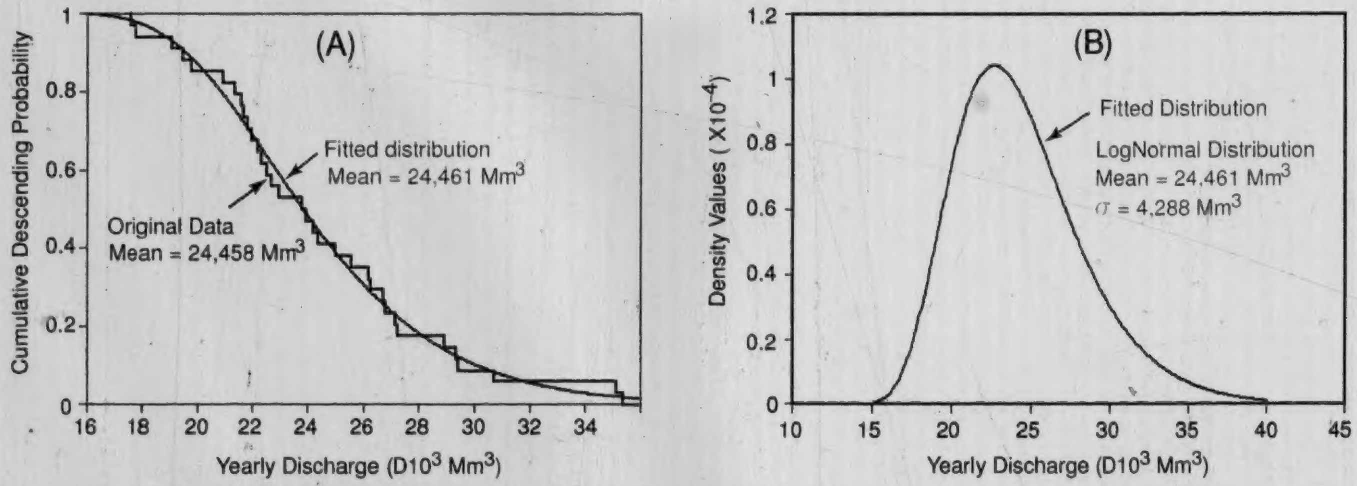

Figure 6.5. (A) Comparison of the yearly discharge data from 1970 to 2003 and the best fit probabilistic distribution and (B) the lognormal probability function resulting from the best fit on yearly discharge data.

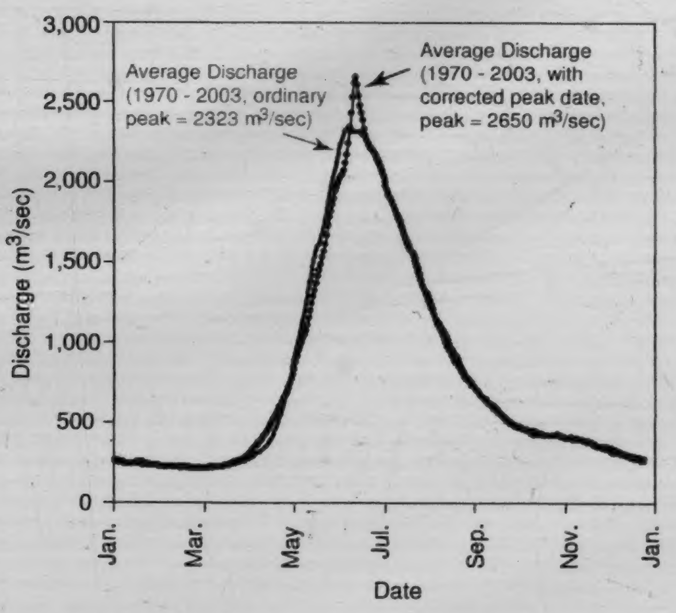

Figure 6.6. The Thompson River average discharge in a normal year, calculated by using peak date correction and without using peak date correction.

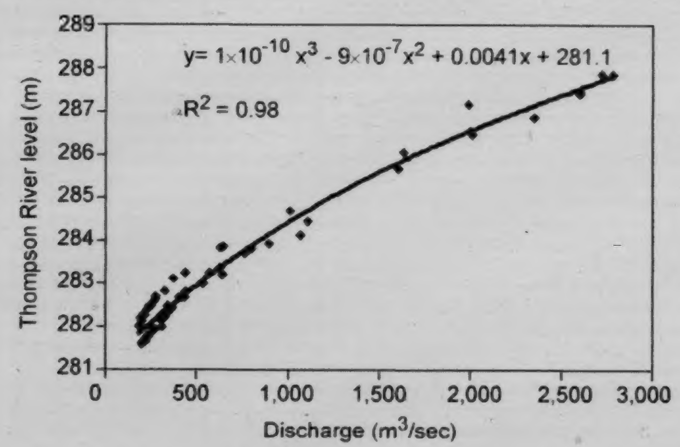

Figure 6.7. Correlation between the Thompson River level at Slide CN50.9 and the Thompson River discharge

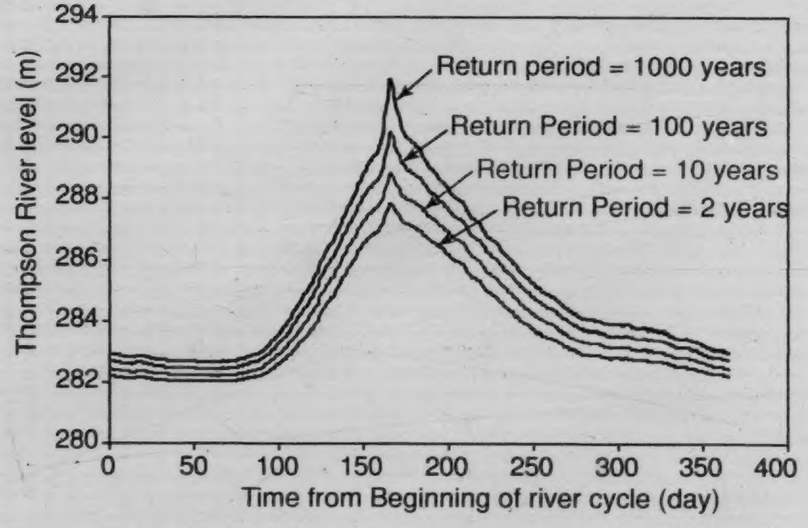

Figure 6.8. The Thompson River level for different yearly discharge return periods

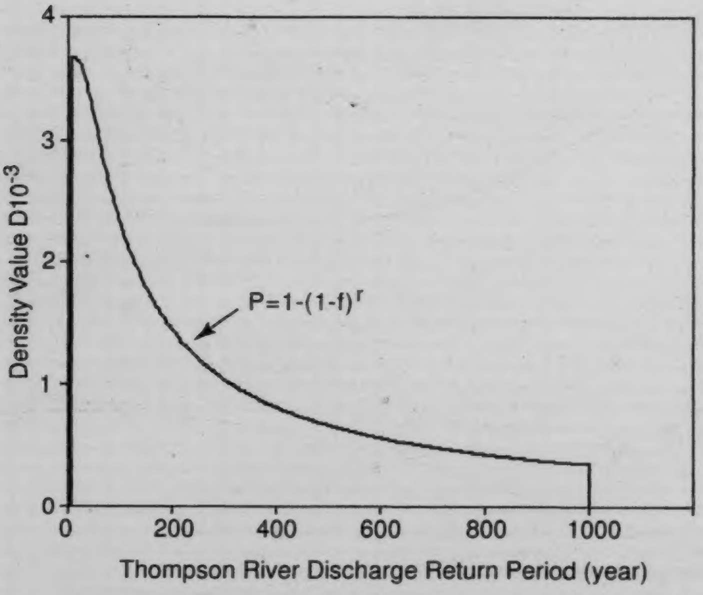

Figure 6.9. Probability of different Thompson River flood return periods within the designed railway lifetime period

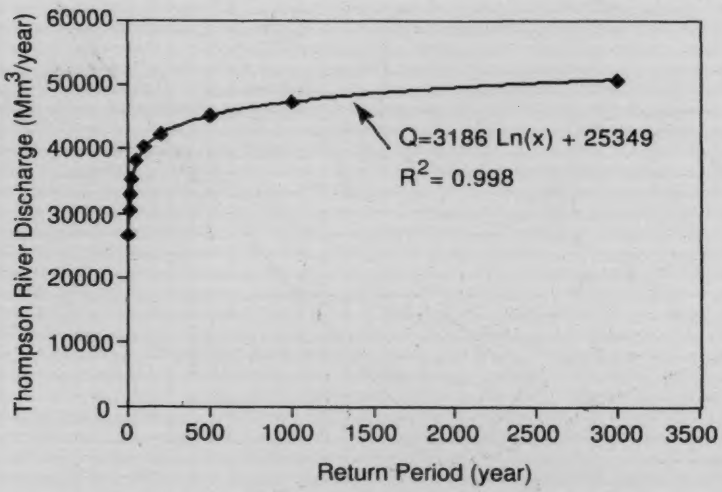

Figure 6.10. Correlation between the Thompson River flood return period and the Thompson River discharge

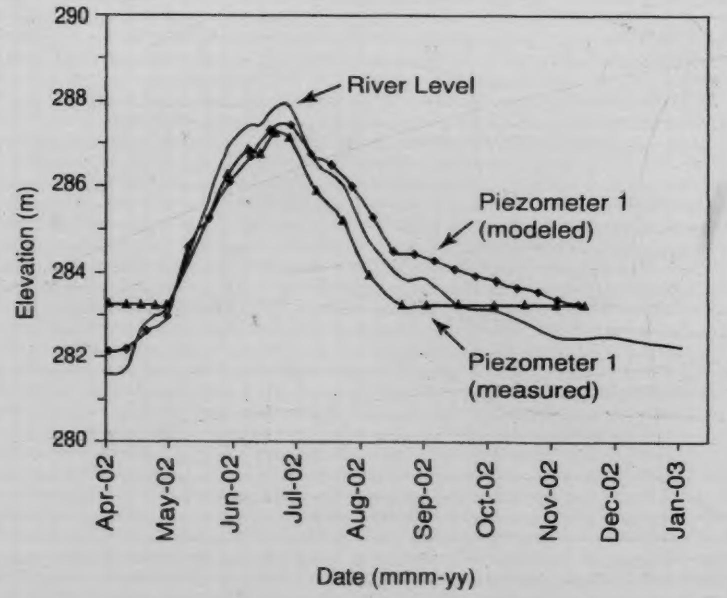

Figure 6.11. Comparison of piezometric modeled response and measured response (from Eshraghian et al. submitted)

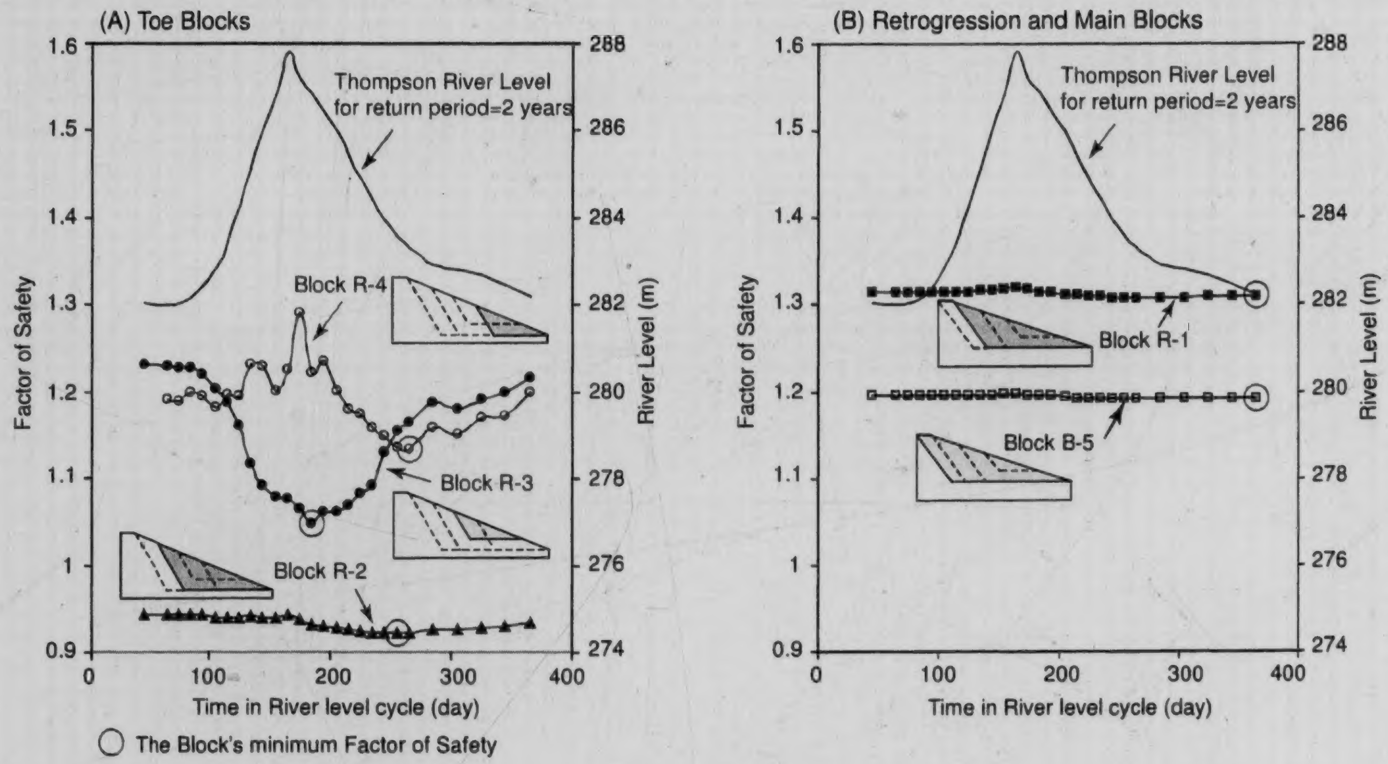

FFigure 6.12. Deterministic stability analysis results with the Thompson River level fluctuation from the Thompson River 2-year return period discharge for (A) reactivation toe blocks, and (B) retrogression and main blocks

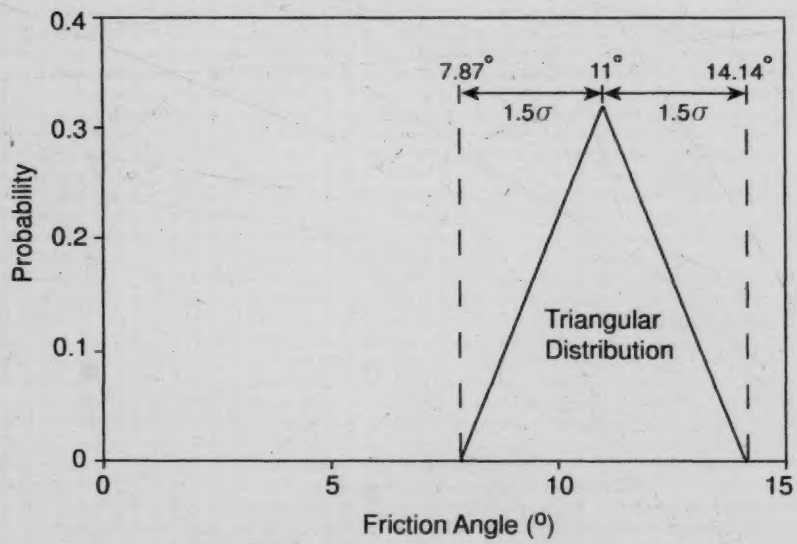

Figure 6.13. A sample material property probability distribution (in this case, the residual friction angle of the disturbed clay-silt layer)

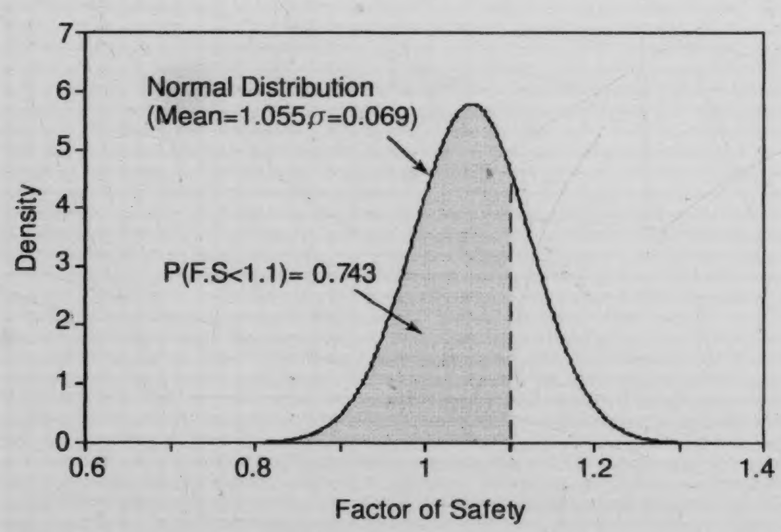

Figure 6.14. The Factor of Safety distribution calculated for block R-3 by using a Thompson River discharge return period of 2 years

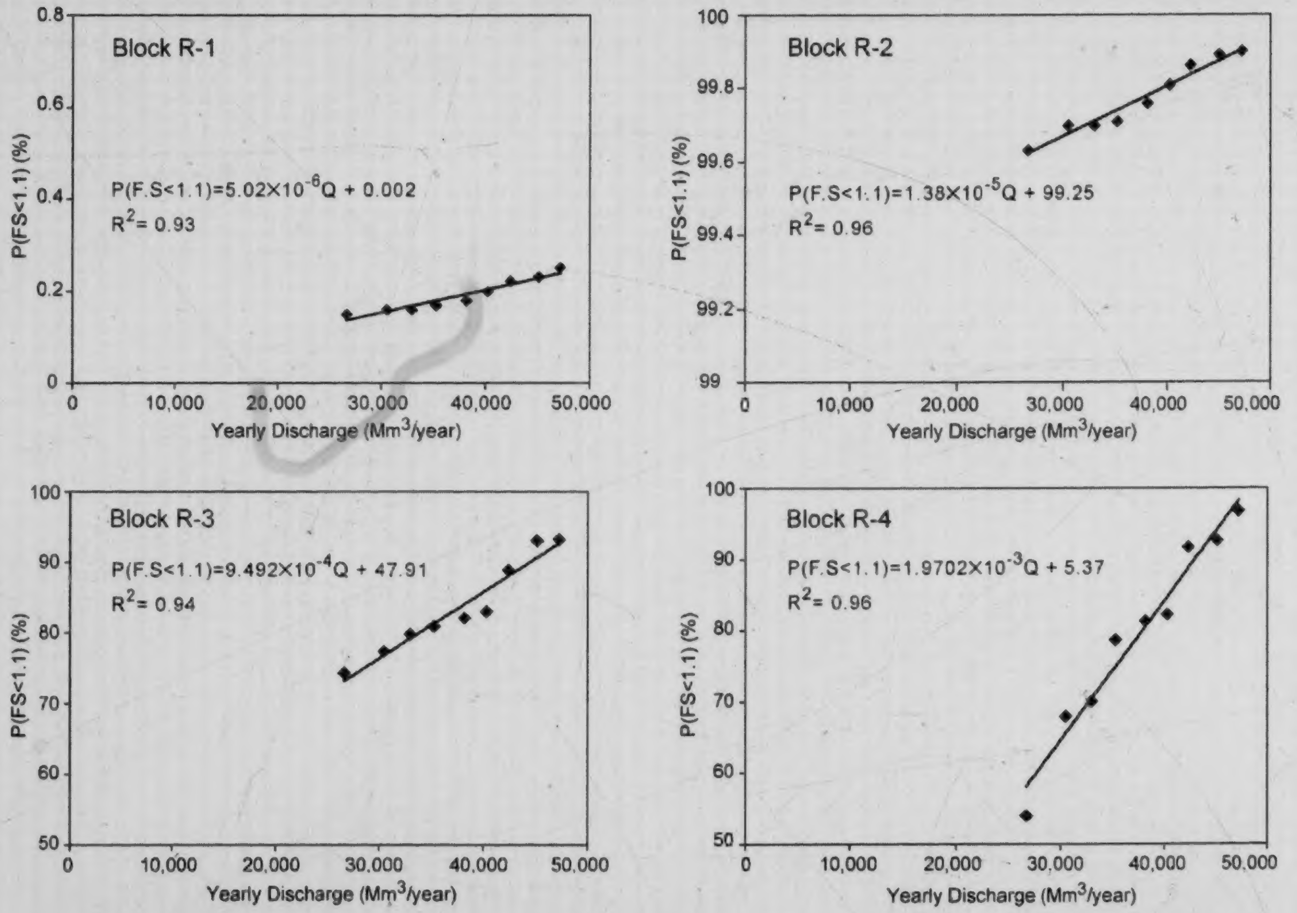

Figure 6.15. Change in the reactivation blocks' probability of Factor of Safety being less than 1.1 with the Thompson River yearly discharge

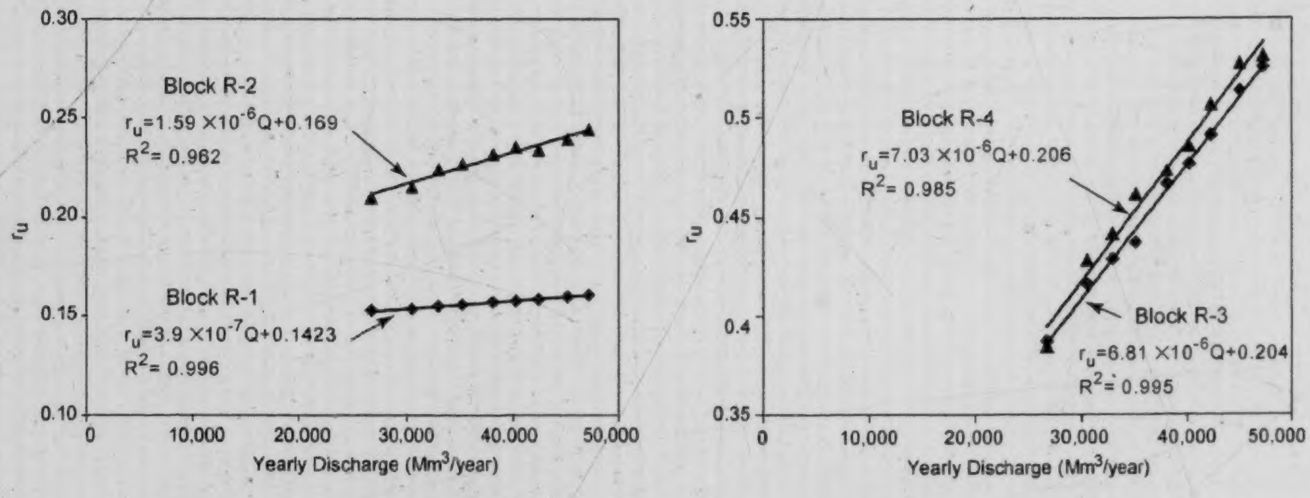

Figure 6.16. Change in the reactivation block pore pressure ratio (ru) with the Thompson River yearly discharge

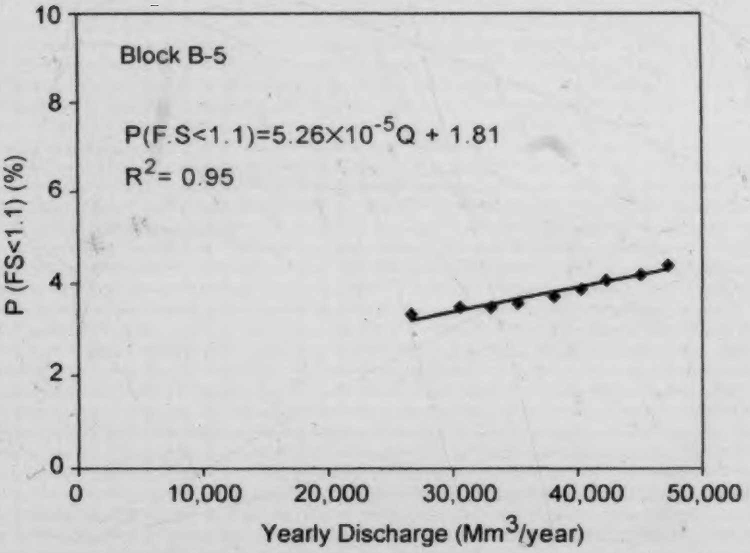

Figure 6.17. Change in the probability of Factor of Safety being less than 1.1 for the retrogressive block (block B-5) with river discharge

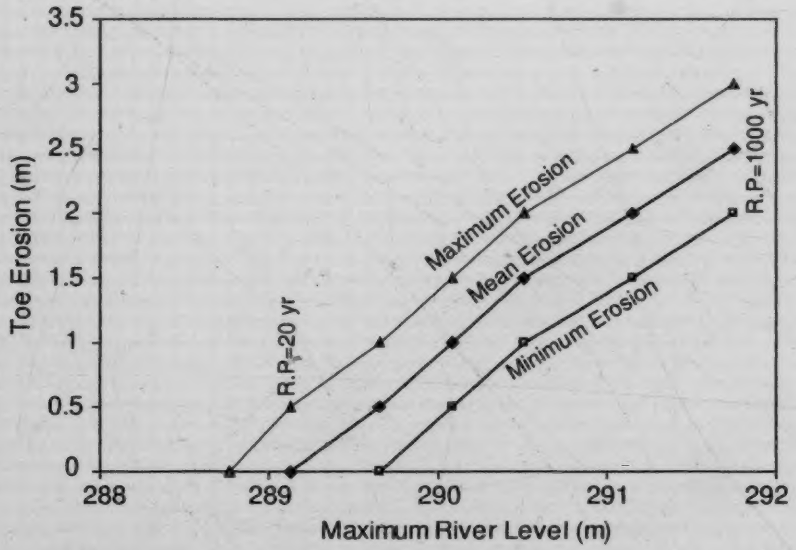

Figure 6.18. Range of possible toe erosion at Slide CN50.9

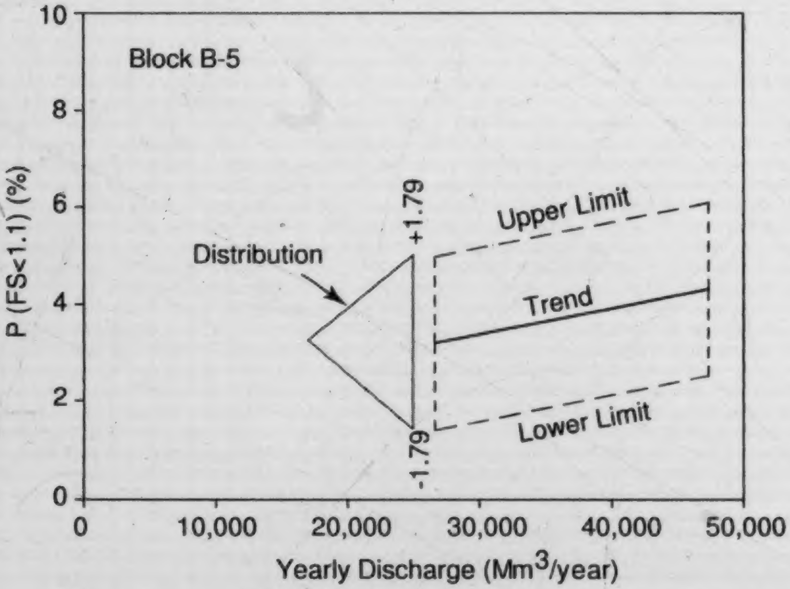

Figure 6.19. Definition of the uncertainty around the trend line fitted on the probabilistic stability analysis (in this case, for the probability of Factor of Safety being less than 1.1 for block R-5)

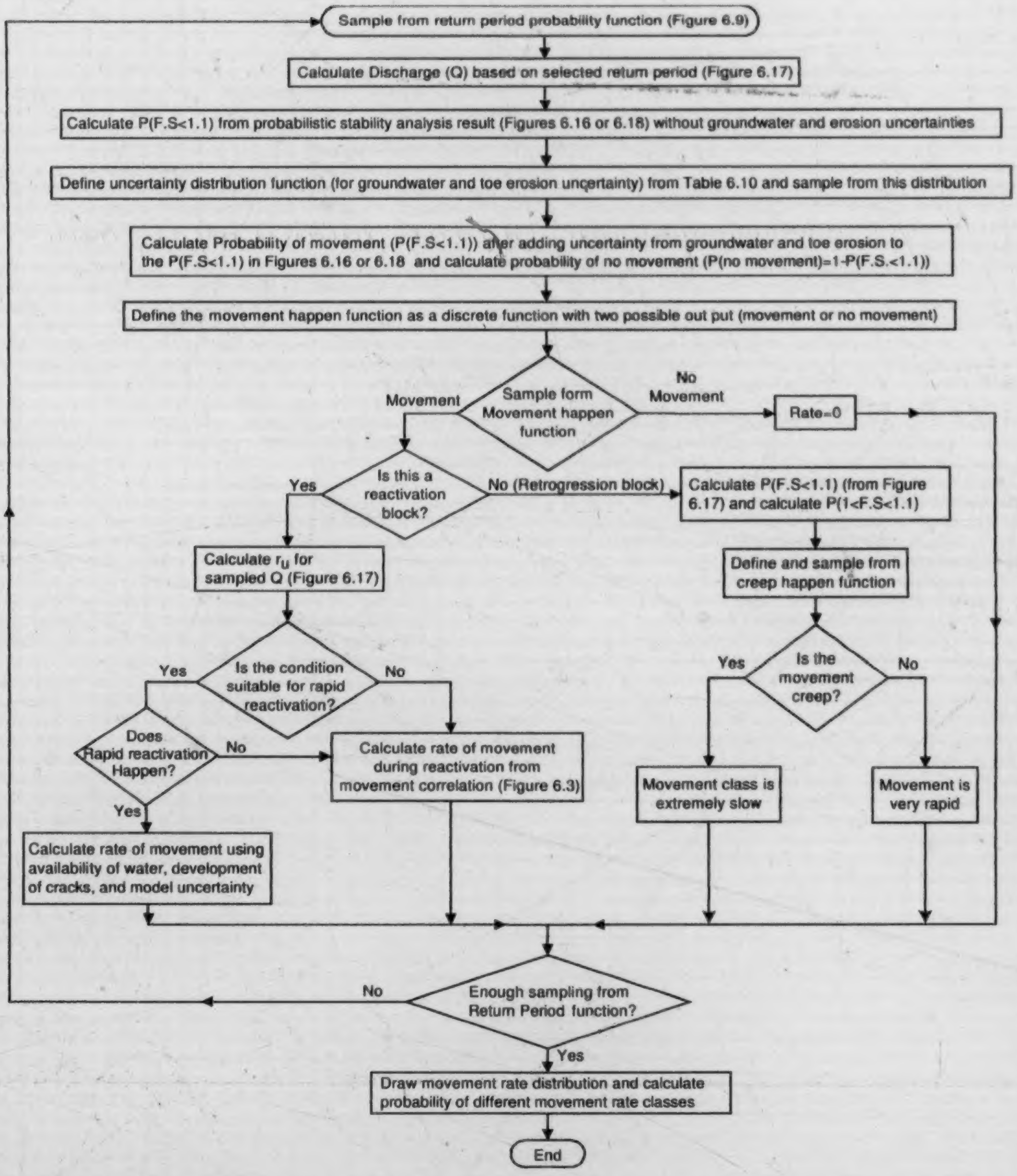
Sample from return period probability function (Figure 6.9)
Calculate Discharge (Q) based on selected return period (Figure 6.17)
Calculate P(F.S<1.1) from probabilistic stability analysis result (Figures 6.16 or 6.18) without groundwater and erosion uncertainties
Define uncertainty distribution function (for groundwater and toe erosion uncertainty) from Table 6.10 and sample from this distribution
Calculate Probability of movement (P(F.S<1.1)) after adding uncertainty from groundwater and toe erosion to the P(F.S<1.1) in Figures 6.16 or 6.18 and calculate probability of no movement (P(no movement)=1-P(F.S.<1.1))
Define the movement happen function as a discrete function with two possible out put (movement or no movement)
Movement
Sample form Movement happen function
No Movement
Rate=0
Yes
Is this a reactivation block?
No (Retrogression block)
Calculate P(F.S<1.1) (from Figure 6.17) and calculate P(1<F.S<1.1)
Calculate r_u for sampled Q (Figure 6.17)
Define and sample from creep happen function
Yes
Is the condition suitable for rapid reactivation?
No
Yes
Is the movement creep?
No
Does Rapid reactivation Happen?
No
Calculate rate of movement during reactivation from movement correlation (Figure 6.3)
Movement class is extremely slow
Movement is very rapid
Yes
Calculate rate of movement using availability of water, development of cracks, and model uncertainty
No
Enough sampling from Return Period function?
Yes
Draw movement rate distribution and calculate probability of different movement rate classes
End

Figure 6.20. Flowchart for calculating probability of different movement rates within the life time of the railway (100 years)

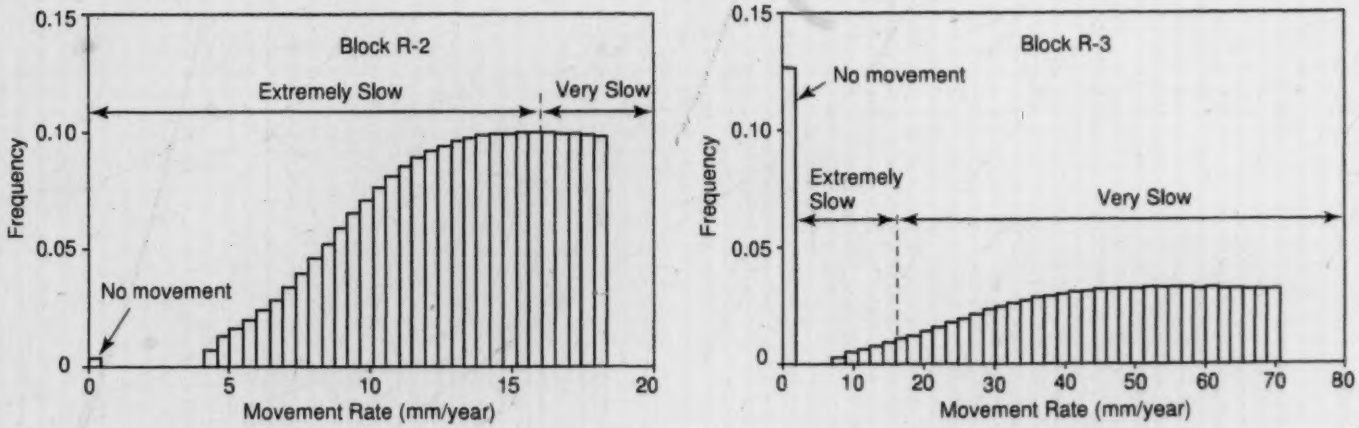

Figure 6.21. Histogram frequency distribution of movement rate for two translational blocks on shallower and deeper rupture surfaces

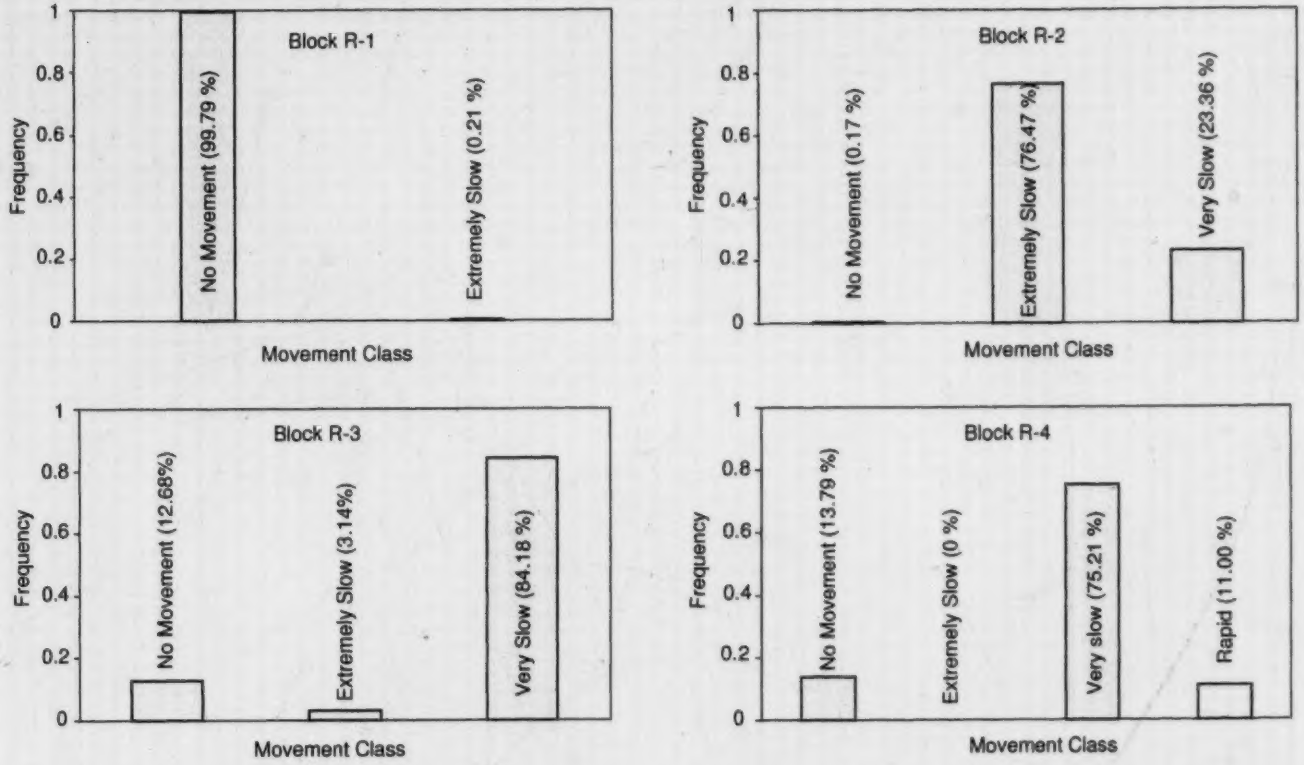

Figure 6.22. Frequency of different movement rate classes for reactivation blocks defined within Slide CN50.9. The duration of calculation is the design life time of the railway (100 years).

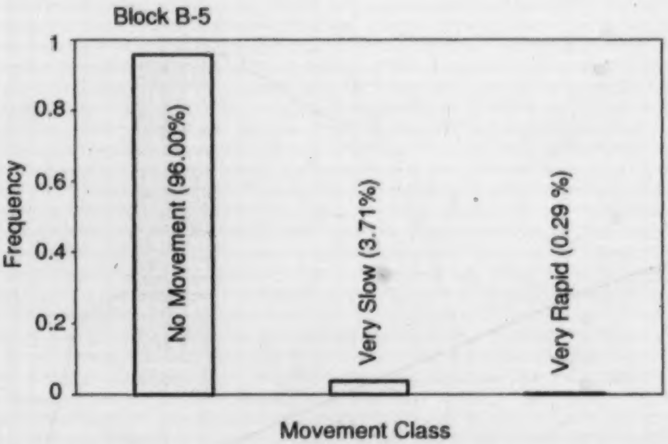

Figure 6.23. Frequency of different movement rate classes for retrogression block (B-5, Figure 6.2)

Chapter 7

Summary and Conclusions

7.1. SUMMARY

In this study, 11 earth slides along 10 kilometres of the Thompson River Valley, Ashcroft, British Columbia were investigated as examples of a common stability problem caused by down-cutting rivers in western Canada and many other parts of the globe. Since the early 1980s, the CN and CPR railway companies have been carrying out geotechnical investigations of these landslides, allowing for the study of the possible triggers of such slides in the walls of a relatively fast down-cutting river through 120 m of glacial sediments. Importing the data from these investigations into a Geographical Information System (GIS) facilitated the study of these slides in a single broader framework.

These slides in the Ashcroft area are large, reactivated, retrogressive, multiple, translational earth slides moving on two rupture surfaces within glaciolacustrine clay-silt unit within Quaternary sediments in this area. The rupture surfaces are within thicker layers of highly-plastic clay within this clay-silt unit. Most of the reactivations have happened in late summer and early fall.

Detailed study of the different possible triggers and the movement frequencies of the landslides in this semi-arid area revealed that these movements' main trigger was the

Thompson River itself. The movement data recorded in boreholes within four of these reactivated landslides showed that the movement rates appeared to respond to drops in the level of the Thompson River after periods of high flows.

Transient groundwater analyses and stability analyses of three of these earth slides were conducted to investigate the possible effects of the Thompson River on these reactivated earth slides. These analyses showed that the Thompson River affects the stability of a slide in its valley walls in two ways: (1) river bank erosion changes the slide geometry and reduces the stability of the slide; and (2) during periods of elevated river levels, the groundwater conditions at the slide toe are modified and can result in a rapid drawdown effect later, which can also reduce the stability of the slide's toe. These effects can act independently or simultaneously. When they act simultaneously, the slide velocities are the greatest. Detailed stability analyses of the slides showed that the relative importance of each of these effects of the Thompson River on a specific block within a slide depends on the river-erosion protection, the size of the block, the depth of the block's rupture surface, and the amount of river-level fluctuation. Seepage analyses of these slides showed that the groundwater system changes mainly within 100-150 metres of the slide toes (Figure 2.15, Figure 4.10, and Figure A1.4). Therefore, the effect of the river-level change on the pore pressure on the rupture surface is mainly on the toe blocks. For larger blocks, the reactivations are more likely to be the result of river erosion or a combination of river erosion and river drawdown.

These slides have been moving at different rates during the last century. A review of their previous movement revealed that most of the previous retrogression movement rates have been very rapid. On the other hand, the current reactivation movements are generally extremely slow to very slow, but the Goddard Slide reactivated rapidly in 1982. The importance of a change from an extremely slow reactivation to a rapid reactivation made a more detailed study of this possibility necessary.

The movement records from the inclinometers installed in 5 of the slides were used to determine the slides' movement behaviours. These data showed the movement rate changed in response to pore pressure changes on a slide's rupture surface. Such detailed information was not available for all the slides and not even for some of the blocks within the slides with detailed movement records. Therefore, a broader study of the movement of the reactivated translational earth slides has been conducted to determine the movement rate behaviour of this type of earth slide. The study of 60 case histories of reactivated translational earth slides around the world helped to increase our understanding of this type of slide's movement behaviour. The result of this study showed that these slides' movement rates change non-linearly with an increase in the pore pressure on their rupture surfaces and that a correlation exists between the acceleration after movement starts and the material properties and stress on the slides' rupture surfaces. The result of this case history review was used to estimate movement behaviour for those blocks without enough movement record data.

The next step of the project was to develop a hazard analysis framework for an active earth slide. While blocks in a reactivated landslide may move at different rates, normal quantitative hazard analysis practice involves probabilistic stability analysis with an assumption of the movement rate after failure. On the other hand, because the consequences of a landslide movement may be closely related to its rate of movement, a hazard analysis should consider the probability of different post-failure movement rates. A new methodology for hazard analysis using probabilistic slope stability and the probabilistic post-failure rate of movement was developed for a sample earth slide in the Ashcroft area (Slide CN50.9). This analysis showed a relatively high probability of the rapid reactivation of Slide CN50.9 toe within the designed lifetime of the project (100 years) with a Thompson River yearly discharge threshold of a return period of 500 years. This threshold is equivalent to a maximum river level of 291 m. The probability of the current main scarp's rapid retrogression for the project's designed lifetime was calculated to be near that of the acceptable practice for a landslide.

7.2. MAIN CONTRIBUTIONS OF THE THESIS

Main contributions of the thesis to the studied subject are summarized as follow.

- Recognized the main trigger of the recent slide reactivations in the Thompson River Valley, south of Ashcroft, British Columbia based on correlations between trigger and number of reactivations among the slides in this area (Chapter 2).
- Expanded previous geological studies in more detailed in a GIS map and added new information to this data base to find similarities among rupture surfaces at the slides (Chapter 3).
- Studied possible kinematics and sequences of sliding for studied slides in the area (Appendix 2).
- Conducted new geotechnical investigations including laboratory tests on new samples from slides shear zone and analysing new inclinometer and piezometric data to gain better understanding of material properties and kinematics of the slides (Appendix 3 and Chapter 3).
- Produced cross sections of the slides for the studied slides based on possible sequences of sliding and matching resulted sections with results of geotechnical investigations (Appendix 2).
- Studied geological information, previous and new geotechnical investigations, and historic data to recognize possible mechanisms of the slides' reactivations (Chapter 3).
- Conducted groundwater analyses (transient analyses) for some of the slides in the area and gained better understanding of changes of groundwater system in the slides (Chapter 4 and Appendix 1)

- Conducted stability analyses of the slides and gained better understanding of effects of the trigger on the stability of the slides and mechanism of reactivations (Chapter 4 and Appendix 1).
- Found correlations between the reactivation rate of slides' blocks and pore pressure on their rupture surfaces (Chapter 4).
- Reviewed case histories of translational reactivated slides and developed correlations for predicting possible movement rate classes for this type of slides (Chapter 5).
- Established characteristics of the Thompson River at the site of a sample slide in Ashcroft area (Chapter 6).
- Conducted probabilistic stability analysis of the sample slide in Ashcroft area (Chapter 6).
- Developed a framework for hazard analysis of reactivated slides and calculated probabilities of different reactivation rates of individual blocks within the sample slide in Ashcroft area (Chapter 6).

7.3. CONCLUSIONS

This study of the earth slides in Ashcroft area increased our understanding of such translational earth slides in glacial-sediment valleys in western Canada. The main conclusions of this study follow:

- In the absence of high precipitation in semi-arid areas, a river may trigger the reactivation of a landslide in two main ways: (1) by changing the geometry of the slope by river erosion action, and (2) by changing the groundwater system and creating a drawdown mechanism.

- The river effects on a specific block's stability in a multiple translational earth slide are (1) a toe erosion effect, (2) a change in the pore pressure on the block rupture surface, and (3) the supporting effect of the river load at the slide toe. Each of these effects' relative importance for a specific block depends on the river erosion protection, the size of the block, the depth of the block's rupture surface, and the amount of river level fluctuation.

- The study of change of reactivation rate from slow to rapid and comparison with the results of stability and seepage analyses showed that if the slide mass is wet and has access to water; cracks previously formed by slow movements may fill with water (chapter 3 section 3.5.2 and chapter 4 section 4.5.2). This process might apply an increased driving force on the tension crack walls and a change of the movement rate to rapid reactivation.

- The reactivation of a translational earth slide may start with Factor of Safety close to unity and, in the case of Ashcroft landslides, with Factor of Safety less than 1.1.

- The rate of reactivation after the movement's start increases non-linearly with the pore pressure increase on the rupture surface.

- The movement acceleration after the movement starts depends on the material on the slide's rupture surface (plasticity index of the material) and the stress level (the depth of the rupture surface). A Ductility Factor can be defined as a function of the Plasticity Index of the material on the rupture surface and the rupture surface's average depth. The acceleration shows a relatively good correlation with the Ductility Factor.

- An increase in the Ductility Factor (an increase in plasticity and/or depth) increases a slide's ductile behaviour and decreases the slide's tendency to accelerate and move at a more rapid rate during its reactivation.

- The hazard analysis of an active landslide requires the calculation of the frequency of different movement rates within the designed lifetime of a project. Such an analysis is possible after gaining a clear understanding of the slide's movement mechanisms.

- In hazard analysis of reactivated translational earth slides triggered by a river, uncertainty in the material's properties, the trigger, river erosion, and pore water pressure modeling should be considered.

7.4. SUGGESTED FUTURE RESEARCH

During the course of this research, several exciting issues were encountered which deserve additional investigation. Some of these issues are presented below.

- Investigation of the possible development of a new, deeper rupture surface within the study area. This study would need a more detailed site investigation targeting to find a new, weak layer among thicker clay layers within the clay-silt unit in the area.

- Development of new hazard analysis methodology for the hazard analysis of slides with a combination of river erosion and river drawdown effects. The current proposed hazard analysis method was used for the hazard analysis of slides with river erosion protection. In this analysis, only sudden toe erosion was considered in such a way that no cumulative toe erosion could be considered (any erosion would be repaired by the following year). In the cases without river erosion protection, continuous toe erosion has to be considered in the hazard analysis.

- Using numerical methods, verification should be sought for the new movement behaviour correlations found for the acceleration of the movement after its start. A numerical method with a proper constitutive model may be useful to verify the change of the movement rate with the pore pressure ratio changes on a slide's rupture surface.
- Investigation of possible new correlations for the movement behaviour of translational earth slides triggered by river erosion, loading at the top, toe cuts, earthquakes, or other triggers. The author suspects that if a procedure similar to that used in this present study were followed, similar correlations could be found for the acceleration of the reactivation of slides due to other triggers unrelated to changes in the groundwater system in a slide.
- Development of a new correlation for the movement behaviour of other types of sliding mechanisms than translational mechanisms. For example, circular sliding or flow slides could be studied.
- Complete risk analysis process for the blocks with relatively high probability of rapid movement and effect of different mitigation options on the risk to help decision makers on selecting appropriate mitigation option.

Appendix 1:

Effect of the Thompson River on the Stability of Earth Slides in Ashcroft Area (South Slide)[1]

A1.1. INTRODUCTION

The main lines of the Canadian National Railway (CN) and Canadian Pacific Railway (CPR) between Kamloops and Vancouver pass through the Thompson River Valley in south-central British Columbia, Canada. Ever since these lines were constructed, both companies have had problems related to the stability of the eleven large translational earth slides along 10 kilometres of their rail lines between the communities of Ashcroft and Spences Bridge (Figure A1.1). In order to analyze the risk imposed by possible rapid movement of these slides, geotechnical studies of the six most active earth slides have been carried out since the 1980s. Porter et al. (2002) and Keegan et al. (2003) presented their geotechnical findings for these landslides. More recently, Eshraghian et al. (2005a) showed that the Thompson River was the main trigger for these slides during their reactivation. The Thompson River is a large river with a five-million-hectare drainage basin upstream of the study area. The average flow, in a normal year, ranges from 230 m^3/second in January to a maximum of 2650 m^3/second in June when snow melt is most active.

---

[1] Published paper:

A version of this chapter has been published in the First North American Landslide Conference, June 2007, Vail, Colorado. Eshraghian, A., Martin, C.D., and Morgenstern, N.R., 2007. Effect of the Thompson River on stability of the South Slide, Ashcroft, British Columbia, Canada.

In this paper, the effect of the Thompson River on the stability of the South Slide is discussed. In particular, the effect of elevated river levels and river-erosion protection on this Slide's stability and movement rate are examined.

A1.2. GEOLOGY AND MOVEMENT HISTORY

Ryder (1976), Monger and McMillan (1989), and Johnsen and Brennand (2004) described this area's geology. Clague and Evans (2003) identified the general stratigraphy of the Quaternary sediments in the Thompson River Valley. The rupture surfaces of these earth slides followed highly plastic overconsolidated clay beds within 45 metres of clay-silt glaciolacustrine sediments. The clay beds in samples taken from the clay-silt sediment in the South Slide were between 1 cm and 40 cm thick, and the rupture surfaces were found to be generally within the thicker clay beds.

Like other slides in this area, the South Slide is moving on two rupture surfaces within the clay-silt glaciolacustrine deposit (Nachtigal 2004). The three scarps at the South Slide (Figure A1.2) suggest three main translational blocks moving on these two rupture surfaces. The toe block (block R-3) is moving on the shallower rupture surface, and the two larger blocks (R-1 and R-2) are moving on the deeper rupture surface (Figure A1.3). Since its most recent retrogression in 1881 (Porter et al. 2002), the South Slide has experienced reactivations including those in the winter of 1977 and in the fall of 1997 (Nachtigal 2004). The 1997 reactivation occurred after a flood which, air photos show, resulted in extensive river erosion and damage to a toe berm built between 1951 and 1971 for erosion protection (Nachtigal 2004). A scour hole had also formed in the Thompson River's bed below this slide as a result of continuous river down-cutting. During these reactivations, the smaller part of the toe, Block R-3, was moving faster than the other two blocks (Porter et al. 2002, Nachtigal

2004). Kosar et al.'s (2004) InSAR analysis showed slow movement in 1997 (rate between 16 mm/year and 1.6 m/year). After the 1997 reactivation, in 1998, the material lost during the 1997 flood was replaced and berm was extended. Since these repairs have been done, the rate of movement has decreased. Kosar et al.'s (2004) InSAR analysis showed extremely slow movement (slower than 16 mm/year) in 1999 and in 2001. The inclinometers at toe have recorded maximum movement rate of 4 mm/year since their installation in summer 2004.

A1.3. GROUNDWATER SYSTEM

A1.3.1. Piezometric Data

Four piezometers were installed in the South Slide in 1998 in boreholes P1 and P2 (Figure A1.3). A summary of the piezometric data is presented in Table A1.1. These data show upward gradients at the toe in both boreholes. The upper gradient is more apparent in borehole P2, which is nearest the toe, than in borehole P1, which is farther away from the toe. Also, piezometers P1-1 and P2-1 show a horizontal gradient. Therefore, these observations indicate that the South Slide toe is a discharge area. Moreover, the changes in the piezometric head during the period discussed in this paper indicate that the closer the piezometers are to the Thompson River, the more the head changes.

A1.3.2. Groundwater Modeling

The data from the piezometers installed in the South Slide boreholes reveal an approximate groundwater system, but a complete groundwater system and its change with the Thompson River level fluctuation was required to study the effect on the slide stability. Therefore, transient seepage analyses were conducted for the period from February 9, 1997 to December 6, 1997 (during the 1997 Thompson River flood).

A1.3.2.1. Procedure

The boundary conditions for the groundwater system analyses were defined according to the Thompson River level fluctuations, the rainfall infiltration on the slide crown terrace, and the rainfall infiltration on the slide slope. The average annual precipitation (mostly rainfall) in the Ashcroft area is 240 mm/year (Porter et al. 2002). The Thompson River level changes more than 6 m in a normal year; however, the Thompson River fluctuation in flood years can be up to 9 m.

In the first step toward a transient groundwater system analysis, the steady state seepage was modeled for the slide by using the 1997 Thomson River minimum level (Elev. 268.8 metres) at the beginning of the study cycle (on February 9, 1997). The steady state seepage was modeled by using constant precipitation on both the slope and the crown terrace. The infiltration on the crown terrace was assumed to be 8% of the mean annual precipitation, according to Chanasyk's (1986) suggestions for the infiltration of a slide 2 km north of the South Slide and composed of similar material. The infiltration on the slope was assumed to be less than the infiltration on the crown terrace, because of the slope angle and also because of the slope's slightly finer material. The infiltration on the slope was assumed to be 4.4×10^{-10} (m/sec) (5% of the mean annual precipitation), to match the piezometric head measurements.

After defining the boundary conditions, the material properties were estimated from the grain size analyses reported by Eshraghian et al. (2005b) and from similar materials reported in the literature (Table A1.2). The selected values of the hydraulic conductivities were adjusted during the steady state seepage analysis to match the predicted heads with the heads measured by the piezometers when the Thompson River was at its minimum level. Because the materials are laminated and also disturbed by slide activity, the ratio of the vertical to the horizontal hydraulic conductivity (k_v/k_h) was assumed to be 0.5. In their groundwater analyses, Pauls et al.

(1999) and Kelly et al. (1995) used a k_v/k_h between 0.2 and 0.5 for the laminated sediments within disturbed material in a landslide. The hydraulic conductivity as a function of the suction for the soil units was defined according to that of similar material reported in the literature.

In the second step of the groundwater system analysis, the steady state seepage analysis results for the Thompson River minimum level were used as the starting point for the transient seepage analysis for the river level's fluctuation cycle. In the transient analyses, a variable head boundary function was used to model the Thompson River level fluctuation at the slide toe. The material hydraulic conductivity was assumed to be the same as the material hydraulic conductivities used in the steady state seepage analysis, and the soil storage functions were defined according to the material data base in the literature. After the transient analyses, the result was compared with the measured responses of the installed piezometers, and the material soil storage functions were adjusted to reach the best agreement between the model response and the piezometric data.

A1.3.2.2. Result

The South Slide modeled groundwater system with the Thompson River at its minimum level (Elev. 268.8 m on February 9) and maximum level (Elev. 274.3 m on June 9) in 1997 is shown in Figure A1.4. This figure demonstrates the groundwater system changes within the slide's 150-metre toe due to the Thompson River level fluctuations. The modeled piezometric elevation responses to the Thompson River level fluctuations are shown in Figure A1.5. The modeled elevation heads of piezometers P2-1 and P2-2 show more response to the river level fluctuation and more upward gradient at the toe. The modeled elevation heads of piezometers P1-1 and P1-2 show higher elevation heads, but less change with the Thompson River level fluctuations. The maximum modeled elevation heads at the locations of piezometers 1 and 2 in borehole P1 were Elev. 289.3 m and Elev. 290.3 m, and the modeled elevation head at piezometer 1 in borehole P2 was Elev. 276.2 (m). These results are in average 0.55 m above the maximum piezometric elevation measured during the record period (Table A1.1). A sensitivity analysis of stability of the blocks in the South Slide showed no change in general behavior of the stability graphs with minimum change in factor of safety of main block (R-1) (less than 1 %) and maximum change in factor of safety of shallow toe block (R-3) (2.5 %). Therefore, the groundwater modeling considered reasonably accurate for the purpose of this study.

A1.4. STABILITY ANALYSES

After completing the groundwater system analyses, the stability of the three main reactivation blocks (Figure A1.3) was analyzed by using the Thompson River level changes in 20-day intervals for the river level's 1997 fluctuation cycle. In order to assess the effect of the toe erosion damage repair after the 1997 reactivation, the stability of the South Slide in 2002 was analyzed after conducting similar groundwater system analyses for the river level's fluctuation cycle in 2002.

A1.4.1. Procedure

The result of the groundwater system modeling by using transient seepage analysis was used for modeling the South Slide stability in 1997. The surface topography was reproduced from a 2-metre by 2-metre mesh of the Light Detecting and Ranging (LiDAR) data recorded in 2003, which had a vertical resolution of ± 0.2 metres. After reviewing aerial photos of the slide prior to and after 1997, it was concluded that this LiDAR data provided the best estimate of the topography but that the profile needed to be shortened by 4 metres to represent the 1997 conditions because of 4 metres toe erosion during the 1997 flood repaired later by the time LiDAR data was recorded in 2003. Therefore, the LiDAR 2003 data were used for estimating the slide topography in 1997, but with a profile 4 metres shorter than its length in 2003 to account for erosion in 1997 and the previous years. The material properties were estimated from a series of index property tests and direct shear tests on the clay beds and silt beds in the clay-silt unit within the slide's body (Table A1.3).

These material properties were used with the Morgenstern and Price (1965) method of slices for calculating the South Slide block factors of safety at different stages of the river level in 1997. At each stage, the change of the river's supporting force at the toe was modeled by using an equivalent pressure on the river bank, and the groundwater system was imported from the transient seepage at that stage. Therefore, the changes in the block factors of safety were caused by changing the pore pressure in the slide mass and changing the Thompson River's supporting load at the slide toe.

After the 1997 reactivation, the material eroded by the river at the toe was replaced by new material, and the toe berm (Figure A1.2) was repaired. The same process for groundwater modeling and stability modeling was followed to investigate the Thompson River's effect on the South Slide stability in 2002. The 2002 slide topography was defined from the 2003 LiDAR data. These analyses provided a methodology for assessing the effect of the South Slide's erosion protection on stability.

In order to investigate the possibility of more main scarp retrogression on the current rupture surface, a new retrogressed block in the undisturbed material was assumed to have formed (Figure A1.3). The movement of the retrogression block was assumed to be on the current deeper rupture surface, which would likely grow from its current scarp. The materials in the new part of the developed rupture surface were assumed to be undisturbed; therefore, the peak parameters (Table A1.3) were used in the stability analyses for this portion of the rupture surface while the residual parameters were used for the rest of the "old" rupture surface length.

A1.4.2. Results

Figure A1.6 shows the results of the South Slide stability analyses for the Thompson River 1997 and 2002 level fluctuations. The factor of safety of all blocks changes with the Thompson River level changes, but these changes in the factor of safety are greater for the toe shallow block (block R-3). While the deep blocks (blocks R-1 and R-2) had a factor of safety above 1.1 in 1997 and 2002, the toe block (block R-3, Figure A1.3) factor of safety in 1997 dropped below unity, and in 2002 was close to unity. These findings explain the South Slide's 1997 faster reactivation movement on the shallower rupture surface at the toe.

The result of the stability analysis for the retrogression block showed a minimum factor of safety of 1.15 with the Thompson River level fluctuations in 1997.

A1.5. DISCUSSION

The large fluctuations of the Thompson River level had two significant effects on the South Slide: (1) the groundwater system within the slides caused pore pressure changes on the rupture surface, and (2) river bank erosion. Both of these effects influenced slide stability.

The groundwater system model shows that the Thompson River level fluctuations change the equipotential lines within 150 metres of the slide toe (Figure A1.4) and the stability analyses (Figure A1.6) show significant changes in the toe block's factor of safety with the Thompson River fluctuations. This change in factor of safety is due to the greater changes in the pore pressure on the slide rupture surfaces in the vicinity of the toe. The change in the pore pressure on the rupture surfaces may bring a marginally stable block to an unstable state. For example, while block R-3 was marginally stable in spring 2002, the pore pressure increases reduced the factor of safety to unity in the summer of that year which caused the extremely slow movement of this block (4 mm/year). Therefore, as long as the river flows do not erode the toe material, the slow reactivation is likely related to the pore pressure increase and the delay in the pore pressure decreasing after the river level reaches its peak and begins to drop, creating a drawdown mechanism.

In 1997, the South Slide toe erosion protection berm was damaged by the Thompson River flood. This erosion resulted in the 1997 reactivation of the slide on its two rupture surfaces with a higher rate of movement on the shallower rupture surface (slow movement, estimated by using Kosar et al.'s (2003) InSAR map). The stability analyses of the toe block (R-3, Figure A1.3) for the 1997 and 2002 slide geometries (Figure A1.6) show that block R-3's starting factor of safety in 1997 and 2002 was 1.01 and 1.03, respectively. The Thompson River minimum levels in 1997 and 2002 were similar; therefore, this 2% improvement in the factor of safety in 2002 is likely due to repair of the 1997 river erosion (4 m).

The analyses showed that the decrease in the South Slide stability due to four metres of toe erosion in 1997 was similar to the decrease caused by the change in the pore pressure on the rupture surface due to the Thompson River drawdown (both decreased the factor of safety by 2%). Eshraghian et al. (2005b) showed that slide reactivation caused by a drawdown mechanism accelerates at the beginning of the drawdown. In contrast, the South Slide fall 1997 reactivation accelerated at the end of the river drop when the flood-induced toe erosion reached a maximum. Therefore, the river erosion was likely the major trigger to the 1997 South Slide reactivation. Figure A1.7 shows the possible change in toe block R-3 factor of safety during 1997 flood event. The block R-3 factor of safety probably changed from no-erosion factor of safety line to full erosion factor of safety line after erosion at the time of maximum Thompson River level in 1997 which caused overflow on top of the berms damage to the berms and then erosion at the slide toe.

A1.6. CONCLUSIONS

The South Slide 1997 reactivation was triggered by toe erosion caused by the Thompson River. Erosion protection and repair of the eroded parts after the 1997 reactivation have improved stability but have not fully stopped the reactivation of the shallow block at the toe. These new extremely slow reactivations are also affected by the drawdown-like mechanism caused by the Thompson River after periods of elevated water levels. The analyses indicate that a rapid retrogression of the South Slide is unlikely to occur with an effective toe erosion protection system in place.

This study of the South Slide, as an example of the translational slide stability in the Ashcroft area, shows that the Thompson River affects the stability of the slide blocks by changing the pore pressure on the rupture surfaces as the river level fluctuates and by altering the slide geometry due to river bank erosion. The South Slide seepage analyses show that the river level fluctuations mainly change the groundwater system and the pore pressures within approximately 150 metres of the slide toe. The rate of slide movement appears very sensitive to small changes in factor of safety caused by these boundary changes in the vicinity of the toe of the slide.

A1.7. REFERENCES

Chanasyk, D.S. 1986. Goddard landslide of September, 1982, summary of the opinion of David S. Chanasyk. Report prepared for court between Canadian Pacific Railway Limited and Highland Valley Cattle Company Limited. Supreme Court of British Columbia.

Clague, J.J., and Evans, S.G. 2003. Geological framework of large historic landslides in Thompson River Valley, British Columbia. Environmental and Engineering Geoscience, **9**: 201-212.

Eshraghian, A., Martin, C.D., and Cruden, D.M. 2005a. Landslides in the Thompson River Valley between Ashcroft and Spences Bridge, British Columbia. In Proceedings of the International Conference on Landslide Risk Management. Vancouver, Canada. May 31 to June 4, 2005, pp. 437-446.

Eshraghian, A., Martin, C.D., and Cruden, D.M. 2005b. Earth slide movements in the Thompson River Valley, Ashcroft, British Columbia. In CD-ROM Proceedings of the 58th Canadian Geotechnical Conference. Saskatoon, Saskatchewan, Canada. September 18-21, 2005.

Johensen, T.F., and Brennand, T.A. 2004. Late-glacial lakes in the Thompson Basin, British Columbia: paleogeolography and evolution. Canadian Journal of Earth Science, **41**: 1367-1383.

Keegan, T., Abbot, B., Cruden, D., Bruce, L., and Pritchard, M. 2003. Railway ground hazard risk scenario: River erosion: Earth-slide. In Proceedings of the 3rd Canadian Conference on Geotechnique and Natural Hazards. Edmonton, Alberta. 9-10 June, 2003. Canadian Geotechnical Society, pp. 269-277.

Kelly, A.J., Sauer, E.K., Christiansen, E.A., Barbour, S.L., and Widger, R.A. 1995. Deformation of the Deer Creek bridge by an active landslide in clay shale. Canadian Geotechnical Journal, **32**: 701-724.

Kosar, K., Rerering, K., Keegan, T., Black, K., and Stewart, L. 2003. Use of spaceborne InSAR to characterize ground movements along a rail corridor and open pit mine. In Proceedings of the 3rd Canadian Conference on Geotechnique and Natural Hazards. Edmonton, Alberta. Canadian Geotechnical Society, 177-184.

Monger, J.W.H., and McMillan, W.J. 1989. Geology, Ashcroft, British Columbia. Geological Survey of Canada.

Nachtigal, B.J. 2004. Thomson 52.80 west-cap geotechnical investigations. Report to Canadian Pacific Railway, Calgary, Alberta. Bruce Geotechnical Consultants Inc., Kamloops, British Columbia.

Pauls, G.J., Sauer, E.K., Christiansen, E.A., and Widger, R.A. 1999. A transient analysis of slope stability following drawdown after flooding of a highly plastic clay. Canadian Geotechnical Journal, **36**: 1151-1171.

Porter, M.J., Savigny, K.W., Keegan, T.R., Bunce, C.M., and Mackay, C. 2002. Controls on stability of the Thompson River landslides. In Proceedings of the 55th Canadian Geotechnical Conference: Ground and Water: Theory to Practice. Edited by D. Stolle, A.R. Piggott, and J.J. Crowder. Niagara Falls, Ontario. 20-23 October, 2002. Canadian Geotechnical Society, pp. 1393-1400.

Ryder, J.M. 1976. Terrain inventory and Quaternary geology, Ashcroft, British Columbia. Geological Survey of Canada, Ottawa.

Table A1.1 Summary of piezometric elevation data from piezometers installed in South Slide.

Borehole	Piezometer	Tip Elevation (m)	Minimum Elev. Head (m)	Maximum Elev. Head (m)	Change in Elev. Head (m)
P1	P1-1	272.7	286.7	288.7	2.0
	P1-2	262.7	288.2	289.7	1.5
P2	P2-1	271.7	272.0	275.7	3.7
	P2-2	248.7	276.7	279.2	2.5

Table A1.2 Material properties were used in groundwater modeling of South Slide.

Material	K_{sat} (cm/sec)
Fluvial sand and gravel at head terrace	6.75×10^{-4}
Glacial Till	9.26×10^{-4}
Glaciolacustrine Silt and Sand	8.1×10^{-6}
Glaciolacustrine Clay-Silt	6.94×10^{-7}
Glaciofluvial Sand and Gravel	3.47×10^{-4}
Fluvial sand and gravel (toe)	1.85×10^{-3}

Table A1.3 Residual and peak properties of material on the South Slide rupture surfaces.

State	Sand and Silt		Clay-Silt		Till		Fluvial	Berm
	φ′ (°)	c′ (kPa)	φ′ (°)	c′ (kPa)	φ′ (°)	c′ (kPa)	φ′ (°)	φ′ (°)
Residual	22	0	12	0	26	0	13	30
Peak	24	25	16	12	26	50	NA	NA

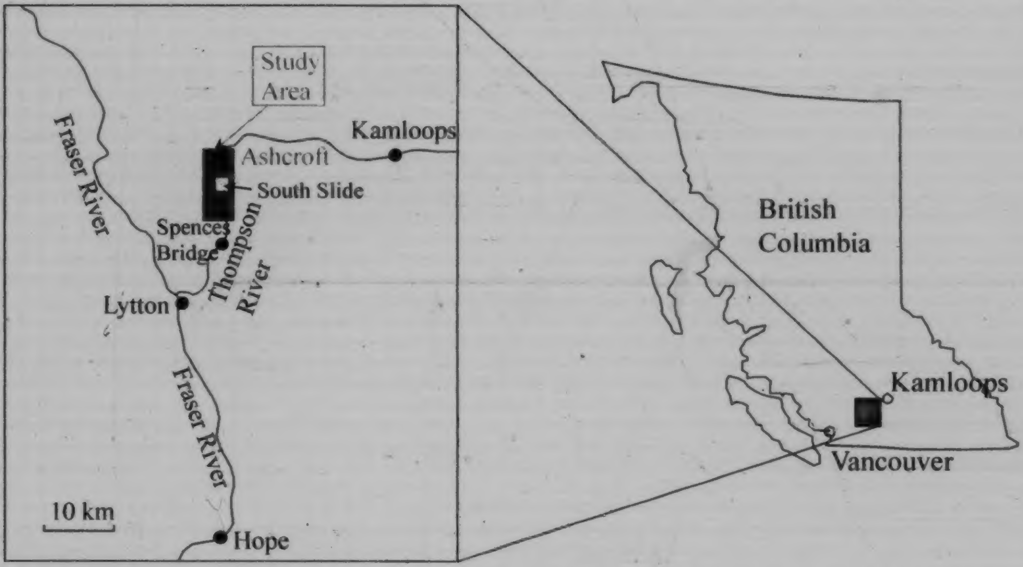
Study Area
Kamloops
Ashcroft
South Slide
Fraser River
Spences Bridge
Thompson River
Lytton
Fraser River
10 km
Hope
British Columbia
Kamloops
Vancouver

Figure A1.1 Study area south of Ashcroft, BC, between 50° 10′ to 50° 20′ N and 121° 15′ to 121° 20′ W.

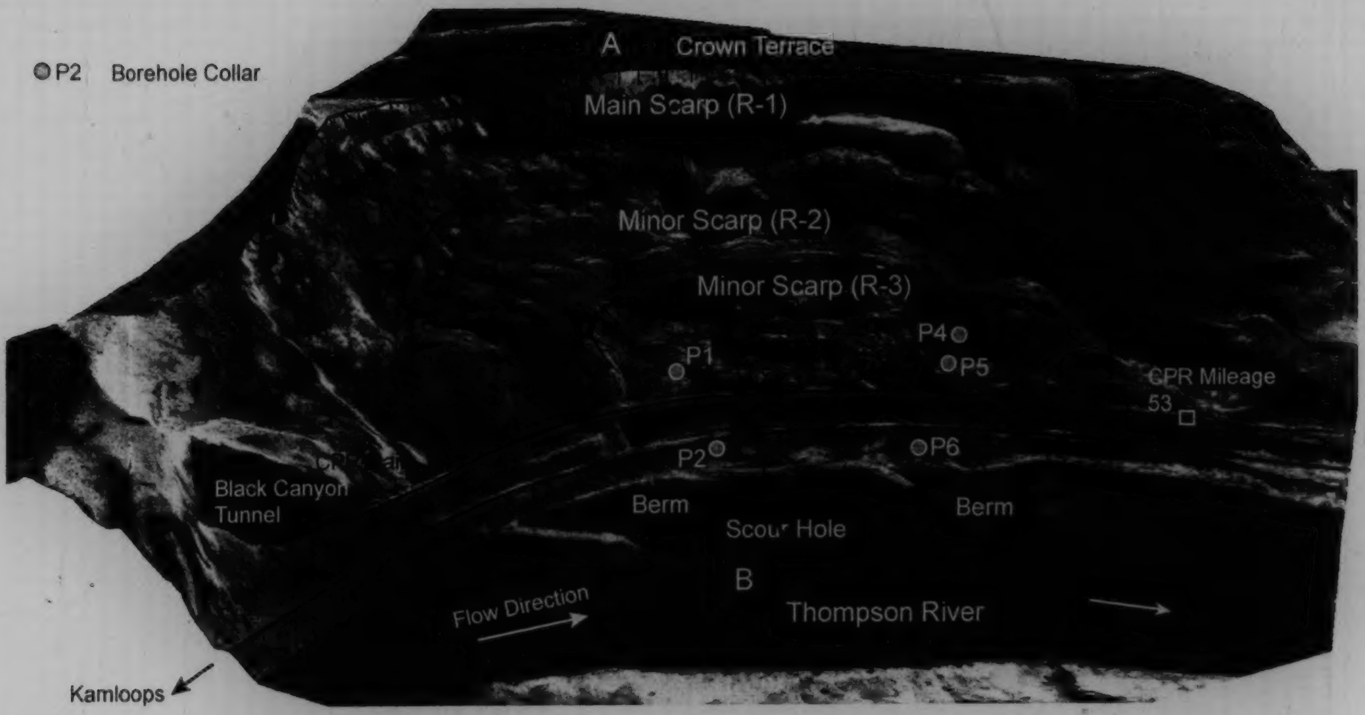
P2 Borehole Collar
A
Crown Terrace
Main Scarp (R-1)
Minor Scarp (R-2)
Minor Scarp (R-3)
P1
P4
P5
CPR Mileage
53
P2
P6
Black Canyon
Tunnel
Berm
Scour Hole
Berm
B
Flow Direction
Thompson River
Kamloops

Figure A1.2 A 3-dimensional view of the South Slide with its three scraps, scour hole at the Thompson River bed, borehole locations, and cross-section line. The slide is 600 metres wide at the river level.

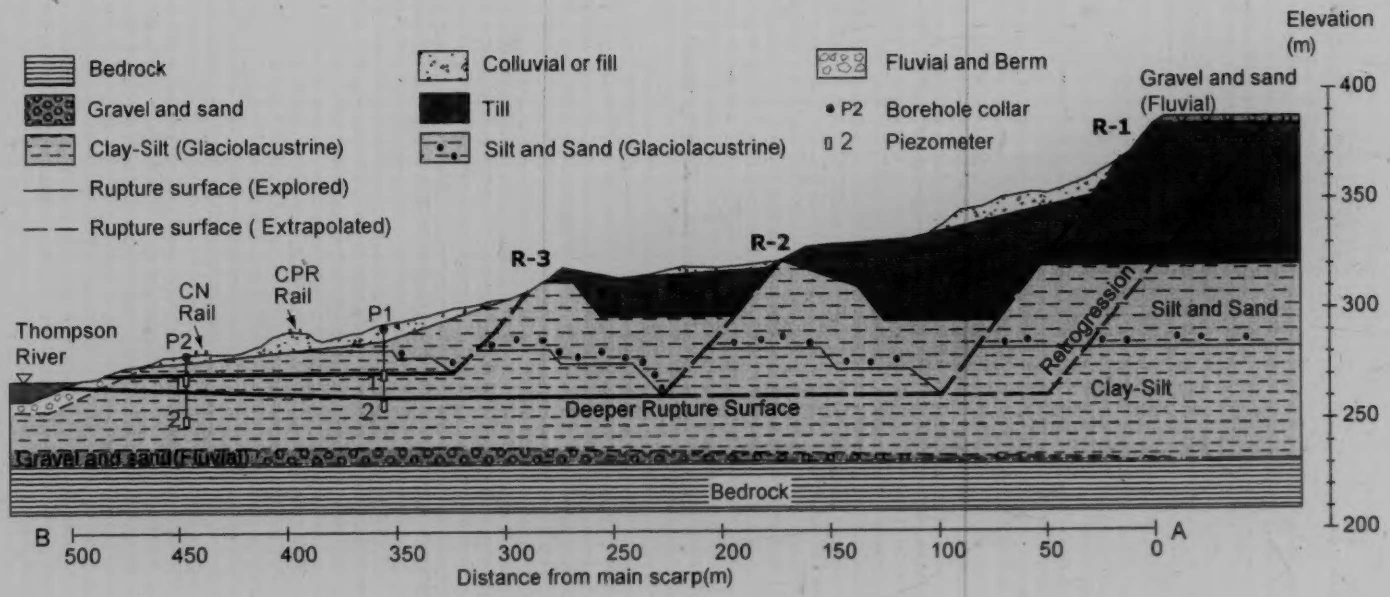
Bedrock
Gravel and sand
Clay-Silt (Glaciolacustrine)
Rupture surface (Explored)
Rupture surface (Extrapolated)
Colluvial or fill
Till
Silt and Sand (Glaciolacustrine)
Fluvial and Berm
• P2 Borehole collar
▯ 2 Piezometer
Elevation (m)
Gravel and sand (Fluvial)
R-1
R-2
R-3
Thompson River
CN Rail
CPR Rail
P1
P2
Retrogression
Silt and Sand
Clay-Silt
Deeper Rupture Surface
Gravel and sand (Fluvial)
Bedrock
B
A
500
450
400
350
300
250
200
150
100
50
0
Distance from main scarp(m)
400
350
300
250
200

Figure A1.3 South Slide's cross section with its three translational blocks, possible future retrogression, and piezometer locations.

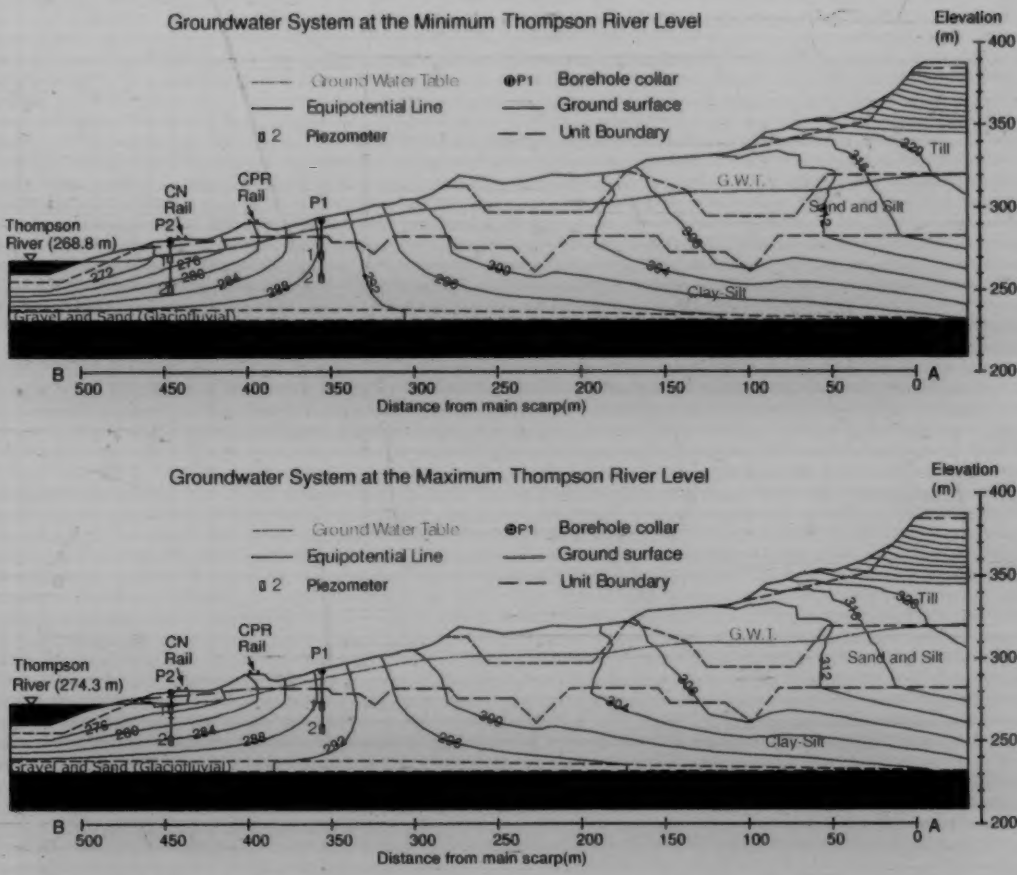
Groundwater System at the Minimum Thompson River Level
Ground Water Table
Equipotential Line
Piezometer
Borehole collar
Ground surface
Unit Boundary
Elevation (m)
Thompson River (268.8 m)
CN Rail
CPR Rail
P1
P2
G.W.T.
Till
Sand and Silt
Clay-Silt
Gravel and Sand (Glaciofluvial)
272
276
280
284
288
292
296
300
304
308
316
320
B
A
500
450
400
350
300
250
200
150
100
50
0
Distance from main scarp(m)
400
350
300
250
200
Groundwater System at the Maximum Thompson River Level
Thompson River (274.3 m)
312

Figure A1.4 Modeled groundwater system for the maximum and minimum Thompson River level in 1997.

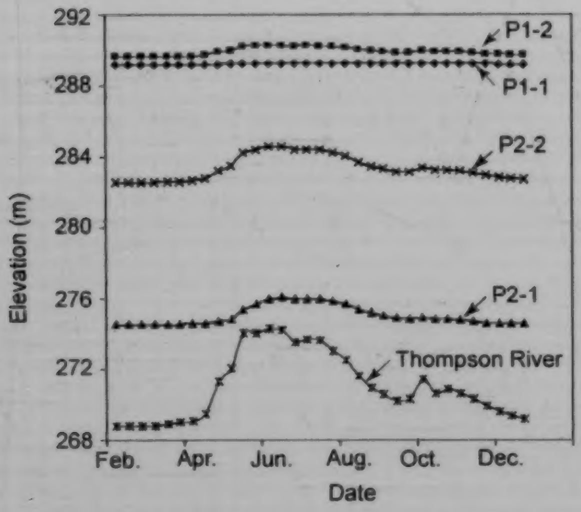

Figure A1.5 Modeled piezometer responses to the Thompson River level fluctuation in 1997.

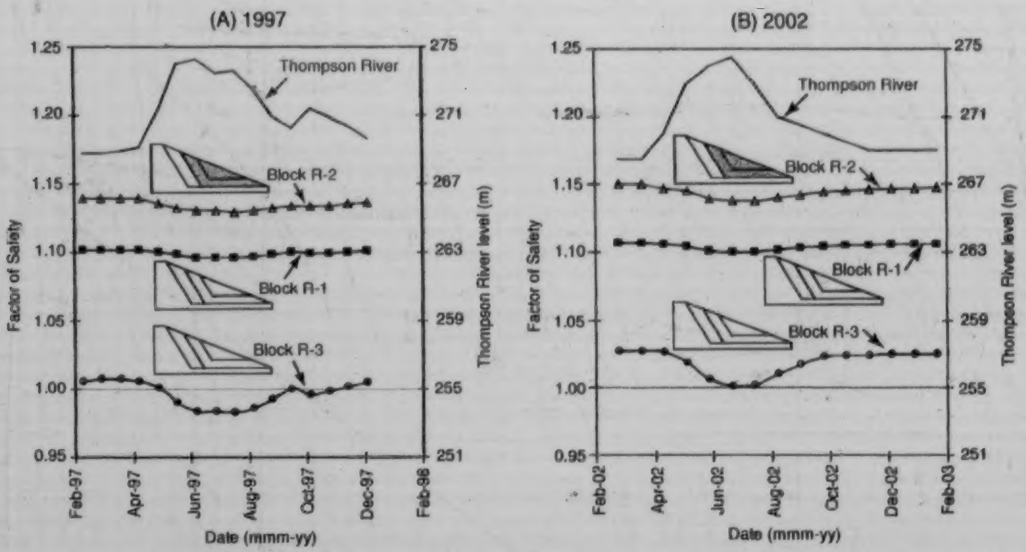

Figure A1.6 Stability of the South Slide in (A) 1997 after erosion took place and before repairing the toe berm protection and the eroded part (B) 2002 after repairing the toe berm protection and the eroded part.

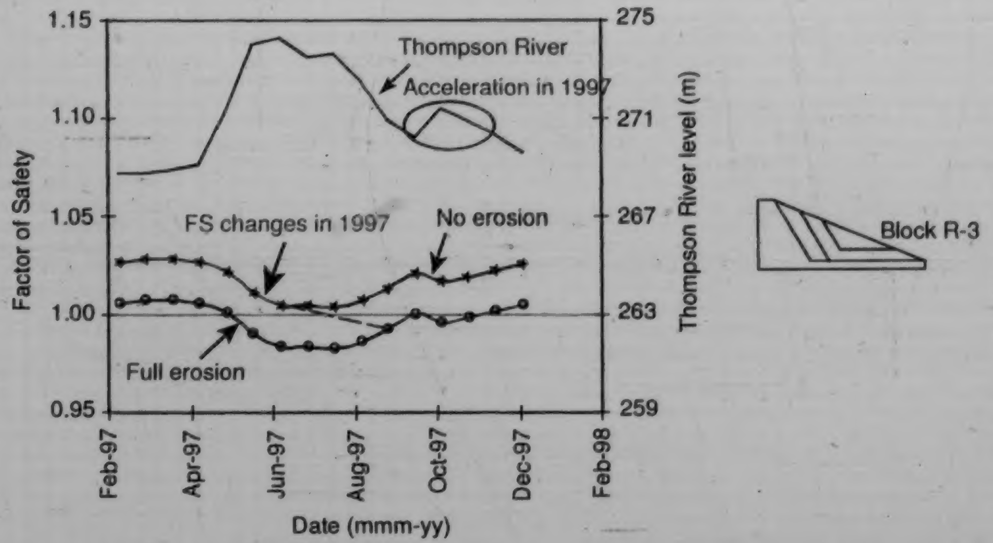

Figure A1.7 Change of Factor of Safety for toe block R-3 during the 1997 flood event.

Appendix 2: Cross Sections of the Earth Slides in Ashcroft Area

---

A2.1. INTRODUCTION

To continue the study of earth slides in the Ashcroft area, complete cross sections of these slides were essential. The ground surface was determined from a Digital Terrain Model (DTM) produced by using Light Detection and Ranging (LiDAR) data collected in 2003 with a resolution of ±0.2 m. Boreholes have been drilled in Slide CN50.9, Goddard Slide, North Slide, South Slide, and Basque Slide sites, mainly at the toes of these slides. With only this information available, producing an accurate cross section for each slide was impeded by lack of information about the strtigraphy within the displaced material, because the boreholes were located either at the toes of the slides or too far from each other to give a clear picture of a slide's cross section.

A2.2. PROCESS

The ground surface was produced from LiDAR data by using a 2-by-2-metre mesh. The comparison of the Triangular Irregular Network (TIN) produced from this data with some of the control points (Boreholes collars) showed accuracy in the order of 0.2 metre. This accuracy seemed satisfactory for estimating the ground surfaces of landslides. The LiDAR data were used for making a ground surface TIN in a Geological Information System (GIS) program (ArcGIS9, http://www.esri.com). This TIN was later used for making a ground surface DTM in the Surpac program (Surpac Minex, http://www.surpac.com). Figure A2.1 shows a sample of the DTM produced in Surpac (in this case, the Basque slide).

The borehole information and locations were entered into GIS program and later entered into the Surpac files for each slide. Then, for each studied slide, one or two cross sections were produced in the Surpac program.

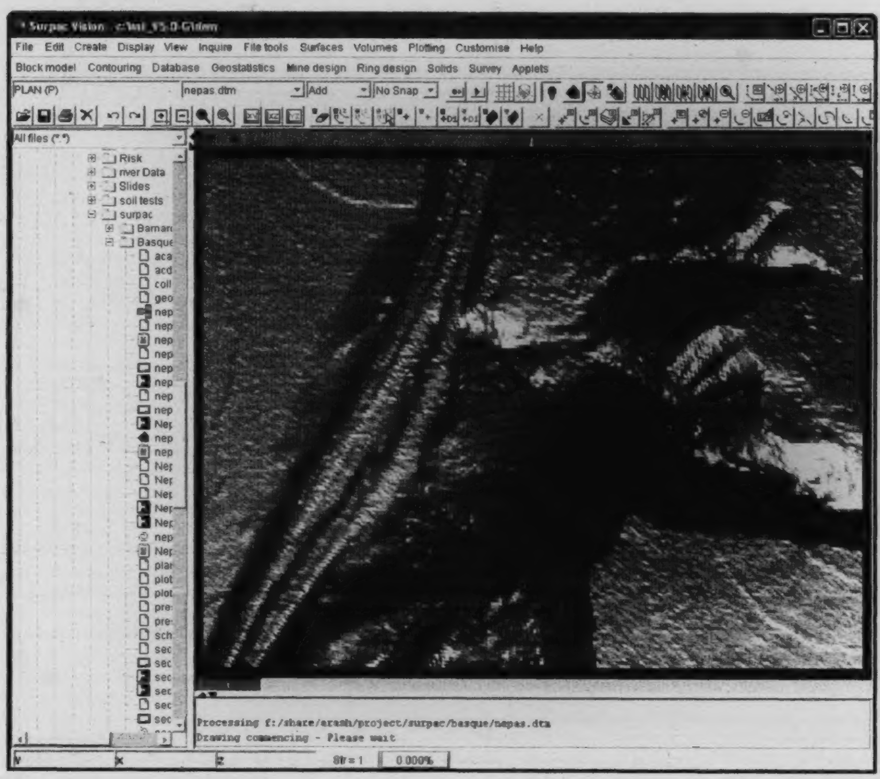
Surpac Vision c:\ssi_V5-0-G\dem
File
Edit
Create
Display
View
Inquire
File tools
Surfaces
Volumes
Plotting
Customise
Help
Block model
Contouring
Database
Geostatistics
Mine design
Ring design
Solids
Survey
Applets
PLAN (P)
nepas.dtm
Add
No Snap
All files (*.*)
Risk
river Data
Slides
soil tests
surpac
Barnar
Basque
Str = 1
0.000%

```
Processing f:/share/arash/project/surpac/basque/nepas.dtm
Drawing commencing - Please wait
```

Figure A2.1 Sample ground surface DTM made in Surpac program (north of Basque Slide).

The cross sections produced in Surpac were saved as Auto plot files (dxf files). This process provided plot files containing ground surface and borehole information (soil layers). Then these files were ready for further processing by the AutoCAD (AutoCAD 2002) program. In AutoCAD, based on the borehole information, the stratigraphy was completed as much as possible. Unfortunately, most of the boreholes are located near the toes of slides and not spread over the whole slide area to give complete information on stratigraphy in the cross sections. Therefore, some assumptions had to be made, and more processing had to be carried out to estimate the stratigraphy within the cross sections.

First, the portion of the unit boundaries in the slides before sliding was estimated. For the units at a higher elevation than that of the shear zones, it was assumed that this position was similar to what was currently visible in the terraces above the slide. Not enough boreholes are present in the upper-level terraces to give the stratification boundaries, but by using the geological evidence presented in previous work (Clague and Evans 2003), the stratigraphy of the sediment fill in Thompson River Valley at Ashcroft could be estimated. Figure A2.2 shows the general stratigraphy of the sediments in the study area. The elevations of the layers' boundaries differ for each slide because of the general elevation decrease from north to south and also because of unconformities, but the sequence is the same. The positions of the undisturbed material in the local geological succession, bedrock, and unit 1 were estimated mainly from borehole information. Whenever the boreholes did not encounter bedrock or unit 1, an elevation was assumed from the nearest slide with adequate borehole information or from the geology of the area. The elevations of the layers higher than rupture surfaces were estimated mainly from the outcrops seen in different locations in the area and by considering the general tilting of the layers from north to south. The end result was stratigraphy in high terraces or the slide body before sliding. Figure A2.3 shows the layers in terraces above the landslides and the location of rupture surfaces in unit 2. The contact elevation between layers decreases from north to south (Figure A2.3).

Because of the slide body's movement, the elevation of the materials encountered in boreholes above the rupture surface changed during sliding. Therefore, directly using this information to estimate the stratigraphy in the rest of the displaced material was not possible. Instead, it was more reasonable to use this information to model the sliding process and to use this sliding model to estimate the complete stratigraphy within the displaced material.

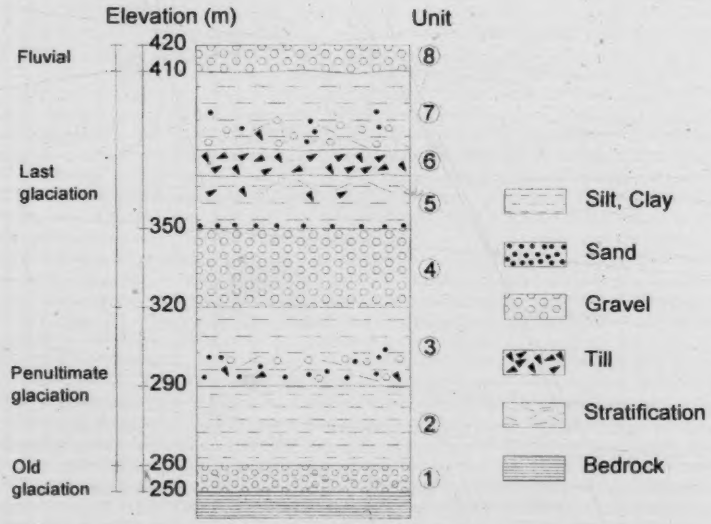
Elevation (m)
Unit
Fluvial
Last glaciation
Penultimate glaciation
Old glaciation
420
410
350
320
290
260
250
⑧
⑦
⑥
⑤
④
③
②
①
Silt, Clay
Sand
Gravel
Till
Stratification
Bedrock

Figure A2.2 Stratigraphy of sediment fill units in Thompson River Valley at Ashcroft and their approximate elevations.

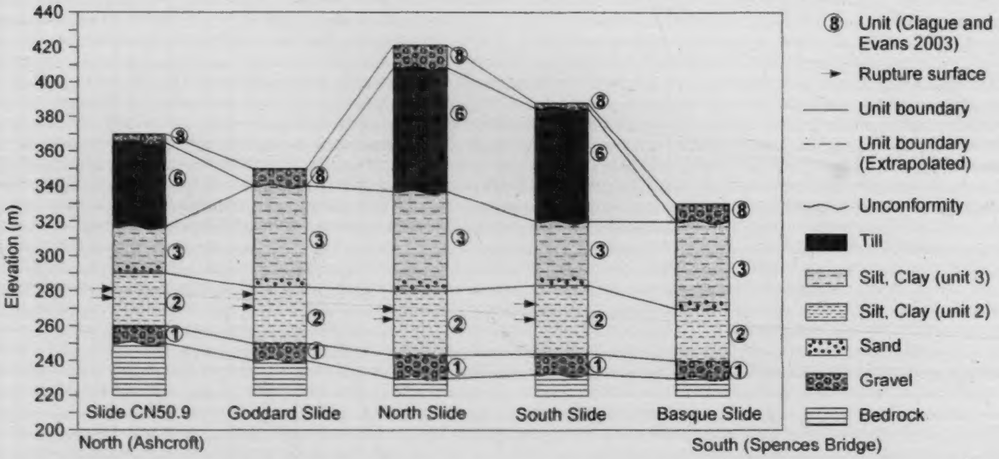

Figure A2.3 Geological units in the earth slides and highland terraces in Ashcroft area (the horizontal distance is not to scale).

Modeling the sliding process required assumptions to be made about the pre-slide situation. As mentioned before, the soil stratigraphy in the terraces can be found from geology, borehole information, site visits, and air photos. The next step was to define the pre-slide ground surface. As we know, during sliding, the displaced material's volume sometimes increases by as much as thirty percent. On the other hand, the Thompson River probably removed most of this displaced material by erosion. Therefore, it was assumed that the area of the pre-slide cross section was between 0 to 20 percent larger than the current cross-section area. Also, it was assumed that the sliding started when the pre-slide ground surface slope was higher than the residual friction angle of the material on the rupture surface and, perhaps, was near to the slope angles of adjacent slopes. With these assumptions, the ground surface and stratigraphy for each slide at the pre-slide stage could be estimated.

The next step in modeling the sliding process was modeling the retrogressions. The number of retrogressions was considered to be equal to the number of scarps in the displaced material. More retrogression might occur in the slides, but the materials were removed from the slide sites by erosion and, therefore, did not affect our modeling. Dormant scarps are detected from site visits, photos, aerial photographs, and also from sudden changes in the slope on the cross-section ground surface. To reconstruct each retrogression on the pre-slide ground, the distances had to be increased during the sliding process because of material dilation. As the slides are mainly translation of slides, blocks directly located on horizontal rupture surfaces have only horizontal movements, but the blocks located on scarps may have both horizontal and vertical movements. The amount of movement could be estimated by the blocks' vertical movements required to reach the current elevation. This process pushes other blocks out toward the river. Later, the river erodes the extra material at the toe. This river erosion and the surface erosion processes change the slide's ground surface, which at the end should be similar to the current ground surface. The end result of the modeling of the retrogression was the current cross section with soil stratigraphy.

Wherever boreholes were available, the validity of the assumptions was checked by comparing the model's results and the borehole information. This comparison shows the assumptions' accuracy. Perhaps drilling boreholes in the terraces and the main bodies of the slides, in the gaps between boreholes, could provide more verification for the general stratigraphy assumptions.

A2.3. ASHCROFT AREA SLIDES' CROSS SECTIONS

A2.3.1. Slide CN50.9

During the previous retrogressions of Slide CN50.9, the river removed most of the displaced material, so, to account for this material loss, the pre-slide volume was assumed to be more than the current volume. The pre-slide cross-section area was assumed to be 15% larger than the current cross-section area. The pre-slide ground surface slope was assumed from the adjacent slopes. Figure A2.4 shows the cross-section location within Slide CN50.9. Figure A2.5 shows the pre-slide slope in Slide CN50.9. The existence of unit 4 (the gravel unit) under unit 6 in the pre-slide stratification is uncertain.

It was assumed that the current situation was the result of two main retrogressions of the main scarp; each could be the result of more than one sliding. The blocks were assumed from evidence on the ground, suggesting the boundaries of the blocks.

The results of the first and second series of sliding are shown in Figures A1.6 and A1.7. The height of the upper block was calculated according to the amount of vertical movement required for the block to reach to the current level. The same process was used for finding the next sliding stage, which is shown in Figure A2.8. As the ground surface shows the last block is tilted slightly. This finding suggests the back part of the main scarp should be slightly curved.

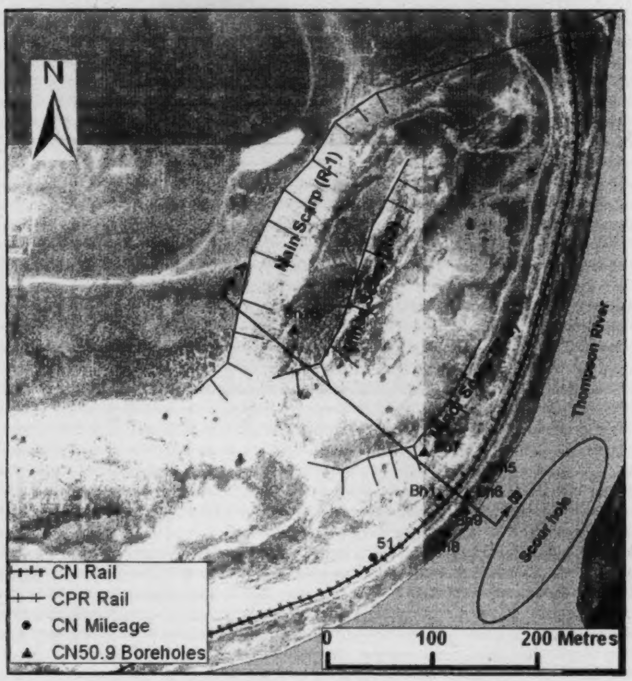
N
Main Scarp (R-1)
Thompson River
Bh1
51
Scour hole
CN Rail
CPR Rail
CN Mileage
CN50.9 Boreholes
0
100
200 Metres

Figure A2.4 A plan view of Slide CN50.9 with cross-section and boreholes locations.

The general shape of the block surfaces after the last retrogression (Figure A2.8) is in agreement with the current ground surface. The extra material at the toe was removed by river erosion. Also, some surficial erosion process has adjusted the ground surface (see Figure A2.9). Figure A2.10 presents the current stratification.

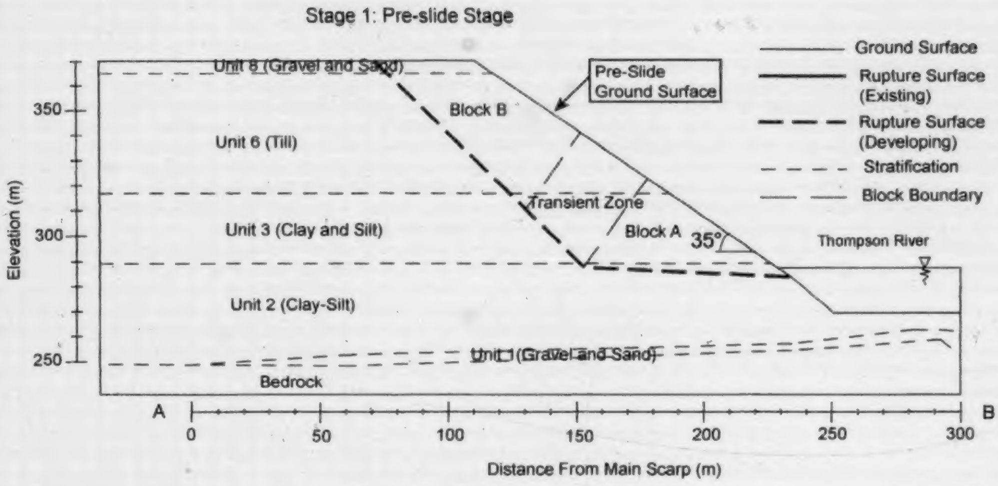
Stage 1: Pre-slide Stage
Ground Surface
Rupture Surface (Existing)
Rupture Surface (Developing)
Stratification
Block Boundary
Unit 8 (Gravel and Sand)
Pre-Slide Ground Surface
Block B
Unit 6 (Till)
Transient Zone
Unit 3 (Clay and Silt)
Block A
35°
Thompson River
Unit 2 (Clay-Silt)
Unit 1 (Gravel and Sand)
Bedrock
Elevation (m)
350
300
250
A
B
0
50
100
150
200
250
300
Distance From Main Scarp (m)

Figure A2.5 Pre-slide stage in Slide CN50.9, Ashcroft area.

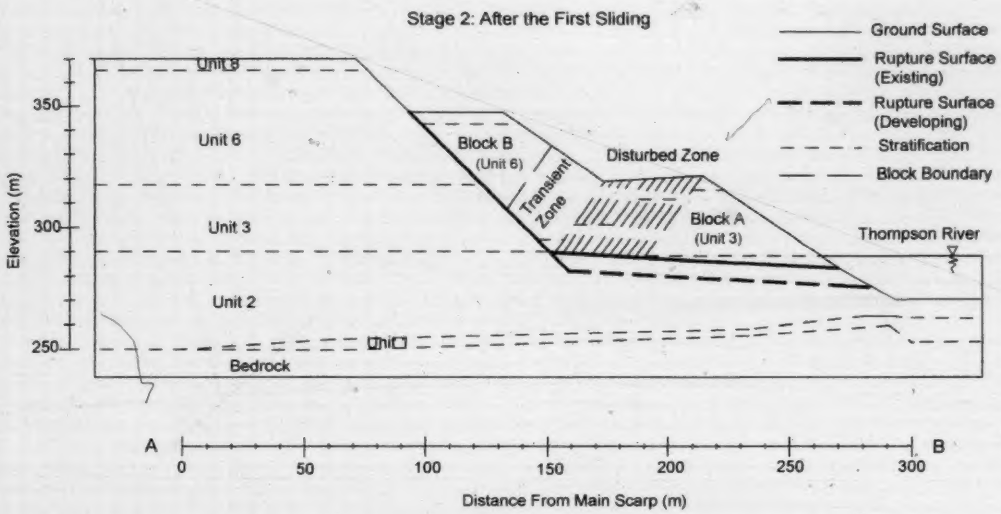
Stage 2: After the First Sliding
Ground Surface
Rupture Surface (Existing)
Rupture Surface (Developing)
Stratification
Block Boundary
Unit 8
Unit 6
Block B (Unit 6)
Disturbed Zone
Transient Zone
Block A (Unit 3)
Unit 3
Thompson River
Unit 2
Unit 1
Bedrock
Elevation (m)
350
300
250
A
B
0
50
100
150
200
250
300
Distance From Main Scarp (m)

Figure A2.6 Slide CN50.9 after first retrogression on shallower rupture surface.

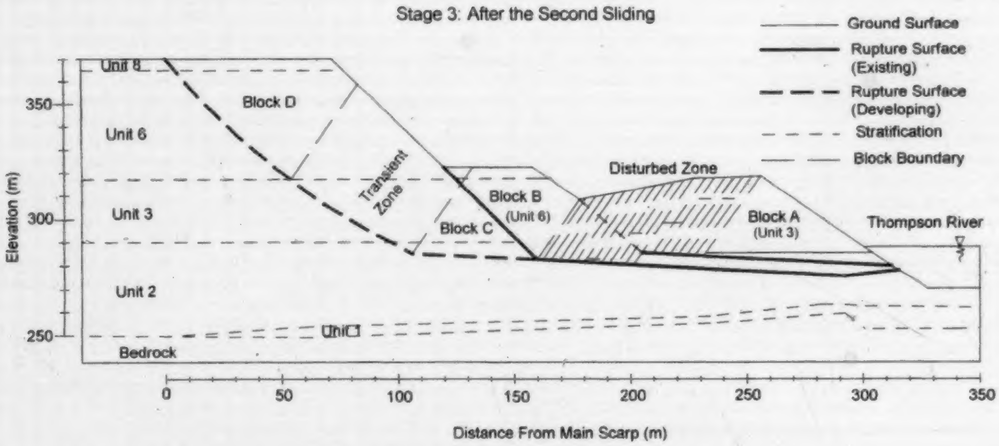
Stage 3: After the Second Sliding
Ground Surface
Rupture Surface (Existing)
Rupture Surface (Developing)
Stratification
Block Boundary
Unit 8
Unit 6
Unit 3
Unit 2
Unit 1
Bedrock
Block D
Transient Zone
Block C
Block B (Unit 6)
Disturbed Zone
Block A (Unit 3)
Thompson River
Elevation (m)
350
300
250
0
50
100
150
200
250
300
350
Distance From Main Scarp (m)

Figure A2.7 Slide CN50.9 after first sliding on deeper rupture surface.

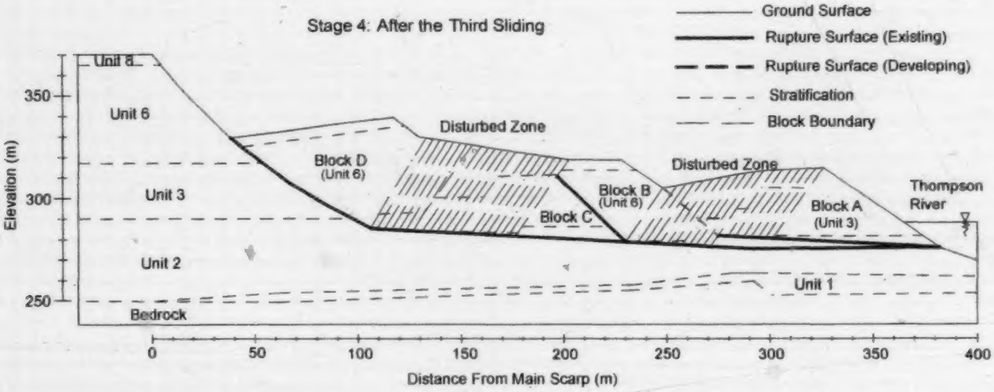
Stage 4: After the Third Sliding
Ground Surface
Rupture Surface (Existing)
Rupture Surface (Developing)
Stratification
Block Boundary
Unit 8
Unit 6
Unit 3
Unit 2
Unit 1
Bedrock
Block D (Unit 6)
Disturbed Zone
Block C
Block B (Unit 6)
Disturbed Zone
Block A (Unit 3)
Thompson River
Elevation (m)
350
300
250
0
50
100
150
200
250
300
350
400
Distance From Main Scarp (m)

Figure A2.8 Slide CN50.9 after second retrogression on the deeper rupture surface.

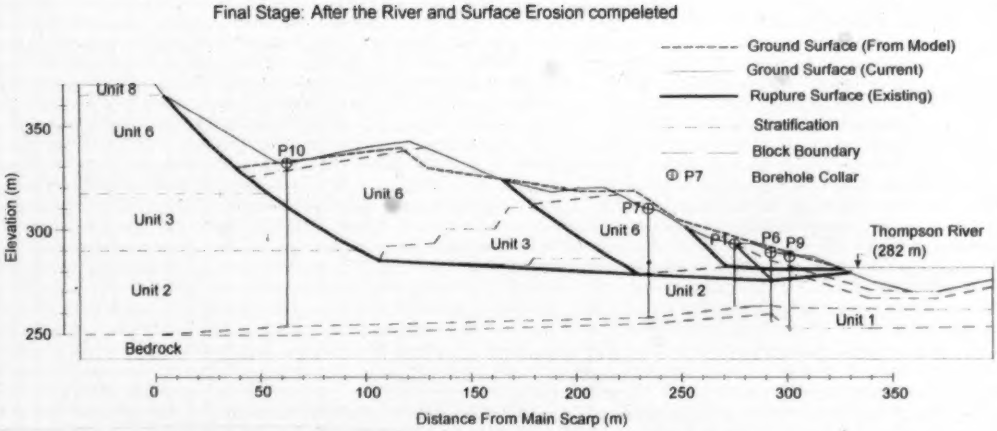
Final Stage: After the River and Surface Erosion compeleted
Ground Surface (From Model)
Ground Surface (Current)
Rupture Surface (Existing)
Stratification
Block Boundary
⊕ P7
Borehole Collar
Unit 8
Unit 6
Unit 3
Unit 2
Bedrock
P10
Unit 6
Unit 3
P7
Unit 6
Unit 2
P1
P6
P9
Unit 1
Thompson River
(282 m)
Elevation (m)
350
300
250
0
50
100
150
200
250
300
350
Distance From Main Scarp (m)

Figure A2.9 Slide CN50.9 end result of sliding process modeling after toe river erosion.

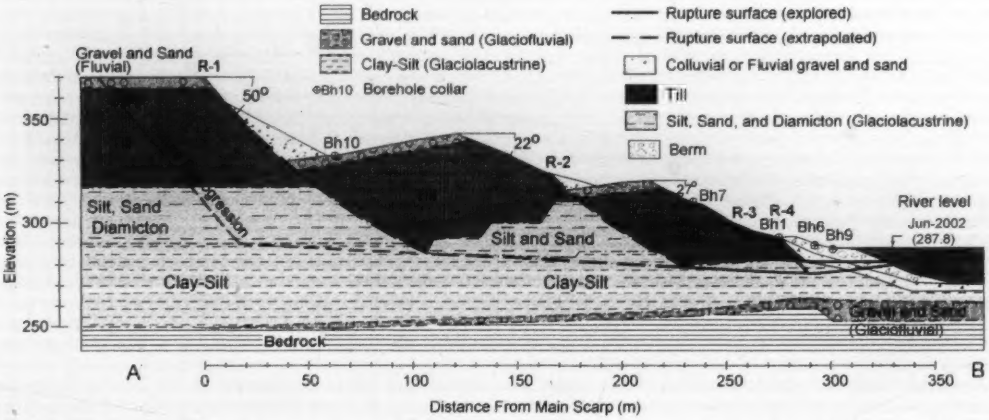
Bedrock
Gravel and sand (Glaciofluvial)
Clay-Silt (Glaciolacustrine)
⊕Bh10 Borehole collar
Rupture surface (explored)
Rupture surface (extrapolated)
Colluvial or Fluvial gravel and sand
Till
Silt, Sand, and Diamicton (Glaciolacustrine)
Berm
Gravel and Sand
(Fluvial)
R-1
50°
Bh10
22°
R-2
27°
Bh7
R-3
R-4
Bh1
Bh6
Bh9
River level
Jun-2002
(287.8)
Silt, Sand
Diamicton
gression
Silt and Sand
Clay-Silt
Clay-Silt
Gravel and Sand
(Glaciofluvial)
Bedrock
Elevation (m)
350
300
250
A
B
0
50
100
150
200
250
300
350
Distance From Main Scarp (m)

Figure A2.10 Slide CN50.9 current stratigraphy based on borehole information and sliding modeling.

A2.3.2. Goddard Slide

The Goddard Slide, with 11 boreholes, has the most boreholes among the slides in the study area. Especially, the boreholes in the terrace above the landslide show the upper part of the stratification at this area. Unfortunately, the boreholes are not deep enough to define the locations of unit 1 and the bedrock. The level of unit 1 and the bedrock was defined based on the data from the adjacent slides, Slide CN50.9 and the South Slide, and by considering the general tilting of layers toward the south. Therefore, the level of unit 1 and the bedrock was assumed to be 5 to 10 metres lower than what was seen in Slide CN50.9.

During the sliding process, the volume of disturbed material increased. On the other hand, the river erosion removed some of the material. Based on trial-and-error to match the current ground surface and the ground surface from the modeling process, the pre-slide cross-section area was assumed to be 5% larger than the current cross-section area. Based on the study of the adjacent slopes, the pre-slide ground slope was assumed to be 16°. Figure A2.11 shows the Goddard Slide's and its cross-section's location.

Based on the visible minor scarps on the ground, the current situation was assumed to be the result of five series of sliding. Figure A2.12 shows the slide situation before the first sliding stage. The stratification was defined based on borehole information, the adjacent slides, and the general stratigraphy of the sediments in this area. The location of the sliding blocks was defined based on ground evidence like that from slope changes and minor scarps. The scarp slopes were defined based on the material's residual friction angle. As the residual friction angle of the material on the slip surface was about 14°, the scarp angle was assumed to be 52° (45+14/2).

Figure A2.13 shows the Goddard Slide after the retrogression on the shallower rupture surface. During this retrogression, the toe block (block A) moved horizontally toward the river while the upper block (block B) moved both horizontally and vertically. A transition-disturbed zone, which may contain many small sheared blocks, was presented between the two blocks.

Figure A2.14 shows the Goddard Slide after the second retrogression on the shallower rupture surface. Again, the same method was used for modeling the movement. Figure A2.15 shows the Goddard Slide after the third sliding process. This time, the retrogression occurred on the deeper rupture surface.

Figure A2.16 shows the Goddard slide after the fourth retrogression on deeper rupture surface. This situation existed before the 1982 reactivation. Figure A2.17 shows the Goddard slide after the 1982 reactivation. During this reactivation, the head block (block H) moved down and toward the river while the rest of material moved toward the river.

Later, the toe material removed by river erosion and further surficial processes adjusted the ground surface. Figure A2.18 shows the current ground surface and stratification within the Goddard Slide resulting from this process of sliding. This result from the sliding process modeling is in good agreement with what is encountered in the boreholes and the material outcrops at the toe.

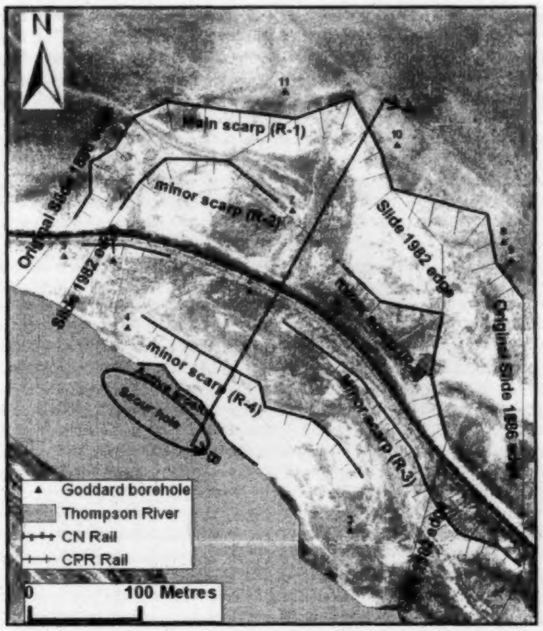
N
11
10
Main scarp (R-1)
minor scarp (R-2)
minor scarp (R-4)
minor scarp (R-3)
Original Slide 1896 edge
Slide 1982 edge
Slide 1982 edge
Original Slide 1896 edge
Scour hole
Goddard borehole
Thompson River
CN Rail
CPR Rail
0
100 Metres

Figure A2.11 Goddard slide boreholes and cross-section location

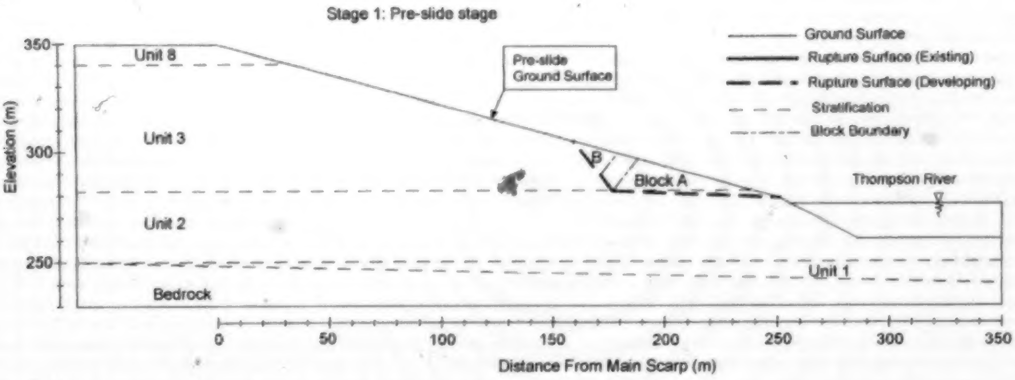
Stage 1: Pre-slide stage
Pre-slide Ground Surface
Unit 8
Unit 3
Unit 2
Bedrock
Unit 1
B
Block A
Thompson River
Ground Surface
Rupture Surface (Existing)
Rupture Surface (Developing)
Stratification
Block Boundary
Elevation (m)
350
300
250
0
50
100
150
200
250
300
350
Distance From Main Scarp (m)

Figure A2.12 Goddard Slide pre-slide situation.

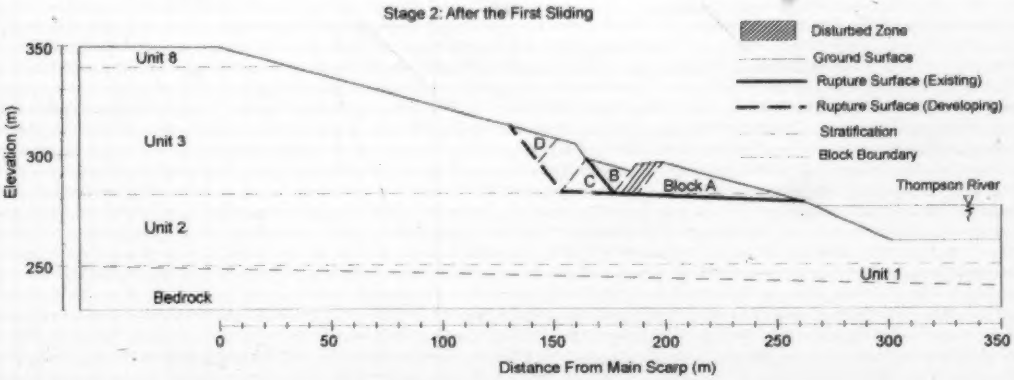
Stage 2: After the First Sliding
Unit 8
Unit 3
Unit 2
Bedrock
Unit 1
D
C
B
Block A
Thompson River
Disturbed Zone
Ground Surface
Rupture Surface (Existing)
Rupture Surface (Developing)
Stratification
Block Boundary
Elevation (m)
350
300
250
0
50
100
150
200
250
300
350
Distance From Main Scarp (m)

Figure A2.13 Goddard Slide after the first retrogression on the shallower rupture surface.

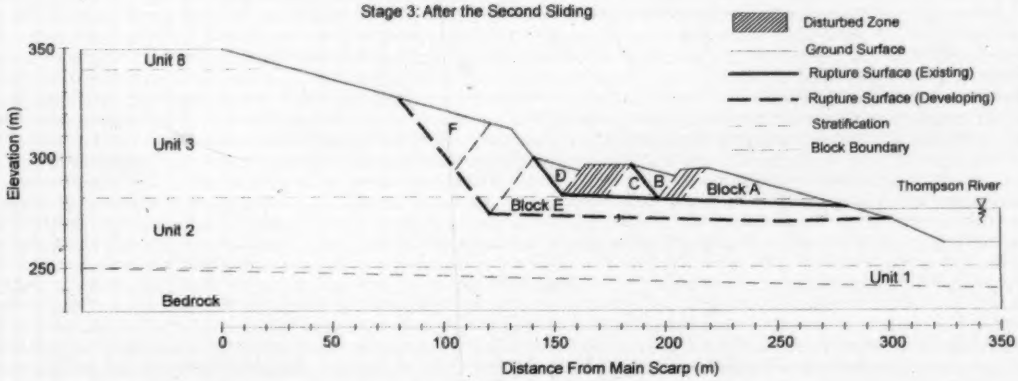
Stage 3: After the Second Sliding
Unit 8
Unit 3
Unit 2
Bedrock
Unit 1
F
D
C
B
Block A
Block E
Thompson River
Disturbed Zone
Ground Surface
Rupture Surface (Existing)
Rupture Surface (Developing)
Stratification
Block Boundary
Elevation (m)
350
300
250
0
50
100
150
200
250
300
350
Distance From Main Scarp (m)

Figure A2.14 Goddard Slide after the second retrogression on the shallower rupture surface.

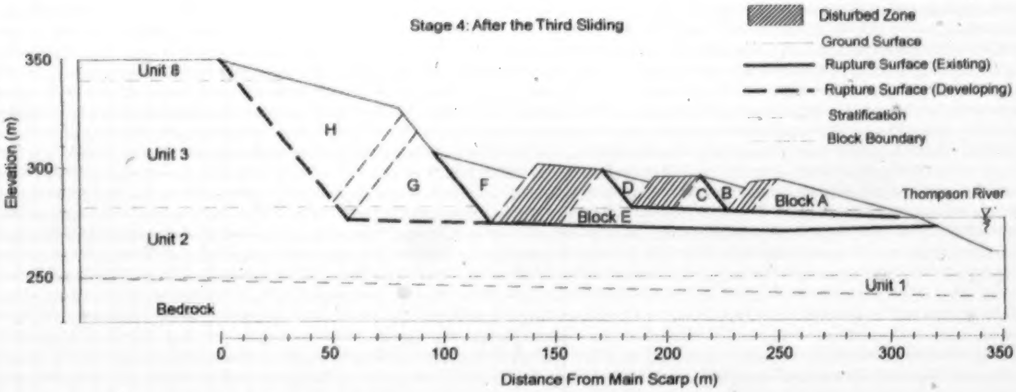
Stage 4: After the Third Sliding
Disturbed Zone
Ground Surface
Rupture Surface (Existing)
Rupture Surface (Developing)
Stratification
Block Boundary
Unit 8
Unit 3
Unit 2
Bedrock
Unit 1
H
G
F
D
C
B
Block A
Block E
Thompson River
Elevation (m)
350
300
250
0
50
100
150
200
250
300
350
Distance From Main Scarp (m)

Figure A2.15 Goddard Slide after the third retrogression on the deeper rupture surface.

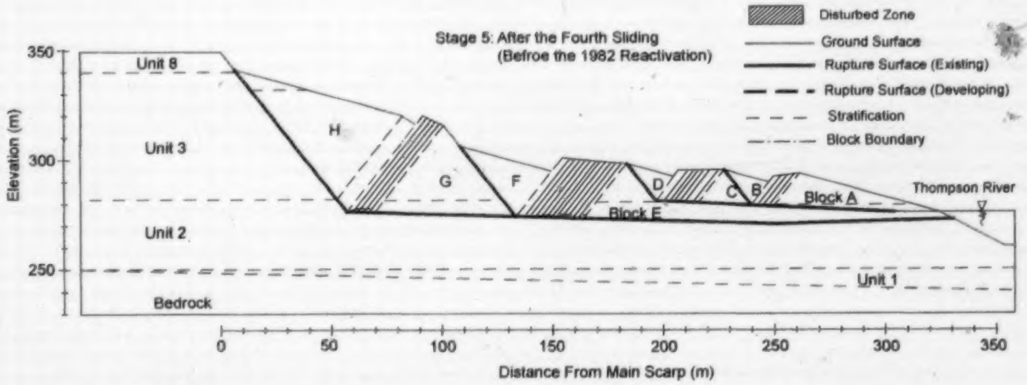
Stage 5: After the Fourth Sliding
(Befroe the 1982 Reactivation)
Disturbed Zone
Ground Surface
Rupture Surface (Existing)
Rupture Surface (Developing)
Stratification
Block Boundary
Unit 8
Unit 3
Unit 2
Bedrock
Unit 1
H
G
F
D
C
B
Block A
Block E
Thompson River
Elevation (m)
350
300
250
0
50
100
150
200
250
300
350
Distance From Main Scarp (m)

Figure A2.16 Goddard Slide after the fourth retrogression on the deeper rupture surface and before the 1982 reactivation.

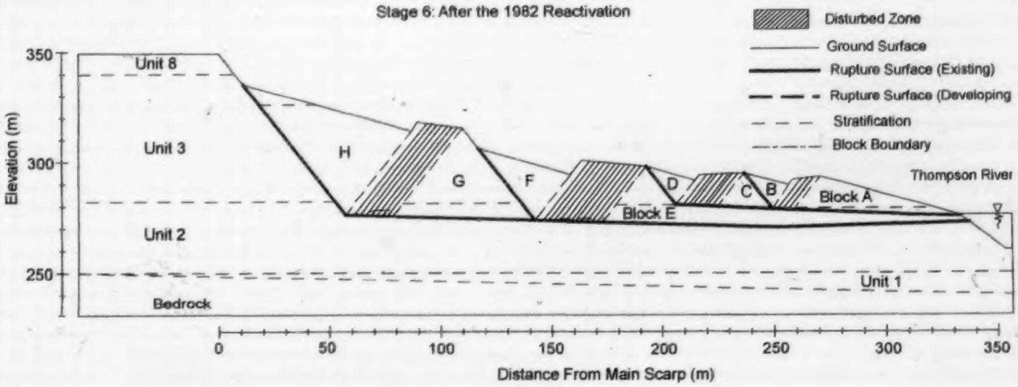
Stage 6: After the 1982 Reactivation
Disturbed Zone
Ground Surface
Rupture Surface (Existing)
Rupture Surface (Developing
Stratification
Block Boundary
Unit 8
Unit 3
Unit 2
Bedrock
Unit 1
H
G
F
D
C
B
Block A
Block E
Thompson River
Elevation (m)
350
300
250
0
50
100
150
200
250
300
350
Distance From Main Scarp (m)

Figure A2.17 Goddard Slide after the 1982 reactivation.

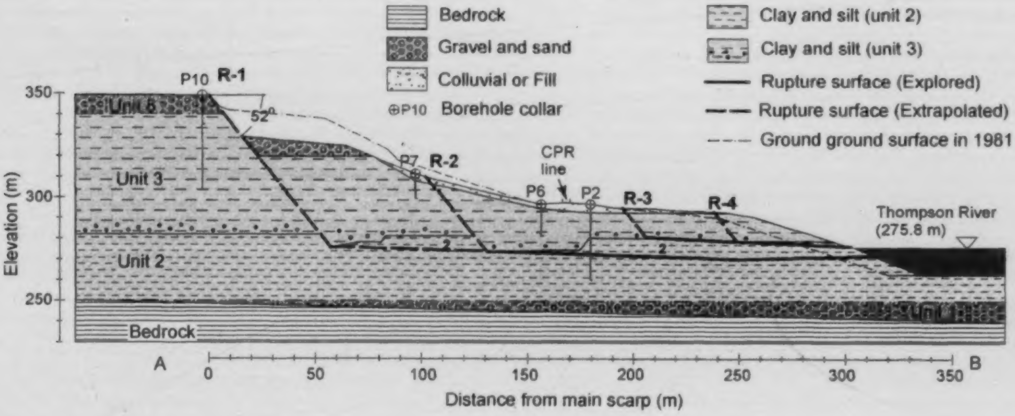
Bedrock
Gravel and sand
Colluvial or Fill
⊕P10 Borehole collar
Clay and silt (unit 2)
Clay and silt (unit 3)
Rupture surface (Explored)
Rupture surface (Extrapolated)
Ground ground surface in 1981
P10
R-1
52°
Unit 8
Unit 3
Unit 2
Unit 1
Bedrock
P7
R-2
CPR line
P6
P2
R-3
R-4
2
2
2
Thompson River (275.8 m)
350
300
250
Elevation (m)
A
B
0
50
100
150
200
250
300
350
Distance from main scarp (m)

Figure A2.18 Current Goddard cross section.

A2.3.3. North Slide

Four boreholes at the toe of the North Slide provide some information about the stratification in this slide. Unfortunately, all these boreholes are located at the toe, which is a small area compared to the whole slide area. This borehole information was reported by Porter and Savigny (2001). The boreholes entered colluvial and fill material at the top and then entered layers of silt and sand, which should be unit 3 or unit 2. None of the boreholes are deep enough to define unit 1's and the bedrock's location; therefore, their location were assumed from the data for the adjacent slide to the south (the South Slide). At the main scarp, a thick layer of till material, unit 6, can be seen. This layer is overlain by a layer of gravel and sand, which should be unit 8. Figure A2.19 shows the North Slide plan view and the produced cross-section location. The cross section is located close to the centre of the slide.

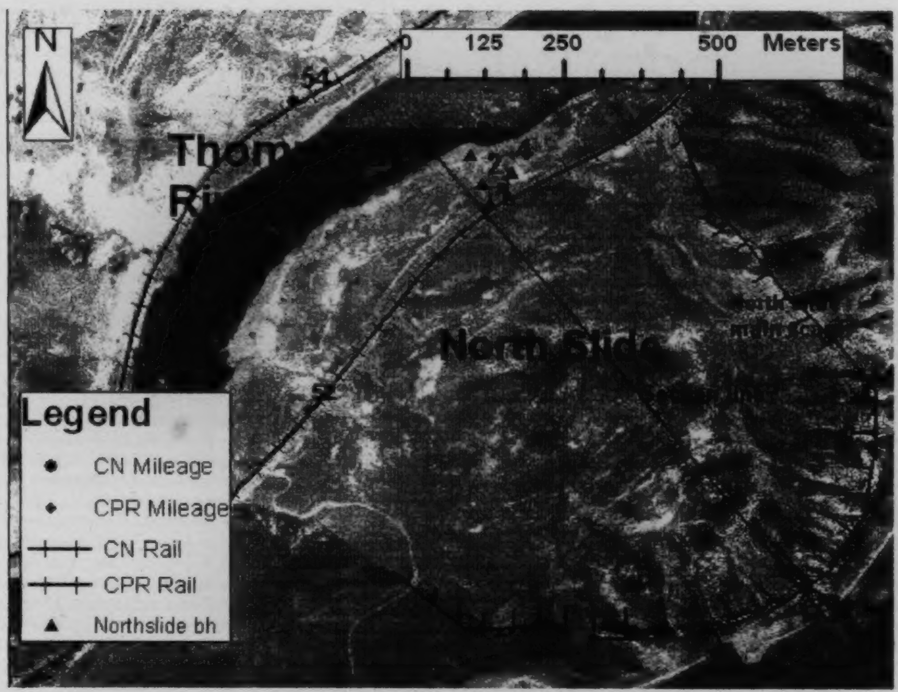
N
0
125
250
500
Meters
Thom
Ri
North Slide
51
52
Legend
● CN Mileage
◆ CPR Mileage
CN Rail
CPR Rail
▲ Northslide bh

Figure A2.19 North Slide's boreholes and cross-section location.

Because some of the sliding material later was removed by river erosion, the pre-slide cross-section area was assumed to be 15% larger than the current cross-section area. Based on the study of the adjacent slopes and the residual friction angle of the materials in this slide, the pre-slide ground slope was assumed to be 20°. In order to satisfy these conditions, the pre-slide ground surface should have a relatively large horizontal terrace. Figure A2.20 shows the North Slide before sliding. The scarp angles were assumed to be 52°.

Figure A2.21 shows the North Slide after the first retrogression on the shallower rupture surface. A lower block moved toward the river. As a result of this block's horizontal movement, the upper block was left unsupported and slid down on a 52° scarp slip surface. Between the two blocks, a transition zone was disturbed during the sliding process.

Figure A2.22 shows the continuing of the sliding process by a second retrogression on the shallower rupture. This retrogression was modeled by using two blocks and a disturbed zone between them.

Figure A2.23 shows how the retrogression process continued in the North Slide's third retrogression. This time, the movement was assumed to be on the deeper rupture surface and to be the result from the Thompson River down-cutting through the sediments. The movement was modeled by using two blocks with a transition zone between them.

Figure A2.24 shows the situation after the fourth retrogression on the deeper rupture surface. Figure A2.25 shows the fifth retrogression on the deeper rupture surface. This figure reveals an accumulation of material at the toe. This extra material was removed by the Thompson River erosion. The ground surface resulting from the block movement model reasonably matches with the current ground surface, which shows the accuracy of the model. Based on the modeled process, the North Slide's current topography and stratification are shown in Figure A2.26.

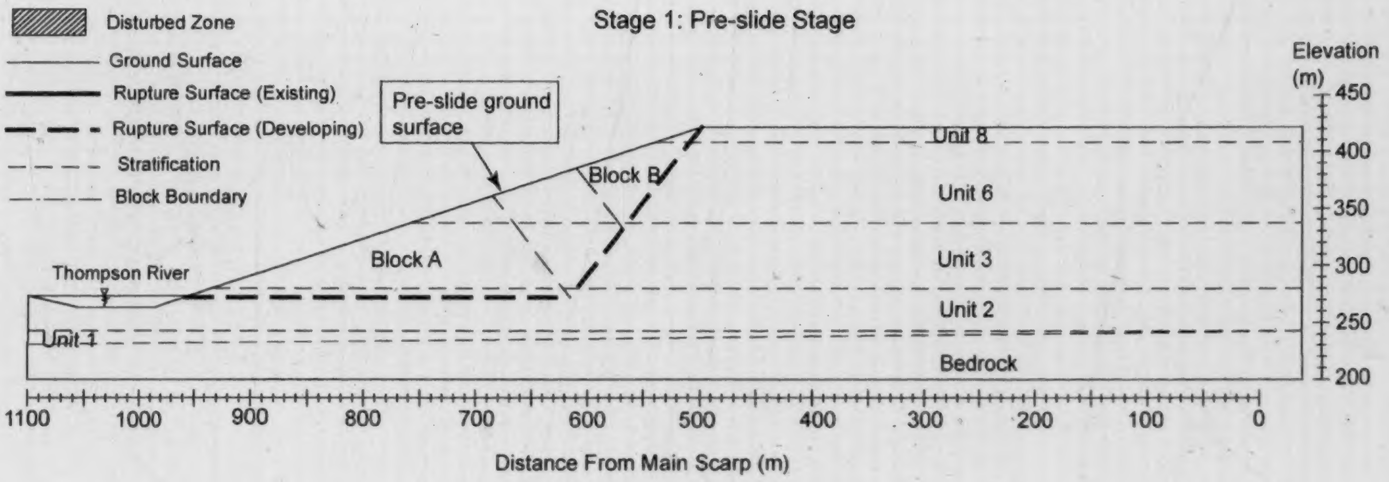

Disturbed Zone
Ground Surface
Rupture Surface (Existing)
Rupture Surface (Developing)
Stratification
Block Boundary
Stage 1: Pre-slide Stage
Pre-slide ground surface
Elevation (m)
450
400
350
300
250
200
Unit 8
Unit 6
Unit 3
Unit 2
Bedrock
Block B
Block A
Thompson River
Unit 1
1100
1000
900
800
700
600
500
400
300
200
100
0
Distance From Main Scarp (m)

Figure A2.20 North Slide pre-slide stage.

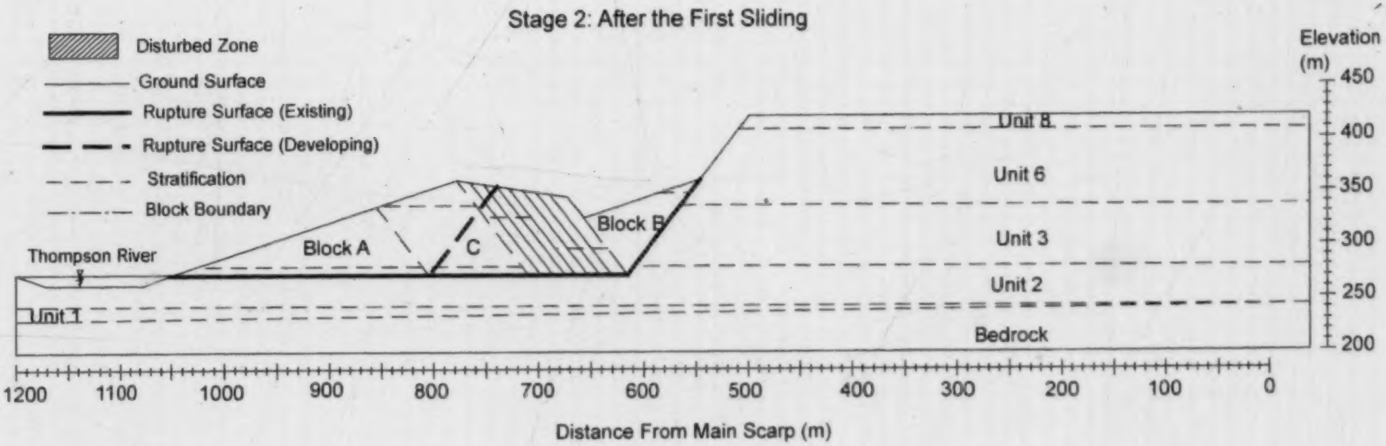
Stage 2: After the First Sliding
▨ Disturbed Zone
Ground Surface
Rupture Surface (Existing)
Rupture Surface (Developing)
Stratification
Block Boundary
Thompson River
Block A
C
Block B
Unit 8
Unit 6
Unit 3
Unit 2
Unit 1
Bedrock
Elevation (m)
450
400
350
300
250
200
1200
1100
1000
900
800
700
600
500
400
300
200
100
0
Distance From Main Scarp (m)

Figure A2.21 North Slide after the first retrogression.

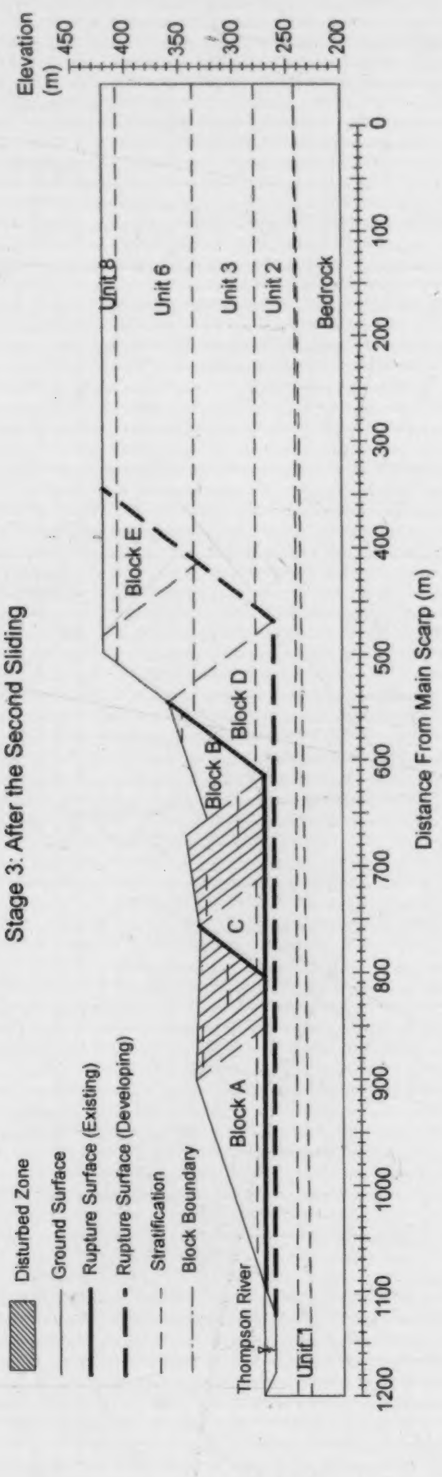
Stage 3: After the Second Sliding
Disturbed Zone
Ground Surface
Rupture Surface (Existing)
Rupture Surface (Developing)
Stratification
Block Boundary
Thompson River
Unit 1
Unit 2
Unit 3
Unit 6
Unit 8
Bedrock
Block A
Block B
C
Block D
Block E
Elevation (m)
450
400
350
300
250
200
Distance From Main Scarp (m)
0
100
200
300
400
500
600
700
800
900
1000
1100
1200

Figure A2.22 North Slide after the second retrogression.

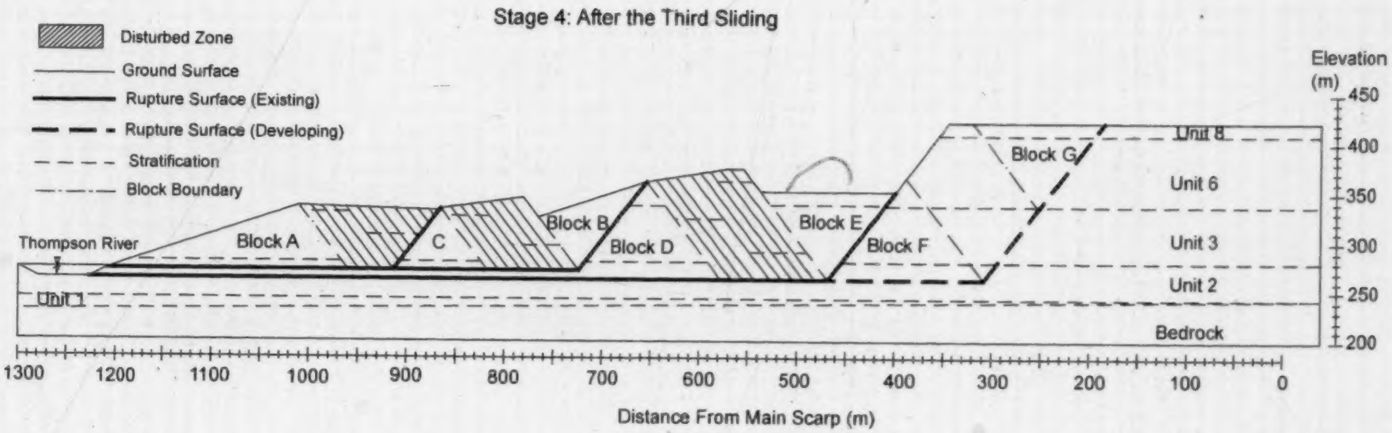

Stage 4: After the Third Sliding

▨ Disturbed Zone
Ground Surface
Rupture Surface (Existing)
Rupture Surface (Developing)
Stratification
Block Boundary
Thompson River
Block A
C
Block B
Block D
Block E
Block F
Block G
Unit 8
Unit 6
Unit 3
Unit 2
Unit 1
Bedrock
Elevation (m)
450
400
350
300
250
200
1300
1200
1100
1000
900
800
700
600
500
400
300
200
100
0
Distance From Main Scarp (m)

Figure A2.23 North Slide after the third retrogression.

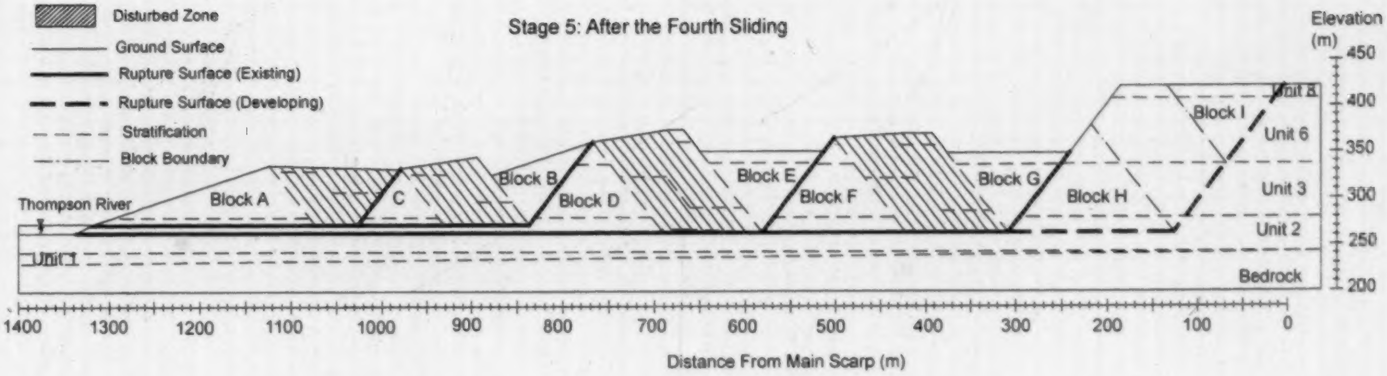
Disturbed Zone
Ground Surface
Rupture Surface (Existing)
Rupture Surface (Developing)
Stratification
Block Boundary
Stage 5: After the Fourth Sliding
Elevation (m)
450
400
350
300
250
200
Thompson River
Block A
C
Block B
Block D
Block E
Block F
Block G
Block H
Block I
Unit 8
Unit 6
Unit 3
Unit 2
Unit 1
Bedrock
1400
1300
1200
1100
1000
900
800
700
600
500
400
300
200
100
0
Distance From Main Scarp (m)

Figure A2.24 North Slide after the fourth retrogression.

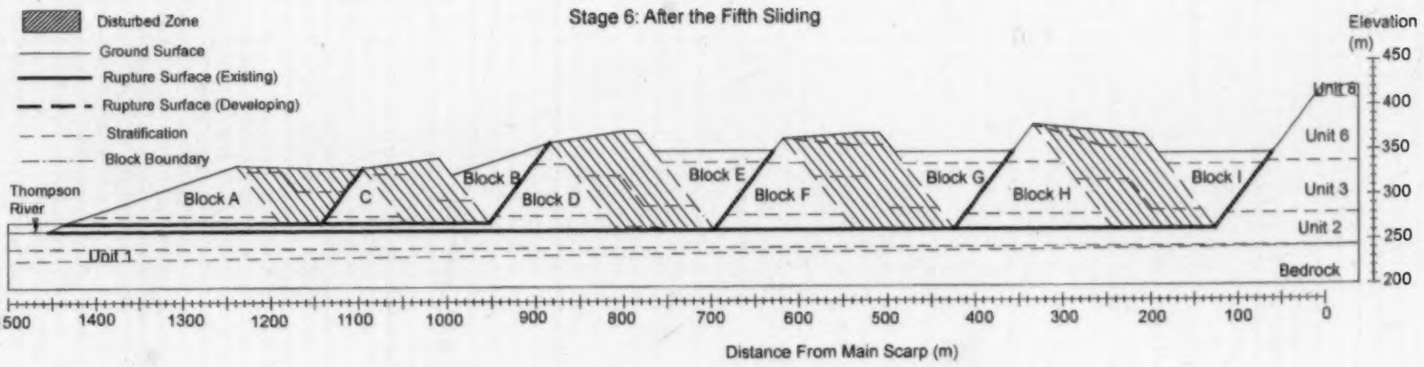
Stage 6: After the Fifth Sliding
Disturbed Zone
Ground Surface
Rupture Surface (Existing)
Rupture Surface (Developing)
Stratification
Block Boundary
Thompson River
Block A
C
Block B
Block D
Block E
Block F
Block G
Block H
Block I
Unit 1
Unit 2
Unit 3
Unit 6
Unit 8
Bedrock
Elevation (m)
450
400
350
300
250
200
1500
1400
1300
1200
1100
1000
900
800
700
600
500
400
300
200
100
0
Distance From Main Scarp (m)

Figure A2.25 North Slide after the most recent retrogression (fifth retrogression).

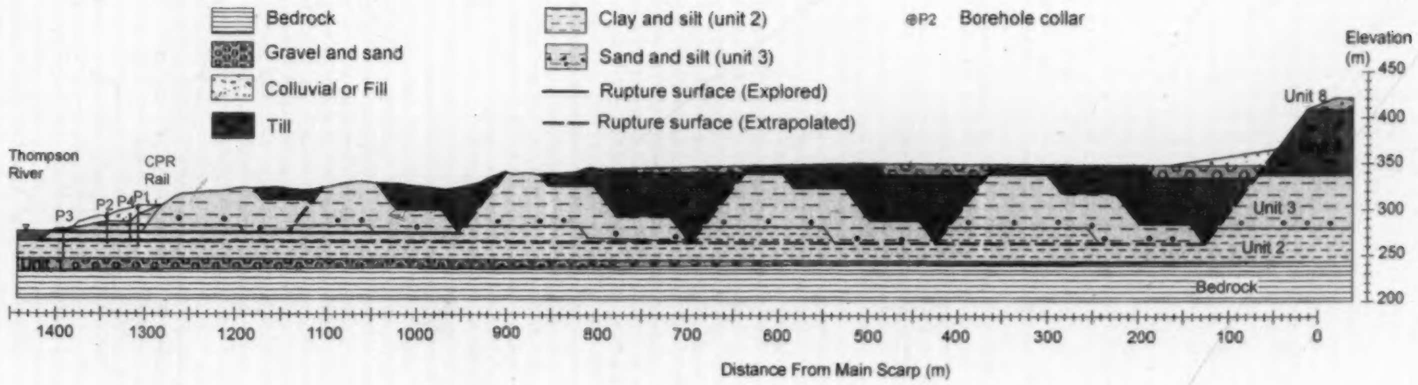
Bedrock
Gravel and sand
Colluvial or Fill
Till
Clay and silt (unit 2)
Sand and silt (unit 3)
Rupture surface (Explored)
Rupture surface (Extrapolated)
⊕P2 Borehole collar
Elevation (m)
450
400
350
300
250
200
Unit 8
Unit 3
Unit 2
Bedrock
Thompson River
CPR Rail
P3
P2
P4
P1
1400
1300
1200
1100
1000
900
800
700
600
500
400
300
200
100
0
Distance From Main Scarp (m)

Figure A2.26 North Slide current cross section.

A2.3.4. South Slide

Figure A2.27 shows a plan view of the South Slide and its cross-section's location, which is close to the centre of the slide.

The South Slide, with seven boreholes, has the most boreholes after the Goddard Slide. Unfortunately, all of these boreholes are located at the toe of the slide. These boreholes entered colluvial and fill material at the top and then entered layers of silt and sand, which are believed to be units 3 and 2. Boreholes DH04-10 and DH04-13 (shown as number 6 in Figure A2.27) were deep enough to reach unit 1 and bedrock. Therefore, the bedrock and unit 1 locations were defined based on these boreholes' information. At the main scarp, a thick layer of till of unit 6 can be seen. This layer is overlain by a layer of gravel and sand, which should be unit 8.

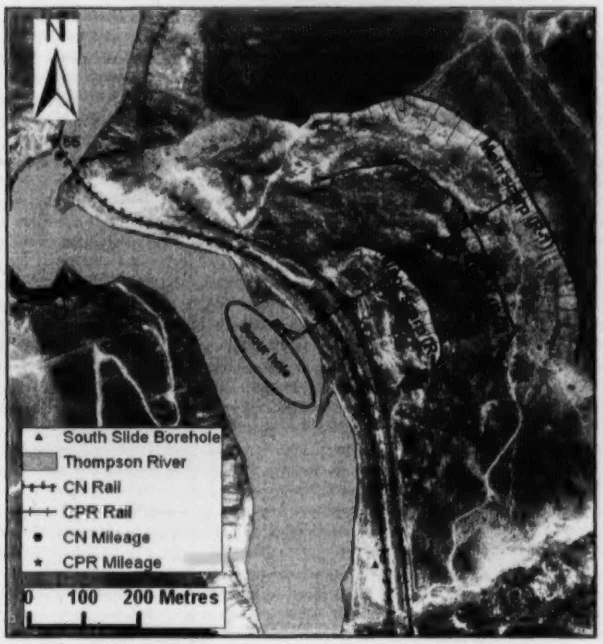
N
Scour hole
South Slide Borehole
Thompson River
CN Rail
CPR Rail
CN Mileage
CPR Mileage
0 100 200 Metres

Figure A2.27 A plan view of South Slide with the cross-section line close to the centre of slide and boreholes.

The pre-slide cross-section area was assumed to be 4% larger than current cross-section area to account for the material lost due to the river erosion. Based on the study of the adjacent slopes and the residual friction angles of the materials in this slide, the pre-slide ground slope was assumed to be 16°.Figure A2.28 shows the South Slide in its pre-slide stage. The scarp angle was assumed to be 52° based on the friction angles of the materials.

South Slide's stratigraphy after the first retrogression is shown in Figure A2.29. A lower block moved toward the river and as a result of this block's horizontal movement, the upper block was left unsupported and slid down on a 52° slip surface. Between the two blocks, a transition zone was disturbed during this process of sliding.

Second retrogression during the sliding process is shown in Figure A2.30. This time, the movement happened on the deeper rupture surface as the result of the Thompson River down-cutting through the sediments. Again, the movement was modeled by using two blocks with a transition zone between them. Figure A2.31 shows the situation after the third retrogression.

Based on the block movement model, the current topography and stratification of South Slide are shown in Figure A2.32. This figure shows the end result of the movement process after the removal of material by the river and surficial modification by other processes.

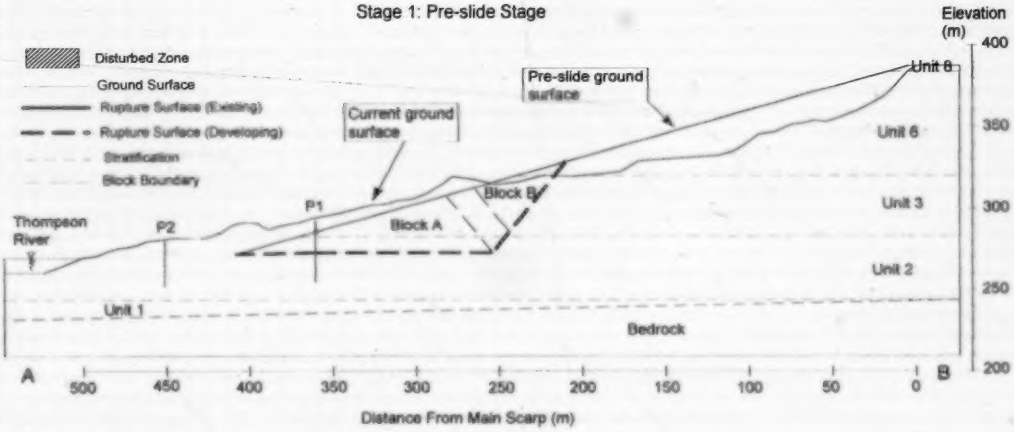
Stage 1: Pre-slide Stage
Disturbed Zone
Ground Surface
Rupture Surface (Existing)
Rupture Surface (Developing)
Stratification
Block Boundary
Current ground surface
Pre-slide ground surface
Thompson River
P2
P1
Block A
Block B
Unit 8
Unit 6
Unit 3
Unit 2
Unit 1
Bedrock
Elevation (m)
400
350
300
250
200
A
B
500
450
400
350
300
250
200
150
100
50
0
Distance From Main Scarp (m)

Figure A2.28 South Slide pre-retrogression stage.

Distance From Main Scarp (m)

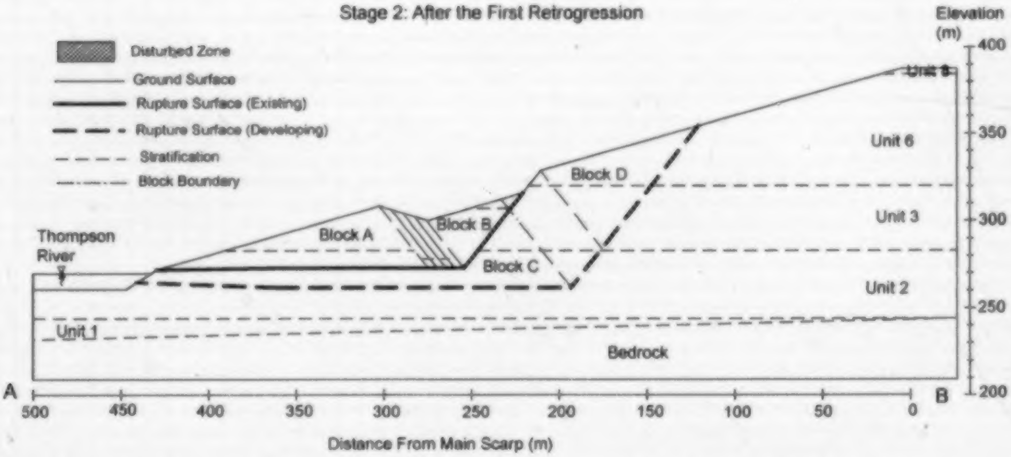
Stage 2: After the First Retrogression
Disturbed Zone
Ground Surface
Rupture Surface (Existing)
Rupture Surface (Developing)
Stratification
Block Boundary
Thompson River
Block A
Block B
Block C
Block D
Unit 8
Unit 6
Unit 3
Unit 2
Unit 1
Bedrock
Elevation (m)
400
350
300
250
200
A
B
500
450
400
350
300
250
200
150
100
50
0
Distance From Main Scarp (m)

Figure A2.29 South Slide after the first retrogression on the shallower rupture surface.

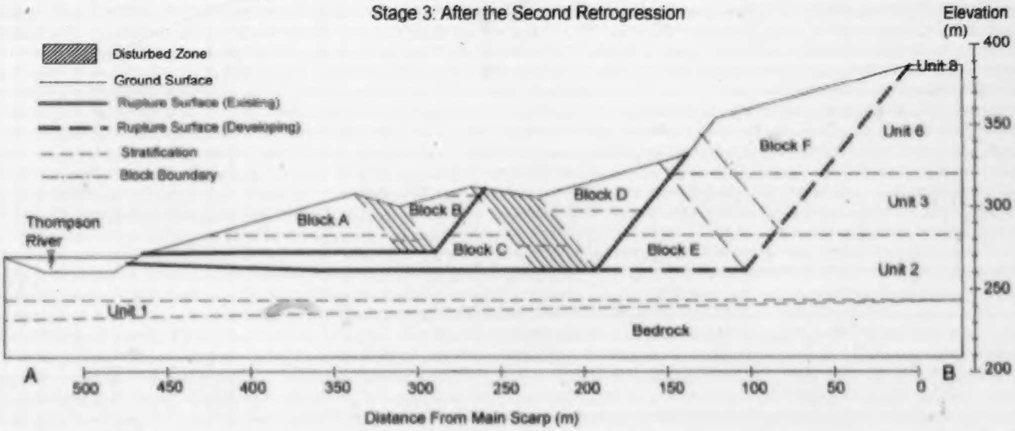
Stage 3: After the Second Retrogression
Disturbed Zone
Ground Surface
Rupture Surface (Existing)
Rupture Surface (Developing)
Stratification
Block Boundary
Elevation (m)
400
350
300
250
200
Unit 8
Unit 6
Unit 3
Unit 2
Unit 1
Bedrock
Block A
Block B
Block C
Block D
Block E
Block F
Thompson River
A
B
500
450
400
350
300
250
200
150
100
50
0
Distance From Main Scarp (m)

Figure A2.30 South Slide after the second retrogression on the deeper rupture surface.

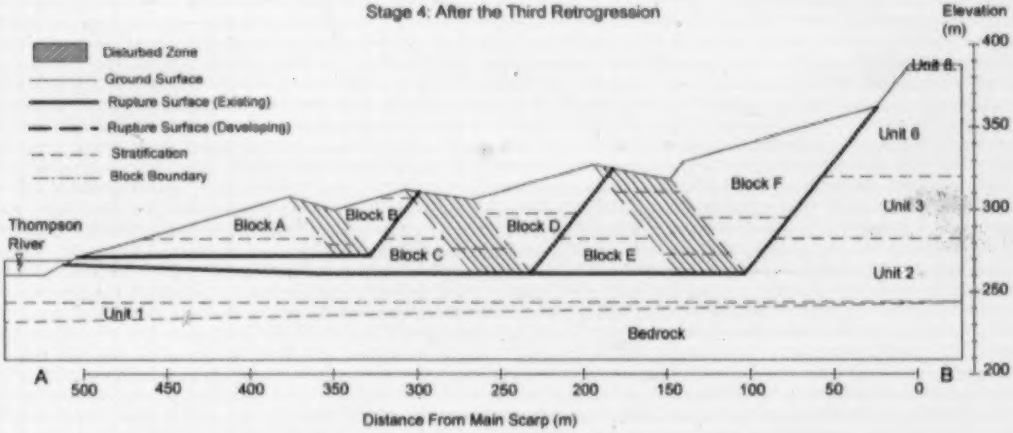
Stage 4: After the Third Retrogression
Disturbed Zone
Ground Surface
Rupture Surface (Existing)
Rupture Surface (Developing)
Stratification
Block Boundary
Elevation (m)
400
350
300
250
200
Unit 8
Unit 6
Unit 3
Unit 2
Unit 1
Bedrock
Block A
Block B
Block C
Block D
Block E
Block F
Thompson River
A
B
500
450
400
350
300
250
200
150
100
50
0
Distance From Main Scarp (m)

Figure A2.31 South Slide after the most recent retrogression on the deeper rupture surface.

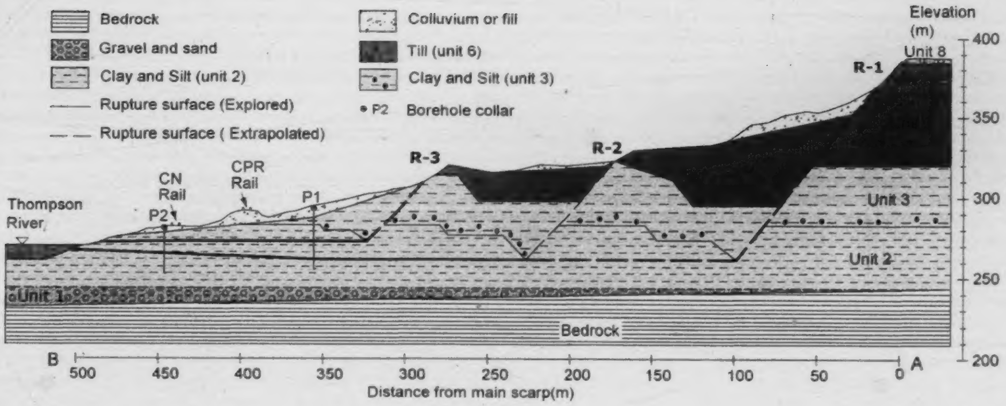
Bedrock
Gravel and sand
Clay and Silt (unit 2)
Rupture surface (Explored)
Rupture surface (Extrapolated)
Colluvium or fill
Till (unit 6)
Clay and Silt (unit 3)
P2 Borehole collar
Elevation (m)
Unit 8
R-1
R-2
R-3
Thompson River
CN Rail
CPR Rail
P2
P1
Unit 3
Unit 2
Unit 1
Bedrock
400
350
300
250
200
B
A
500
450
400
350
300
250
200
150
100
50
0
Distance from main scarp(m)

Figure A2.32 Current South Slide cross section.

A2.3.5. Basque Slide

The Basque Slide's extent, boreholes' location, and cross-section line are shown on a plan view of the site in Figure A2.33.

Information from the four boreholes drilled in this site was used for making the slide's stratification. All the boreholes are located at the toe, and none is deep enough to reach unit 1 and bedrock. They entered colluvial material; sand-silt unit 3; and clay-silt, unit 2. Therefore, the bedrock and unit 1 locations were defined based on their level in the South Slide. The terrace is at a relatively low level; therefore, no unit 6, till, is present in this slide.

The pre-slide cross-section area was assumed to be 20% larger than the current cross-section area to account for the material eroded by river erosion. Based on the study of the adjacent slopes and the residual friction angle of the material in this slide, the pre-slide ground slope was assumed to be 22°. Figure A2.34 shows the Basque Slide in the pre-slide stage. Based on previous experiences of similar slides in the area, it was assumed that the slide moved on two rupture surfaces, one at river-level elevation and the other 8 metres deeper at the river-bed elevation.

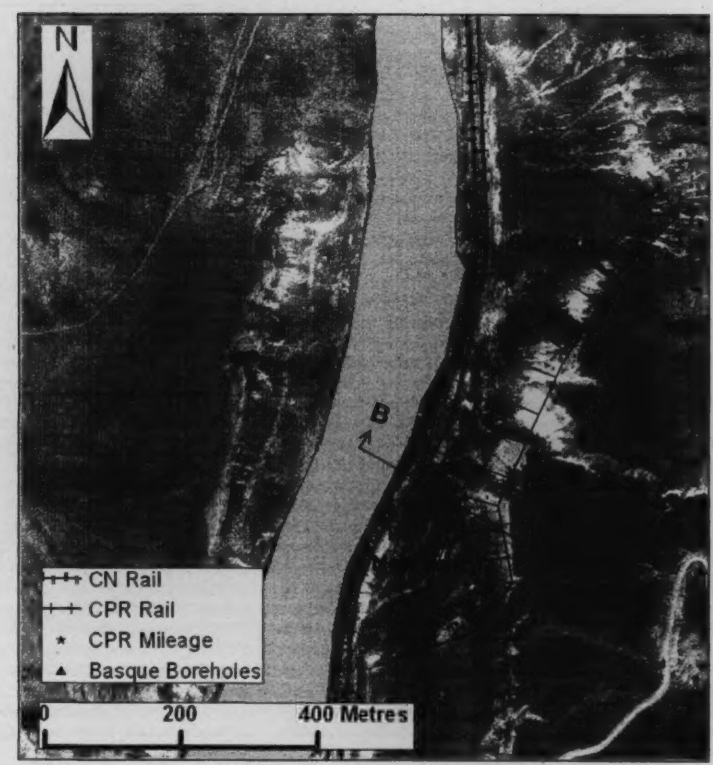
N
B
CN Rail
CPR Rail
CPR Mileage
Basque Boreholes
0
200
400 Metres

Figure A2. 33 A plan view of Basque Slide showing the section line, boreholes, and slide extend.

The Basque Slide after the first retrogression at the toe on the shallower rupture surface is shown in Figure A2.35. A transition zone between the two moved blocks was disturbed during the sliding process.

Figure A2.36 shows the Basque Slide after the second retrogression. This time, the movement occurred on the deeper rupture surface. The movement was modeled by using two blocks with a transition zone between them. Figure A2.37 shows the situation after the third retrogression.

Figure A2.38 shows the final result after the toe material was removed by river erosion. The materials seen in the boreholes are similar to what would be seen if block movement occurred. These findings verify the validity of the assumptions regarding the number of blocks and the nature of their movement.

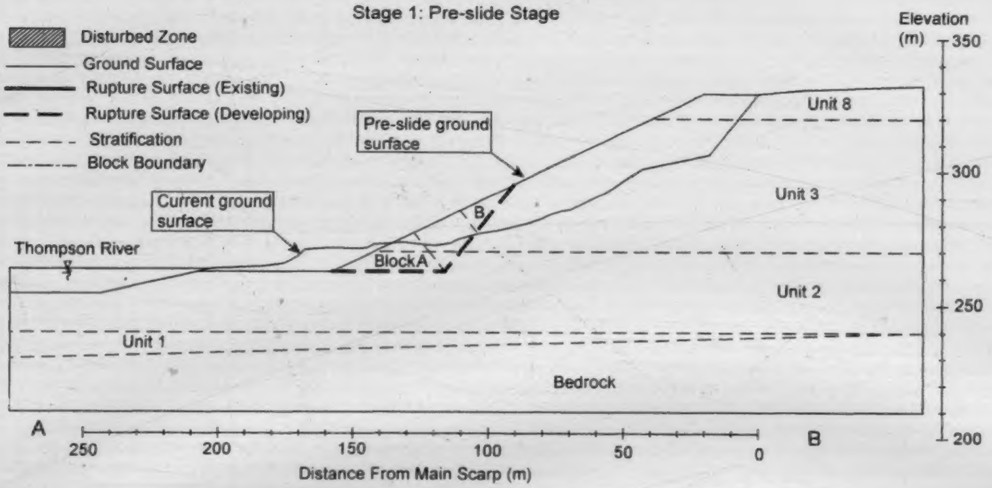
Stage 1: Pre-slide Stage
▨ Disturbed Zone
Ground Surface
Rupture Surface (Existing)
Rupture Surface (Developing)
Stratification
Block Boundary
Pre-slide ground surface
Current ground surface
Thompson River
Block A
B
Unit 8
Unit 3
Unit 2
Unit 1
Bedrock
Elevation (m)
350
300
250
200
A
B
250
200
150
100
50
0
Distance From Main Scarp (m)

Figure A2.34 Basque Slide pre-slide stage.

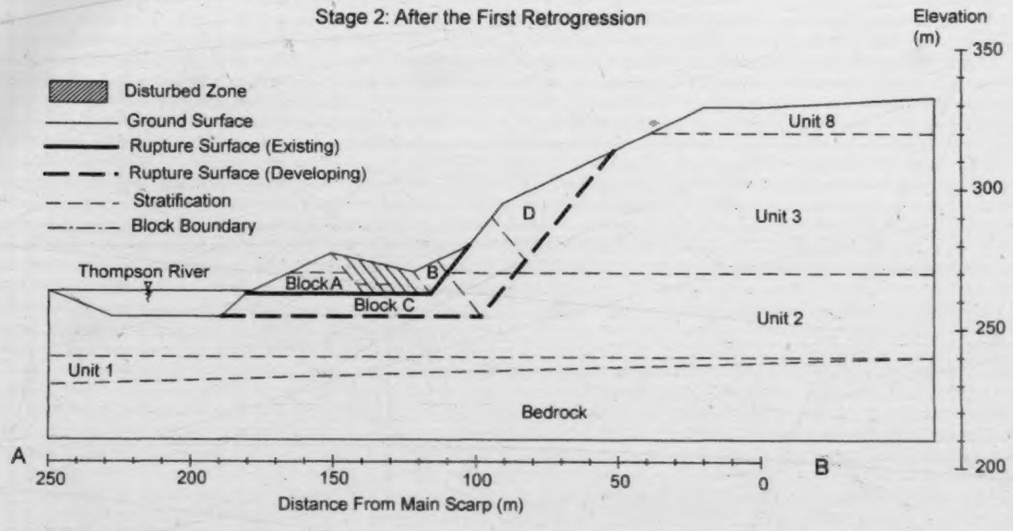
Stage 2: After the First Retrogression
▨ Disturbed Zone
Ground Surface
Rupture Surface (Existing)
Rupture Surface (Developing)
Stratification
Block Boundary
Thompson River
Block A
B
Block C
D
Unit 8
Unit 3
Unit 2
Unit 1
Bedrock
Elevation (m)
350
300
250
200
A
B
250
200
150
100
50
0
Distance From Main Scarp (m)

Figure A2.35 Basque Slide after the first retrogression on the shallower rupture surface.

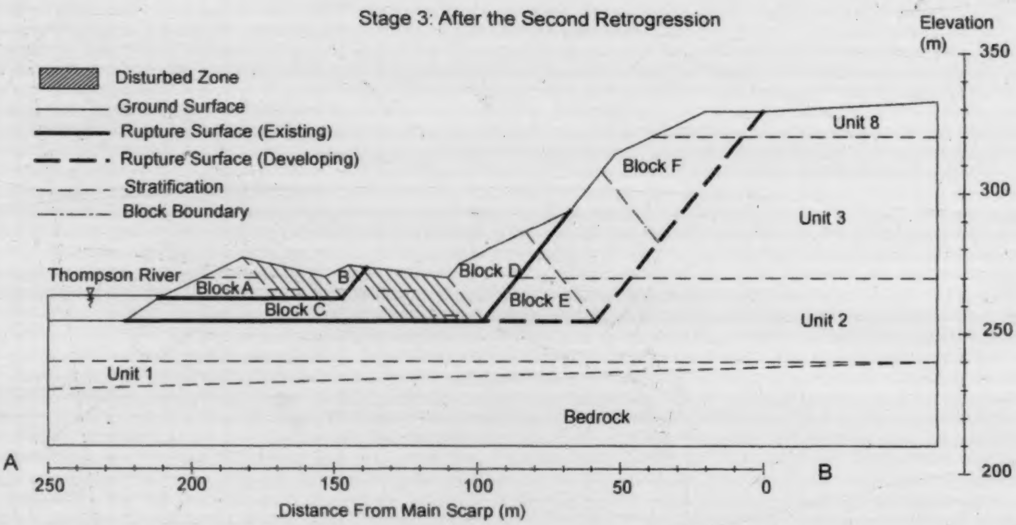
Stage 3: After the Second Retrogression
Disturbed Zone
Ground Surface
Rupture Surface (Existing)
Rupture Surface (Developing)
Stratification
Block Boundary
Elevation (m)
350
300
250
200
Unit 8
Block F
Unit 3
Thompson River
Block A
B
Block D
Block E
Block C
Unit 2
Unit 1
Bedrock
A
B
250
200
150
100
50
0
Distance From Main Scarp (m)

Figure A2.36 Basque Slide after the second retrogression by movement on the deeper rupture surface.

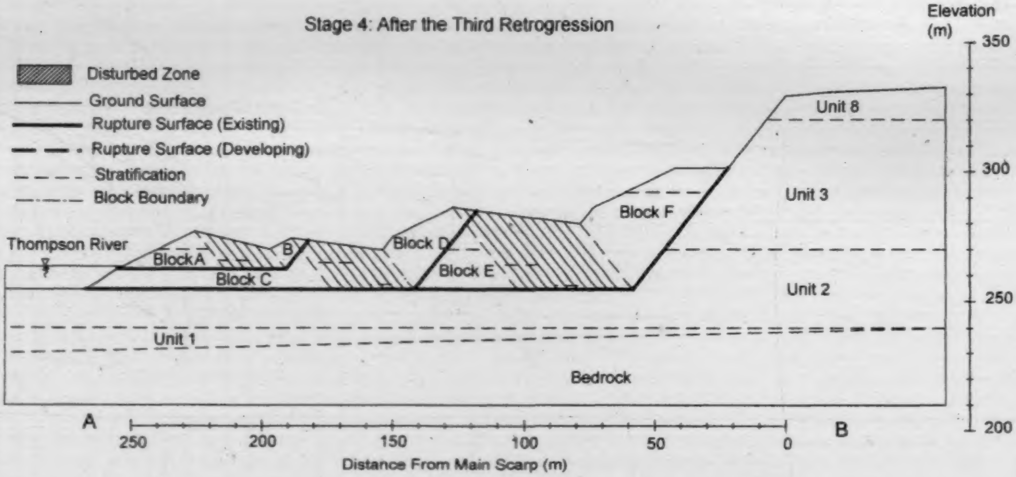
Stage 4: After the Third Retrogression
Disturbed Zone
Ground Surface
Rupture Surface (Existing)
Rupture Surface (Developing)
Stratification
Block Boundary
Elevation (m)
350
300
250
200
Unit 8
Unit 3
Block F
Thompson River
Block A
B
Block D
Block E
Block C
Unit 2
Unit 1
Bedrock
A
B
250
200
150
100
50
0
Distance From Main Scarp (m)

Figure A2.37 Basque Slide after the most recent retrogression on the deeper rupture surface.

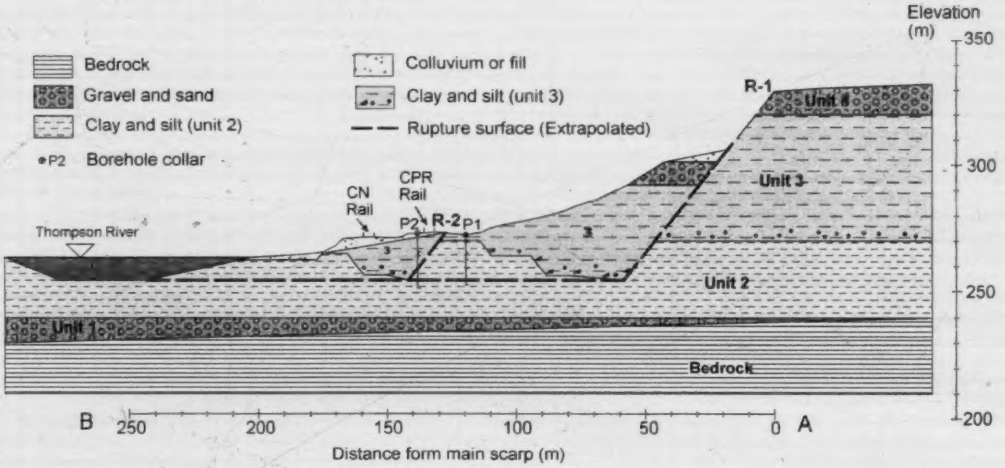
Bedrock
Gravel and sand
Clay and silt (unit 2)
•P2 Borehole collar
Colluvium or fill
Clay and silt (unit 3)
Rupture surface (Extrapolated)
Elevation (m)
350
300
250
200
R-1
Unit 4
Unit 3
Unit 2
Unit 1
Bedrock
3
CN Rail
CPR Rail
P2
R-2
P1
Thompson River
B
250
200
150
100
50
0
A
Distance form main scarp (m)

Figure A2.38 Basque cross section.

A2.3.6. Conclusions

The cross sections of five of the landslides in the Ashcroft area were produced by using block movement modeling. The boreholes' information, geology, ground surface LiDAR data, aerial photos, and site-visit information were used to model the sliding processes as block movements on rupture surfaces.

Wherever the boreholes were available, a comparison between the material in the boreholes and the material predicted by the block movement model was carried out. These comparisons showed a reasonable agreement between the assumptions and reality. Therefore, it can be concluded that this method can be used for finding stratification whenever the borehole information alone is not complete. Also, this method provides a sense of the sliding process in each of the slides.

Most of the boreholes either are at the toe of the slides or are not deep enough. Deeper boreholes at the middle of the slides or on the terraces could probably help in making more accurate stratigraphies for these slides.

Appendix 3: Soil Tests

A3.1. INTRODUCTION

Most of the rupture surfaces length of the translational landslides in the Ashcroft area are within the clay-silt glaciolacustrine sediments (unit 2). In the scarps, the rupture surfaces pass through higher-elevation sediments of sand and silt (unit 3), till (unit 6), and fluvial material on the crown terrace (unit 8). The index property tests were done on samples from the boreholes in Slide CN50.9, the Goddard Slide, North Slide, South Slide, Nepa Slide, and Basque Slide. Because of the importance of the characteristics of the clay-silt sediments of unit 2, more detailed tests had to be run on this material. The clay layers in the clay-silt sediment of unit 2 are highly plastic and are believed to be the main cause of the slide activity in this area. The specimens had to be taken from the clay-silt samples in such a way that these specimens contained the highly plastic clay layers needed for the separate tests on this material.

In order to test the characteristics of the clay-silt sediments of unit 2, samples were taken from the South Slide shear zone in boreholes DH04-02 (P1), DH04-05 (P5), and DH04-13 (P6) (Figure A3.1). Table 1 shows the borehole and sample information.

Table A3.1 South Slide borehole and sample information

Tube	Slip 1	Slip 2	Ground	Tube Elevation	
(borehole)	(m)*	(m)*	(m)*	Begin (m)	End (m)
1 (DH04-02)	260.2	272.7	293.3	272.73	272.12
2 (DH04-05)	259.7	276.2	291	282.56	281.95
3 (DH04-13)	259	-	276	269.29	268.3
4 (DH04-13)	259	-	276	261.67	260.15
5 (DH04-13)	259	-	276	260.15	258.63

* Elevation from sea level in metre.

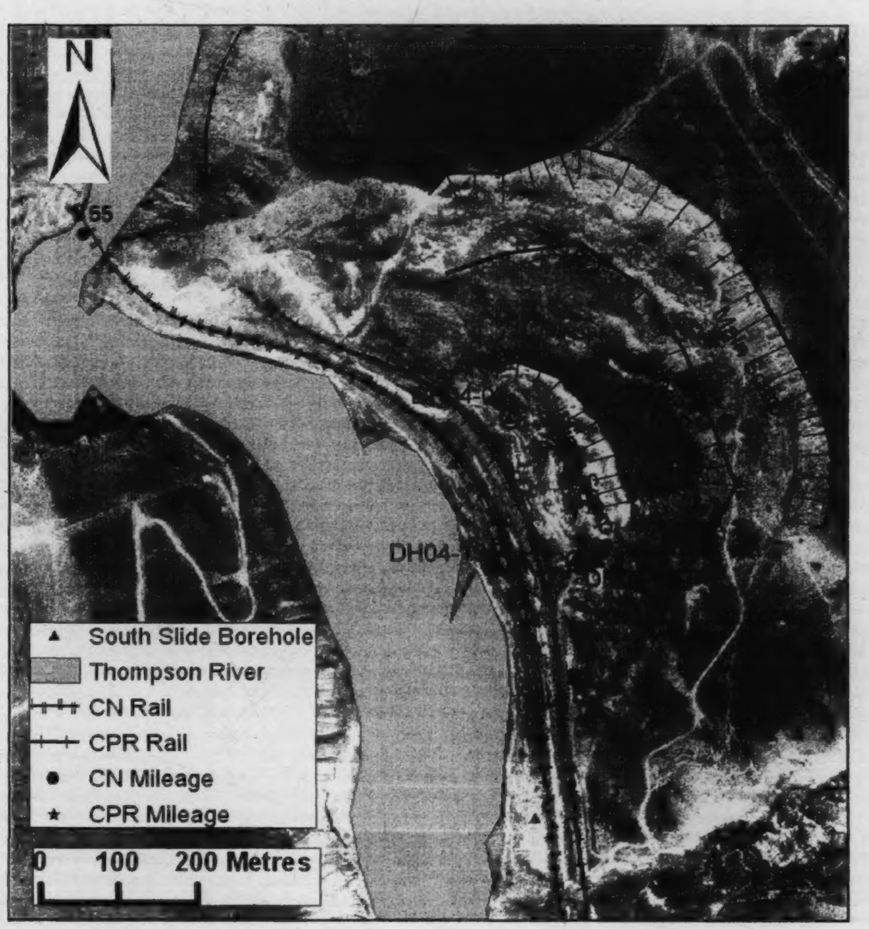
N
55
DH04-1
▲ South Slide Borehole
Thompson River
CN Rail
CPR Rail
● CN Mileage
★ CPR Mileage
0 100 200 Metres

Figure A3.1 South Slide

A3.2. CONSOLIDATION TEST

A specimen for the consolidation test was taken from sample 5, borehole DH04-13, from a ground surface depth of 16.1 m (elevation 259.1 m). Therefore, the sample was taken from the deeper rupture zone (slip surface 1). Table A3.2 presents the sample's general information, and Table A3.3 presents information about the load and vertical stress applied to the sample during consolidation.

The consolidation test results are shown in Table A3.4 and Figure A3.2 presents the cumulative log-time/settlement curves for all stages of loading and unloading.

Table A3.2 Consolidation specimen's information.

General Information	
Start date : July 29, 2005	
Sample location : Borehole DH04-13, South Slide, Ashcroft	
Sample Depth : 16.1 (m)	
Sample Elevation : 259.9 (m)	
Specimen information	
$L_{(initial)}$: 27.55 (mm)	$D_{(initial)}$: 50.7 (mm)
$A_{(initial)}$: 2019 (mm^2)	Volume $_{(total)}$: 55.62 (cm^2)
$\rho_{(wet)}$: 1.964 (gr/cm^3)	$\rho_{(dry)}$: 1.509 (gr/cm^3)
G_s : 2.7 (assumed)	
$e_0 = G/\rho_D - 1 = 0.79$	
V_s : 31.09 (cm^3)	V_v: 24.529 (cm^3)
H_s (equivalent solid height) : 15.39 (mm)	
S_r (initial) : 100%	
W.C (from trimming) : 30.1 %	

Table A3.3 Consolidation loading stages.

Loading Stage	Load (kg)	Normal Stress (kPa)
1	4.46	21.65
2	10.46	50.78
3	20.262	98.36
4	50.002	242.72
5	106.248	515.75

Table A3.4 Consolidation test result's summary.

Load (kg)	Normal stress (kPa)	d_i (mm)	d_c (mm)	d_0 (mm)	d_{100} (mm)	t_{90} (min)	t_{50} (min)
4.46	21.65	0.00	0.00	0.0185	0.0455	1927	500
10.46	50.78	0.0365	0.0668	0.0661	0.0780	1200	100
20.26	98.36	0.0780	0.1319	0.1305	0.1495	1500	103
50.00	242.72	0.1489	0.4092	0.4095	0.4595	1500	58
106.25	515.75	0.4612	0.6873	0.6895	0.7635	1306	32
20.26	98.36	0.7640	0.6285	0.6285	0.6135	103	8
4.46	21.65	0.6084	0.5243	0.5255	0.4815	450	15

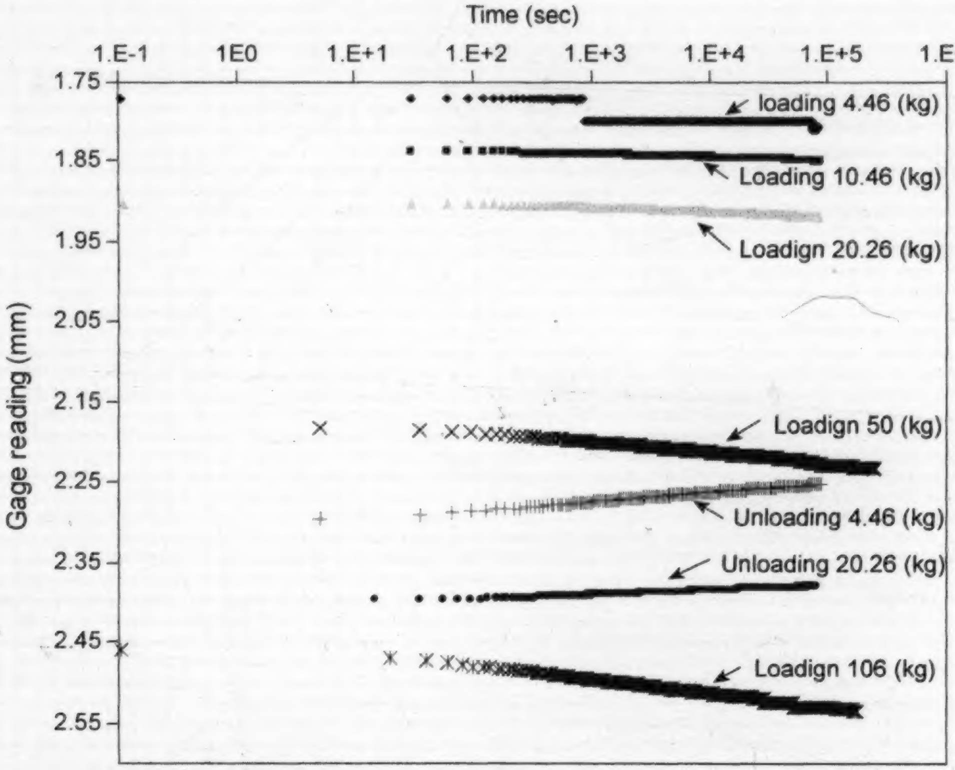

Figure A3.2 Cumulative log-time gauge reading for consolidation test on the selected specimen.

The coefficient of volume compressibility, coefficient of consolidation and coefficient of hydraulic conductivity were calculated from the consolidation test results. Table A3.5 presents the data for calculating the coefficient of volume compressibility, and Table A3.6 presents the data for calculating the coefficients of consolidation and coefficient of hydraulic conductivity. Figure A3.3 shows the void ratio versus the logP and C_v changes with pressure.

Table A3.5 Coefficient of volume compressibility calculation data.

Increment #	Void Ratio calculation				Volume compressibility			
	P (kPa)	ΔH (mm)	Δe= ΔH/H_s	e= e_0-Δe	δe	δP (kPa)	1+e_1	m_v= δe/δP(1000/(1+e)) (m^2/MN)
0	0.0	0	0	0.789	0	0	-	-
1	21.65	0.045	0.0030	0.786	0.0030	21.6	1.789	0.0763
2	50.78	0.078	0.0051	0.784	0.0021	29.1	1.786	0.0406
3	98.36	0.150	0.0097	0.779	0.0046	47.6	1.784	0.0547
4	242.72	0.460	0.0298	0.759	0.0201	144.4	1.779	0.0784
5	515.75	0.764	0.0496	0.739	0.0197	273.0	1.759	0.0411
6	98.36	0.614	0.0398	0.749	-0.0097	-417.4	-	-
7	21.65	0.482	0.0313	0.758	-0.0086	-76.4	-	-

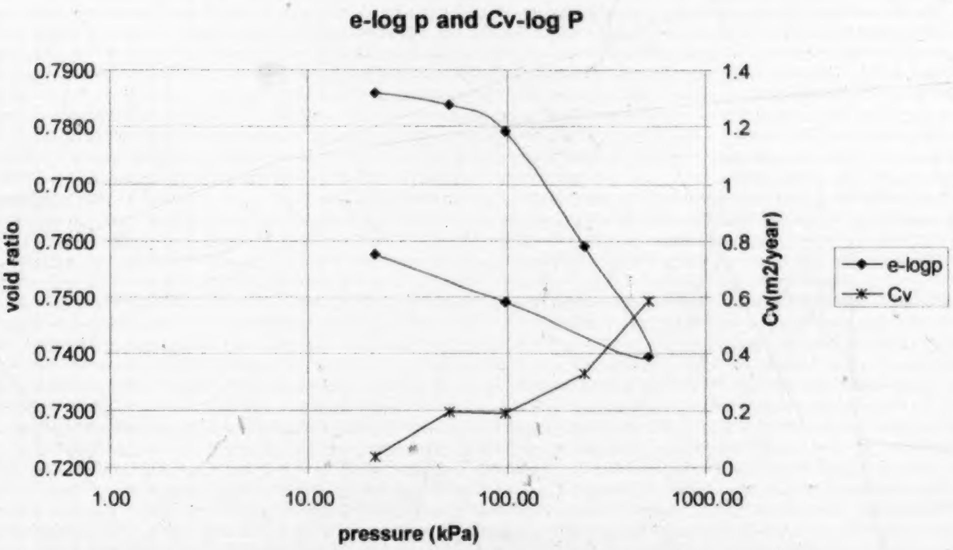

Figure A3.3 Void ratio versus log P and coefficient of consolidation (C_v) versus log P.

Table A3.6 Coefficient of consolidation and hydraulic conductivity data.

Iteration #	Coefficient of consolidation								Conductivity
	P (kPa)	ΔH (mm)	t_{50} (min)	H (mm)	$H_{average}$ (mm)	d (mm)	C_v (mm^2/ min)	C_v (m^2/year)	K (m/year)
0	0.0	0	-	27.55	-	-	-	-	-
1	21.65	0.045	500	27.50	27.53	13.76	0.075	0.039	9.3E-13
2	50.78	0.078	100	27.47	27.49	13.74	0.372	0.196	2.5E-12
3	98.36	0.150	103	27.40	27.44	13.72	0.359	0.189	3.2E-12
4	242.72	0.460	58	27.09	27.25	13.62	0.627	0.329	8.0E-12

From e-logp graph, coefficient of compression (C_c) was calculated to be 0.06. Although the material was believed to be overconsolidated, the graph shows an over consolidation ratio of around unity. Because the sample was taken from the shear zone, the overconsolidation ratio (OCR) for the soil from this sample could not be determined. The coefficient of hydraulic conductivity was calculated to be in the range of 7.5E-12 to 9.3E-13. The average conductivity of the soil layer should be much higher as the horizontal layering and sand lenses can increase the conductivity, especially in the horizontal direction.

A3.3. DIRECT SHEAR TESTS

Specimens from the samples taken from the shear zone were tested in a direct shear apparatus. Figure A3.4 to Figure A3.7 show the direct shear test graphs for the tested specimens. Table A3.7 provides the general information for the tested specimens and the results of the direct shear tests on the specimens.

Table A3.7 Specimens general information.

Specimen #	Sample tube	Borehole ID	Specimen depth (m)	Specimen Elev. (m)	Water content (%)	Normal stress (kPa)	τ_{Peak} (kPa)
1	5	DH04-13	16.1	259.9	30.1	21.65	34.5
2	5	DH04-13	16.3	259.7	36.4	242.72	128
3	5	DH04-13	17	259	47.5	242.72	80.5
4	5	DH04-13	16.7	259.3	44.6	515.75	160
5	4	DH04-13	14.6	261.4	38.5	515.75	190.2
6	4	DH04-13	15.3	260.7	37.1	98.35	56.3
7	4	DH04-13	15.0	261	42.5	197.03	88.7

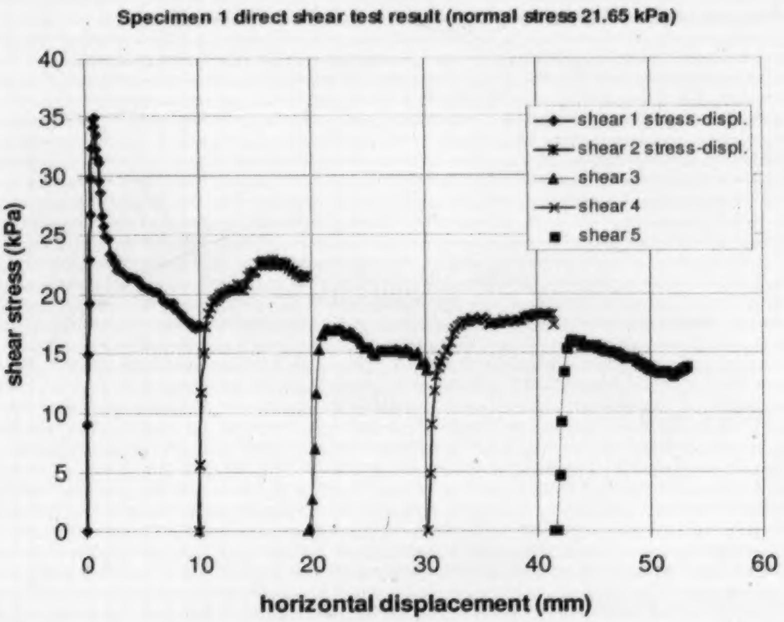

Figure A3.4 Specimen one direct shear test graph.

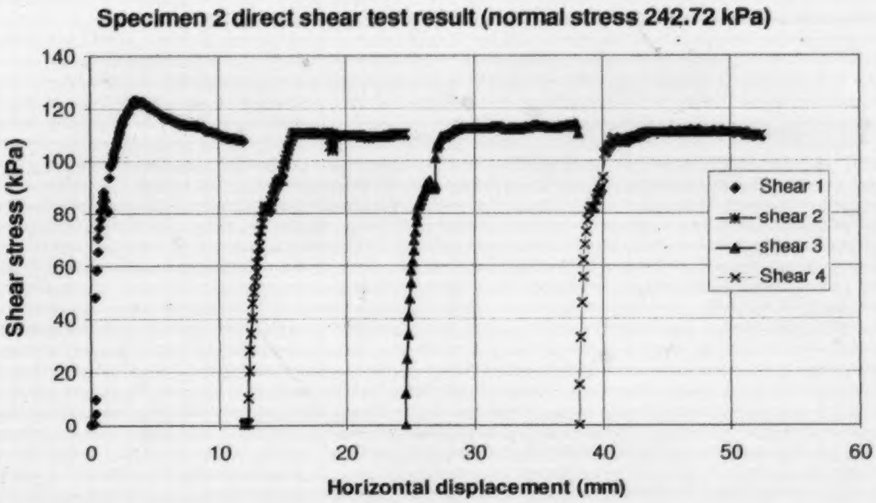

Figure A3.5 Specimen two direct shear test graphs.

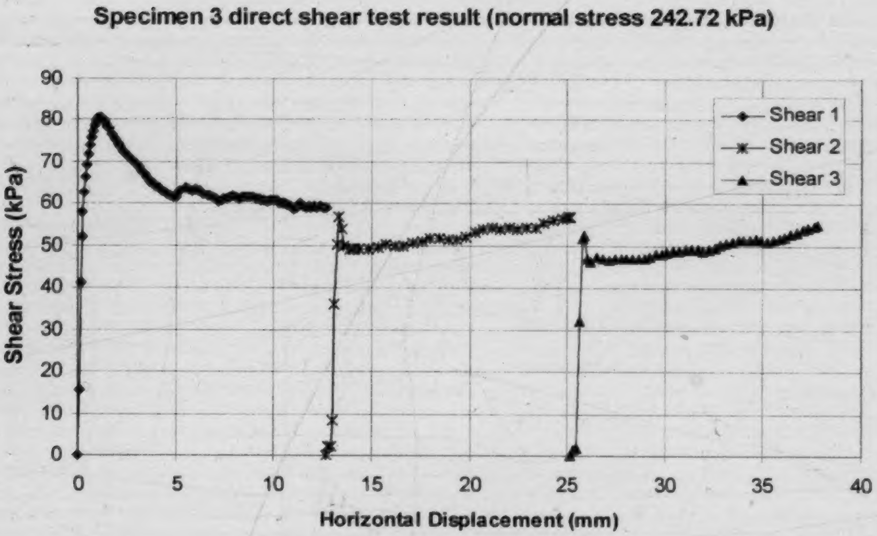

Figure A3.6 Specimen three direct shear test graphs.

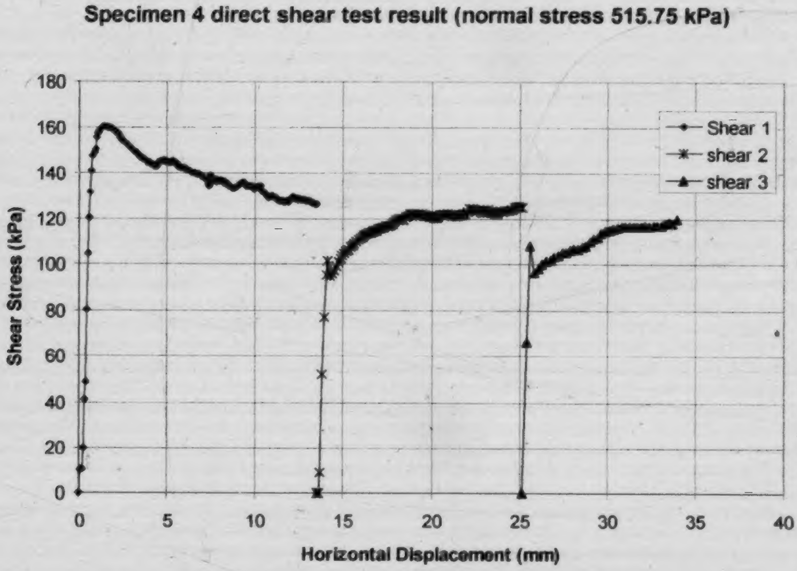

Figure A3.7 Specimen four direct shear test graphs.

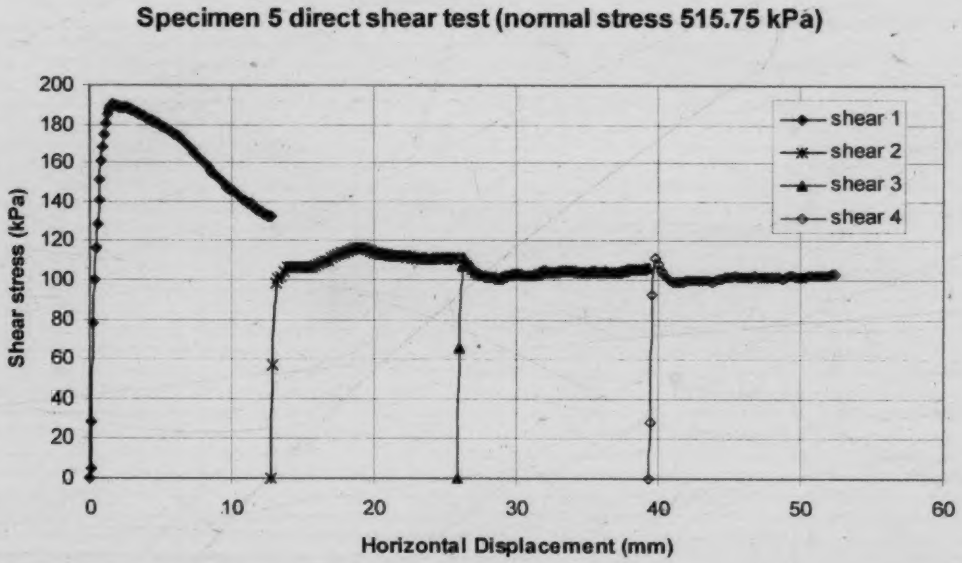

Figure A3.8 Specimen five direct shear test graphs.

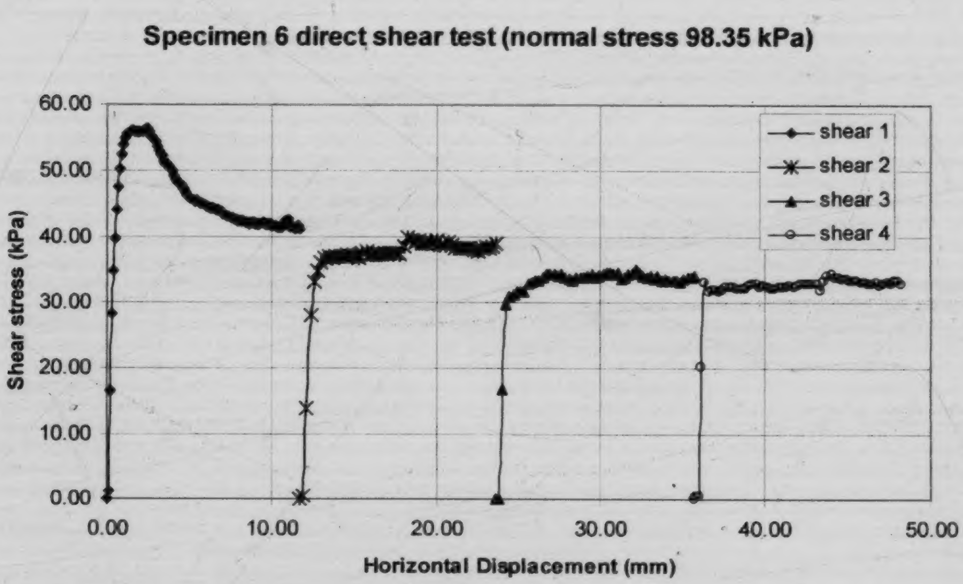

Figure A3.9 Specimen six direct shear test graphs.

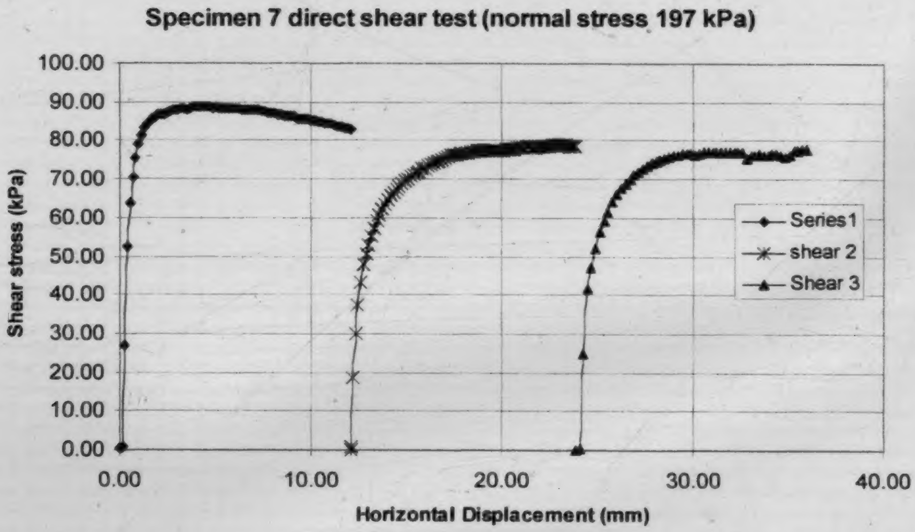

Figure A3.10 Specimen seven direct shear test graphs.

A3.4. MOISTURE CONTENT AND INDEX TESTS

Specimens for the liquid limit and plastic limit tests were taken from the trims of the direct shear specimens, and, in some cases, direct shear test specimens themselves were used directly. A Casagrande apparatus was used for the liquid limit test. The moisture contents of the specimens were calculated from the trims from the direct shear test specimens.

Table A3.8 to Table A3.15 show the calculation sheets for the Atterberg Limit tests on specimens. Figure A3.11 to Figure A3.18 show the liquid limit curves and the changes in the blow numbers with the water content. Table A3.16 presents the summary of the moisture content and the Atterberg Limit results for the tested specimens.

Table A3.8 Atterberg limit calculation sheet (specimen 1).

Specimen Number: 1		$W_{natural}$: 30.12 %		Test Date: August 17, 2005		
Liquid Limit	Trial #	1	2	3	4	5
	# Blows	10	14	17	40	24
	Container #	1	2	3	4	5
	W (wet soil+cont.)(gr)	13.5	10.8	10.38	12.14	15.85
	W(dry soil+cont.) (gr)	9.42	7.67	7.56	8.99	11.56
	W(water) (gr)	4.08	3.13	2.82	3.15	4.29
	W(container) (gr)	0.95	0.97	0.96	0.96	0.94
	W(dry soil) (gr)	8.47	6.7	6.6	8.03	10.62
	Water content (%)	48.17	46.72	42.73	39.23	40.40
Plastic Limit	Trial #	1	2	3	4	Average
	Container #	6	7	8		
	W (wet soil+cont.)(gr)	11.88	11.07	11.42		
	W(dry soil+cont.) (gr)	9.82	9.17	9.55		
	W(water) (gr)	2.06	1.9	1.87		
	W(container) (gr)	0.94	0.92	0.94		
	W(dry soil) (gr)	8.88	8.25	8.61		
	Water content (%)	23.20	23.03	21.72		22.65

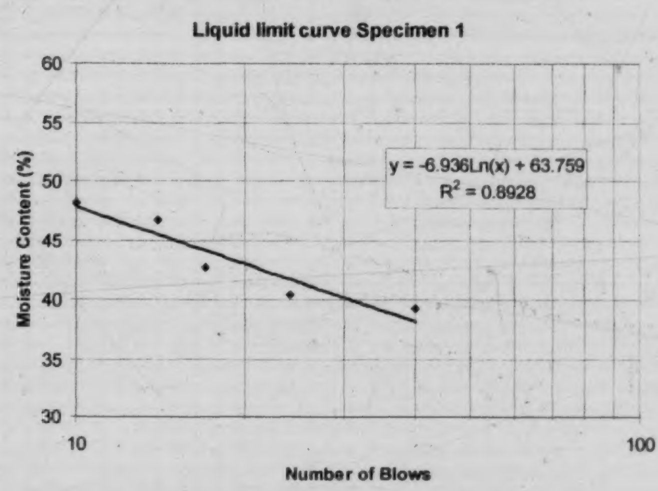

Figure A3.11 Liquid limit curve for specimen one.

Table A3.9 Atterberg limit calculation sheet (specimen 2).

	Specimen Number: 2	$W_{natural}$: 36.41 %		Test Date: August 30, 2005		
Liquid Limit	Trial #	1	2	3	4	5
	# Blows	5	10	35	24	23
	Container #	1	2	3	4	5
	W (wet soil+cont.)(gr)	10.89	13.94	14,84	19.2	16.53
	W(dry soil+cont.) (gr)	7.41	9.63	10.88	13.84	11.95
	W(water) (gr)	3.48	4.31	3.96	5.36	4.58
	W(container) (gr)	0.94	0.94	0.93	0.96	0.94
	W(dry soil) (gr)	6.47	8.69	9.95	12.88	11.01
	Water content (%)	53.79	49.60	39.80	41.61	41.60
Plastic Limit	Trial #	1	2	3	4	Average
	Container #	6	7	8		
	W (wet soil+cont.)(gr)	8.69	12.06	11.40		
	W(dry soil+cont.) (gr)	7.23	9.99	9.40		
	W(water) (gr)	1.46	2.07	2.00		
	W(container) (gr)	0.94	0.96	0.96		
	W(dry soil) (gr)	6.29	9.03	8.44		
	Water content (%)	23.21	22.92	23.70		23.28

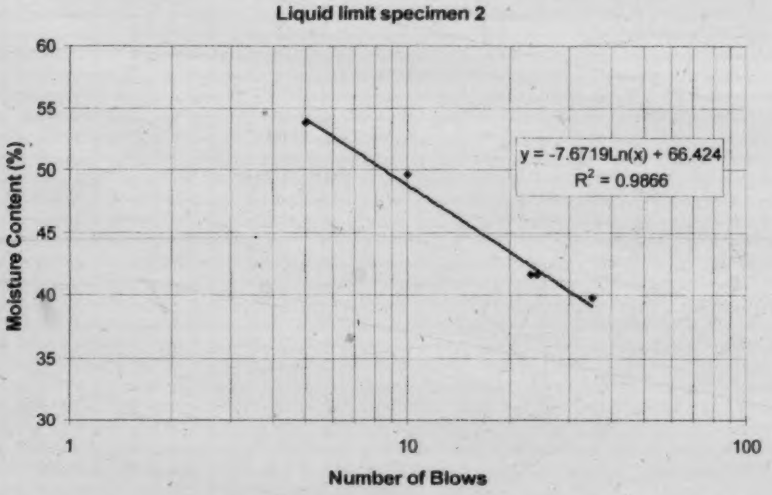

Figure A3.12 Liquid limit curve for specimen 2.

Table A3.10 Atterberg limit calculation sheet (specimen 3).

Specimen Number: 3 W $_{natural}$: 47.47 % Test Date: September 9, 2005

Liquid Limit	Trial #	1	2	3	4	5
	# Blows	13	37	23	18	45
	Container #	1	2	3	4	5
	W (wet soil+cont.)(gr)	12.2	13.35	16.80	12.97	15.53
	W(dry soil+cont.) (gr)	7.25	8.08	10.01	7.74	9.26
	W(water) (gr)	4.95	5.27	6.79	5.23	6.27
	W(container) (gr)	0.92	0.93	0.93	0.95	0.95
	W(dry soil) (gr)	6.33	7.15	9.08	6.79	8.31
	Water content (%)	78.20	73.71	74.78	77.03	75.45
Plastic Limit	Trial #	1	2	3	4	Average
	Container #	6	7	8		
	W (wet soil+cont.)(gr)	7.16	6.10	10.86		
	W(dry soil+cont.) (gr)	5.59	4.81	8.43		
	W(water) (gr)	1.57	1.29	2.43		
	W(container) (gr)	0.94	0.97	0.96		
	W(dry soil) (gr)	4.65	3.84	7.47		
	Water content (%)	33.76	33.59	32.53		33.30

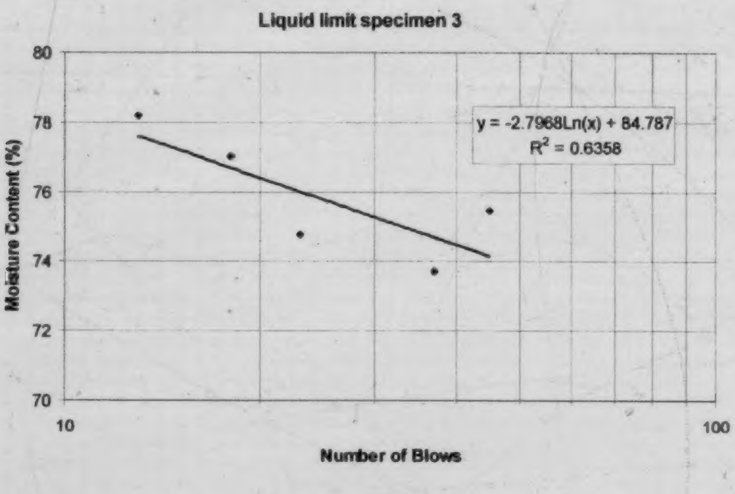

Figure A3.13 Liquid limit curve for specimen 3.

Table A3.11 Atterberg limit calculation sheet (specimen 4).

Specimen Number: 4		W $_{natural}$: 44.62 %		Test Date: September 17, 2005		
Liquid Limit	Trial #	1	2	3	4	5
	# Blows	13	28	34	34	18
	Container #	1	2	3	4	5
	W (wet soil+cont.)(gr)	14.12	17.48	18.00	15.03	18.42
	W(dry soil+cont.) (gr)	8.68	11.09	11.21	9.42	11.20
	W(water) (gr)	5.44	6.39	6.79	5.61	7.22
	W(container) (gr)	0.94	0.94	0.94	0.94	0.93
	W(dry soil) (gr)	7.74	10.15	10.27	8.48	10.27
	Water content (%)	70.28	62.96	66.11	66.16	70.30
Plastic Limit	Trial #	1	2	3	4	Average
	Container #	6	7	8		
	W (wet soil+cont.)(gr)	14.24	11.01	10.15		
	W(dry soil+cont.) (gr)	11.13	8.1	8.75		
	W(water) (gr)	3.11	2.91	1.4		
	W(container) (gr)	0.93	0.93	0.93		
	W(dry soil) (gr)	10.2	7.17	7.82		
	Water content (%)	30.49	40.59	17.90		29.66

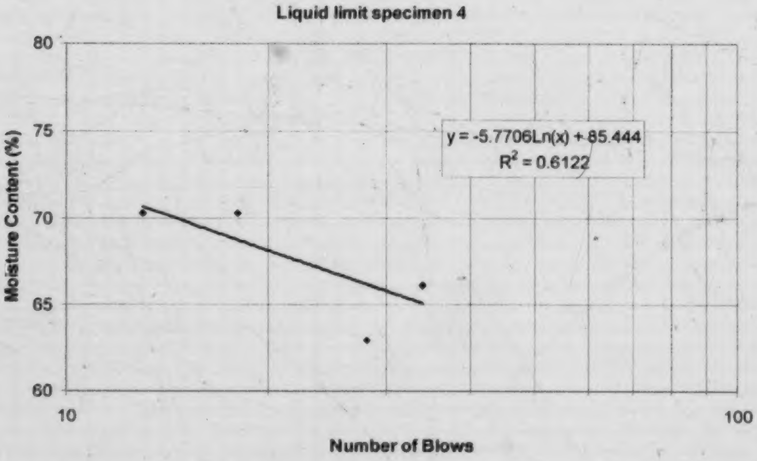

Figure A3.14 Liquid limit curve for specimen 4.

Table A3.12 Atterberg limit calculation sheet (specimen 5).

Specimen Number: 5		$W_{natural}$: 38.53 %		Test Date: September 2005		
Liquid Limit	Trial #	1	2	3	4	5
	# Blows	14	17	26	33	50
	Container #	1	2	3	4	5
	W (wet soil+cont.)(gr)	13.88	9.94	13.81	15.87	17.38
	W(dry soil+cont.) (gr)	9.13	6.75	9.38	10.79	11.91
	W(water) (gr)	4.75	3.19	4.43	5.08	5.47
	W(container) (gr)	0.97	0.94	0.95	1	0.94
	W(dry soil) (gr)	8.16	5.81	8.43	9.79	10.97
	Water content (%)	58.21	54.91	52.55	51.89	49.86
Plastic Limit	Trial #	1	2	3	4	Average
	Container #	6	7	8		
	W (wet soil+cont.)(gr)	11.52	10.7	11.84		
	W(dry soil+cont.) (gr)	9.4	8.78	9.66		
	W(water) (gr)	2.12	1.92	2.18		
	W(container) (gr)	0.95	1.03	0.95		
	W(dry soil) (gr)	8.45	7.75	8.71		
	Water content (%)	25.09	24.77	25.03		24.96

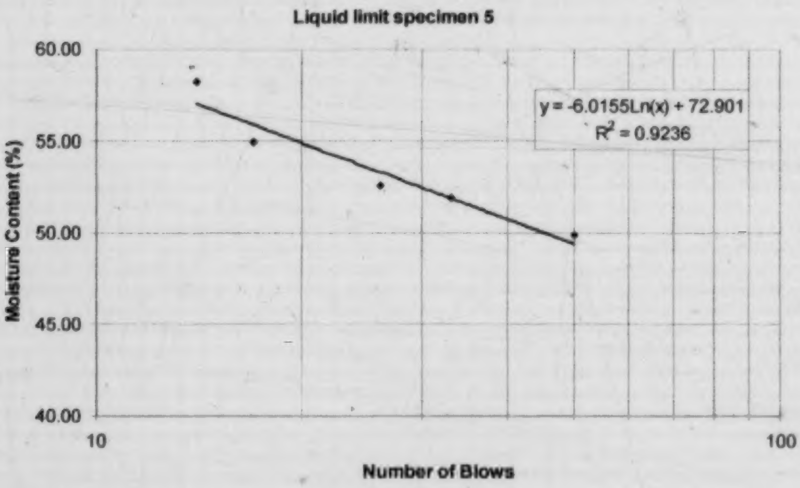

Figure A3.15 Liquid limit curve for specimen 5.

Table A3.13 Atterberg Limit calculation sheet (specimen 6).

Specimen Number: 6		$W_{natural}$: 37.05 %		Test Date: October, 2005		
Liquid Limit	Trial #	1	2	3	4	5
	# Blows	20	30	43	39	23
	Container #	1	2	3	4	5
	W (wet soil+cont.)(gr)	12.38	12.73	13.45	15.56	18.08
	W(dry soil+cont.) (gr)	8.53	8.84	9.41	10.78	12.31
	W(water) (gr)	3.85	3.89	4.04	4.78	5.77
	W(container) (gr)	0.96	0.95	0.96	0.96	0.96
	W(dry soil) (gr)	7.57	7.89	8.45	9.82	11.35
	Water content (%)	50.86	49.30	47.81	48.68	50.84
Plastic Limit	Trial #	1	2	3	4	Average
	Container #	6	7	8		
	W (wet soil+cont.)(gr)	16.69	10.23	10.51		
	W(dry soil+cont.) (gr)	13.61	8.4	8.64		
	W(water) (gr)	3.08	1.83	1.87		
	W(container) (gr)	0.95	0.95	0.94		
	W(dry soil) (gr)	12.66	7.45	7.7		
	Water content (%)	24.33	24.56	24.29		24.39

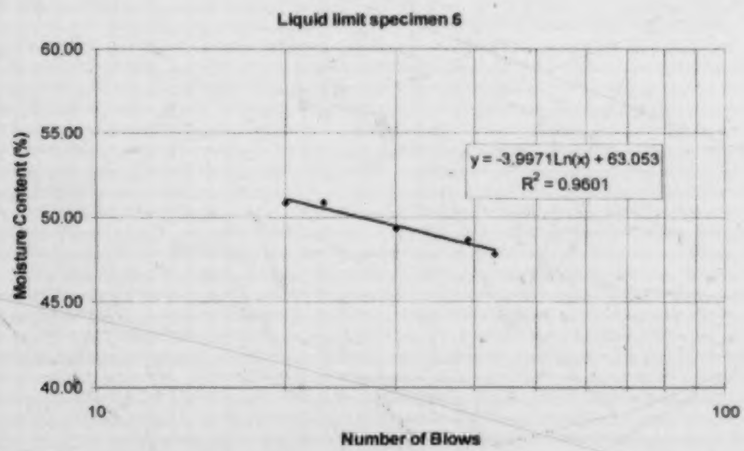

Figure A3.16 Liquid limit curve for specimen 6.

Table A3.14 Atterberg limit calculation sheet (specimen 7).

Specimen Number: 7		W $_{natural}$: 42.53 %		Test Date: October, 2005		
Liquid Limit	Trial #	1	2	3	4	5
	# Blows	27	50	38	18	12
	Container #	1	2	3	4	5
	W (wet soil+cont.)(gr)	16.85	14.66	12.54	14.79	15
	W(dry soil+cont.) (gr)	11.32	10.09	8.51	9.75	9.84
	W(water) (gr)	5.53	4.57	4.03	5.04	5.16
	W(container) (gr)	0.95	0.97	0.97	0.96	0.94
	W(dry soil) (gr)	10.37	9.12	7.54	8.79	8.9
	Water content (%)	53.33	50.11	53.45	57.34	57.98
Plastic Limit	Trial #	1	2	3	4	Average
	Container #	6	7	8		
	W (wet soil+cont.)(gr)	10.53	10.06	9.71		
	W(dry soil+cont.) (gr)	8.64	8.28	7.96		
	W(water) (gr)	1.89	1.78	1.75		
	W(container) (gr)	0.95	0.95	0.94		
	W(dry soil) (gr)	7.69	7.33	7.02		
	Water content (%)	24.58	24.28	24.93		24.60

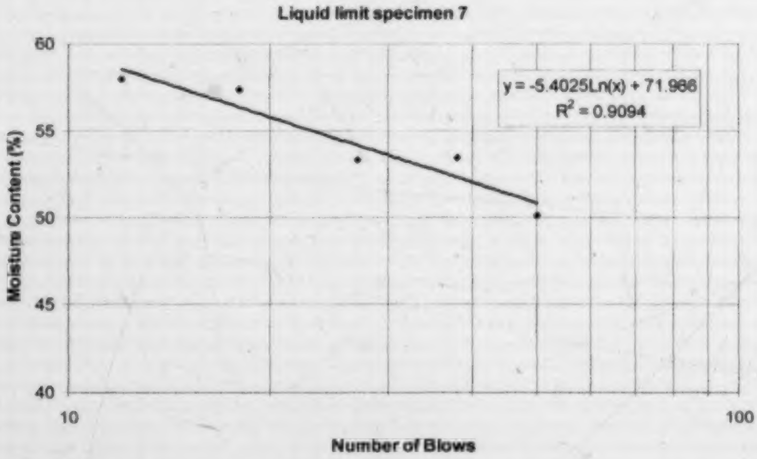

Figure A3.17 Liquid limit curve for specimen 7.

Table A3.15 Atterberg limit calculation sheet (specimen 8).

Specimen Number: 8		$W_{natural}$: 34.50 %		Test Date: November, 2005		
Liquid Limit	Trial #	1	2	3	4	5
	# Blows	10	15	20	35	50
	Container #	1	2	3	4	5
	W (wet soil+cont.)(gr)	14.56	15.69	16.53	14.34	14.07
	W(dry soil+cont.) (gr)	9.41	10.16	10.81	9.62	9.35
	W(water) (gr)	5.15	5.53	5.72	4.72	4.72
	W(container) (gr)	0.94	0.96	0.94	0.95	0.96
	W(dry soil) (gr)	8.47	9.2	9.87	8.67	8.39
	Water content (%)	60.80	60.11	57.95	54.44	56.26
Plastic Limit	Trial #	1	2	3	4	Average
	Container #	6	7	8		
	W (wet soil+cont.)(gr)	14.43	11.36	10.47		
	W(dry soil+cont.) (gr)	11.8	9.34	8.6		
	W(water) (gr)	2.63	2.02	1.87		
	W(container) (gr)	0.95	0.95	0.94		
	W(dry soil) (gr)	10.85	8.39	7.66		
	Water content (%)	24.24	24.08	24.41		24.24

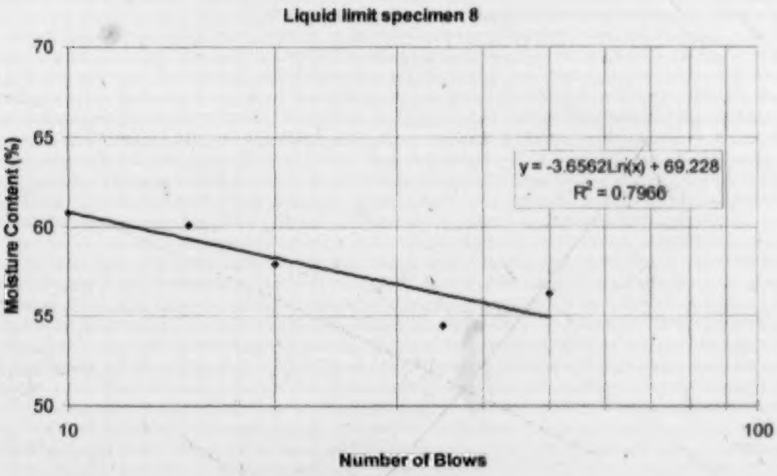

Figure A3.18 Liquid limit curve for specimen 8.

Table A3.16 Results of water content and Atterberg Limit tests.

Specimen #	Tube #	W.C. (%)	Liquid Limit (LL) (%)	Plastic Limit (LL) (%)	Plasticity Index (PI) (%)
1	5	30.12	41	23	18
2	5	36.41	42	23	19
3	5	47.47	76	33	43
4	5	44.62	67	30	37
5	4	38.53	54	25	29
6	4	37.05	50	24	26
7	4	42.53	55	25	31
8	1	34.50	57	24	33

A3.5. PARTICLE-SIZE DISTRIBUTION

The specimens tested in the Atterberg Limit and water content tests were used to conduct particle-size distribution tests. As all the specimens were fine-grained soil, only hydrometry tests had to be conducted on them.

A hydrometer type 152H was used in all cases. The test was conducted according to ASTM D422 procedure. For each specimen, two hydrometry tests were run at the same time to confirm the accuracy of the test. The results from these two identical hydrometry tests for each specimen are presented in two tables for each specimen. The average particle-size distribution for each specimen is also presented in a figure.

Figure A3.27 presents the summary of the particle-size distribution curves, and Table A3.33 provides the summary of the particle-size analysis of the specimens.

Table A3.17 Hydrometry test data sheet (test 1, specimen 1).

Specimen 1		Test 1	Gs:2.70		Date: Aug 23, 2005			Cd=1	Cm=1	
t (min)	R'_h	Temp. (°C)	Ct	R_h	R'_h+C_m	L (cm)	L/t	K	Finer %	D (mm)
0.5	53	21	0.2	52.2	54	7.4	14.89	0.0139	100	0.0536
1	51	21	0.2	50.2	52	7.8	7.767	0.0139	99.40	0.0387
2	50	21	0.2	49.2	51	7.9	3.966	0.0139	97.42	0.0277
4	49	21	0.2	48.2	50	8.1	2.024	0.0139	95.44	0.0198
8	46	21	0.2	45.2	47	8.6	1.073	0.0139	89.50	0.0144
16	43	21	0.2	42.2	44	9.1	0.567	0.0139	83.56	0.0105
30	37	21	0.2	36.2	38	10.1	0.336	0.0139	71.68	0.0081
60	31	21	0.2	30.2	32	11.0	0.184	0.0139	59.80	0.0060
120	26	21	0.2	25.2	27	11.9	0.099	0.0139	49.90	0.0044
240	23	21	0.2	22.2	24	12.4	0.052	0.0139	43.96	0.0032
480	18	21	0.2	17.2	19	13.2	0.028	0.0139	34.06	0.0023
1380	14	21	0.2	13.2	15	13.8	0.010	0.0139	26.14	0.0014
1920	9	21	0.2	8.2	10	14.7	0.008	0.0139	16.24	0.0012
2820	6	21	0.2	5.2	7	15.2	0.005	0.0139	10.30	0.0010

Table A3. 18 Hydrometry test data sheet (test 2, specimen 1).

Specimen 1		Test 2	Gs:2.70		Date: Aug 23, 2005			Cd=1	Cm=1	
t (min)	R'_h	Temp. (°C)	Ct	R_h	R'_h+C_m	L (cm)	L/t	K	Finer %	D (mm)
0.5	54.0	21	0.2	53.2	55.0	7.3	14.55	0.0139	100	0.0530
1	52.0	21	0.2	51.2	53.0	7.6	7.60	0.0139	100	0.0383
2	50.0	21	0.2	49.2	51.0	7.9	3.97	0.0139	97.42	0.0277
4	49.0	21	0.2	48.2	50.0	8.1	2.02	0.0139	95.44	0.0198
8	47.0	21	0.2	46.2	48.0	8.4	1.05	0.0139	91.48	0.0143
15	43.0	21	0.2	42.2	44.0	9.1	0.60	0.0139	83.56	0.0108
30	37.0	21	0.2	36.2	38.0	10.1	0.335	0.0139	71.68	0.0081
60	31.0	21	0.2	30.2	32.0	11.0	0.184	0.0139	59.80	0.0060
120	28.0	21	0.2	27.2	29.0	11.5	0.096	0.0139	53.86	0.0043
240	23.0	21	0.2	22.2	24.0	12.4	0.051	0.0139	43.96	0.0032
480	19.0	21	0.2	18.2	20.0	13.0	0.027	0.0139	36.04	0.0023
1380	15.0	21	0.2	14.2	16.0	13.7	0.01	0.0139	28.12	0.0014
1920	10.0	21	0.2	9.2	11.0	14.5	0.007	0.0139	18.22	0.0012
2820	7.0	21	0.2	6.2	8.0	15.0	0.005	0.0139	12.28	0.0010

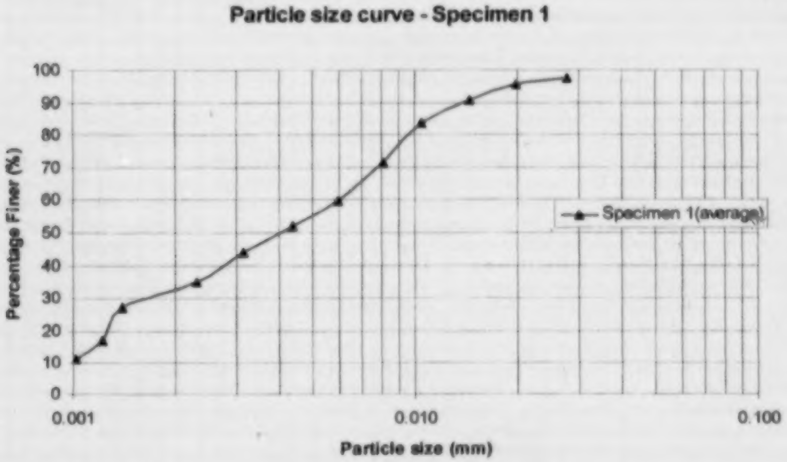

Figure A3.19 Average particle size distribution curve for specimen 1.

Table A3.19 Hydrometry test data sheet (test 1, specimen 2).

Specimen 2 Test 1 Gs:2.70 Date: Sept. 1, 2005 C_d=2 C_m=1

t (min)	R'_h	Temp. (°C)	Ct	R_h	R'_h+C_m	L (cm)	L/t	K	Finer %	D (mm)
0.5	55.0	21	0.2	53.2	56.0	7.1	14.22	0.0139	100	0.0524
1.0	52.0	21	0.2	50.2	53.0	7.6	7.60	0.0139	99.40	0.0383
2.0	52.0	21	0.2	50.2	53.0	7.6	3.80	0.0139	99.40	0.0271
4.0	51.0	21	0.2	49.2	52.0	7.8	1.95	0.0139	97.42	0.0194
8.0	49.5	21	0.2	47.7	50.5	8.0	1.00	0.0139	94.45	0.0139
15.0	46.0	21	0.2	44.2	47.0	8.6	0.573	0.0139	87.52	0.0105
30.0	40.0	21	0.2	38.2	41.0	9.6	0.319	0.0139	75.64	0.0079
60.0	34.0	21	0.2	32.2	35.0	10.6	0.176	0.0139	63.76	0.0058
120.0	28.0	21	0.2	26.2	29.0	11.5	0.096	0.0139	51.88	0.0043
240	25.0	21	0.2	23.2	26.0	12.0	0.050	0.0139	45.94	0.0031
480	20.0	21	0.2	18.0	21.0	12.9	0.027	0.0141	35.64	0.0023
1410	15.5	21	0.2	13.7	16.5	13.6	0.01	0.0139	27.13	0.0014
1581	14.0	21	0.2	12.2	15.0	13.8	0.009	0.0139	24.16	0.0013

Table A3.20 Hydrometry test data sheet (test 2, specimen 2).

Specimen 2		Test 1	Gs:2.70		Date: Sept. 1, 2005			C_d=2	C_m=1	
t (min)	R'_h	Temp. (°C)	Ct	R_h	R'_h+C_m	L (cm)	L/t	K	Finer %	D (mm)
0.5	54.0	21	0.2	52.2	55.0	7.3	14.55	0.0139	100	0.0530
1.0	53.0	21	0.2	51.2	54.0	7.4	7.439	0.0139	100	0.0379
2.0	53.0	21	0.2	51.2	54.0	7.4	3.719	0.0139	100	0.0268
4.0	52.0	21	0.2	50.2	53.0	7.6	1.900	0.0139	99.40	0.0192
8.0	50.0	21	0.2	48.2	51.0	7.9	0.991	0.0139	95.44	0.0138
15.0	46.0	21	0.2	44.2	47.0	8.6	0.572	0.0139	87.52	0.0105
30.0	41.0	21	0.2	39.2	42.0	9.4	0.314	0.0139	77.62	0.0078
60.0	35.0	21	0.2	33.2	36.0	10.4	0.173	0.0139	65.74	0.0058
120.0	29.0	21	0.2	27.2	30.0	11.4	0.095	0.0139	53.86	0.0043
240	25.0	21	0.2	23.2	26.0	12.0	0.050	0.0139	45.94	0.0031
480	21.5	21	0.2	19.7	22.5	12.6	0.026	0.0139	39.01	0.0023
1410	16.5	21	0.2	14.5	17.5	13.4	0.01	0.0141	28.71	0.0014
1581	15.0	21	0.2	13.2	16.0	13.7	0.009	0.0139	26.14	0.0013

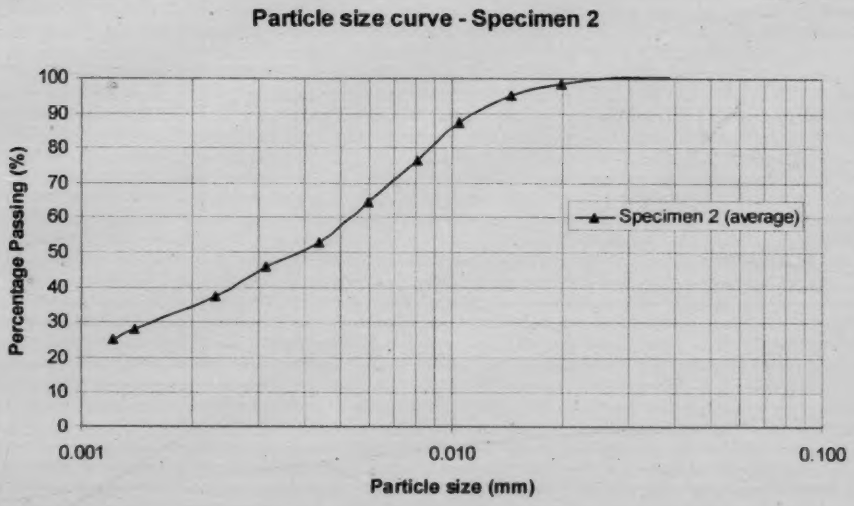

Figure A3.20 Average particle size distribution curve for specimen 2.

Table A3.21 Hydrometry test data sheet (test 1, specimen 3).

Specimen 3		Test 1	Gs:2.70		Date: Sept. 2005			C_d=1	C_m=1	
t (min)	R'_h	Temp. (°C)	Ct	R_h	R'_h+C_m	L (cm)	L/t	K	Finer %	D (mm)
0.5	54.5	20.0	0.00	50.0	55.5	7.2	14.38	0.0141	100	0.0535
1.0	54.5	20.0	0.00	50.0	55.5	7.2	7.192	0.0141	99.00	0.0378
2.0	54.5	20.0	0.00	50.0	55.5	7.2	3.596	0.0141	99.00	0.0267
4.0	54.0	20.0	0.00	49.5	55.0	7.3	1.818	0.0141	98.01	0.0190
8.0	54.0	20.0	0.00	49.5	55.0	7.3	0.909	0.0141	98.01	0.0134
15.0	53.0	20.0	0.00	48.5	54.0	7.4	0.496	0.0141	96.03	0.0099
30.0	52.0	20.0	0.00	47.5	53.0	7.6	0.253	0.0141	94.05	0.0071
60.0	52.0	20.0	0.00	47.5	53.0	7.6	0.127	0.0141	94.05	0.0050
120.0	50.5	20.0	0.00	46.0	51.5	7.8	0.065	0.0141	91.08	0.0036
240	50.0	20.0	0.00	45.5	51.0	7.9	0.033	0.0141	90.09	0.0026
480	48.0	20.0	0.00	43.5	49.0	8.3	0.017	0.0141	86.13	0.0018
1440	43.0	20.0	0.00	38.5	44.0	9.1	0.006	0.0141	76.23	0.0011
2880	38.0	20.0	0.00	33.5	39.0	9.9	0.003	0.0141	66.33	0.0008

Table A3.22 Hydrometry test data sheet (test 2, specimen 3).

Specimen 3		Test 2	Gs:2.70		Date: Sept. 2005			C_d=1	C_m=1	
t (min)	R'_h	Temp. (°C)	Ct	R_h	R'_h+C_m	L (cm)	L/t	K	Finer %	D (mm)
0.5	54.0	20.0	0.00	49.5	55.0	7.3	14.55	0.0141	98.01	0.0538
1.0	54.0	20.0	0.00	49.5	55.0	7.3	7.274	0.0141	98.01	0.0380
2.0	54.0	20.0	0.00	49.5	55.0	7.3	3.637	0.0141	98.01	0.0269
4.0	54.0	20.0	0.00	49.5	55.0	7.3	1.819	0.0141	98.01	0.0190
8.0	54.0	20.0	0.00	49.5	55.0	7.3	0.909	0.0141	98.01	0.0134
15.0	53.5	20.0	0.00	49.0	54.5	7.4	0.490	0.0141	97.02	0.0099
30.0	53.0	20.0	0.00	48.5	54.0	7.4	0.248	0.0141	96.03	0.0070
60.0	52.0	20.0	0.00	47.5	53.0	7.6	0.127	0.0141	94.05	0.0050
120.0	52.0	20.0	0.00	47.5	53.0	7.6	0.063	0.0141	94.05	0.0035
240	50.0	20.0	0.00	45.5	51.0	7.9	0.033	0.0141	90.09	0.0026
480	48.0	20.0	0.00	43.5	49.0	8.3	0.017	0.0141	86.13	0.0018
1440	45.0	20.0	0.00	40.5	46.0	8.8	0.006	0.0141	80.19	0.0011
2880	34.0	20.0	0.00	29.5	35.0	10.6	0.004	0.0141	58.41	0.0009

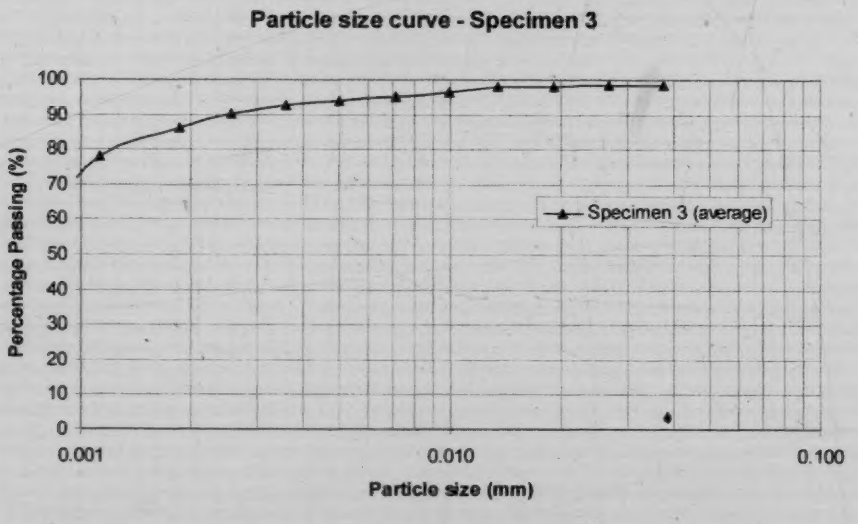

Figure A3.21 Average particle size distribution curve for specimen 3.

Table A3.23 Hydrometry test data sheet (test 1, specimen 4).

Specimen 4		Test 1	Gs:2.70		Date: Sept. 2005			C_d=4	C_m=1.5	
t (min)	R'_h	Temp. (°C)	C_t	R_h	R'_h+C_m	L (cm)	L/t	K	Finer %	D (mm)
0.5	54.5	20.0	0.00	50.5	56.0	7.1	14.22	0.0141	100	0.0532
1.0	54.5	20.0	0.00	50.5	56.0	7.1	7.11	0.0141	99.99	0.0376
2.0	54.5	20.0	0.00	50.5	56.0	7.1	3.55	0.0141	99.99	0.0266
4.0	54.5	20.0	0.00	50.5	56.0	7.1	1.778	0.0141	99.99	0.0188
8.0	54.5	20.0	0.00	50.5	56.0	7.1	0.889	0.0141	99.99	0.0133
15.0	54.0	20.0	0.00	50.0	55.5	7.2	0.479	0.0141	99.00	0.0098
30.0	53.0	20.0	0.00	49.0	54.5	7.4	0.245	0.0141	97.02	0.0070
60.0	51.5	20.0	0.00	47.5	53.0	7.6	0.127	0.0141	94.05	0.0050
120.0	50.0	20.0	0.00	46.0	51.5	7.8	0.065	0.0141	91.08	0.0036
240	48.0	20.0	0.00	44.0	49.5	8.2	0.034	0.0141	87.12	0.0026
480	45.0	20.0	0.00	41.0	46.5	8.7	0.018	0.0141	81.18	0.0019
1440	43.0	20.0	0.00	39.0	44.5	9.0	0.006	0.0141	77.22	0.0011
2880	31.0	20.0	0.00	27.0	32.5	11.0	0.004	0.0141	53.46	0.0009

Table A3.24 Hydrometry test data sheet (test 2, specimen 4).

Specimen 4		Test 1	Gs:2.70		Date: Sept. 2005			C_d=4	C_m=1.5	
t (min)	R'_h	Temp. (°C)	C_t	R_h	R'_h+C_m	L (cm)	L/t	K	Finer %	D (mm)
0.5	54.5	20.0	0.00	50.5	56.0	7.1	14.22	0.0141	100	0.0532
1.0	54.5	20.0	0.00	50.5	56.0	7.1	7.11	0.0141	100	0.0376
2.0	54.5	20.0	0.00	50.5	56.0	7.1	3.55	0.0141	100	0.0266
4.0	54.5	20.0	0.00	50.5	56.0	7.1	1.77	0.0141	100	0.0188
8.0	54.5	20.0	0.00	50.5	56.0	7.1	0.888	0.0141	99.99	0.0133
15.0	54.0	20.0	0.00	50.0	55.5	7.2	0.479	0.0141	99.00	0.0098
30.0	53.0	20.0	0.00	49.0	54.5	7.4	0.245	0.0141	97.02	0.0070
60.0	51.5	20.0	0.00	47.5	53.0	7.6	0.126	0.0141	94.05	0.0050
120.0	50.0	20.0	0.00	46.0	51.5	7.8	0.065	0.0141	91.08	0.0036
240	47.5	20.0	0.00	43.5	49.0	8.3	0.034	0.0141	86.13	0.0026
480	45.0	20.0	0.00	41.0	46.5	8.7	0.018	0.0141	81.18	0.0019
1440	41.0	20.0	0.00	37.0	42.5	9.3	0.006	0.0141	73.26	0.0011
2880	29.0	20.0	0.00	25.0	30.5	11.3	0.004	0.0141	49.50	0.0009

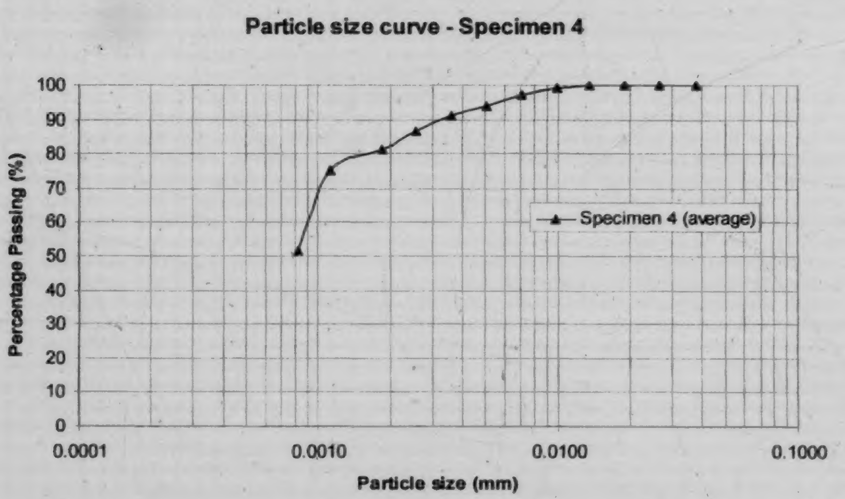

Figure A3.22 Average particle size distribution curve for specimen 4.

Table A3.25 Hydrometry test data sheet (test 1 specimen 5).

Specimen 5		Test 1	Gs:2.70		Date: Sept. 2005			C_d=5	C_m=1	
t (min)	R'_h	Temp. (°C)	C_t	R_h	R'_h+C_m	L (cm)	L/t	K	Finer %	D (mm)
0.5	52.5	20.0	0.0	47.5	53.5	7.5	15.04	0.0141	94.05	0.0547
1.0	52.0	20.0	0.0	47.0	53.0	7.6	7.60	0.0141	93.06	0.0389
2.0	52.0	20.0	0.0	47.0	53.0	7.6	3.80	0.0141	93.06	0.0275
4.0	51.5	20.0	0.0	46.5	52.5	7.7	1.92	0.0141	92.07	0.0195
8.0	50.5	20.0	0.0	45.5	51.5	7.8	0.98	0.0141	90.09	0.0140
15.0	48.0	20.0	0.0	43.0	49.0	8.3	0.55	0.0141	85.14	0.0105
30.0	45.0	20.0	0.0	40.0	46.0	8.8	0.29	0.0141	79.20	0.0076
60.0	41.0	20.0	0.0	36.0	42.0	9.4	0.157	0.0141	71.28	0.0056
120.0	38.0	20.0	0.0	33.0	39.0	9.9	0.083	0.0141	65.34	0.0040
240	33.5	20.0	0.0	28.5	34.5	10.6	0.044	0.0141	56.43	0.0030
508	30.0	20.0	0.0	25.0	31.0	11.2	0.022	0.0141	49.50	0.0021
1440	25.0	20.0	0.0	20.0	26.0	12.0	0.008	0.0141	39.60	0.0013
2880	22.0	20.0	0.0	17.0	23.0	12.5	0.004	0.0141	33.66	0.0009

Table A3.26 Hydrometry test data sheet (test 2 specimen 5).

Specimen 5		Test 2	Gs:2.70		Date: Sept. 2005			C_d=5	C_m=1	
t (min)	R'_h	Temp. (°C)	C_t	R_h	R'_h+C_m	L (cm)	L/t	K	Finer %	D (mm)
0.5	52.0	20.0	0.0	47.0	53.0	7.6	15.20	0.0141	93.06	0.0550
1.0	52.0	20.0	0.0	47.0	53.0	7.6	7.60	0.0141	93.06	0.0389
2.0	51.5	20.0	0.0	46.5	52.5	7.7	3.84	0.0141	92.07	0.0276
4.0	51.0	20.0	0.0	46.0	52.0	7.8	1.94	0.0141	91.08	0.0196
8.0	50.5	20.0	0.0	45.5	51.5	7.8	0.981	0.0141	90.09	0.0140
15.0	48.5	20.0	0.0	43.5	49.5	8.2	0.545	0.0141	86.13	0.0104
30.0	45.0	20.0	0.0	40.0	46.0	8.8	0.292	0.0141	79.20	0.0076
60.0	41.5	20.0	0.0	36.5	42.5	9.3	0.155	0.0141	72.27	0.0056
120.0	38.0	20.0	0.0	33.0	39.0	9.9	0.083	0.0141	65.34	0.0040
240	34.0	20.0	0.0	29.0	35.0	10.6	0.044	0.0141	57.42	0.0030
508	29.5	20.0	0.0	24.5	30.5	11.3	0.022	0.0141	48.51	0.0021
1440	25.0	20.0	0.0	20.0	26.0	12.0	0.008	0.0141	39.60	0.0013
2880	22.0	20.0	0.0	17.0	23.0	12.5	0.004	0.0141	33.66	0.0009

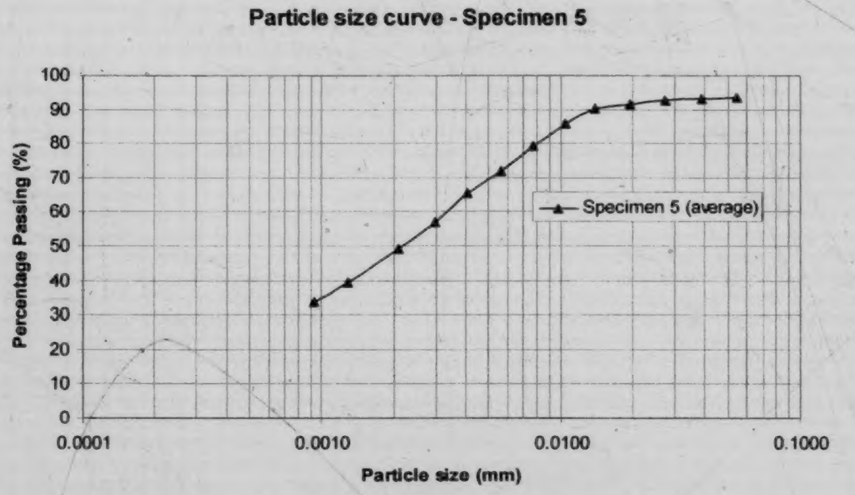

Figure A3.23 Average particle size distribution curve for specimen 5.

Table A3.27 Hydrometry test data sheet (test 1 specimen 6).

Specimen 6		Test 1	Gs:2.70		Date: Oct. 2005			C_d=6	C_m=1.5	
t (min)	R'_h	Temp. (°C)	C_t	R_h	R'_h+C_m	L (cm)	L/t	K	Finer %	D (mm)
0.5	54.0	20.0	0.0	48.0	55.5	7.2	14.38	0.0141	95.04	0.0535
1.0	53.5	20.0	0.0	47.5	55.0	7.3	7.27	0.0141	94.05	0.0380
2.0	53.5	20.0	0.0	47.5	55.0	7.3	3.63	0.0141	94.05	0.0269
4.0	52.5	20.0	0.0	46.5	54.0	7.4	1.86	0.0141	92.07	0.0192
8.0	51.5	20.0	0.0	45.5	53.0	7.6	0.95	0.0141	90.09	0.0137
15.0	49.0	20.0	0.0	43.0	50.5	8.0	0.534	0.0141	85.14	0.0103
30.0	46.0	20.0	0.0	40.0	47.5	8.5	0.284	0.0141	79.20	0.0075
60.0	42.5	20.0	0.0	36.5	44.0	9.1	0.151	0.0141	72.27	0.0055
120.0	38.5	20.0	0.0	32.5	40.0	9.7	0.081	0.0141	64.35	0.0040
240	35.0	20.0	0.0	29.0	36.5	10.3	0.043	0.0141	57.42	0.0029
480	32.0	20.0	0.0	26.0	33.5	10.8	0.023	0.0141	51.48	0.0021
1470	27.0	20.0	0.0	21.0	28.5	11.6	0.008	0.0141	41.58	0.0013
2080	25.0	20.0	0.0	19.0	26.5	12.0	0.006	0.0141	37.62	0.0011

Table A3.28 Hydrometry data sheet (test 2 specimen 6).

Specimen 6		Test 2	Gs:2.70		Date: Oct. 2005			C_d=6	C_m=1.5	
t (min)	R'_h	Temp. (°C)	C_t	R_h	R'_h+C_m	L (cm)	L/t	K	Finer %	D (mm)
0.5	54.5	20.0	0.0	48.5	56.0	7.1	14.22	0.0141	96.03	0.0532
1.0	54.0	20.0	0.0	48.0	55.5	7.2	7.19	0.0141	95.04	0.0378
2.0	54.0	20.0	0.0	48.0	55.5	7.2	3.59	0.0141	95.04	0.0267
4.0	53.0	20.0	0.0	47.0	54.5	7.4	1.84	0.0141	93.06	0.0191
8.0	50.5	20.0	0.0	44.5	52.0	7.8	0.971	0.0141	88.11	0.0139
15.0	48.5	20.0	0.0	42.5	50.0	8.1	0.540	0.0141	84.15	0.0104
30.0	45.0	20.0	0.0	39.0	46.5	8.7	0.289	0.0141	77.22	0.0076
60.0	41.0	20.0	0.0	35.0	42.5	9.3	0.155	0.0141	69.30	0.0056
120.0	38.0	20.0	0.0	32.0	39.5	9.8	0.082	0.0141	63.36	0.0040
240	34.0	20.0	0.0	28.0	35.5	10.5	0.044	0.0141	55.44	0.0029
480	31.0	20.0	0.0	25.0	32.5	11.0	0.023	0.0141	49.50	0.0021
1470	26.5	20.0	0.0	20.5	28.0	11.7	0.008	0.0141	40.59	0.0013
2080	25.0	20.0	0.0	19.0	26.5	12.0	0.006	0.0141	37.62	0.0011

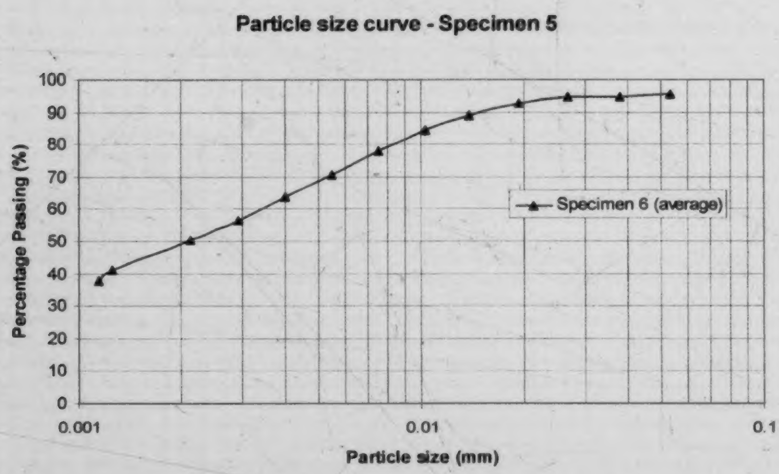

Figure A3.24 Average particle size distribution curve for specimen 6.

Table A3.29 Hydrometry data sheet (test 1 specimen 7).

Specimen 7		Test 1	Gs:2.70		Date: Nov. 2005			C_d=4.5	C_m=1.5	
t (min)	R'_h	Temp. (°C)	C_t	R_h	R'_h+C_m	L (cm)	L/t	K	Finer %	D (mm)
0.5	54.5	20.0	0.00	50.0	56.0	7.1	14.22	0.0141	99.00	0.0532
1.0	54.5	20.0	0.00	50.0	56.0	7.1	7.11	0.0141	99.00	0.0376
2.0	54.5	20.0	0.00	50.0	56.0	7.1	3.55	0.0141	99.00	0.0266
4.0	53.5	20.0	0.00	49.0	55.0	7.3	1.82	0.0141	97.02	0.0190
8.0	52.0	20.0	0.00	47.5	53.5	7.5	0.94	0.0141	94.05	0.0137
15.0	49.5	20.0	0.00	45.0	51.0	7.9	0.529	0.0141	89.10	0.0103
30.0	45.5	20.0	0.00	41.0	47.0	8.6	0.286	0.0141	81.18	0.0075
60.0	41.5	20.0	0.00	37.0	43.0	9.2	0.154	0.0141	73.26	0.0055
145.0	37.0	20.0	0.00	32.5	38.5	10.0	0.069	0.0141	64.35	0.0037
275	32.5	20.0	0.00	28.0	34.0	10.7	0.039	0.0141	55.44	0.0028
480	29.5	20.0	0.00	25.0	31.0	11.2	0.023	0.0141	49.50	0.0022
1690	23.0	20.0	0.00	18.5	24.5	12.3	0.007	0.0141	36.63	0.0012

Table A3.30 Hydrometry data sheet (test 2 specimen 7).

Specimen 7		Test 2	Gs:2.70		Date: Nov. 2005			C_d=4.5	C_m=1.5	
t (min)	R'_h	Temp. (°C)	C_t	R_h	R'_h+C_m	L (cm)	L/t	K	Finer %	D (mm)
0.5	54.0	20.0	0.0	49.5	55.5	7.2	14.38	0.0141	98.01	0.0535
1.0	54.0	20.0	0.0	49.5	55.5	7.2	7.192	0.0141	98.01	0.0378
2.0	54.0	20.0	0.0	49.5	55.5	7.2	3.596	0.0141	98.01	0.0267
4.0	54.0	20.0	0.0	49.5	55.5	7.2	1.798	0.0141	98.01	0.0189
8.0	53.0	20.0	0.0	48.5	54.5	7.4	0.920	0.0141	96.03	0.0135
15.0	51.0	20.0	0.0	46.5	52.5	7.7	0.512	0.0141	92.07	0.0101
30.0	48.0	20.0	0.0	43.5	49.5	8.2	0.273	0.0141	86.13	0.0074
60.0	43.5	20.0	0.0	39.0	45.0	8.9	0.149	0.0141	77.22	0.0054
145.0	39.0	20.0	0.0	34.5	40.5	9.7	0.067	0.0141	68.31	0.0036
275	36.0	20.0	0.0	31.5	37.5	10.1	0.037	0.0141	62.37	0.0027
480	32.0	20.0	0.0	27.5	33.5	10.8	0.023	0.0141	54.45	0.0021
1690	25.0	20.0	0.0	20.5	26.5	12.0	0.007	0.0141	40.59	0.0012

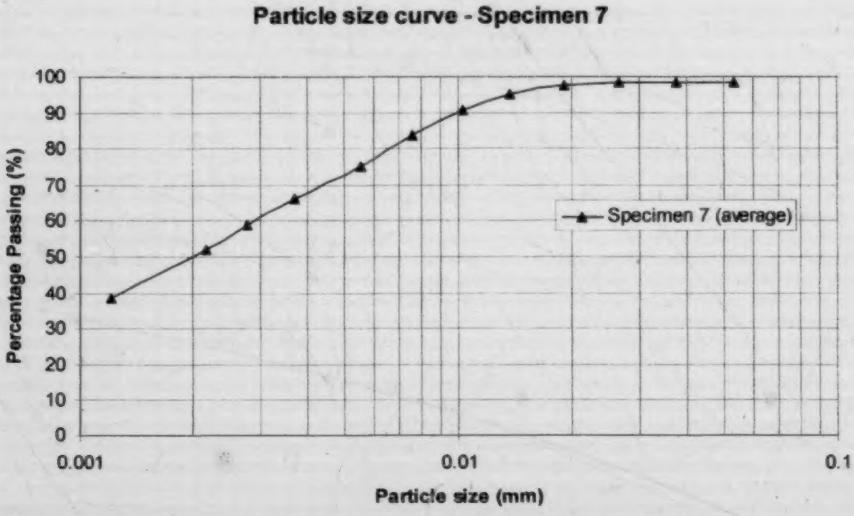

Figure A3.25 Average particle size distribution curve for specimen 7.

Table A3.31 Hydrometry data sheet (test 1 specimen 8).

Specimen 8		Test 1	Gs:2.70		Date: Nov. 2005			C_d=5	C_m=1.0	
t (min)	R'_h	Temp. (°C)	C_t	R_h	R'_h+C_m	L (cm)	L/t	K	Finer %	D (mm)
0.5	55.0	20.0	0.00	50.0	56.0	7.1	14.22	0.0141	99.00	0.0532
1.0	54.5	20.0	0.00	49.5	55.5	7.2	7.192	0.0141	98.01	0.0378
2.0	54.5	20.0	0.00	49.5	55.5	7.2	3.596	0.0141	98.01	0.0267
4.0	54.0	20.0	0.00	49.0	55.0	7.3	1.819	0.0141	97.02	0.0190
8.0	53.5	20.0	0.00	48.5	54.5	7.4	0.920	0.0141	96.03	0.0135
15.0	51.5	20.0	0.00	46.5	52.5	7.7	0.512	0.0141	92.07	0.0101
30.0	50.0	20.0	0.00	45.0	51.0	7.9	0.264	0.0141	89.10	0.0072
60.0	45.5	20.0	0.00	40.5	46.5	8.7	0.144	0.0141	80.19	0.0054
120.0	41.5	20.0	0.00	36.5	42.5	9.3	0.078	0.0141	72.27	0.0039
240	38.0	20.0	0.00	33.0	39.0	9.9	0.041	0.0141	65.34	0.0029
480	35.0	20.0	0.00	30.0	36.0	10.4	0.022	0.0141	59.40	0.0021
1440	30.0	20.0	0.00	25.0	31.0	11.2	0.008	0.0141	49.50	0.0012

Table A3.32 Hydrometry data sheet (test 2 specimen 8).

Specimen 8		Test 2	Gs:2.70		Date: Nov. 2005			C_d=5	C_m=1.0	
t (min)	R'_h	Temp. (°C)	C_t	R_h	R'_h+C_m	L (cm)	L/t	K	Finer %	D (mm)
0.5	55.0	20.0	0.00	50.0	56.0	7.1	14.22	0.0141	99.00	0.0532
1.0	55.0	20.0	0.00	50.0	56.0	7.1	7.11	0.0141	99.00	0.0376
2.0	55.0	20.0	0.00	50.0	56.0	7.1	3.55	0.0141	99.00	0.0266
4.0	54.5	20.0	0.00	49.5	55.5	7.2	1.798	0.0141	98.01	0.0189
8.0	54.0	20.0	0.00	49.0	55.0	7.3	0.909	0.0141	97.02	0.0134
15.0	52.5	20.0	0.00	47.5	53.5	7.5	0.501	0.0141	94.05	0.0100
30.0	49.5	20.0	0.00	44.5	50.5	8.0	0.267	0.0141	88.11	0.0073
60.0	46.0	20.0	0.00	41.0	47.0	8.6	0.143	0.0141	81.18	0.0053
120.0	43.0	20.0	0.00	38.0	44.0	9.1	0.076	0.0141	75.24	0.0039
240	39.0	20.0	0.00	34.0	40.0	9.7	0.041	0.0141	67.32	0.0028
480	35.5	20.0	0.00	30.5	36.5	10.3	0.021	0.0141	60.39	0.0021
1440	30.5	20.0	0.00	25.5	31.5	11.1	0.008	0.0141	50.49	0.0012

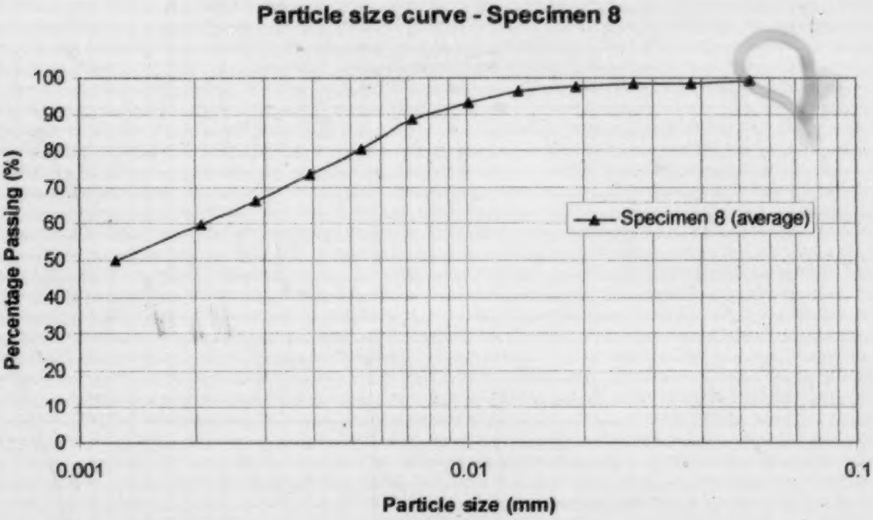

Figure A3.26 Average particle size distribution curve for specimen 8.

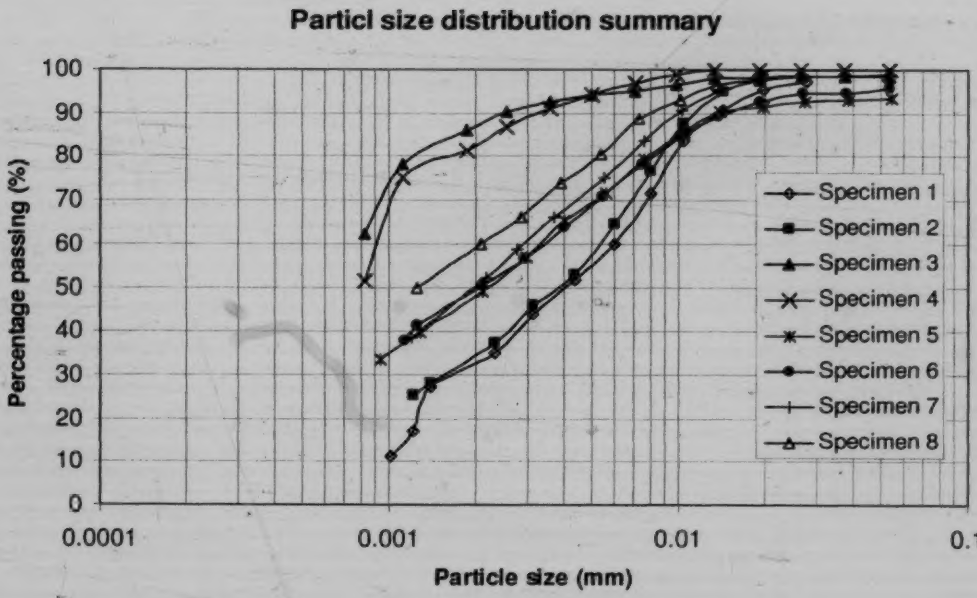

Figure A3.27 Summary of particle size distribution curves of all tested specimens from clay-silt unit.

Table A3.33 Summary of particle size distribution analysis result.

Specimen	Sand (%)	Silt (%)	Clay (%)
1	0	67	33
2	0	66	34
3	0	13	87
4	0	18	82
5	5	46	49
6	3	47	50
7	0	49	51
8	0	41	59

A3.6. MINERALOGY TESTS

Four samples were taken for soil mineralogy tests (Figure A3.28). Two pieces from each sample were tested under a Scanning Electron Microscope (SEM) (Figure A3.29). All specimens were taken from the clay-silt material of unit 2 in the shear zone. Table A3.34 presents the specimens' information. Specimen 2 was taken from the clay part of the direct shear sample #4 in borehole DH04-13 (P6, Figure A3.1). Minimum shear strength and slickensides were visible in this specimen. Similar material was encountered in the borehole, and specimen 4 was taken from that clay part. Specimens 1 and 3 were silty clay material which was sampled to check for the differences between the dark brown clay layers and this light brown silty clay material.

Samples of SEM pictures from each specimen are showed in Figure A3.30. This figure shows that the specimens from the dark brown clay layers (specimens 2 and 4) contain more than 80% clay-sized particles. The material in the bright brown silty clay specimens (specimens 1 and 3) is a mixture of clay and silt. Table A3.35 shows the results of X-ray fluorescence (energy dispersive x-ray micro fluorescence) tests on these specimens, revealing the relative amounts of elements in them.

Table A3.34 SEM specimens' general information.

SEM Specimen #	Borehole ID	Depth (m)	Elevation (m)	Description
1	DH04-13 (P6)	16.7	259.3	Bright brown silty clay, above clay seam in direct shear sample #4
2	DH04-13 (P6)	16.7	259.3	Dark brown clay from direct shear test sample #4 at the slickenside in sample
3	DH04-13 (P6)	15.5	260.5	Bright brown silty clay
4	DH04-13 (P6)	15.0	261.0	Dark brown clay seam similar to material in specimen #2

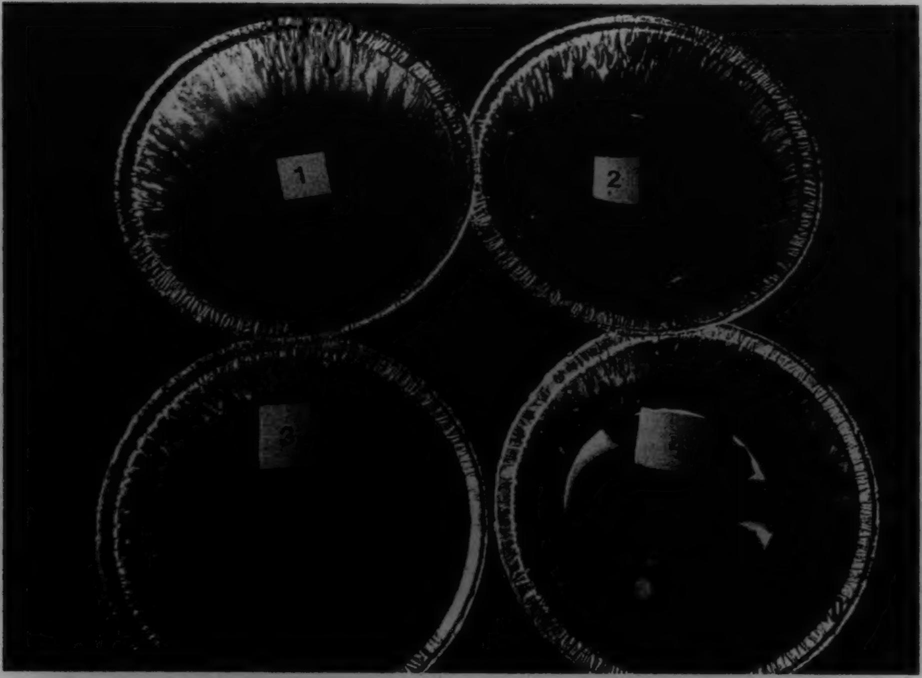

Figure A3.28 Four specimens from clay-silt unit (unit 2) for mineralogy tests.

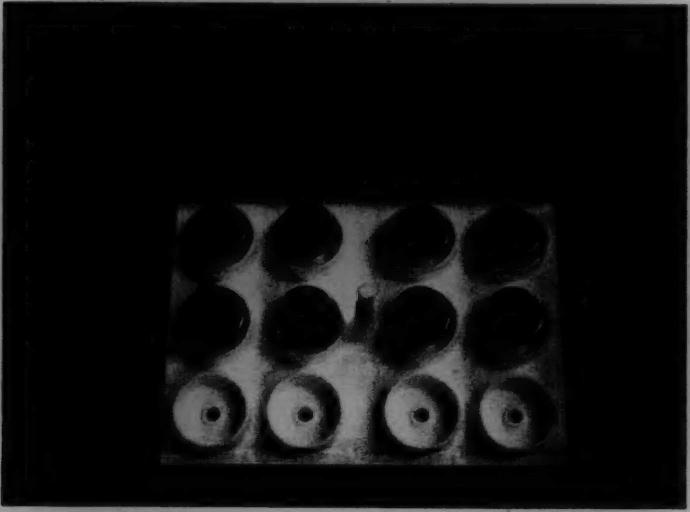

Figure A3.29 Gold coated specimens ready for Scanning Electronic Microscope.

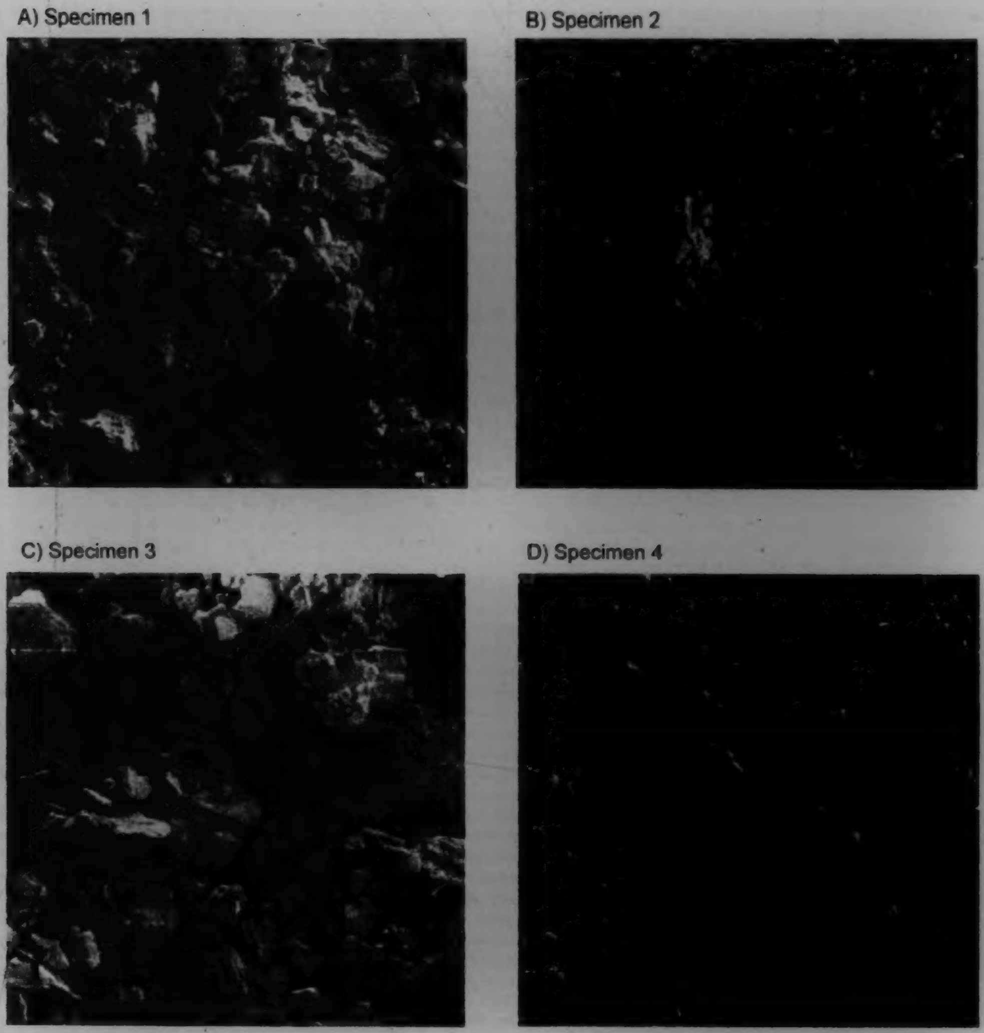

A) Specimen 1

B) Specimen 2

C) Specimen 3

D) Specimen 4

Figure A3.30 SEM pictures of four tested specimens from South Slide borehole DH04-13.

Table A3.35 X-ray fluorescence (energy dispersive x-ray micro fluorescence) test results on specimens.

Specimen	Dominant Elements
1	Si (52%), Al (15.8%), Fe (11.7 %), Ca (8.8%), other
2	Si (50%), Al (17.9%), Fe (14.6%), Mg (7.1%), others
3	Si (49.5%), Al (15.8%), Fe (15.01%), Ca (8.8%), others
4	Si (50%), Al (16.8%), Fe (16.3%), Mg (7.5%), others

A3.7. CONCLUSIONS

A summary of all test results for the specimens from the boreholes in the South Slide done in University of Alberta is shown in Table A3.36. Based on these results, the material in the clay-silt unit, unit 2, can be divided into three classes (Table A3.37). Class 1, the highly plastic brown clay soil has the lowest residual friction angle. Near the rupture surface, this layer is thicker. Therefore, this material controls the stability of slope in the reactivation mode. The peak strength parameters are useful for material outside of the rupture surfaces (Figure A3.31, Table A3.37). Class 2 is a mixture of clay and silt layers which separating these two beds were not possible. The silt layers in unit 2, shown as material class 3 in Table A3.37, are similar to the silt layers in the sand and silt unit, unit 3; therefore; its parameters can be used for part of the rupture surface passes through unit 3.

The SEM pictures and the X-ray fluorescence (energy dispersive x-ray micro fluorescence) tests on the clay layers in the clay-silt unit, unit 2, show that this material consists of highly plastic non-expansive clays (Illite or Kaolinite). The main difference between the shear zones and the rest of the clay-silt sediment is the thickness of the brown clay layers. In the shear zones, the thickness of the highly-plastic brown clay layers is between 20 and 40 cm while in the rest of the sediment sequence, the brown-clay thickness is generally less than 10 cm. The mineralogies of the clay layers are basically the same.

Table A3.36 Summary of test results on soil specimens from clay-silt sediment, unit 2, South Slide.

Specimen #	Tube #	Depth (m)	Elevation (m)	Clay (%)	L.L (%)	P.L (%)	P.I (%)	Water Content (%)	Activity	L.I	φ_r (°)(Stark.)	φ_r (°)(Test)
1	5	16.1	259.9	33	41	23	18	30.12	0.55	0.40	24	31.2
2	5	16.3	259.7	34	42	23	19	36.41	0.56	0.71	24	23.9
3	5	17	259	87	76	33	43	47.47	0.49	0.34	12	12.8
4	5	16.7	259.3	82	67	30	37	44.62	0.45	0.40	13	13.1
5	4	14.6	261.4	49	54	25	29	38.53	0.59	0.47	16	11.3
6	4	15.3	260.7	50	50	24	26	37.05	0.52	0.50	17	19
7	4	15	261	51	55	25	30	42.53	0.61	0.60	16	21.56
8	1	20.9	272.4	59	57	24	33	34.5	0.56	0.32	15	NA

Table A3.37 Summary of test results on clay-silt sediments in South Slide.

Test	Class 1	Class 2	Class 3
Specimens (#)	3 an 4	5, 6, 7,and 8	1 and 2
Liquid Limit (%)	71.5 (67-76)	54 (50-57)	41.5 (41-42)
Plastic Limit (%)	31.5 (30-33)	24.3 (24-25)	23 (23-23)
Plasticity Index (%)	40 (37-43)	29.8 (26-33)	18.5 (18-19)
Water Content (%)	46.0 (44.6-47.5)	38.1 (34.5-42.5)	33.3 (30.1-36.4)
Clay Fraction (%)	84.5 (82-87)	52.3 (49-59)	33.5 (33-34)
Activity	0.47 (0.45-0.49)	0.57 (0.52-0.61)	0.55 (0.55-0.56)
Liquidity Index	0.37 (0.34-0.40)	0.47 (0.32-0.6)	0.55 (0.40-0.71)
φ_r (°) (Stark.)	12.5 (12-13)	16 (15-17)	24 (24-24)
φ_r (°) (Test)	13	17.3	23.5
φ_{peak} (°) (Test)	16	18	23
C_{peak} (kPa) (Test)	10	25	25
Descriptions	High plastic brown clay (CH)	Relatively thin layers of brown clay (CH) (class 1) between layers of olive colour silty clay (CI) (class 3) layers	Olive colour Clayey silt (CI)

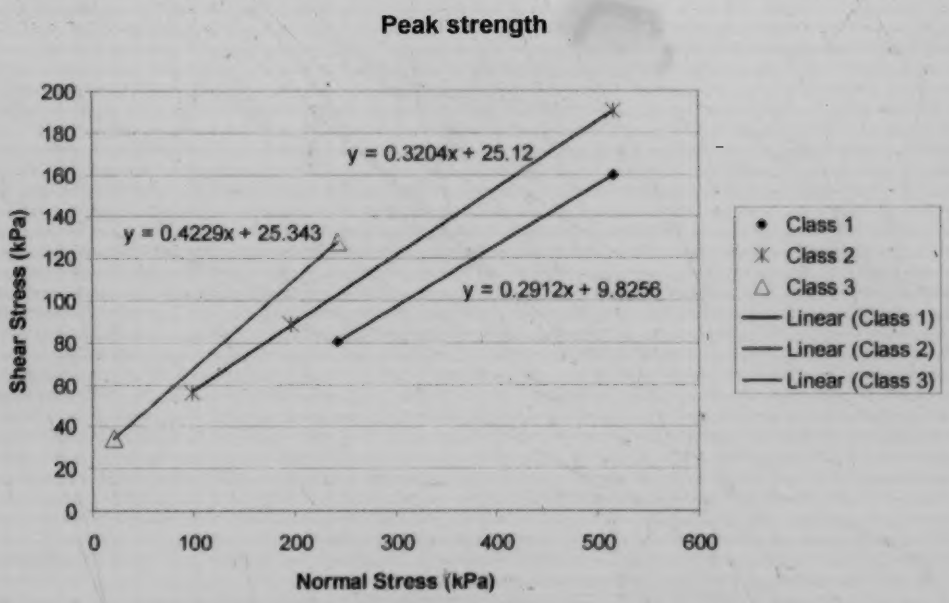

Figure A3.31 Peak strength envelope from direct shear tests for three classes of material in clay-silt unit, unit 2.